

Epithelial-mesenchymal dialogue during skin wound healing

Chong, Kelvin Han Chung

2014

Chong, K. H. C. (2014). Epithelial-mesenchymal dialogue during skin wound healing.
Doctoral thesis, Nanyang Technological University, Singapore.

<https://hdl.handle.net/10356/61824>

<https://doi.org/10.32657/10356/61824>

Epithelial-mesenchymal dialogue during skin wound healing

Chong Han Chung, Kelvin
(*B.Sc., University of Melbourne*)

A thesis submitted in partial fulfilment of the requirement for the degree of
Doctor of Philosophy

School of Biological Sciences
Nanyang Technological University

2014

ACKNOWLEDGEMENTS

It would never be possible to finish this doctoral thesis without the esteemed help from people around me, my committee members, friends and support from my family.

First and foremost I offer my deepest gratitude to my supervisor, Assistant Professor Tan Nguan Soon, Andrew, for his excellent guidance and patience ever since I started research from 2007. His enthusiasm for scientific research and pursue of research excellence in this field motivated me to become an independent researcher. I have learned a lot from his brilliant thoughts and ideas and was fortunate to impart some of his lab skills during his demonstrations at times. His patience in correcting my writing and diligent effort in reviewing all my manuscripts are greatly appreciated.

My sincere thanks must also go to the members of my thesis advisory committee: Assistant Professor Ravi Kambadur and Assistant Professor Thirumaran s/o Thanabalu. They generously gave their time to offer me valuable comment toward improving my work. I would also like to extend my utmost gratitude to the examiners who reviewed my thesis.

To all my current and ex-lab colleagues for great advices, assistances and the wonderful researching journey spent in the laboratory: Dr. Mintu Pal, Dr. Goh Yan Yih, Dr. Tan Chek Kun, Dr. Zhu Pengcheng, Dr. Ivan Lam, Dr. Wang Xiaoling, Dr. Dalton Tay, Ming Keat Sng, Brian Teo, Jeremy Chan, Royston Huang, Selin Foo and a special regard to M.J. Tan. Not forgetting my friends who went through hard times together with me, cheered me on, and celebrated each of our accomplishment: Andy Lam, Kevin Eng, Y Y Han, C L Chia and K Y Pang.

On a special note, my academic journey would not have begun or proceed smoothly if not for my parents constant support and belief in my abilities to pursue PhD. I would like to thank my mother, Iris for her unconditional trust and devotion. Special thanks to my father, Peter for the financial support throughout my studies and endless patience. Not to be excluded are my sisters, Brenda and Esther and brother, Edwin for their wonderful companions and they have been generous with their love. Finally, I would like to dedicate this thesis to my wife, Alicia for her personal support and my son, Jayren for filling me with joys through the hard times.

TABLE OF CONTENTS

TABLE OF CONTENTS.....	4
LIST OF TABLES.....	10
LIST OF ABBREVIATIONS.....	11
SUMMARY	17
CHAPTER 1: REGULATION OF EPITHELIAL-MESENCHYMAL INTERLEUKIN-1 SIGNALING BY PPAR β/δ IS ESSENTIAL FOR SKIN HOMEOSTASIS AND WOUND HEALING	19
1.1 ABSTRACT.....	20
1.2 INTRODUCTION.....	21
1.2.1 Skin	21
1.2.2 Wound healing.....	22
1.2.2.1 Inflammatory phase (phase 1)	25
1.2.2.2 Proliferative or migratory phase (phase 2)	29
1.2.2.3 Maturational phase (phase 3)	34
1.2.3 Cells of the Epidermis	36
1.2.4 Cells of the Dermis	40
1.2.5 Dermal Fibroblasts.....	42
1.2.6 Intercellular communication between fibroblasts and keratinocytes	44
1.2.7 Peroxisome proliferator-activated receptors (PPARs) in the skin	49
1.2.8 Biological role of the Interleukin 1 receptor antagonist in skin	50
1.3 MATERIALS AND METHODS.....	53
1.3.1 Reagents	53
1.3.2 Total RNA isolation, Reverse transcription PCR and qPCR	53
1.3.3 Lentivirus-mediated knockdown of PPAR β/δ and sIL-1ra	54
1.3.4 Transactivation assay	55
1.3.5 Chromatin immune-precipitation (ChIP)	55
1.3.6 Organotypic tissue culture (OTC).....	56
1.3.7 Immunofluorescence	57
1.3.8 Wounding experiment	58

1.3.9	Measurement of cytokines by Enzyme-linked immunosorbent assay (ELISA)	58
1.3.10	Protein arrays	59
1.3.11	Western blot analysis.....	59
1.3.12	Statistical analysis	59
1.4	RESULTS	62
1.4.1	PPAR β/δ knockdown in dermal fibroblasts results in increased keratinocytes proliferation.....	62
1.4.2	Organotypic cultures with F _{PPARβ/δ} show increased expression of mitogenic factors	68
1.4.3	Increased expression of mitogenic factors by F _{PPARβ/δ}	71
1.4.4	Neutralization of IL-1 α/β signalling abolishes the mitogenic action of F _{PPARβ/δ}	76
1.4.5	Human sIL-1ra gene is a direct target of PPAR β/δ in fibroblasts.....	80
1.4.6	sIL-1ra knockdown fibroblasts increase keratinocytes proliferation	85
1.4.7	PPAR β/δ KO mice show reduced sIL-1ra expression during early wound healing	92
1.5	DISCUSSION.....	96
1.6	FUTURE STUDIES	100
1.6.1	Tumor-stroma interaction during cancer progression: effect of nuclear receptors including PPAR β/δ in Cancer-associated fibroblasts (CAFs)	100
1.6.1.1	Reduced expression of PPAR β/δ in fibroblast results in increased A5RT3 proliferation	103
1.6.1.2	Organotypic culture with F _{PPARβ/δ} show increased expression of mitogenic factors	108
1.6.1.3	Expression Profiles of Nuclear Receptor in CAFs from Squamous Cell Carcinoma.....	110
1.6.1.4	Effect of Modified CAFs on the Adjacent Tumour Growth using Organotypic Co-culture.....	111
1.6.2.4	Orthotropic Surface Transplantation Assay in Nude Mice	112
CHAPTER 2: REGULATION OF EPITHELIAL-MESENCHYMAL NITRIC OXIDE SIGNALING BY ANGIOPOIETIN-LIKE 4 ACCELERATE CUTANEOUS WOUND HEALING IN DIABETIC MICE		114
2.1	ABSTRACT.....	115

2.2	INTRODUCTION.....	116
2.2.1	Diabetes wound repair	116
2.2.2	Mouse models of diabetes	118
2.2.2.1	Mutant genes causing diabetes-obesity syndromes in mice	119
2.2.2.2	Streptozotocin induced diabetic mice	120
2.2.2.3	Diabetes induced by diabetogens such as alloxan monohydrate	121
2.2.2.4	Type 2 diabetes mellitus in mouse model induced by high fed diet.....	122
2.2.3	Topical therapeutic strategies for treating diabetic wound.....	123
2.2.4	Nitric oxide and wound healing	124
2.2.5	The role of matricellular proteins in wound healing	128
2.2.5.1	Angiopoietin like protein 4.....	132
2.3.1	Reagents	137
2.3.2	Recombinant cANGPTL4 expression, purification and endotoxin removal.	137
2.3.3	Genotyping of diabetic mice.....	138
2.3.4	Full excisional splinted wounding.....	140
2.3.5	Tissue preparation and sectioning	140
2.3.6	Assessment of wound healing	141
2.3.7	Van gieson elastic stain	141
2.3.8	Focused real-time PCR array	142
2.3.9	Hydroxyproline assay	144
2.3.10	Nitric oxide determination	145
2.3.11	Immunofluorescence staining	145
2.3.13	Proximity ligation assay	146
2.3.14	<i>In vitro</i> diabetic wound assay	147
2.3.15	Chromatin Immunoprecipitation (ChIP)	148
2.3.16	Transmission Electron Microscopy	149
2.3.17	Scanning Electron Microscopy.....	149
2.3.18	Laser capture microdissection (LCM).....	150
2.3.19	Immunoblotting	150
2.3.20	RNA extraction and reverse transcription.....	151
2.3.21	Isolation of cells.	152

2.3.22	Intracellular staining and Flow cytometry.	152
2.3.23	Transient suppression of STAT3 in keratinocytes.	153
2.3.24	Statistical analysis	154
2.4	RESULTS	154
2.4.1	Reduced ANGPTL4 expression in impaired diabetic wound healing.	154
2.4.2	Topical application of cANGPTL4 improves the healing rate of diabetic wounds.	155
2.4.3	ANGPTL4 induces angiogenesis in diabetic wounds	156
2.4.4	ANGPTL4 increases nitric oxide (NO) production as an angiogenic mediator in diabetic wounds.	178
2.4.5	ANGPTL4 regulates iNOS expression via STAT3 activation in keratinocytes.	186
2.6	FUTURE STUDIES.....	195
2.6.1	The effect of cANGPTL4 in tissue remodelling and collagen scar formation	195
2.6.1.1	Recombinant cANGPTL4 reduces collagen scar deposition in ob/ob diabetic wounds.....	197
2.6.1.2	Improved biomechanical properties of cANGPTL4-treated wounds.	200
2.6.1.3	ANGPTL4 restores wound fibroblast migration into wound bed	202
2.6.1.4	Potential mechanism for scarring: ANGPTL4 inhibits collagen 1 alpha-2 (COL1A2) expression in a β -catenin-dependent manner	204
2.7	GENERAL CONCLUSION.....	207
	REFERENCES	214
	PUBLICATIONS	245

LIST OF FIGURES

Figure 1. Phases of repair in acute wound healing.....	23
Figure 2. Skin layers	38
Figure 3. Schematic illustration of keratinocyte-fibroblast cross-talk.....	47
Figure 4 Increased PPAR β/δ expression in both keratinocytes and fibroblasts.	64
Figure 5. K _{PPARβ/δ} reduced the expression of terminal differentiation markers.....	66
Figure 6. . F _{PPARβ/δ} potentiate the adjacent epithelial proliferation.....	67
Figure 7. Reduced fibroblast PPAR β/δ expression up-regulated AP-1-controlled mitogenic target genes.....	70
Figure 8. Reduced fibroblast PPAR β/δ expression increases IL-1 α activation of TAK1.	74
Figure 9. Increased c-Jun binding to AP-1 site of human KGF and GM-CSF gene in F _{PPARβ/δ}	75
Figure 10. Neutralizing antibodies against IL-1 α/β or against KGF, GMCSF and IL-6 abolished the mitogenic effect of F _{PPARβ/δ}	78
Figure 11. Neutralizing antibodies against IL-1 α/β or against KGF, GMCSF and IL-6 abolished the mitogenic effect of F _{PPARβ/δ}	79
Figure 12. Reduced sIL-1ra in PPAR β/δ deficient fibroblasts.	81
Figure 13. Human sIL-1ra is encoded in a direct PPAR β/δ target gene in fibroblasts... ..	84
Figure 14. Reduced sIL-1ra in fibroblasts potentiates epidermal keratinocyte proliferation.	87
Figure 15. Reduced fibroblasts sIL-1ra increases epidermal proliferation.	88
Figure 16. Increased c-JUN binding to AP-1 site of human KGF, GMCSF and IL-6 gene promoter in F _{sIL-1ra}	91
Figure 17. Regulation of IL-1 β signaling via PPAR β/δ during wound repair in PPAR β/δ -null mice.	94
Figure 18. Laser capture microdissection (LCM) of normal and wound biopsies.	95
Figure 19. The autonomous and non-autonomous actions of PPAR β/δ	97
Figure 20. Heatmap shows changes in gene expression of 48 nuclear receptor (NRs) in normal skin fibroblasts (NF) or cancer-associated fibroblasts (CAFs).	104
Figure 21. Reduced PPAR β/δ and sIL-1ra in cancer-associated fibroblasts.....	106
Figure 22. PPAR β/δ -deficient fibroblasts increase epithelial tumor cell proliferation... ..	107
Figure 23. Graft transplantation assay.	112
Figure 24. Signaling mechanisms of selected matricellular proteins.....	130
Figure 25. Structure and biological functions of ANGPTL4.....	135
Figure 26. Analysis of centrally dissected ob/+ and ob/ob wound sections.....	159
Figure 27. Expression of ANGPTL4 was reduced in diabetic wounds.	160
Figure 28. Specificity of monoclonal antibodies against mouse ANGPTL4.....	161
Figure 29. Topical application of ANGPTL4 improves diabetic wound healing.	163

Figure 30. ANGPTL4 implications on several biological gene functions.	173
Figure 31. ANGPTL4 improves wound-related angiogenesis.	174
Figure 32. Immunofluorescence staining of wound biopsies	175
Figure 33 ANGPTL4 induced angiogenesis in ob/ob wound.	176
Figure 34 ANGPTL4 has no direct effect on endothelial cells survival and proliferation.	177
Figure 35. ANGPTL4 regulates NO production in wound epithelium.	181
Figure 36. Laser capture microdissection (LCM) of saline- and cANGPTL4-treated ob/ob.	183
Figure 37. ANGPTL4 regulates iNOS expression.	184
Figure 38. Effect of ANGPTL4 on <i>in vitro</i> endothelial tubule formations.	185
Figure 39. ANGPTL4 activates the integrin signaling pathway.	188
Figure 40. ANGPTL4 activates JAK1/STAT3 signalling to regulate iNOS expression in keratinocytes.....	190
Figure 41. Schematic illustration of the autocrine and paracrine effect of ANGPTL4 on cutaneous wound healing.	193
Figure 42. Reduced collagen deposition in cANGPTL4 treated ob/ob wounds.....	198
Figure 43. Scanning and transmission electron microscopy imaging of connective tissues	199
Figure 44. biomechanical properties of cANGPTL4-treated wounds	201
Figure 45. ANGPTL4 restores wound fibroblast migration.....	203
Figure 46.reduced id3 and collagen expression in cANGPTL4 treated fibroblasts	205
Figure 47. Schematic Illustration of keratinocyte-fibroblast and keratinocyte-endothelial cell crosstalks during wound healing.....	210

LIST OF TABLES

Table 1: Sequence of primers	60
Table 2: Relative fold change of protein expression in OTCs with $F_{PPAR\beta/\delta}$ compared with F_{CTRL}	69
Table 3: Relative fold change of protein expression in OTCs with F_{sIL1ra} compared to F_{CTRL}	90
Table 4: Relative fold change in growth factors/ cytokines expression in HaCaT-A5RT3 OTCs with $F_{sIL-1ra}$ compared to HaCat-A5RT3 OTCs with F_{CTRL}	109
Table 5: List of primer pairs sequences.....	143
Table 6. Gene expression in ob/+ wound	164
Table 7. Gene expression in Saline-treated ob/ob wound.	167
Table 8. Gene expression in cANGPTL4-treated ob/ob wound.	170

LIST OF ABBREVIATIONS

ANGPTL4	Angiopoietin-like 4
A5RT3	Human metastatic skin squamous cell carcinoma
AG	Aminoguanidine hydrochloride
AP-1	Activator protein 1
ATP	Adenosine triphosphate
AU	Arbitrary fluorescence unit
BCC	Basal cell carcinoma
CAFs	Cancer associated fibroblasts
CCN-1	Cysteine-rich protein 61
CCR2	C-C chemokine receptor 2
CD31	Marker for endothelial cells
CD68	Marker for monocytes and macrophages
ChIP	Chromatin immunoprecipitation
CK5	Keratin 5
CK10	Keratin 10
CMC	Carboxymethylcellulose
COL1A2	Collagen type 1 alpha-2
CRP	C-reactive protein
CXCL1	Chemokine ligand 1
DAF	4,5-diamino-fluorescein
DAPI	4',6-diamidino-2-phenylindole
DC	Dendritic cells
DFU	Diabetic foot ulcer

DNA	Deoxyribonucleic acid
DM	Diabetes mellitus
DMAB	p-dimethylaminobenzaldehyde
DMEM	Dulbecco's Modified Eagle's Medium
DMSO	Dimethyl sulfoxide
DR1	Direct repeat 1
ECM	Extracellular matrix
EGF	Epidermal growth factor
ELISA	Enzyme-linked immunosorbent assay
eNOS	Endothelial nitric oxide synthase/nitric oxide synthase 3
EMSA	Electrophoretic mobility shift assay
ERK	Extracellular signal-regulated kinases
eNOS	Endothelial nitric oxide synthase
EMSA	Electrophoretic mobility shift assay
F4/80	Macrophage marker
FACS	Fluorescence-activated cell sorting
FAD	Flavine adenine dinucleotide
FBS	Fetal bovine serum
FITC	Fluorescein isothiocyanate
F _{CTRL}	Control or normal fibroblasts
F _{PPARβ/δ}	PPAR β/δ knockdown fibroblasts
FsIL-1ra	PPARsIL-1ra knockdown fibroblasts
FFPE	Formalin-fixed, paraffin-embedded
FGF2	Fibroblast growth factor 2
FMN	Flavine mononucleotide

GM-CSF	Granulocyte macrophage colony stimulating factor
GW501516	PPAR β/δ agonist
GRO- α	Growth-related oncogene
H&E	Haematoxylin and eosin
HaCaT	Immortalized human keratinocytes
HBSS	Hank's buffered salt solution
HIF- α	Hypoxia-inducible factors alpha
HGF/SF	hepatocyte growth factor/scatter factor
I-309	a member of the CC subfamily of chemokines
icIL-1ra	Intracellular IL-1R antagonist
ID3	Inhibitor of DNA binding 3
IgG	Immunoglobulin G
IGF	Insulin-like growth factor
IL-1	Interleukin 1
IL-1R	Interleukin 1 receptor
IL-6	Interleukin 6
IL-8	Interleukin 8
iNOS	Inducible nitric oxide synthase
INF- γ	Interferon gamma
JAK1	Janus kinase 1
Ker _{STAT3}	STAT3-knockdown keratinocytes
Ki67	Proliferation marker
KGF/FGF7	Keratinocyte growth factor
KO	PPAR β/δ knockout mice
LCM	Laser capture micro dissection

LPS	Lipopolysaccharide
NADPH	Nicotinamide-adenine-dinucleotide phosphate
NGS	Normal goat serum
NO	Nitric oxide
NFs	Normal dermal fibroblasts
NRs	Nuclear receptors
MEd	Malic enzyme distal PPRE
MMPs	Matrix metalloproteinases
ob/+ or WT	Normal or wild-type mice
ob/ob	Diabetic mice
OCT	Optimum cutting temperature
OPN	Osteopontin
OTC	Organotypic tissue culture
PARP	Poly (ADP-ribose) polymerase
PCNA	Proliferating cell nuclear antigen
PDGF	Platelet-derived growth factor
PE	Phycoerythrin
PLA	Proximity ligation Assay
PKC α	Protein kinase C
PIGF	Placental growth factor
PFA	Paraformaldehyde-PBS
PNFs	Stromal fibroblasts from peri-normal tissue
PMSF	Phenylmethylsulfonyl fluoride
PPAR β/δ	Peroxisome proliferator-activated receptor β/δ

PPRE	Peroxisome proliferator response element
PVDF	Polyvinylidene difluoride
pVHL	von Hippel-Lindau tumor suppressor
qPCR	Quantitative polymerase chain reaction
RAR	Retinoic acid receptor
RPLP0	Ribosomal protein P0
RT	Room Temperature
RXR	Retinoid X receptor
SCC	Squamous cell carcinoma
SDF-1	Stromal-derived growth factor-1
SDS	Sodium dodecyl sulfate
sIL-1ra	Secreted IL-1R antagonist
siRNA	Small interfering ribonucleic acid
SPARC	Secreted Protein, Acidic and Rich in Cysteine
STZ	Streptozotocin
TAK1	Transforming growth factor-activated kinase 1
TBE	Tcf-binding sites
Tgase 1	Transglutaminase 1
TGF- β	Transforming growth factor beta
TNC	Tenascin
TNF α	Tumor necrosis factor alpha
TPA	12-O-Tetradecanoylphorbol-13-Acetate
TUNEL	Terminal deoxynucleotidyl transferase Biotin-dUTP nick end labelling

VDR	Vitamin D receptor
VE-cadherin	Vascular endothelial cadherin
VEGF	Vascular endothelial growth factor
WT	Wildtype

SUMMARY

The skin epidermis forms mainly by the stratification or differentiation of keratinocytes which dividing begin from the basal region right above the dermis. As the keratinocytes moved outward, they cease dividing and initiate their terminal differentiation process such as enucleation and keratinization. This regeneration and maintenance of the epidermis is dependent on the precise regulation of cellular proliferation, differentiation and apoptosis orchestrated with the underlying dermal tissue. Once the skin integrity is damaged, it is critical to activate the repair process in place to prevent the host from being exposed to foreign particle and infectious agents. The regulation of wound healing is also dictated by epithelial-mesenchymal interactions and purportedly mediated by the action of central players, such as chemokines and growth factors. The synchrony of this interaction is important to prevent excessive or insufficient wound repair. This complex interplay demands the expression of soluble factors exerting autocrine and paracrine activity, and importantly the integration of such diverse signals culminating in appropriate cellular responses. Apart from wound healing, a collective research has also revealed the involvement of stromal fibroblasts in cancer development. It is conceivable that irregularities or aberrations in the epithelial-stromal interaction can either enhance or attenuate tumor cell proliferation and metastasis. Though the importance of the epithelial-mesenchymal communication is well realized, the mechanism underlying this event needs in-depth study.

Thus, this study aims to understand the molecular communications between fibroblasts and keratinocytes during skin homeostasis and wound healing. Using a combination of molecular biology techniques, *in vitro* organotypic cultures and *in vivo* animal

experimentation, we analyze the growth characteristics of normal epithelial cells and the wound microenvironment. A better understanding of the molecular dialogue between fibroblasts and the epithelium opens a new avenue for the development of new therapies for wound treatment.

CHAPTER 1: REGULATION OF EPITHELIAL-MESENCHYMAL INTERLEUKIN-1 SIGNALING BY PPAR β/δ IS ESSENTIAL FOR SKIN HOMEOSTASIS AND WOUND HEALING

This work had been published in year 2009. Copyright permission has been granted to reuse portions or all of the author own material in a thesis without submitting a request to JBC.

Publication:

Chong, H.C., Tan, M.J., Philippe, V., Tan, S.H., Tan, C.K., Ku, C.W., Goh, Y.Y., Wahli, W., Michalik, L. and Tan, N.S. (2009). Regulation of epithelial-mesenchymal IL-1 signaling by PPAR β/δ is essential for skin homeostasis and wound. *J. Cell Biol.* 184(6):817-831. (IF: 10.264) (CI: 33)

This article was featured in the inaugural "In Focus- Time (and PPAR β/δ) heals all wound, and mentioned in Cover Page of J. Cell Biol

HCC and **MJT** performed, and analysed most of the experiments in this study, with intellectual input from **WW**. **VP** and **LM** performed animal wounding studies and collection of wound fluids for ELISA. **SHT**, **CKT**, **CWK** and **GY** performed some experiments and provided technical help. **NST** performed the EMSA and ChIP assay. **NST** provided overall coordination with respect to the conception, design, and supervision of the study. **HCC** and **NST** wrote the manuscript with comments from co-authors

1.1 ABSTRACT

The maintenance of skin function and integrity during normal skin hemostasis or wound repair involved complex epithelial-mesenchymal interactions. We show a novel paracrine effect of fibroblast PPAR β/δ on epithelial cell growth. IL-1 produced by keratinocytes activates PPAR β/δ expression in underlying fibroblasts, which in turn stimulates the production of the secreted IL-1 receptor antagonist (sIL-1ra) in the fibroblasts. sIL-1ra acts in an autocrine fashion onto the IL-1R1 expressed on the fibroblasts modulate the IL-1-mediated signalling events and consequently decreases production of several AP-1 mediated mitogenic factors. The mitogenic factors exert a reduced paracrine effect on the epithelial growth via their cognate receptors. Therefore, PPAR β/δ in the fibroblasts plays an important homeostatic role in maintaining epidermal homeostasis and proper wound healing. The absence of PPAR β/δ in the fibroblasts can result in significant epidermal proliferation similar to a tumour characteristic. Together, these findings provide evidence for a novel homeostatic control of keratinocyte proliferation and differentiation mediated via PPAR β/δ regulation in dermal fibroblasts of IL-1 signalling. Given the ubiquitous expression of PPAR β/δ other epithelial-mesenchymal interactions may also be regulated in a similar manner.

1.2 INTRODUCTION

1.2.1 Skin

The skin is the largest organ of the human body, covering a surface of approximately 20 square feet and weighing roughly 16% of our total body weight. The skin serves a variety of functions¹. It provides a protective shield against external environmental insults, such as pathogens and ultraviolet radiation, and helps sense the surroundings^{2,3}. Basic protection against environmental insults includes the use of pigmentation, which protects the underlying tissues from dehydration and from ultraviolet radiation injury^{3,4}. The skin can sense extreme temperatures through sensory detection from nerve endings that perceive pain¹. The physical structures of the skin prevent most pathogens and environmental toxins from harming the host⁵. Beyond this physical structure is the host innate immune system, which includes monocytes/macrophages, dendritic cells, and polymorphonuclear leukocytes (PMNs), providing an overall effective host defense against foreign pathogens². The human skin is primarily built by three main layers: a thin outer epidermis, an inner dermis and a subcutis that is also known as the hypodermis. The epidermis mainly consists of keratinocytes and, to a lesser extent, melanocytes, Merkel cells and Langerhans cells¹. The boundary between the epidermis and the dermis is known as the basement membrane and consists of a densely packed layer of proteins, such as proteoglycans and laminins. The basement membrane provides the anchorage for the basal keratinocytes. The dermis provides a structural and nutritional support with an established vascular network. This network is composed of a collagen and elastin fiber matrix with a residing population of fibroblasts, endothelial cells,

macrophages and mast cells. Specialized components of the skin, such as hair follicles, sebaceous glands and sweat glands are found anchored in the hypodermis. The hypodermis also contains fat lobules separated by layers of connective tissue¹.

1.2.2 Wound healing

Normal wound healing occurs through a series of events involving the interaction between multiple cells, proteins, growth factors and extracellular matrix components. The process of wound healing can be characterized into three considerably overlapping phases: the inflammatory phase, the proliferative phase and the maturational phase^{6,7} (Figure 1).

Briefly, the inflammatory phase is characterized by hemostasis and inflammation. Hemostasis is triggered upon activation of the intrinsic and extrinsic clotting cascade. In addition, skin injury triggers the release of potent vasoconstrictors, such as thromboxane A₂ and prostaglandin 2 alpha, leading to the extravasation of blood constituents⁸. The extravasated blood forms a clot to reinforce the hemostatic plug, which helps to limit hemorrhage. Once hemostasis is achieved, the surrounding capillaries will vasodilate and become leaky, resulting in the release of local histamine through the local activation of the complement cascade⁹. Furthermore, the altered vascular permeability allows the migration of inflammatory cells to the wound bed, and the presence of foreign organisms stimulates the activation of the alternate complement pathway¹⁰. Activation of Complement C3 results in a cascade of non-enzymatic protein

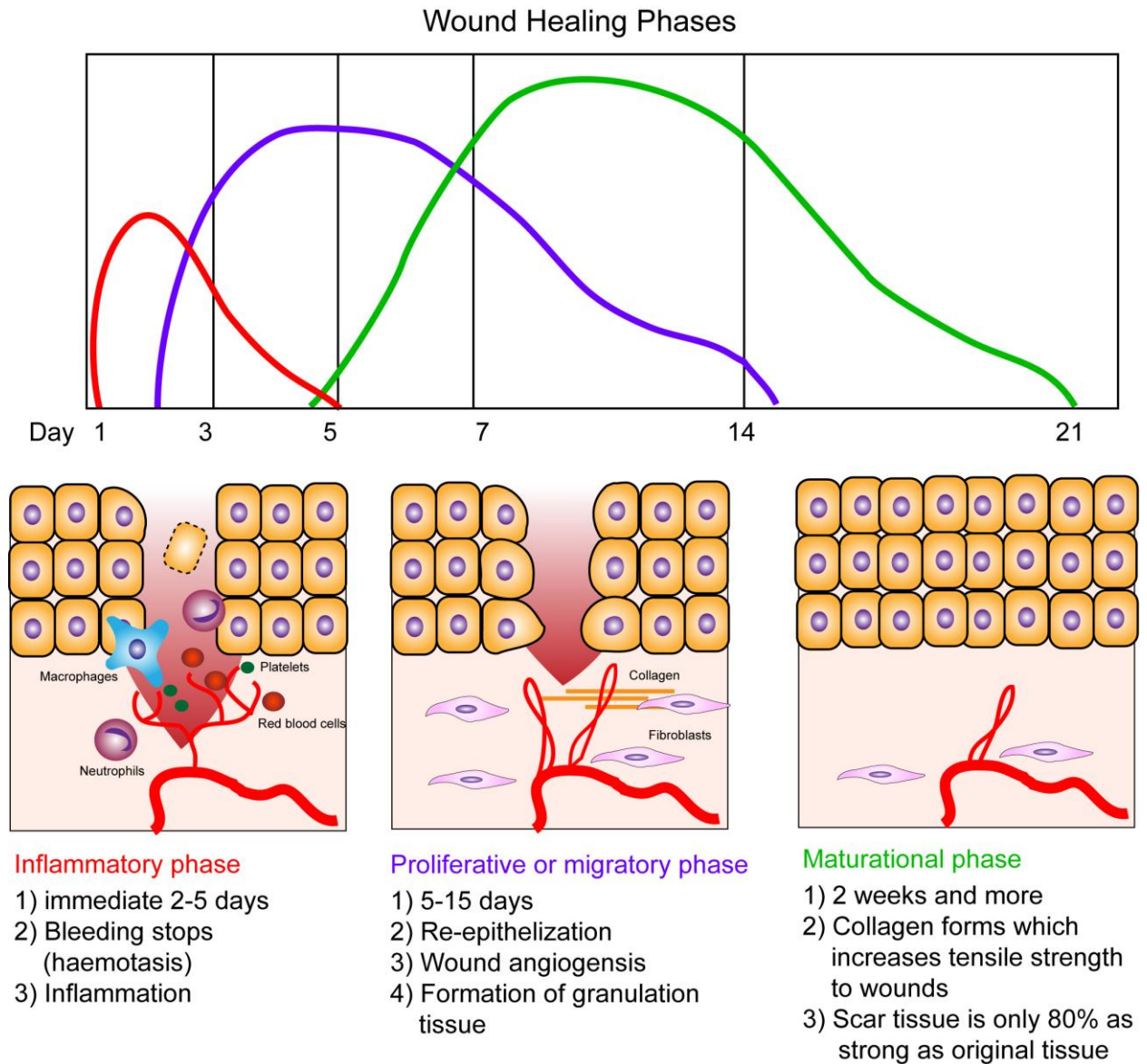


Figure 1. Phases of repair in acute wound healing

These processes, which are triggered by tissue injury, involve the three overlapping but well-defined phases of inflammatory (red), proliferative (blue) and maturational (green). Basic descriptions of each phase are noted below.

cleavage and interactions that eventually activate inflammatory cells and lead to bacterial killing¹⁰. In addition, the infiltration of neutrophils is responsible for debris scavenging, complement mediated opsonization and the lysis of foreign organisms as well as bacterial destruction via oxidative burst mechanisms, such as superoxide and hydrogen peroxide formation¹⁰.

The proliferative phase is marked by epithelialization, angiogenesis, granulation tissue formation, and collagen deposition¹¹. Epithelialization usually occurs a few hours after injury, but this process depends on the severity of the wound damage. In cases such as skin abrasion or first degree burn, the basement membrane is still intact and the epithelial cells can migrate in their normal orientation, with the epithelial progenitor cells remaining intact below the wound¹¹. The normal layers of epidermis can be restored within a few days. However, if the basement membrane has been damaged, as is the case for a deeper burn or a full thickness cutaneous wound, then the normal epidermal cells from skin appendages (e.g., hair follicles and sweat glands) will reepithelialize the wound from the wound edges¹¹. The formation of new blood vessels is necessary to deliver nutrients to the wound and help to maintain the granulation tissue bed. Angiogenesis has been linked to many cytokines and growth factors, including fibroblast growth factor, vascular endothelial growth factor, transforming growth factor β , tumor necrosis factor alpha, and thrombospondin^{12,13}. In clinical complications from diseases such as diabetes, poor capillary formation results in an insufficient nutrient supply to sustain the tissue deposition in the granulation phase and thus leads to the development of a chronically unhealed wound. The formation of granulation tissue marks the end of the proliferative phase¹⁴. As the new stroma begins

to invade the wound bed region, this invasion also provides an entry point for cells, such as macrophages and fibroblasts. Macrophages can supply growth factors to further stimulate angiogenesis and fibroplasia¹⁵. The secreted platelet derived growth factor and transforming growth factor β , along with extracellular matrix molecules, can stimulate fibroblast differentiation to myofibroblasts and the production of collagen¹⁵. Fibroblasts are key players in the synthesis, deposition, and remodeling of the extracellular matrix, providing strength and contraction to the wound.

The final phase of wound healing is the maturational phase. This is characterized by the transition from granulation tissue to scar formation^{7,14}. Weeks after injury, the wound undergoes contraction, ultimately resulting in the formation of apparent scar tissue¹⁶. Collagen continues to be produced by fibroblasts for a prolonged period of time, lasting up to several weeks after tissue injury and resulting in an overall increase in collagen deposition¹⁷.

1.2.2.1 Inflammatory phase (phase 1)

The inflammatory phase is often referred to as the second phase of wound healing and is characterized by increased vascular permeability and the sequential migration of leukocytes into the extravascular space¹⁸. One of the key functions of inflammation is to recruit inflammatory cells to the wounded area¹⁹. These cells are essential to remove dead cell debris, bacteria and damaged matrix, thus enabling the repair processes²⁰. Signs of inflammation, including erythema and heat, develop soon after wound injury as a result of vasodilatation. Simultaneously, the endothelial cells lining the capillaries in

the wound region develop gaps, which allow for the leakage of plasma into the extravascular compartment²¹. Edema is then generated from the migration of fluid into the injured area and contributes to the sensation of pain. Endothelial products and mast cell-derived factors, such as leukotrienes, prostaglandins and, in particular, histamine, contribute to this vasodilation.

Although the primarily capillary leakage is mediated by the release of histamine and prostaglandins, there is an additional influence from thrombin and the complement system. Complement factors C3a and C5a promote capillary leakage and also act as chemoattractants for neutrophils and monocytes²². Their chemotactic function is dependent on the release of TGF- β and formyl-methionyl peptides²³. The migration of leukocytes into the wounded area is stimulated by complement factors, collagen and immunomodulatory factors, including TGF- β , tumor necrosis factor- α (TNF- α), interleukin-1 (IL-1), PDGF, leukotriene B₄, and platelet factor IV. Leukocytes anchor and adhere to endothelial cells lining the capillaries in the wounded area through an interaction of intracellular adhesion molecules on the endothelial cell membranes and integrins expressed on the cell surface of the leukocytes. Leukocytes then transmigrate across the endothelium through a facilitated mechanism involving the expression of CD11/CD18, an integrin on the neutrophil surface²⁴. As the monocytes migrate into the extravascular space, they are transformed into macrophages by the stimulation of chemotactic factors such as fibronectin, elastin from the damaged matrix, complement components, TGF- β , and other factors. Macrophages can then be activated by IL-2 and INF- γ derived from T lymphocytes²⁵. Activated macrophages and neutrophils then initiate cellular wound debridement by phagocytosing bacteria and other foreign

materials^{25,26}. Both cell types present specific surface receptors that allow them to recognize, bind, and engulf foreign materials²⁷. Once the bacteria and debris are engulfed, they are digested by oxygen radicals and hydrolytic enzymes within the inflammatory cells²⁷. In addition, macrophages also contribute to extracellular breakdown by releasing matrix metalloproteinases into the wounded area²⁸. In addition, macrophages are also a primary source of cytokines that mediate several aspects of the wound healing process. Unlike polymorphonuclear leukocytes, the removal of macrophages from the healing environment significantly alters and impedes the healing process¹⁹. The presence of polymorphonuclear leukocytes will only alter the rate of wound infection²⁹. The role of the macrophage is complex as it is involved in many aspects of healing through the production of cytokines and immunomodulatory factors³⁰. Macrophage-produced cytokines are involved in angiogenesis, fibroblast migration and proliferation, collagen production, and possibly wound contraction³⁰. TGFb, IL-1, insulin-like growth factor-1 (IGF-1), FGF-2, and PDGF are several of the more critical macrophage-derived cytokines²³. TGF-b regulates its own production by macrophages in an autocrine manner³¹. It also stimulates macrophages to secrete PDGF, FGF-2, TNF-a, and IL-1 through binding to the epidermal growth factor receptor²³. Furthermore, macrophages also release nitric oxide, which may serve an antimicrobial function, among other functions, during the healing process. The inhibition of nitric oxide release has been found to impair wound healing in an in vivo mouse model³². The complete role of nitric oxide in wound healing has yet to be fully delineated (refer to 2.2.4 Nitric oxide and wound healing). As the healing process proceeds, inflammatory cells trapped within clots are sloughed³³. Neutrophils remaining within the wound become senescent and

undergo apoptosis³⁴. Apoptosis is characterized by the activation of endogenous calcium dependent endonucleases. The activation of these endonucleases results in the cleavage of chromatin into oligonucleosome DNA fragments and is indicative of irreversible cell death³⁵. The stimuli that lead to inflammatory cell apoptosis during tissue repair and scar formation have yet to be determined. Neutrophils are the first of the inflammatory cells to become apoptotic. They are then phagocytosed by macrophages²⁶. Macrophages and lymphocytes remain in the wound for approximately 7 days, after which they gradually diminish in number unless a noxious stimulant or further inflammation persists. Inflammatory cell apoptosis influences antigen presentation and, more importantly, contributes to the modulation of cytokine concentrations²¹.

The wound-healing process is, in large part, regulated by the ordered production of cytokines that control the gene activation responsible for cellular migration and proliferation and synthetic activities. As mentioned, platelets and macrophages are key cytokine sources, although many other cells produce cytokines as well. The control of cytokine release is regulated, in part, by other cytokines and by the characteristics of the surrounding tissue milieu^{36,37}. An often underreported signal for cytokine release is tissue hypoxia. Hypoxia has been shown to stimulate the release of TNF- α , TGF- β , vascular endothelial growth factor (VEGF), and IL-8 (IL-8) from fibroblasts, endothelial cells, and macrophages³⁸⁻⁴¹. "Cytokine networks" exist where multiple cell types involved in the healing process have receptors for the same cytokine. This permits the simultaneous stimulation of multiple activities by single cytokines⁴². This redundancy is most likely important in that it allows different factors to play greater or lesser roles at different time points or at different sites. In an individual cell, many cytokines can also

stimulate several different cellular functions that are often dependent on the concentration of the cytokine. This further allows individual cytokines to have varying effects at different points during the healing process. TGF- β , for example, is a macrophage chemoattractant when circulating in the femtomolar range but cannot stimulate collagen synthesis by fibroblasts until found in the nanomolar range²¹. In addition, PDGF facilitates chemotaxis for fibroblasts but only at a 100-fold greater concentration gradient than is necessary to stimulate fibroblast proliferation⁴³. Cellular activity is also regulated by the balance of cytokines and cytokine isoforms with conflicting activities. Cytokines such as PDGF, TGF- β , and FGF-2 accelerate collagen synthesis scar formation⁴⁴. Other cytokines slow collagen synthesis, including the $\beta 3$ isoform of TGF- β and INF- α ⁴⁵. Cellular activity is therefore modulated by the balance of cytokines with competing functions. A loss of this network balance has been implicated in chronic wound healing pathways³⁸.

1.2.2.2 Proliferative or migratory phase (phase 2)

The cellular situation in wounds changes dramatically after the initial phase. The fibrin–fibronectin matrix of the wound bed is heavily populated by inflammatory cells, whereas fibroblasts and endothelial cells needed for revascularization begin to predominate as healing progresses⁴⁶. The reestablishment of the epithelial surface of the damaged area will also be initiated. Cytokine networks continue to be a part of the process because cytokine release contributes to fibroplasia, epithelialization, and angiogenesis⁴². Although much is known about the cytokine signals that stimulate these processes during the proliferative phase of healing, less is known about the signals that modulate

or control these processes. Negative feedback mechanisms that deactivate cells after they have completed their work are also essential for normal healing. The recruitment of additional fibroblasts is required in the healing wound because the resident cells are lost or damaged in any injury^{42,47}. Fibroblasts can repopulate the wounded area through migration from adjacent tissues or through the proliferation of the resident cells in the wound⁴⁵. Integrin expression and several other factors, including PDGF⁴⁷, TGF- β ⁴⁵, EGF⁴⁸, and fibronectin⁴⁶, are vital for the migration of fibroblasts and other cell types. There are several different integrin molecules, and most present both α and β subunits²⁴. Different cells express different integrins, and individual cells commonly express more than one integrin, often under the influence of varied cytokines. Briefly, most cell migration requires that cell membrane-bound integrins adhere to fibronectin within the extracellular matrix⁴⁹. The migrating cell then forms lamellipodia that extend outward to another binding site within the matrix⁵⁰. The cell will then release itself from the primary binding site and pull the secondary site. The orientation of fibers in the matrix can influence cellular migration because cells tend to migrate along fibers. The migratory fibroblasts may be impeded by residual debris found in the wound matrix. To facilitate migration through such debris, TGF- β -stimulated fibroblasts can secrete several proteolytic enzymes to degrade obstacles, including matrix metalloproteinase-1 (MMP-1), gelatinase (MMP-2), and stromelysin (MMP-3)^{31,51-54}. The proliferation of resident fibroblasts in the wounded area as well as fibroblasts that have migrated to the wounded area is regulated by a variety of cytokines, including PDGF and TGF- β . PDGF often works in concert with IGF to facilitate fibroblast proliferation⁴⁷. PDGF primarily stimulates cell progression through the early G0 and G1 phases of the cell cycle. IGF,

which is derived primarily from hepatocytes and fibroblasts, then facilitates progression through the subsequent S1, G2, and M phases of the cell cycle⁴³. TGF- β can induce FGF-2 signaling in fibroblasts, leading to induction of fibroblast proliferation and fibrotic activation through the ERK kinase pathway⁵⁵.

1.2.2.2.1 Re-epithelization or Keratinocyte migration

Wound epithelization is critical for the reconstruction of injured epithelium and the re-establishment of the skin barrier functions. Re-epithelization of injured epithelium begins almost immediately upon wound injury. After injury, basal epithelial cells at the wound edge elongate and begin to migrate across the exposed wound surface³⁸. If the epithelial appendages, such as hair follicles and sweat glands, are still intact after the injury, these structures can contribute migratory epithelial cells for the re-epithelization process⁵⁶. Basically, these migratory epithelial cells form a monolayer across the wounded region. After the initiation of cellular migration, basal cells at the wound edge or from the appendages begin to proliferate, contributing additional cells to this monolayer. The migration of epithelial cells continues until overlap is achieved with other epithelial cells migrating from different directions. At that point, the cell to cell contact results in the cessation of cellular migration. The processes of cellular migration and proliferation occur under the control of various cytokines including EGF, TGF- α , platelet-derived EGF, and FGF-7⁵⁶⁻⁵⁸. Cellular migration may also require the secretion of MMPs to penetrate wound scabs. Cell migration requires formation of actin filaments within the cytoplasm of migratory cells and the removal of desmosomes that assist cells to link to one another and to the basement membrane. These processes are dependent

on changes in the expression of integrins on the cell membranes⁵⁹. It is believed that decreased calcium or increased magnesium concentrations stimulate the downregulation of the critical integrins, although the precise signal is not yet known⁴⁹. Migratory cells can simply migrate over the basement membrane if it is still intact. However, in wounds where the basement membrane has been destroyed, the cells have to migrate over the fibrin–fibronectin provisional matrix. As they migrate across the matrix, the epithelial cells can then regenerate a new basement membrane^{60,61}. This re-establishment of a basement membrane involves the secretion of several matrix proteins such as tenascin, vitronectin, and type I and V collagens⁶². When cellular contact is established via these matrix proteins, the hemidesmosomes link can reform between the cells and the basement membrane, and tenascin and vitronectin secretion will slowly diminishes^{63,64}. The cells become more basaloid, and further cellular proliferation generates a multi-laminated neo-epidermis that is covered by keratin⁶⁵. The neo-epidermis is similar to the native epidermis, although it is slightly thinner, its basement membrane is flatter, and the ridges that normally penetrate the dermis are absent⁶⁵.

1.2.2.2.2 Wound angiogenesis

The angiogenic process becomes active within 2 days after wounding⁶⁶. Various factors in the wound environment can contribute to angiogenesis. These factors included high lactate levels, acidic pH, and decreased oxygen tension, all of which occur in a hypoxic state⁶⁷. Severe hypoxia in the wound milieu is most likely due to the disruption of vasculature and increased oxygen consumption by cells, as active proliferating cells consume oxygen much faster than resting cells³³. During angiogenesis, endothelial cells

migrate and proliferate from the intact capillaries at the wound periphery⁶⁸. The endothelial cells develop a curvature and begin to produce a lumen as the chain of endothelial cells elongates. Eventually, the endothelial sprout comes into contact with a sprout derived from a different capillary, and the two interconnect to generate a new capillary⁶⁸. The migration of endothelial cells involves interactions of integrin domains within the provisional fibrin–fibronectin matrix in a similar manner to fibroblasts⁶⁹. The upregulation of $\alpha v \beta 3$ integrins on the endothelial cells has strong association with angiogenesis⁶⁸. Endothelial cell migration is also facilitated by the cell's ability to produce matrix metalloproteinases that break down collagen and the plasminogen activator, facilitating movement through the matrix^{51,54}. The angiogenic process is regulated by a variety of cytokines. The angiogenic factors that contribute to wound angiogenesis include FGF-2⁷⁰, VEGF⁷¹, TGF- β , angiopoietin and PDGF^{43,68}. This change in angiogenic cytokines may facilitate the maturation of the vascular system. Cytokine concentrations diminish as the wounded area becomes revascularized.

1.2.2.2.3 Formation of granulation tissue

The formation of acute granulation tissue is the final step in the proliferation phase and represents the beginning of the remodeling phase. As transitional tissue replaces the fibrin-/fibronectin-based provisional wound matrix, it produces a scar by maturation^{6,7,9,72-74}. This granulation tissue is characterized by a high density of fibroblasts, granulocytes, macrophages, capillaries and loosely organized collagen bundles⁷⁴. At this stage, the angiogenesis is also not completely finished; therefore, the granulation tissue is highly vascular⁷⁴. However, the dominating cell in this phase is the fibroblast, which fulfils

different functions, such as producing collagen and ECM substances. The formation of the ECM represents another important step because it provides a scaffold for cell adhesion and critically regulates and organizes the growth, movement and differentiation of the cells within it^{75,76}. The fibroblast is, therefore, the precursor of the provisional wound matrix within which the subsequent cell migration and organization takes place⁷⁷. At the end of this phase, the number of maturing fibroblasts is reduced by myofibroblast differentiation and consecutive apoptosis⁷⁸.

1.2.2.3 Maturation phase (phase 3)

This phase is considered the last phase of wound healing and can also be called the remodeling phase⁷⁴. Briefly, the maturation phase involves the remodeling of collagen from type III to type I; cellular activity diminishes, and the blood vessels in the wounded area regress and decrease in number; the formation of granulation tissue stops via apoptosis; therefore, a mature wound is usually characterized as both avascular and acellular⁷⁴. During wound maturation, the ECM components undergo remodeling. Collagen III, which was produced in the proliferative phase, is now replaced by the stronger collagen I. Collagen I is arranged in small parallel bundles and is therefore different from the basket-weave collagen structure found in healthy unwounded dermis^{74,79}. After the remodeling, myofibroblasts can attach to these collagen fibers for wound contraction, which helps to reduce the surface of the developing scar. Lastly, as the angiogenic processes diminish, the wound blood flow will decline, and the wound metabolism will slow.

1.2.2.3.1 Scarring

Scar formation usually marks the endpoint of mammalian wound repair. There is evidence suggesting that the process of wound healing is directly linked to the extent of scar formation. Fetal wound healing is known to be scarless up to a certain age due to the lack of an inflammatory response^{80,81}. In addition, studies showed that the presence of low levels of reproductive hormones, such as estrogen in mice, can lead to excessive inflammation, scarring, and a corresponding impairment in the rate of healing^{80,82}.

Excessive scarring is a fibrotic disorder that results from a disruption in the normal wound healing process. Most non-healing wounds fail to progress through the normal phases of wound repair and instead remain in a chronic inflammatory state⁸³. This leads to abnormal wound repair and the formation of hypertrophic or keloid scars⁸⁴. Keloids scars are usually made up of thick collagen fibers, whereas hypertrophic scars contain thin fibers organized into nodules⁸⁵. During the maturation phase, the abnormal remodeling of collagen from type III to type I can contribute to the change in excessive scar formation¹⁶. The granulation tissue continues to grow due to the excessive secretion of growth factors and the lack of molecules necessary for the initiation of apoptosis or ECM remodeling. Hypertrophic scars contain excessive microvessels, which are mostly occluded due to the over proliferation and functional regression of endothelial cells induced by myofibroblast hyperactivity and by excessive collagen production⁸⁶.

Scarring is a major cause of physical and psychological morbidity. While various studies have utilized a range of model systems to increase our understanding of the pathways and processes underlying scar formation, they have typically not translated to

the development of effective therapeutic approaches for scar management. This is evidenced by the fact that despite a number of potential treatment regimens, no single therapy is accepted universally as the standard of care. As such, scar improvement still remains an area of clear medical need. Currently, there are no registered pharmaceuticals for the prophylactic improvement of scarring, and no single therapy is accepted universally as the standard of care^{87,88}.

1.2.3 Cells of the Epidermis

The epidermis is clearly defined by its name: “epi” in Greek means top, while “dermis” means skin⁸⁹. The epidermis is a multilayered keratinized epithelium consisting of cells such as melanocytes and Langerhans cells (Figure 2). The cell type that predominates in the epidermis is the keratinocyte. Keratinocytes produce keratins, which are the main structural proteins of the skin epidermis, hair and nails⁸⁹. The epidermis is the skin's outer structure, which serves a protective function, and consists of five defined layers. The proliferation, differentiation and migration of epidermal cells begin in the basal layer known as the stratum basale (the inner-most layer closer to the dermis). As the basal cells divide and differentiate, they accumulate and are pushed upwards toward the surface. Keratinocytes go through phases of maturation, starting with an early differentiated cell layer known as the stratum spinosum, where the shape of the cells changes from columnar to polygonal⁸⁹. The cells switch from the expression of keratins K14 and K5 to K1 and K10^{90,91}. They exhibit spine-like cytoplasmic processes to which the desmosomes are anchored. In the granular layer (stratum granulosum), enzymes induce the degradation of nuclei and organelles⁸⁹. Granules attach to the cell membrane and release keratohyalin, which contributes to cell adhesion and to the cornified layer.

At this point, the keratinocytes no longer require metabolic activity to start a process of self-destruction that resembles apoptosis. The product of this process forms the cornified layer (stratum corneum), which is the outermost epidermal layer consisting of tightly packed enucleated and flattened cells⁸⁹. Another layer (stratum lucidum) that is found between the granular and cornified layer has no real distinction from the cornified dead cell layer except that keratinization can be observed⁸⁹. The skin epidermis forms an impenetrable seal that is continually replenished as inner layer cells move outwards and are sloughed from the skin surface⁸⁹. During skin perturbation, the restoration of an intact epidermal barrier through wound epithelialization is an essential feature. The migration of keratinocytes directed by a complex balance of signaling factors and surface proteins regulated in a temporospatial manner is critical to wound re-epithelialization⁷⁴. Re-epithelialization of the wound can be simply viewed as the product of overlapping functions of keratinocyte migration, proliferation, and differentiation⁷⁴. Keratinocytes are believed to begin re-epithelialization with the dissolution of cell-cell and cell-substratum contacts followed by the polarization and initiation of migration of basal keratinocytes over the provisional wound matrix¹¹. A group of keratinocytes found closer to the wound edge, but not within the wound bed itself, then undergoes mitosis to induce keratinocyte proliferation¹¹. Finally, the induction of keratinocyte differentiation forms a multilayer epidermis with a restored functionality. The clinical phenotype of chronic non-healing wounds is mostly associated with problems in keratinocyte migration rather than problems in keratinocyte proliferation or differentiation⁹².

Langerhans cells are antigen-presenting dendritic cells that are localized to the suprabasal region of the epidermis^{93,94}. There is also a substantial number of existing

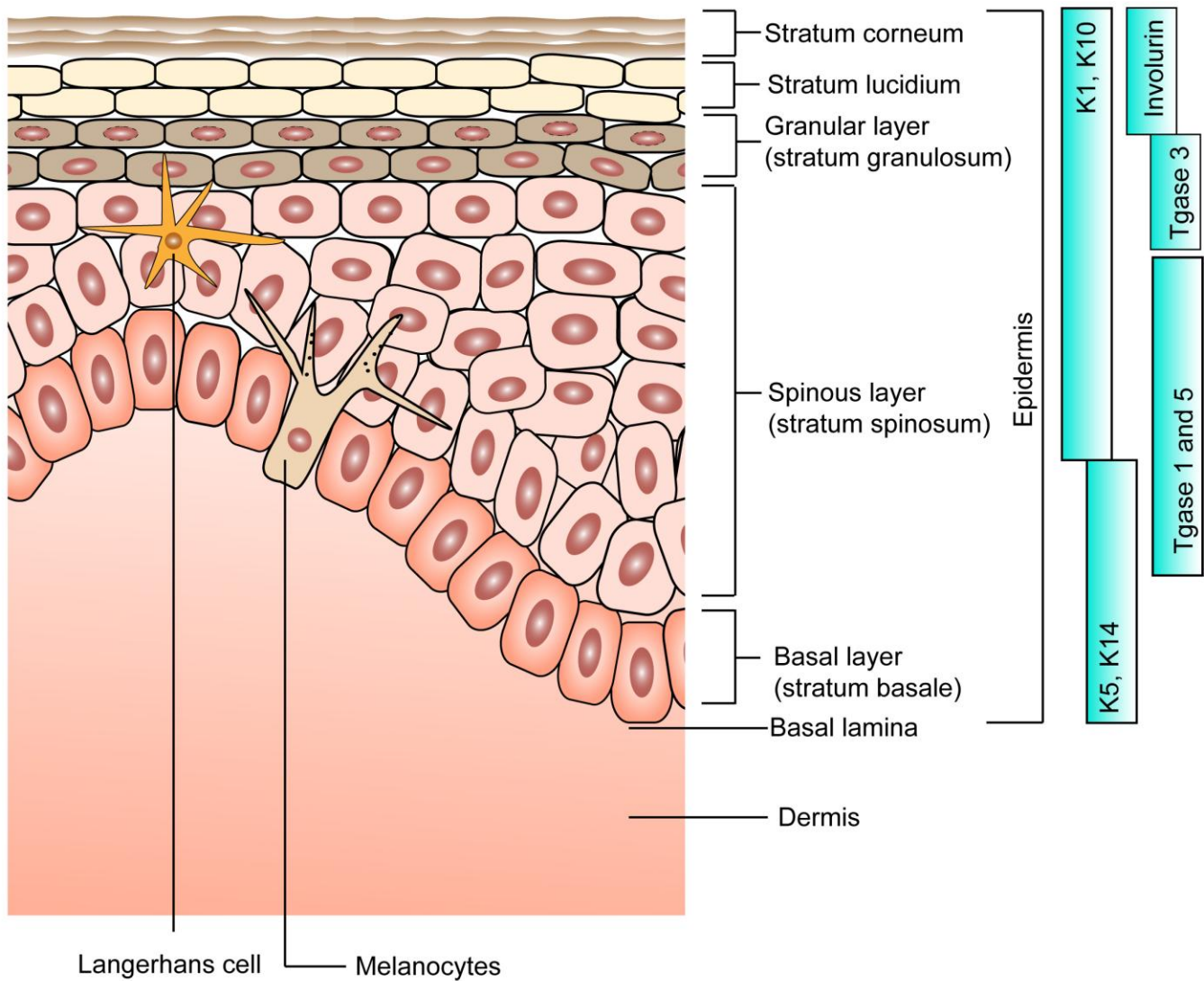


Figure 2. Skin layers

The epidermis is the outermost layer of the skin and is separated from the underlying dermis by the basal lamina. Keratinocytes, which compose the epidermis, proliferate within the basal layer. As differentiation proceeds, keratinocytes progress upwards through the different epidermal layers (the spinous layer, granular layer, stratum lucidum and stratum corneum), becoming anucleated and increasingly compacted in size, before being eventually lost from the skin surface by desquamation. Each stage of epidermal differentiation is characterised by the expression of specific proteins, and examples of these are listed on the right of the figure.

dendritic leukocytes in the dermis. Although some of these leukocytes may represent Langerhans cells on their way into or out of the epidermis, most of these cells are phenotypically slightly different from Langerhans cells and are generally referred as dermal dendritic cells⁹³. These cells populate the epidermis during ontogeny and were originally thought to be constantly replenished by bone-marrow-derived cells^{93,95}. However, it has recently been shown that Langerhans cells are self-renewing⁹³. When Langerhans cells are depleted by irradiation with ultraviolet light, they are replenished from circulating bone-marrow-derived precursors in a CCR2-dependent manner, indicating that a circulating precursor is only utilized when the system is under stress⁹³. Similar observations have been made in the case of human hand-allograft transplantation. At 4.5 years after transplantation, the Langerhans cells were solely of donor origin, supporting the idea that the replacement of Langerhans cells by recipient bone-marrow precursors is rare under steady-state conditions. Whether the CCR2-dependent recruitment of the Langerhans-cell precursor involves the recruitment of an inflammatory monocyte or a lineage-committed precursor is unclear. During skin homeostasis, dendritic cells are sensors and guardians of peripheral tolerance due to their capacity to process self-antigens and signal tolerance to the T-cell pool upon evading the peripheral organs via the lymphatics to reach regional lymph nodes⁹⁵. This functional property constantly assures the quiescence of the immune system in homeostasis⁹⁵. Dendritic cells and tissue macrophages share certain functions, such as particle phagocytosis and danger recognition/signaling upon the recognition of pathogens⁹⁵. Hence, these two cell types are together referred to as the mononuclear phagocyte system. The importance of circulating precursors in the repopulation of

tissue-resident dendritic cell (DC) populations is not fully understood. Furthermore, the nature of the type of precursor, such as a peripheral-blood monocyte or a circulating lineage-committed precursor is still unclear.

Melanocytes originate in neural crest melanoblasts that migrate to different destinations, including the basal layer of the epidermis and the hair follicles. Their migration, proliferation, and differentiation into melanin-producing cells depend on mediators produced by keratinocytes, which bind the c-Kit receptor tyrosine kinase in melanocytes⁹⁶. Melanocytes are surrounded by keratinocytes and are regulated by a paracrine system. This system is responsible for melanin production and distribution through a process called melanogenesis⁹⁶. Melanogenesis is a complex process with multiple stages involving melanocyte-keratinocyte interactions. When disturbed, this interaction may determine different types of pigmentation defects, which are classified as hypo or hyperpigmentation of the skin. This may occur with or without an altered number of melanocytes⁹⁶.

1.2.4 Cells of the Dermis

The dermis is organized into papillary and reticular regions. The distinction between the two zones is based largely on differences in their connective tissue organization, cell density, and neurovascular patterns. The papillary dermis is proximal to the epidermis and follows the epidermal contours⁹⁷. The epidermis and proximal dermis exchange a number of cytokines and growth factors, and matrix components of the dermis are linked to the cytoskeleton of the epidermis through transmembrane receptors⁹⁷. Therefore, it is possible that the organization and composition of the papillary dermis reflects the influence of the epidermis through some soluble and diffusible factors. The

papillary dermis has a high density of fibroblastic cells that proliferate more rapidly, have a higher rate of metabolic activity and synthesize different types of proteoglycans compared with those in the reticular dermis⁹⁷. The reticular dermis is the dominant region of the dermis and constitutes the bulk of the skin. It is woven with large diameter collagen fibrils organized into large fiber bundles⁹⁷. Elastic fibers form a superstructure around the collagen fiber bundles. This fiber organization is integrated to provide the dermis with strong resilient mechanical properties⁹⁷. Dermal fibroblasts, macrophages and endothelial cells are regular residents of the dermis⁹⁷. They are found at a high density in healthy skin within the papillary dermis, but they can also occur in the reticular dermis, where they are found in the interstices between collagen fiber bundles⁹⁷. A small number of lymphocytes can also be found near the blood vessels in normal skin.

Dermal macrophages are heterogeneous and can be grouped into two types: tissue resident macrophages (M2-like) and recruited inflammatory macrophages (M1-like)^{98,99}. The M1-M2 classification of macrophages represents a simplified operational concept to find distinctions within the heterogeneous macrophage populations but has often been over-interpreted as a true functional classification. Tissue resident macrophages are mainly involved in immune surveillance by contributing to the priming of adaptive immunity and tissue homeostasis after skin injury or infection⁹⁴. They can be maintained locally by proliferative self-renewal. Macrophages can persist through all stages of the repair response and can promote a return to homeostasis by the removal of apoptotic cells and cell debris in all repair stages⁹⁴. During the resolution of inflammation, recruited inflammatory macrophages are often greater in number than resident macrophages and are likely to resume the role of apoptotic cell clearance⁹⁹.

However, the distinction of their roles between tissue-resident and recruited inflammatory macrophages in various disease settings remains unknown.

Dermal microvascular endothelial cells play a major role in stabilizing and destabilizing vascular structures by balancing cellular processes such as proliferation, quiescence, apoptosis, and senescence¹⁰⁰. The rate of new blood vessel formation must equal the rate of the loss of old blood vessels to achieve homeostasis¹⁰⁰. During angiogenesis, the proliferation of endothelial cells occurs in an area proximal to the tip of the new vessel. Controlling the rate of angiogenesis is considered a major therapeutic target in pathological diseases such as cancer, acute lung infection and chronic wounds. Many angiogenic and angiostatic factors are believed to influence the level of endothelial proliferation.

Dermal fibroblasts are an essential component of the skin and are critical in the maintenance of skin homeostasis. They not only produce and organize the extracellular matrix of the dermis, but they also communicate with themselves and other cell types to play a crucial role in regulating skin physiology¹⁰¹⁻¹⁰³. Fibroblasts are important in cutaneous wound repair and influence tumor biology through interactions with multiple cells; however, their mechanisms and extensive crosstalk are not yet fully understood. (Refer to section 1.2.5 for more details on dermal fibroblasts).

1.2.5 Dermal Fibroblasts

Dermal fibroblasts are a dynamic and diverse population of cells whose functions in the skin are poorly understood. Their phenotypic differences are demonstrated in a variety of ways, such as through extracellular matrix production and organization, the

production of growth factors/cytokines, and involvement with inflammatory responses¹⁰⁴⁻¹⁰⁸. Normal adult human skin contains at least three distinct populations of fibroblasts, all of which occupy unique niches in the dermis. Two subpopulations of fibroblasts reside in distinct dermal layers: the papillary dermis and the reticular dermis. A third population is associated with hair follicles, which lie in the dermal papilla region of the follicle and along its shaft. These subpopulations exhibit characteristic phenotypic differences¹⁰⁹.

During the proliferation phase of wound healing, multiple cells are recruited to wound sites by the localized release of growth factors/cytokines. Fibroblasts enter the wound site with new sprouting vasculature. Fibroblasts can differentiate into a specialized but transient cell type called the myofibroblast¹¹⁰. Myofibroblasts produce a provisional wound matrix that is enriched in fibronectin and hyaluronan in response to certain factors^{33,111,112}. These cells also provide the motive force to contract the wound. Myofibroblasts disappear from the wound site, apparently by apoptosis, and are replaced by newly recruited fibroblasts that initiate the formation of a collagenous matrix¹¹³. However, their ability to organize this matrix is impaired, resulting in the formation of scar³³. Fetal skin is repaired without scar formation^{114,115}. This is mainly due to the differences in fetal and adult fibroblast phenotypes¹¹⁶. The low production of certain growth factors/cytokine fetal cells, such as TGF- β 1, appears to be a major factor for scarless formation¹¹⁷⁻¹¹⁹. The aberrant fibroblast phenotype also appears to contribute to fibrotic disorders, such as keloid formation and scleroderma^{120,121}. Signals such as TGF- β and connective tissue growth factor play a significant role in the latter process¹⁰⁷.

In tumor progression, stroma cells including fibroblasts, endothelial cells and inflammatory cells can interact with tumor cells by influencing the tumor growth^{122,123}.

This tumor/stroma crosstalk not only modifies and controls angiogenesis, suppressing immune responses in the tumor but also modulates the composition of the extracellular matrix and secreting factors, which in turn, alters cell physiology as well as the cellular composition of the tumor microenvironment^{122,124,125}. Normal fibroblasts or early cancer phase fibroblasts are believed to have certain tumor suppressing activities. However, the phenotype of these fibroblasts can be altered to a tumor promoting state as carcinogenesis progresses. This switch in the fibroblast phenotype occurs in two stages in which a reversible “primed” fibroblasts type is generated first and then followed by the manifestation of irreversible “tumor promoting” fibroblasts¹²³. These “tumor promoting” fibroblasts, or so-called cancer associated fibroblasts (CAFs), have properties distinct from those of normal fibroblasts¹²³. They actively promote tumorigenesis in a variety of cancers. The idea of CAFs is relatively new in the field of tumor biology research. (Refer to this review article “Insidious Changes in Stromal Matrix Fuel Cancer Progression” for more details¹²⁶).

1.2.6 Intercellular communication between fibroblasts and keratinocytes

Regeneration and maintenance of epithelial tissue homeostasis requires a complex interplay with neighbouring cells and extracellular matrix of the adjacent stroma. This is well understood in skin based on data from wound healing, transplantation and cell culture studies, which strongly indicate that epidermal tissue regeneration is regulated by a network of cytokines and growth factors controlling functional behaviour of keratinocytes and dermal fibroblasts¹²⁷⁻¹³⁰. Keratinocytes and fibroblasts engage in paracrine and autocrine interactions in skin^{127,128,131} (Figure 3). It is shown in a

conventional cell culture system where keratinocyte proliferation is strongly enhanced by a feeder layer co-culture with dermal fibroblasts^{132,133}. Accumulating data strongly indicate that this stromal cell support of epithelial cell proliferation is, for the most part, mediated by diffusible factors. Importantly, the support of keratinocyte proliferation is not based on their passive utilization of growth factors constitutively produced by fibroblasts but represents an active interplay between both cell types in a double paracrine mechanism¹³². A series of recent studies have highlighted the importance of stromal factors in the regulation of keratinocyte proliferation and differentiation in health and disease. This led to the identification of stromal factors that regulate keratinocyte proliferation, including keratinocyte growth factor/fibroblast growth factor 7 (KGF/FGF-7). This is a member of the fibroblast growth factor (FGF) family that is exclusively produced by stromal cells. However, only epithelial cells express the KGF receptor and, hence, respond to KGF-1. Fibroblasts also produce other factors that regulate the proliferation of keratinocytes and play roles in wound repair. These include granulocyte-macrophage colony-stimulating factor (GM-CSF), epidermal growth factor (EGF), hepatocyte growth factor/scatter factor (HGF/SF), FGF-10, interleukin-1 (IL-1) and interleukin 6 (IL-6)¹²⁷. Fibroblasts release growth factors/cytokines that play a significant role in wound repair by modulating the activity of keratinocytes. It was first found out that coculture of fibroblasts and keratinocytes results in increased levels of KGF-1, IL-6 and GM-CSF mRNAs¹²⁷. The level of KGF-1 mRNA and the amount of protein released into culture medium by cultured dermal fibroblasts were upregulated by treatment of these cells with IL-1. KGF-1 produced by fibroblasts can in turn enhance the release of IL-1 α by keratinocytes. Thus, a paracrine loop is established between the dermal

fibroblasts and keratinocytes. Soluble factors released by fibroblasts do not possess inductive characteristics with respect to interfollicular keratinocytes. Nonetheless, these factors can modulate specific aspects of epidermal formation. An Abnormal overexpression of KGF-1 can result in a hyperproliferative epidermis and suppression of terminal differentiation of the keratinocytes. By contrast, overexpression of GM-CSF results in increased apoptosis of cultured keratinocytes, and overexpression of KGF-2 could accelerate keratinocyte differentiation. These observations have led to the proposal that the epidermal response to fibroblast-derived signaling molecules depends upon the ratio of these factors. It is believed that the ratio of KGF-1 to GM-CSF presented to epidermal cells determines the status of this tissue. Site-matched papillary and reticular dermal fibroblasts differ significantly in the release of KGF-1 and GM-CSF where the ratio of GM-CSF to KGF-1 is higher in papillary fibroblasts than in corresponding reticular cells. Thus, these two populations of cells exert subtle differences on epidermal proliferation and differentiation. Communication between fibroblasts and keratinocytes appears to involve AP-1 target genes in dermal fibroblasts¹³³. Fibroblasts from Jun-knockout mouse were found to produce very low levels of KGF-1 and GM-CSF, whereas fibroblasts from JunB^{-/-} knockout mouse produced elevated levels of these factors¹³³. Incorporation of these fibroblasts into bi-layered skin equivalents with normal adult human keratinocytes for the epidermal layer led to strikingly different results. Epidermal layers on skin equivalents containing Jun^{-/-} fibroblasts were atrophic, basal cell proliferation was reduced, and terminal differentiation was delayed. JunB^{-/-} fibroblasts caused epidermal hyperplasia. IL-1 and other inflammatory factors, such as tumor necrosis factor (TNF)- α , activate AP-1-

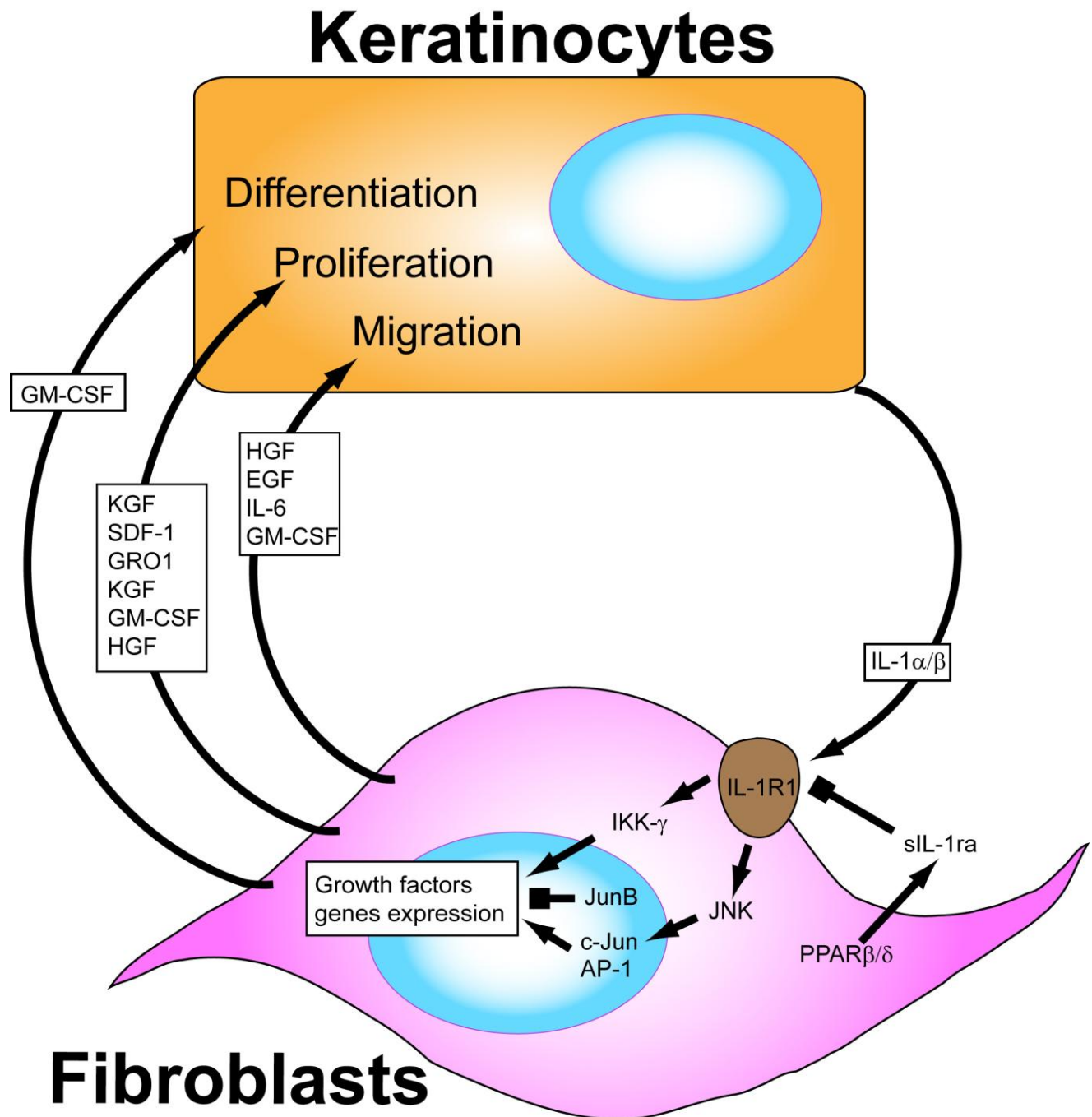


Figure 3. Schematic illustration of keratinocyte-fibroblast cross-talk

Keratinocyte-derived IL-1 α/β stimulates expression and secretion of multiple growth factors in fibroblasts through the c-Jun/AP-1 and JunB transcription factors. Growth factors such as HGF, KGF and GM-CSF are then released by fibroblasts and stimulate keratinocyte proliferation, migration and differentiation in a paracrine manner. sIL-1ra, a target protein of PPAR β/δ from fibroblast can modulate keratinocyte derived IL-1 signaling on stimulates multiple growth factors expression in fibroblasts.

mediated transcription and enhance the activity of NF- κ B¹³⁴. Differences in the phenotypes of fibroblasts in skin might be related to how these cells respond to external signals and modulate the diverse group of genes regulated by AP-1 transcription factors¹³⁵. Obviously, these signaling molecules are only part of a more complex regulatory mechanism of epithelial-stromal interactions controlling tissue regeneration and homeostasis. Recently, a group of transcriptional factors/ nuclear hormone receptor, called peroxisome proliferator-activated receptors (PPARs) have also been shown to be involved in epidermal skin hemostasis and wound repair^{136,137}. Furthermore, they stimulate keratinocyte migration and differentiation and promote keratinocyte survival¹³⁷⁻¹³⁹. Upon injury, a cascade of inflammatory signals produced from other cells can target the AP-1 site in the PPAR beta/delta promoter in the keratinocytes resulting in increased survival¹³⁷. This transcriptional regulation of epithelial-stromal communication during wound repair is less studied and a better model system to study this interaction is needed. Thus, for studying in detail the complex basic mechanisms of epidermal-dermal cell interactions, a standardized and reproducible in vitro skin equivalent model would be advantageous. In this thesis, the creation of a standardized skin equivalent model system also known as organotypic culture (OTC) will be introduced. This model is useful for the study of epithelial-stromal interaction which supports keratinocyte growth and differentiation as well as growth of fibroblasts to produce multiple growth factors and extracellular matrices.

1.2.7 Peroxisome proliferator-activated receptors (PPARs) in the skin

The PPARs belong to a subfamily of nuclear hormone receptors comprised of three different isoforms: PPAR α , PPAR β/δ and PPAR γ ¹⁴⁰. These subtypes are encoded by separate genes, exhibit different tissue distributions and functions and, to some extent, different ligand specificities¹⁴⁰. After ligand binding, PPARs regulate gene expression by binding to peroxisome proliferator response elements (PPRE) in target genes as heterodimers with the retinoid X receptors (RXR)¹⁴⁰. PPAR activation has been shown to play an important role in the regulation of energy homeostasis, modulating glucose and lipid metabolism and transport¹⁴⁰. Moreover, recent studies have demonstrated that PPARs regulate important cellular functions in the skin and other organs, including inflammation, immune responses, cell proliferation, cell differentiation and apoptosis¹⁴¹. All three PPARs contribute to epidermis homeostasis in both rodents and humans. PPAR β , which is the most abundantly expressed isotype, and PPAR α both participate in keratinocyte differentiation and contribute to skin repair after injury^{136,137}. The contribution of PPAR γ is less well understood, although it appears to be important for epidermal functions.

PPAR β expression is strongly reactivated in keratinocytes at the edges of wounds, and its activation is maintained during the entire repair process. The expression of PPAR β is increased following the activation of the stress-associated protein kinase pathway in response to inflammatory cytokines, such as TNF- α , that are released after an injury¹⁴². In addition to the stimulation of PPAR β expression, the inflammatory response also induces the production of endogenous ligands, which are required for PPAR β activation in keratinocytes. After its maximal expression during the inflammatory phase, PPAR β

expression is progressively reduced in the healing epithelium, finally reaching levels observed in the unwounded skin¹⁴². The mechanism of this downregulation is controlled by TGF β -1, which inhibits the binding of AP-1 to the PPAR β promoter¹⁴². In genetically impaired PPAR β -null mice, wound repair is delayed, demonstrating that PPAR β is an important transcriptional regulator in the wounded epidermis¹⁴². PPAR β promotes keratinocyte survival at the wound edges via the activation of the PI3K/PKB α /Akt1 pathway and regulates keratinocyte adhesion and migration, two key processes that occur during re-epithelialization¹³⁹. Keratinocyte proliferation during wound healing is also fine-tuned by a PPAR β -dependent interaction between epidermal keratinocytes and dermal fibroblasts¹⁴². Interleukin-1 (IL-1) is produced by keratinocytes and stimulates the activity of the AP-1 (Jun/Fos) transcription complex in dermal fibroblasts, resulting in an increased production of mitogenic cytokines that enhance keratinocyte proliferation. In parallel, the work presented here highlights a novel paracrine effect of PPAR β/δ in fibroblasts on epithelial cell growth; the expression of PPAR β/δ in the fibroblasts stimulates the production of secreted IL-1 receptor antagonist (sIL-1ra), which results in the autocrine downregulation of the IL-1 signaling pathway. As a consequence, there is a reduced production of secreted mitogenic factors by the IL-1-stimulated fibroblasts, which contributes to the homeostatic control of keratinocyte proliferation.

1.2.8 Biological role of the Interleukin 1 receptor antagonist in skin

The interleukin 1 receptor antagonist (IL1Ra) family of molecules now includes one secreted isoform (sIL1ra) and three intracellular isoforms (icIL1ra1, 2, and 3). Extensive

evidence suggests that the sole biological function of sIL1ra is to competitively inhibit the binding of IL1 to cell-surface receptors. Although intracellular IL1Ra1 may be released from keratinocytes under some conditions, the intracellular isoforms of IL1Ra may perform additional intracellular roles.

The IL1Ra gene (IL1RN) is found on the long arm of human chromosome 2 at band 2q14, adjacent to the IL1 α and IL1 β genes¹⁴³⁻¹⁴⁵. The first described intracellular isoform of IL1Ra (icIL1ra1) is created by an alternative transcriptional splice of an upstream exon into the amino terminus of sIL1ra, creating an 18 kDa protein that lacks a signal peptide¹⁴⁶. IcIL1ra1 is a major protein in keratinocytes and other epithelial cells, and it is also produced with delayed kinetics by monocytes and macrophages. The cDNA for a second intracellular isoform of IL1Ra (icIL1Ra2) was cloned from human neutrophils and contained a 63-bp sequence inserted between the first and second exons for icIL1ra1^{147,148}. This cDNA was present in fibroblasts, keratinocytes, and human myelomonocytic cells, although the predicted 25-kDa protein has not yet been described as a natural product in any cell. Thus, it remains unknown whether icIL1Ra2 exists as a protein in vivo. A third intracellular isoform of IL1Ra (icIL1Ra3) was recently described as a 16-kDa product, predominately of sIL1ra mRNA, that is created by alternative translational initiation^{149,150}. IcIL1Ra3 is a major protein in hepatocytes and neutrophils. It is also present in smaller amounts in monocytes, macrophages, and keratinocytes. The major function of sIL1ra is to regulate the pleiotropic effects of IL1 by competitively blocking its binding to cell surface receptors¹⁵¹. Thus, sIL1ra functions as a major naturally occurring anti-inflammatory protein; when the balance between IL1 and IL1Ra is upset, inflammatory disease and tissue damage may ensue. The

administration of recombinant human sIL1ra has been effective in preventing the onset of disease or in ameliorating established inflammatory diseases. The biological effects of the intracellular isoforms of IL1ra have been less thoroughly investigated. icIL1ra1 and icIL1Ra2 bind to IL1RI as well as sIL1ra and inhibit the stimulatory effects of IL1. In contrast, icIL1ra3, which predominates in neutrophils and hepatocytes, is only a weak inhibitor of IL1 receptor binding¹⁴⁹. Keratinocytes may express on their plasma membrane and release icIL1ra1 from that location¹⁵². Although keratinocytes possess small amounts of active IL1RI, biologically inactive IL1RII predominates on these cells, particularly after activation. IL1RII is cleaved from expressing cells, avidly binds IL1 β , and functions in the cell microenvironment as an IL1 inhibitor¹⁵³. Thus, although keratinocytes are capable of releasing small amounts of icIL1ra1, the functional importance of this cytokine as an extracellular receptor blocker in the skin remains unclear.

Here, we provide evidence for a novel paracrine effect of PPAR β/δ on epithelial cell growth. We find that fibroblast PPAR β/δ attenuates keratinocyte proliferation by directly increasing the expression of sIL-1ra, thereby repressing IL-1 signaling. Epithelial-mesenchymal communications and IL-1 signaling are responsible for a wide range of biological events, such as epidermis homeostasis, wound repair and tumorigenesis. Our results underscore the paracrine role of PPAR β/δ in the control of cell proliferation involving epithelial-mesenchymal interactions.

1.3 MATERIALS AND METHODS

1.3.1 Reagents

Antibodies and suppliers: anti-Ki67, anti-keratin 10, anti-involucrin, anti-keratin 5, anti-transglutaminase, anti-cyclin D1, anti-PCNA (Novacastra); anti- β -tubulin (Santa Cruz); anti-PPAR α , β/δ and γ (Chemicon and Affinity BioReagent); Cytokines: IL-1 α , TNF α and neutralizing antibodies against IL-1 α , β , KGF, IL-6 and GM-CSF (PeproTech), anti-caspase 3, anti-c-JUN, anti-phospho(Ser63)-c-JUN, anti-TAK1 and anti-phospho-TAK1 (Cell Signaling); Alexa488-conjugated goat anti-mouse antibody, Alexa488-conjugated goat anti-rabbit antibody and ProLong[®] Gold anti-fade reagent with DAPI (Molecular Probes). Real-time reagent SYBR GreenER (Invitrogen). Rat tail collagen type I (BD Biosciences). Transfection reagent Superfect (Qiagen). All restriction enzymes and DNA/RNA modifying enzymes (Fermentas). Double-promoter lentivirus-based siRNA vector and pFIV Packaging kit (System Biosciences). The PPAR α , β/δ and γ Complete Transcription Factor Assay Kit was from Cayman Chemical. Primary neonatal human fibroblasts and keratinocytes were obtained from Cascade Biologics. GW501516 was from Alexis Biochemicals. Otherwise, chemicals were from Sigma-Aldrich.

1.3.2 Total RNA isolation, Reverse transcription PCR and qPCR

Total RNA was extracted from fresh tissues using Aurum total RNA kit (Bio-Rad) following the supplier's protocol. Five μ g of total RNA was reverse-transcribed with oligo-dT primers using RevertAid[™] H Minus M-MuLV. After reverse transcription, the RNAs were removed by RNase H digestion. Quantitative real-time PCR (qPCR) was performed with platinum Taq polymerase and SYBR greener supermixes using a

MiniOpticon PCR machine (Bio-Rad). Melt curve analysis was included to assure that only one PCR product was formed. Primers were designed to generate a PCR amplification product of 100 to 250 bp. Only primer pairs yielding unique amplification products without primer dimer formation were subsequently used for real-time PCR assays. Expression was related to the control gene ribosomal protein P0 (RPLP0), which did not change under any of the experimental conditions studied. The sequence of primers is available in Table 1. For each wound biopsies, ten 8 µm-thick tissues were microdissected and pooled. RNA was isolated from microdissected paraformaldehyde-fixed, paraffin embedded sections (FFPE) using RecoverAll™ total nucleic acid isolation kit for paraformaldehyde-fixed, paraffin-embedded tissues (Ambion). Five ng of RNA was subjected to Full Spectrum™ Complete Transcriptome RNA Amplification (System Biosciences) prior qPCR.

1.3.3 Lentivirus-mediated knockdown of PPARβ/δ and siL-1ra

Two siRNAs targeting the human PPARβ/δ, one against siL-1ra and one unrelated control siRNA were subcloned into the lentiviral-based siRNA vector pFIV-H1/U6-puro (System Biosciences). The correct pFIV siRNA constructs were verified by sequencing using H1 primer. The sequence of the siRNAs was as given in Table S1. Transduction-ready pseudoviral particles were produced and harvested as described by manufacturer. Transduced cells were enriched by puromycin selection for 1 week. Western blot analysis, ELISA or qPCR were used to assess the efficiency of knockdown.

1.3.4 Transactivation assay

A ~4.4 kb (-1572 to -5980) promoter of the human sIL-1ra was PCR amplified from human genomic DNA using Pfu polymerase. The primer pairs used is given in Table S1. The resulting fragment was used for a second PCR amplification step introducing SacI and BglII sites which were used for subcloning into the pGL-3 Basic vector (Promega). Site-directed mutagenesis of the 3 putative PPREs (PPRE1 at -1038/-1050, PPRE2 at -1072/-1084, PPRE3 at -4067/-4079) were achieved using QuikChange site-directed mutagenesis kit (Stratagene). Human fibroblasts were routinely grown in Medium 106 (Cascade Biologics). Fibroblasts in culture were cotransfected with a luciferase reporter driven by the various sIL-1ra promoter constructs and pEF1- β -galactosidase as a control of transfection efficiency using Superfect. After transfection, cells were incubated in the presence or absence of 500 nM of PPAR β/δ ligand GW501516 and IL-1 α for 24 h prior to lysis. Transfections with the positive control reporter pGL-3xPPRE-tk-Luc were included. Luciferase activity was measured using the Promega luciferase assay on a Microbeta Trilux (Perkin Elmer). β -galactosidase activity was measured in the cell lysate by a standard assay using 2-nitrophenyl- β D-galactopyranoside as a substrate.

1.3.5 Chromatin immune-precipitation (ChIP)

Chromatin immunoprecipitation was performed as described previously (Tan et al., 2004) with minor modifications. Briefly, epidermis from OTC was physically separated from the collagen-embedded human fibroblasts, following of Dispase treatment (2.5 U/ml) at 37 °C for 20 min. The dermal equivalents were thoroughly washed with PBS. The collagen gel was cut into small pieces prior digestion with 0.5 % collagenase I at 37

°C. The fibroblasts were retrieved and crosslinked with 1 % formaldehyde for 15 min at 37 °C prior sonication in lysis buffer. Monoclonal anti-PPAR β/δ antibody was used. The immunoprecipitates were reverse crosslinked for PCR by heating at 65 °C for 6 h. The primer pairs used were given in Table 1.

1.3.6 Organotypic tissue culture (OTC)

Primary human keratinocytes and fibroblasts were routinely maintained in EpiLife® Defined Keratinocyte Medium and Medium 106, respectively, as described by the manufacturer (Invitrogen). Organotypic skin cultures were performed as previously described¹³³ in serum-free OTC medium with some modifications. One volume of 10x Hanks' balanced salt solution (HBSS) containing phenol red was mixed with 8 volumes of 4 mg/ml rat tail type I collagen (BD Biosciences). The acetic acid was neutralized with 1N NaOH on ice. Fibroblasts were resuspended in one volume of 1x HBSS and added drop wise to the neutralized collagen to achieve a final fibroblast density of 1×10^5 cells/ml of collagen. Three ml of this fibroblast/collagen mixture was dispensed into a 24 mm diameter Transwell culture insert (3 μ m pore size, BD Biosciences). The culture insert was placed in a 6-well Deep-Well Plate (BD Biosciences) and was allowed to gel in a 37 °C, 5% CO₂, 70% humidity incubator (ThermoFisher). Glass rings (outer diameter, 20 mm; thickness, 1.2 mm and height, 12 mm) was centrally placed on to the collagen. This glass rings serves to compress the collagen and delimit the area for the seeding of keratinocytes. The fibroblast-embedded collagen was submerged and cultured in serum-free OTC medium overnight. The serum-free OTC contains basal medium: 3: 1 (v/v) of DMEM (low glucose):Ham's F-12 nutrient mixture; basal

supplements: 5 µg/ml insulin, 1 ng/ml epidermal growth factor, 0.4 µg/ml hydrocortisone, 100 nM adenine, 10 µM serine, 100 nM cholera toxin, 10 µM carnitine, 1 mg/ml fatty-acid free albumin; lipid supplements: 0.05 mM ethanolamine, 1 µM isoproterenol, 1 µM α-tocopherol and 50 µg/ml ascorbic acid. The following day, the medium was removed and 1×10^6 keratinocytes were seeded into the center of the glass ring. OTC medium was added to air-liquid interface and the setup was once again incubated at 37 °C with 5% CO₂ for 24 h to allow the keratinocytes to attach. The next day, the glass ring was removed and culture was maintained at air-liquid interface. Medium was changed every 3 days for a total of 2-weeks. Neutralizing antibodies (each at 400 ng/ml) were freshly supplemented at every change of medium throughout the 2-weeks culture period.

1.3.7 Immunofluorescence

Organotypic skin cultures were fixed with 2% paraformaldehyde in PBS for 2 h at 25 °C. The fixed OTCs were washed twice with PBS and embedded in Tissue-Tek OCT compound medium (Sakura) overnight at 4 °C. The skin cultures were subsequently frozen at -70 °C for cryosectioning. Ten µm cryostat tissue sections were mounted on SuperFrost Plus slides. The sections were processed for immunofluorescence as described previously¹³⁶ except that Alexa488-conjugated goat anti-mouse secondary antibody was used. The apoptotic keratinocytes were detected using the TUNEL assay according to the manufacturer's protocol (Roche). As positive control for TUNEL assay, the section was pre-treated with DNase I. The slides were mounted with ProLong® Gold anti-fade reagent with DAPI. Images were taken with Nikon inverted microscope

ECLIPSE TE2000-U using a Plan Fluor 20x/0.45 objective, QImaging Retiga-EXi FAST Cooled Mono 12-bit camera, and Image-Pro[®] Plus software.

1.3.8 Wounding experiment

Wounding of the mice dorsal skin was performed as previously described¹³⁶. Wound biopsies and fluids were isolated as previously described¹⁵⁴ and were immediately snap-frozen in liquid nitrogen for further analysis. Topical application of exogenous IL-1ra treatment was performed as previously described¹⁵⁵ except that 3 applications of 2.5 µg of recombinant IL-1ra were added over 3 days.

1.3.9 Measurement of cytokines by Enzyme-linked immunosorbent assay (ELISA)

The concentration of sIL-1ra and icIL-1ra measured using sandwich ELISA (R&D System). Briefly, 2×10^5 cells were cultured in a 35 mm culture dish with 750 µl of medium and subjected to the indicated treatments. After 24 h, the media were harvested and treated with by addition of complete protease inhibitors (Roche). The level of sIL-1ra was measured in culture supernatants accordingly to the manufacturer's instruction. To measure icIL-1ra, the cells were washed thoroughly, harvested by treatment with trypsin and collected by centrifugation in fresh serum-free culture medium. The cell pellet was resuspended in 750 µl of medium, disrupted by sonication and the debris was removed by centrifugation. The concentration of icIL-ra in the supernatant was measured as above.

1.3.10 Protein arrays

Human Inflammation antibody array 3 and Growth Factor antibody array membranes were processed according to the manufacturer's protocol (RayBiotech). Protein spots were detected by chemiluminescence. Signal intensities were quantified using ImageJ analysis software and were normalized with the mean intensity of the positive controls on each membrane.

1.3.11 Western blot analysis

Epidermis was physically separated from OTC after a 20 min treatment with Dispase. Fibroblasts embedded in collagen were isolated after collagenase treatment. For western blot, protein extracts were made in ice-cold lysis buffer (20 mM Na₂H₂PO₄, 250 mM NaCl, 1% Triton-100, 0.1% SDS). Equal amount of protein extracts (50 µg) were resolved by SDS-PAGE and electrotransferred onto PVDF membranes. Membranes were processed as described by the manufacturer of antibodies and proteins were detected by chemiluminescence (Millipore). Coomassie blue-stained membrane or tubulin was used to check for equal loading and transfer.

1.3.12 Statistical analysis

Statistical analyses were performed using two-tailed Mann-Whitney tests or two-way ANOVA using SPSS v.19 software (IBM Corporation, USA). Values are expressed as mean ± SEM. A P value of <0.05 was considered statistically significant.

Table 1: Sequence of primers

Real-time quantitative PCR	Sequence
Human	
PPAR α (forward)	5'-ATGTCACACAACGCGATTC-3'
PPAR α (reverse)	5'-TCTTGGCCAGAGATTTGAGA-3'
PPAR δ (forward)	5'-AGGAGCCATTCTGTGTGTGA-3'
PPAR δ (reverse)	5'-TCCTGCCAGCAGAGAGTGAT-3'
PPAR γ (forward)	5'-AATGTGAAGCCCATTGAAGA-3'
PPAR γ (reverse)	5'-TGCAGTAGCTGCACGTGTTT-3'
siL-1ra (forward)	5'-CCGCAGTCACCTAATCACTCTCCT-3'
siL-1ra (reverse)	5'-CTCAGATAGAAGGTCTTCTGG-3'
icL-1ra (forward)	5'-GAAGACCTCAGAAGACCTCCTGTCC-3'
icL-1ra (reverse)	: 5'-CTCAGATAGAAGGTCTTCTGG-3'
RPLP0 (forward)	5'-AACTCTGCATTCTCGCTTCC-3'
RPLP0 (reverse)	5'-TCGTTTGTACCCGTTGATGA-3'
KGF (forward)	5'-CATGACTCCAGAGCAAATGGC-3'
KGF (reverse)	5'-TCCTCAGGTACCACTGTGTTTCG-3'
GMCSF (forward)	5'-AGCAGCACTGCCCTCCAAC-3'
GMCSF (reverse)	5'-CAGCAGTCAAAGGGGATGAC-3'
IL-6 (forward)	5'-CCCACACAGACAGCCACTCA-3'
IL-6 (reverse)	5'-CCAGTGCCTCTTTGCTGCTT-3'
IL-8 (forward)	5'-GAACCTAGATGTCAGTGCAT-3'
IL-8 (reverse)	5'-CCAGACAGAGCTCTCTTCCATC-3'
IL-1 β (forward)	5'-CTGTACCTGTCCTGCGTGTT-3'
IL-1 β (reverse)	5'-GTGCTGATGTACCAGTTGGG-3'
IL-1 α (forward)	5'-CAGTGCTGCTGAAGGAGATG-3'
IL-1 α (reverse)	5'-AGTTTGGATGGGCAACTGAT-3'
IL-1R1 (forward)	5'-GGTGGTTCATCTGAAGAGCA-3'
IL-1R1 (reverse)	5'-ACTGTGGTCCCTGTGTAAAGTC-3'
IL-1RII (forward)	5'-CCACGCCAGGAATATTCAGA-3'
IL-1RII (reverse)	5'-CCTTGACTGTGGTGCGTAGT-3'
Mouse	
siL-1ra (forward)	5'-GCTCATTGCTGGGTACTTACAA-3'
siL-1ra (reverse)	5'-CCAGACTTGGCACAAGACAGG-3'
icL-1ra (forward)	5'-CAGTTCCACCCTGGGAAGGT-3'
icL-1ra (reverse)	5'-AGCCATGGGTGAGCTAAACAGGACA-3'
GMCSF (forward)	5'-TCGTCTCTAACGAGTTCTCCTT-3'
GMCSF (reverse)	5'-GCAGTATGTCTGGTAGTAGCTGG-3'
IL-6 (forward)	5'-TAGTCCTTCCACCCCAATTTCC-3'
IL-6 (reverse)	5'-TTGGTCCTTAGCCACTCCTTC-3'
KC (forward)	5'-CTGGGATTCACCTCAAGAACATC-3'
KC (reverse)	5'-CAGGGTCAAGGCAAGCCTC-3'
IL-10 (forward)	5'-GCTCTTACTGACTGGCATGAG-3'
IL-10 (reverse)	5'-CGCAGCTCTAGGAGCATGTG-3'
IL-16 (forward)	5'-AAGAGCCGGAAATCCACGAAA-3'
IL-16 (reverse)	5'-GTCTCAAAAGGGTCAGGGTACT-3'
siRNA primers	

PPARβ/δ11 (sense)		5'-AAAGGGAAGCAGTTGGTGAATGG-3'
PPARβ/δ11 (antisense)		5'-AAAACCATTCACCAACTGCTTCC-3'
PPARβ/δ9 (sense)		5'-AAAGGAGCGCAGCTGCAAGATTC-3'
PPARβ/δ9 (antisense)		5'-AAAAGAATCTTGCAGCTGCGCTC-3'
control (sense)		5'-AAAGCTGTCTTCAAGCTTGATATCGAAGACTA-3'
control (antisense)		5'-AAAATAGTCTTCGATATCAAGCTTGAAGACAG-3'
slL-1ra (sense)		5'-AAAGATCACTCTCCTCCTCTTCCTG-3'
slL-1ra (antisense)		5'-AAAACAGGAAGAGGAGGAGAGTGAT-3'
H1 sequencing primer		5'-CTGGGAAATCACCATAAACGTGAA-3'
<hr/> Promoter primers		
hsL-1ra (forward)	promoter	5'-GACCAACTCTCCTGCTGAGAATAACTAG-3'
hsL-1ra promoter (reverse)		5'-CTGCCATTGCGGGCCCAGAGTTGTGG-3'
<hr/> chIP primers		
PPRE1 (forward)		5'- AGCCCGGGGCTGGAGGTCAGAAGACCT -3'
PPRE2 (reverse):		5'- AACCTCTGCCACTTGCCTTGTGCCACC-3'
PPRE3 (forward):		5'-TTTACTCCTGGGGACATGTGCTGGTTTC-3'
PPRE3 (reverse):		5'-GGCTGCCCCTGATTCAAATCCATGATT-3'
control (forward):	sequence	5'-GGCTGGGAGTGCAGGGCAGGAGC-3'
control (reverse):	sequence	5'-CACACAATGTGCAGAGCCTGTCTT-3'

1.4 RESULTS

1.4.1 PPAR β/δ knockdown in dermal fibroblasts results in increased keratinocytes proliferation

Earlier studies have shown that ligand-activated PPAR β/δ stimulated the differentiation of human keratinocytes in monolayer cultures¹⁵⁶. In this study, the autocrine and paracrine consequences of PPAR β/δ deficiency during human epidermis formation using the organotypic skin culture (OTC) model were examined. In this skin reconstruction assay, keratinocytes were cultured on a collagen matrix containing dermal fibroblasts. In line with the above-mentioned objective, the expression pattern of the three PPAR isotypes in fibroblasts and keratinocytes of control OTC was first examined. Both qPCR and ELISA analyses performed on mechanically separated dermis and epidermis equivalents of OTCs revealed that PPAR β/δ is the predominant isotype in both the keratinocytes and dermal fibroblasts, whereas the lower levels of PPAR α and PPAR γ are comparable (Fig. 4A). We next assessed the knockdown efficiency of PPAR β/δ expression in human keratinocytes and fibroblasts by lentivirus-mediated siRNAs using qPCR and immunoblot analyses. qPCR revealed a >95% reduction of PPAR β/δ expression in cells transduced with the siRNA PPAR β/δ 11 sequence (Fig. 1B, left panel). Consistent with this result, immunoblot analysis showed negligible levels of PPAR β/δ protein in the transduced cells (Fig. 4B, right panel). These cells were used for subsequent experiments.

Next, OTCs were reconstructed using control and PPAR β/δ -knockdown keratinocytes (K_{CTRL} vs $K_{PPAR\beta/\delta}$) and fibroblasts (F_{CTRL} vs $F_{PPAR\beta/\delta}$) in various combinations. Immunoblot analysis and immunofluorescence staining of the 2-week old

control K_{CTRL}/F_{CTRL} OTCs with unmanipulated levels of PPAR β/δ displayed the expected keratinocyte differentiation markers, keratin 5, 10 and involucrin (Fig. 5A & 5B). OTCs with $K_{PPAR\beta/\delta}$ showed a reduced expression of terminal markers, consistent with the known pro-differentiation role of PPAR β/δ (Fig. 5A & 5B)¹³⁸. No difference in keratin 5 expression, localized to the basal layer of the epidermis, was observed among the various OTCs (Fig. 5A & 5B). This provided evidence for a cell-autonomous action of PPAR β/δ in keratinocyte differentiation. Interestingly, OTC with $F_{PPAR\beta/\delta}$ led to increased keratinocyte proliferation as evidenced by an increase in cyclin D1, PCNA expressions (Fig. 6B) and Ki67-positive cells with respect to the control OTC (Fig. 6A). Notably, the $K_{PPAR\beta/\delta}/F_{PPAR\beta/\delta}$ OTC similarly displayed this enhanced proliferation of keratinocytes, regardless of the impaired differentiation of the $K_{PPAR\beta/\delta}$ (Fig. 5A & 5B). Furthermore, OTC with $K_{PPAR\beta/\delta}$ showed 3-fold more apoptotic cells (TUNEL-positive) and higher level of cleaved caspase 3 as compared to OTC with K_{CTRL} (Fig. 6A & 6B). A dynamic epithelial-mesenchymal interaction is essential for the proper formation of the basement membrane¹⁵⁷. The reduced laminin 5 staining in OTCs with either $K_{PPAR\beta/\delta}$ or $F_{PPAR\beta/\delta}$ suggested a dysregulated epithelial-mesenchymal communication (Fig. 5B). Altogether, these results are consistent with the observations from PPAR β/δ -null mice^{137,158}, and revealed a potent proliferation stimulatory effect of $F_{PPAR\beta/\delta}$ on co-cultured keratinocytes, providing evidence for an important non-cell autonomous PPAR β/δ -dependent mechanism regulating keratinocyte proliferation.

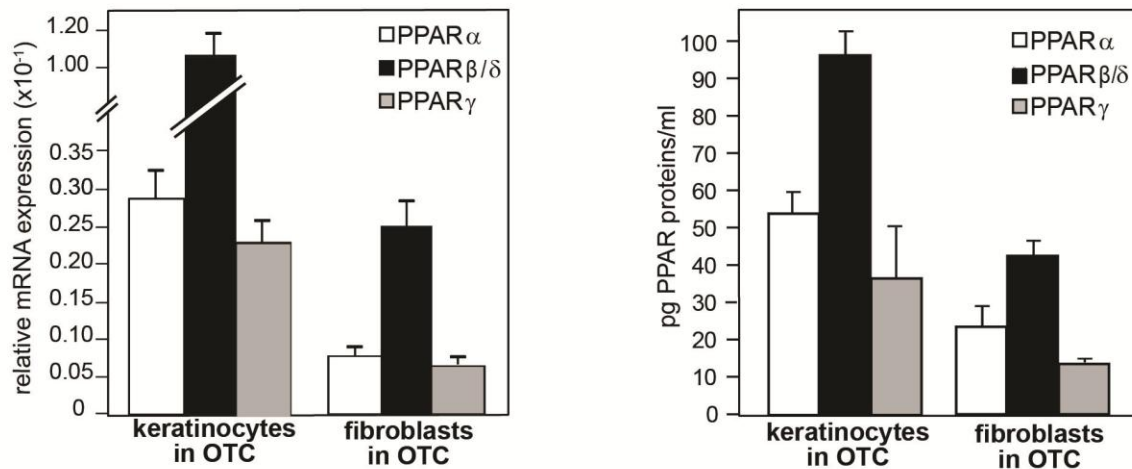
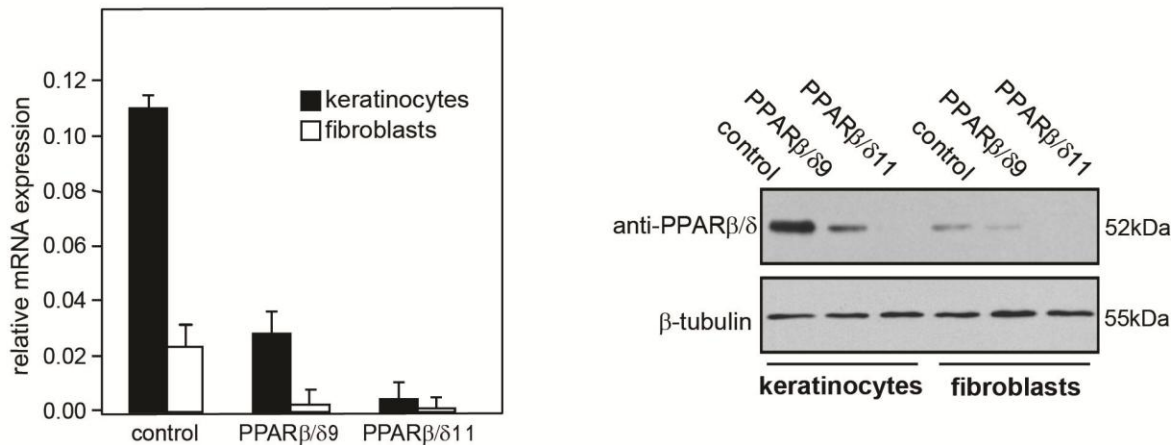
A**B**

Figure 4 Increased PPAR β/δ expression in both keratinocytes and fibroblasts.

(A) Expression profile of PPARs in OTC keratinocytes and fibroblasts. Total RNA and protein were extracted from keratinocytes and fibroblasts in OTC. Expression levels of PPAR mRNA (*left*) and protein (*right*) were monitored by qPCR and PPAR transcription factor assay kit, respectively. PPAR β/δ mRNA was normalized with control ribosomal protein P0 mRNA. **(B)** Human keratinocytes or fibroblasts were transduced with a lentiviral vector harbouring a control or two different PPAR β/δ (PPAR $\beta/\delta 9$ and PPAR $\beta/\delta 11$) siRNAs.

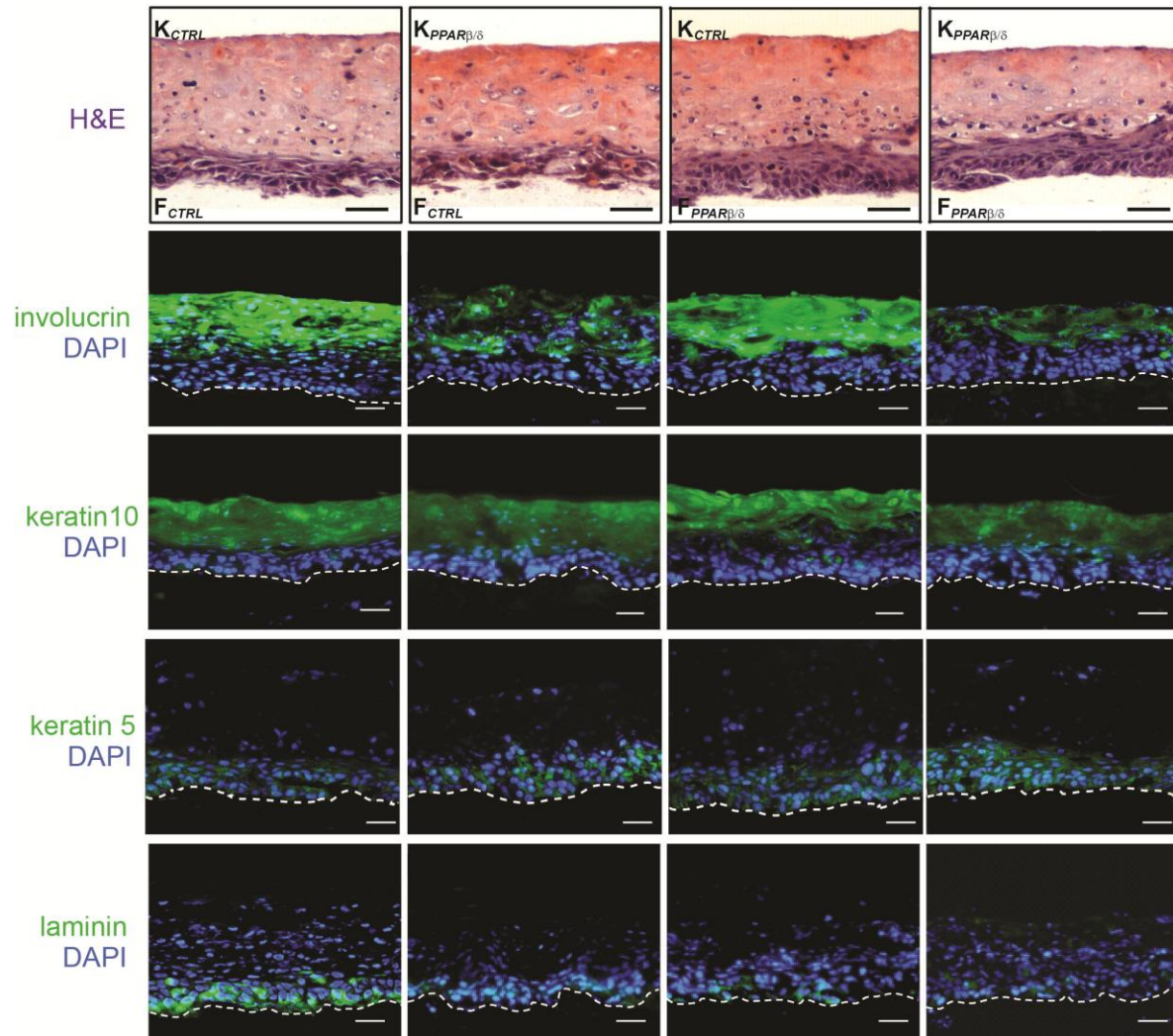
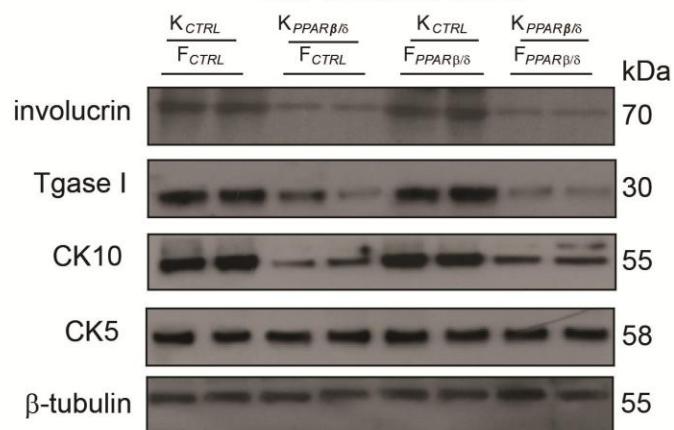
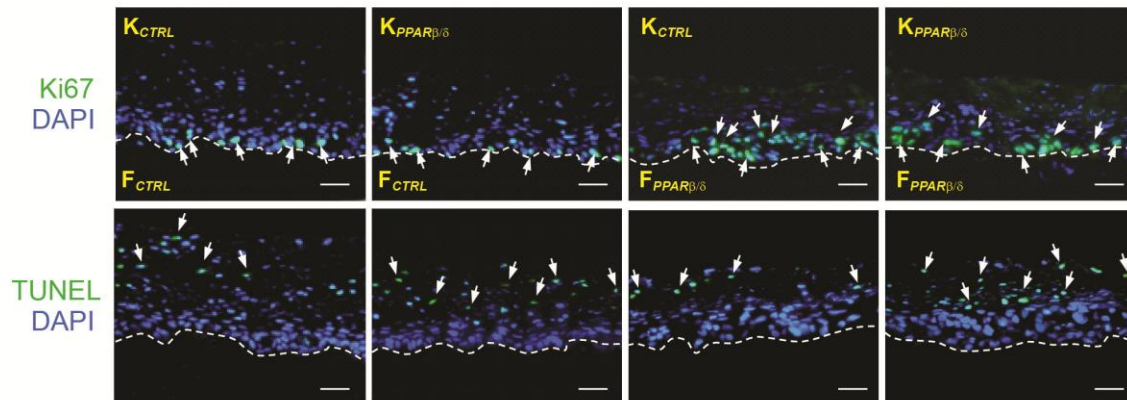
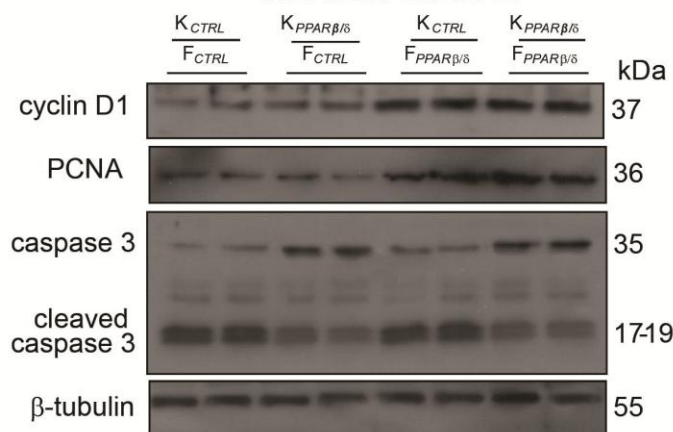
A**Two-week old organotypic skin cultures****B****Two-week old OTCs**

Figure 5. $K_{PPAR\beta/\delta}$ reduced the expression of terminal differentiation markers

(A) Immunofluorescence staining of two-week old organotypic skin cultures. Organotypic skin cultures (OTC) constructed with control or $PPAR\beta/\delta$ -knockdown keratinocytes (K_{CTRL} vs $K_{PPAR\beta/\delta}$) and fibroblasts (F_{CTRL} vs $F_{PPAR\beta/\delta}$). Pictures from representative immunostained sections are shown. H&E: Hematoxylin and eosin staining; Bar: 40 μ m. Involucrin, terminal differentiation marker; keratin 10, intermediate differentiation marker; keratin 5, early differentiation marker; laminin, Basal lamina membrane (green) and DAPI (blue): nuclear staining. Dotted white lines show the epidermal-dermal junction. Bar: 20 μ m. **(B)** Immunoblot analysis of epidermis from 2-week old OTCs constructed using control- or $PPAR\beta/\delta$ -knockdown human keratinocytes (K_{CTRL} vs $K_{PPAR\beta/\delta}$) and fibroblasts (F_{CTRL} vs $F_{PPAR\beta/\delta}$). Involucrin and transglutaminase I (Tgase I): terminal differentiation markers; keratin 10 (CK10): early differentiation marker. Keratin 5 (CK5) identifies the basal keratinocytes. Representative immunoblots of epidermis from 2 OTCs are shown.

A**Two-week old organotypic skin cultures****B****Two-week old OTCs****Figure 6. . $F_{PPAR\beta/\delta}$ potentiate the adjacent epithelial proliferation**

(A) Immunofluorescence staining of two-week old organotypic skin cultures. Organotypic skin cultures (OTC) constructed with control or PPAR β/δ -knockdown keratinocytes (K_{CTRL} vs $K_{PPAR\beta/\delta}$) and fibroblasts (F_{CTRL} vs $F_{PPAR\beta/\delta}$). Pictures from representative immunostained sections are shown. H&E: Hematoxylin and eosin staining; Bar: 40 μ m. Ki67: cell proliferation (white arrows), TUNEL: cellular apoptosis (white arrows) and DAPI (blue): nuclear staining. Dotted white lines show the epidermal-dermal junction. Bar: 20 μ m. Mean numbers of proliferating and apoptotic cells were derived from 5 standardized microscopic fields per section, performed on 3 sections from 4 independent OTC constructions for each combination. Mean Ki67-positive cells per microscopic field (K_{CTRL}/F_{CTRL} , 10 ± 1.1 ; $K_{PPAR\beta/\delta}/F_{CTRL}$, 9 ± 1.8 ; $K_{CTRL}/F_{PPAR\beta/\delta}$, 32.5 ± 2.11 ; $K_{PPAR\beta/\delta}/F_{PPAR\beta/\delta}$, 26.4 ± 3.3). **(B)** Immunoblot analysis of epidermis from 2-week old OTCs constructed using control- or PPAR β/δ -knockdown human keratinocytes (K_{CTRL} vs $K_{PPAR\beta/\delta}$) and fibroblasts (F_{CTRL} vs $F_{PPAR\beta/\delta}$). Cell proliferation was measured using PCNA and cyclin D1. Apoptosis was detected using caspase 3. β -tubulin showed equal loading and transfer. Representative immunoblots of epidermis from 2 OTCs are shown.

1.4.2 Organotypic cultures with $F_{PPAR\beta/\delta}$ show increased expression of mitogenic factors

The paracrine effect of $F_{PPAR\beta/\delta}$ on epidermal proliferation is likely mediated by changes in the production and secretion of mitogenic or anti-mitogenic factors by the fibroblasts. To understand the mechanism underlying the enhanced epidermal proliferation in OTC with $F_{PPAR\beta/\delta}$ an unbiased protein array was done. Inflammatory cytokine and growth factor arrays were used to compare conditioned media from OTCs reconstructed using wildtype keratinocytes with either F_{CTRL} or $F_{PPAR\beta/\delta}$. A total of 76 distinct proteins were screened and the results showed that the protein expression of several mitogenic factors and cytokines were increased in OTC with $F_{PPAR\beta/\delta}$ (Table 2). Notably, most of the proteins whose expression was increased have a known mitogenic action on keratinocytes. The expression of transforming growth factor- β 1 (TGF- β 1), which exerts a pronounced anti-proliferative effect on keratinocytes, and the highly abundant IL-1 α , constitutively produced by keratinocytes, remained unchanged. The expression of two pro-angiogenic factors, namely vascular endothelial growth factor (VEGF) and placental growth factor (PIGF), were reduced in OTC with $F_{PPAR\beta/\delta}$ when compared to F_{CTRL} .

To verify that a reduced PPAR β/δ expression leads to a transcriptional up-regulation of mitogenic factor expression, we performed qPCR on selected mitogenic genes from OTC F_{CTRL} and $F_{PPAR\beta/\delta}$ in the absence or presence of the PPAR β/δ agonist GW501516. Consistent with the protein array results, F_{CTRL} exposed to GW501516 for 12 h showed a decrease in the expression of these genes (Fig. 7A). Importantly, $F_{PPAR\beta/\delta}$ expressed higher basal levels of these mitogenic factors and, as expected, ligand treatment had no effect. Altogether, fibroblasts deficient in PPAR β/δ have an increased expression of mitogenic factors (Fig. 7A).

Table 2: Relative fold change of protein expression in OTCs with $F_{PPAR\beta/\delta}$ compared with F_{CTRL}

Cytokines /Growth Factors	^a Fold change
^b Keratinocyte growth factor (KGF)	4.01±0.11**
^b Interleukin-6 (IL-6)	5.56±0.02**
^b Interleukin-8 (IL-8)	2.94±0.14*
Interleukin-10 (IL-10)	2.13±0.07**
Interleukin-16(IL-16)	2.86±0.11*
^b Granulocyte-macrophage colony-stimulating factor (GMCSF)	5.26±0.10**
I-309	3.33±0.16**
Eotaxin-2	3.03±0.12**
Vascular endothelial growth factor (VEGF)	0.25±0.011*
Placental growth factor (PIGF)	0.33±0.014*

^aThe intensities of signals were quantified by densitometry. Positive control in the array blot, as provided manufacturer, was used to normalise the results from different membranes being compared. Values obtained from the control OTC derived using WT keratinocytes and fibroblasts were arbitrarily assigned a value of 1. Values represent the mean fold increase as compared to control OTC (n=3).

^bThe mRNA expression level of these genes were further verified by qPCR.

* denotes $p < 0.1$

** $p < 0.01$.

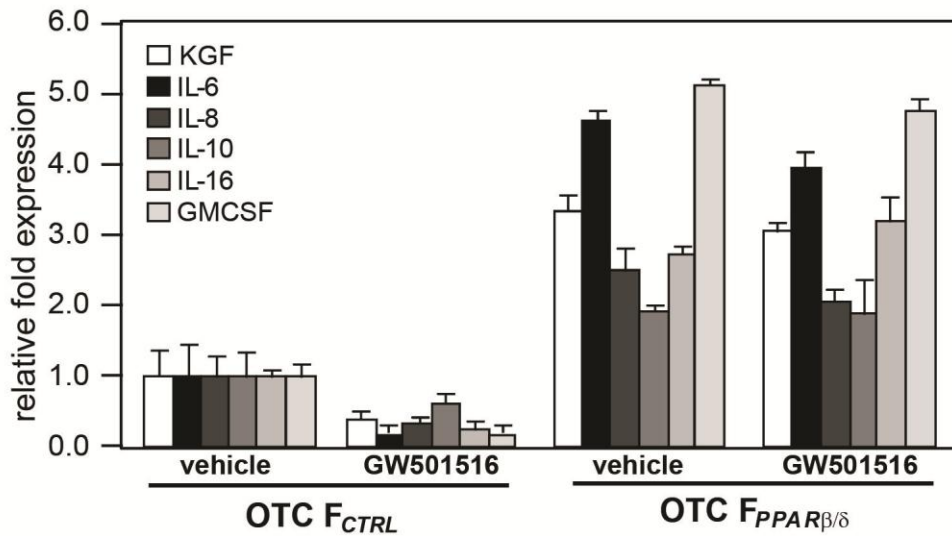
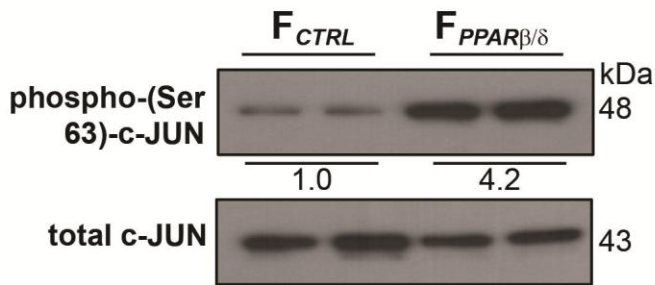
A**B**

Figure 7. Reduced fibroblast $PPAR\beta/\delta$ expression up-regulated AP-1-controlled mitogenic target genes.

(A) Expression of mitogenic factor mRNAs in 2-week old OTC $F_{PPAR\beta/\delta}$ and F_{CTRL} treated with $PPAR\beta/\delta$ agonist (GW501516, 500 nM, 24 h) or vehicle. The expression levels of the indicated mitogenic factors were analyzed by qPCR and normalized to control ribosomal protein P0. Results are represented in fold induction as compared to OTC F_{CTRL} . KGF: keratinocyte growth factor, interleukin (IL)-6, -8, -10, -16, GMCSF: granulocyte macrophage-colony stimulating factor. Data are mean \pm SEM, $n = 3$. **(B)** Immunoblot analysis of phosphorylated c-JUN from $F_{PPAR\beta/\delta}$ and F_{CTRL} extracted from $K_{CTRL}/F_{PPAR\beta/\delta}$ and K_{CTRL}/F_{CTRL} OTCs ($n=2$), respectively. Total c-JUN and TAK1 protein expression level, which remains unchanged, showed equal loading and transfer.

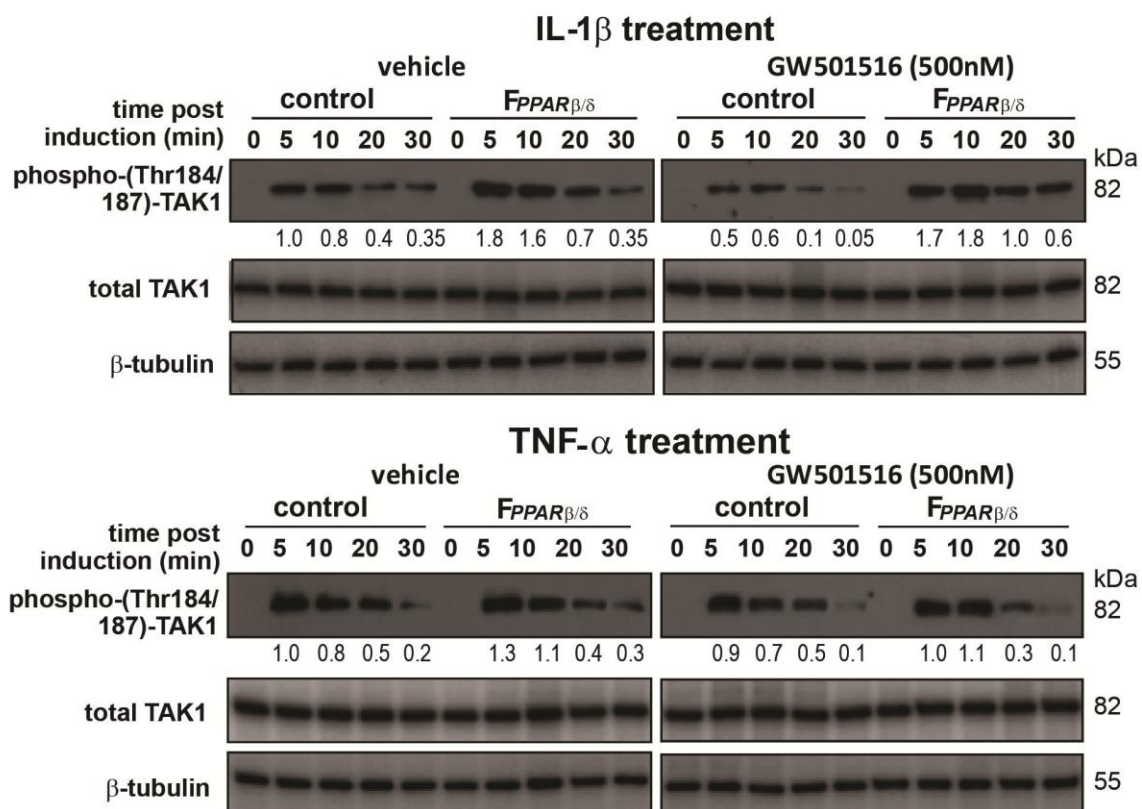
1.4.3 Increased expression of mitogenic factors by $F_{PPAR\beta/\delta}$

To gain further insight into this mechanism, we sought to identify the signaling cascade that culminates in the up-regulation of the mitogenic growth factors in the $F_{PPAR\beta/\delta}$. Interestingly, the expression of the genes encoding these mitogenic factors is known to be regulated by the transcription factor AP-1^{154,159}. Although direct regulation of eotaxin-2 by AP-1 has not been reported, the expression of this gene is stimulated by IL-1^{160,161}. The increased expression of I-309 is likely the consequence of increased IL-8 level¹⁶². We first addressed the hypothesis that AP-1 belongs to the pathway through which $PPAR\beta/\delta$ regulates the expression of mitogenic factors in the $F_{PPAR\beta/\delta}$. We examined the levels of phosphorylated (activated) c-JUN in $F_{PPAR\beta/\delta}$ and F_{CTRL} fibroblasts extracted from $K_{CTRL}/F_{PPAR\beta/\delta}$ and K_{CTRL}/F_{CTRL} OTCs, respectively. Immunoblot analysis showed that $F_{PPAR\beta/\delta}$ isolated from the $K_{CTRL}/F_{PPAR\beta/\delta}$ OTCs had enhanced phosphorylated c-JUN, which is consistent with an increased activity of the AP-1 complex (Fig. 7B) and increased production of growth factors.

The transforming growth factor activated kinase-1 (TAK1) plays a pivotal role in the activation of many genes, including genes encoding mitogenic factors, via activation of AP-1^{159,163}. The IL-1 α/β released by keratinocytes and TNF- α present in wound sites activate TAK1¹⁶⁴. To investigate the effect of $PPAR\beta/\delta$ on TAK1 activation, we examined the expression of phosphorylated (active) TAK1 (phospho-(Thr184/187)-TAK1) in F_{CTRL} and $F_{PPAR\beta/\delta}$ after IL-1 α and TNF- α stimulations. F_{CTRL} and $F_{PPAR\beta/\delta}$ were treated with either vehicle (DMSO) or $PPAR\beta/\delta$ agonist (GW501516) for 24 h prior stimulation by either IL-1 α or TNF- α . As expected, there was an increase in phospho-TAK1 in vehicle-

treated F_{CTRL} exposed to either IL-1 α or TNF- α (Fig. 8). Co-treatment of these fibroblasts with IL-1 α and GW501516 significantly prevented the increase in phospho-TAK1 levels in a dose-dependent manner (Fig. 8A & 8B). In the $F_{PPAR\beta/\delta}$, a more robust increase in phospho-TAK1 was observed, which was only marginally affected by GW501516, showing that the ligand effect in F_{CTRL} was PPAR β/δ -specific (Fig. 8B). In contrast, neither ligand-activated PPAR β/δ nor PPAR β/δ deficiency had an effect on TNF- α -mediated TAK1 activation (Fig. 8B). To further this observation, we performed chromatin immunoprecipitation (ChIP) using phospho-c-JUN antibodies on the KGF and GMCSF gene promoters in fibroblasts from K_{CTRL}/F_{CTRL} and $K_{CTRL}/F_{PPAR\beta/\delta}$ OTCs (Fig. 9A & 9B). There was more phospho-c-JUN immunoprecipitated chromatin from $F_{PPAR\beta/\delta}$ when compared to F_{CTRL} , pointing to enhanced AP-1 binding and activation of the KGF and GMCSF genes in $F_{PPAR\beta/\delta}$ (Fig. 9A & 9B). Together, these results indicate that PPAR β/δ specifically attenuates IL-1 α -mediated TAK1 activation and thus AP-1 activity.

A



B

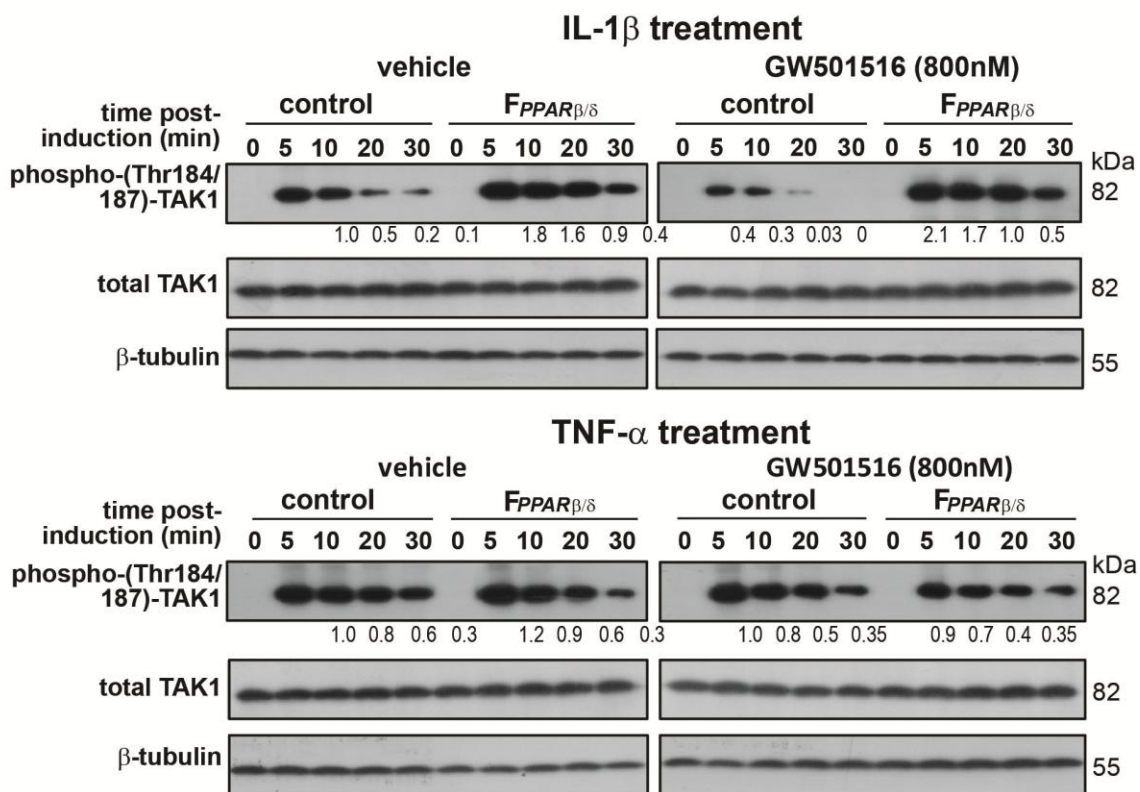


Figure 8. Reduced fibroblast PPAR β/δ expression increases IL-1 β activation of TAK1.

Immunoblot analysis of IL-1 β and TNF- α activation of TAK1 in F_{CTRL} or F_{PPAR β/δ} . Cells were treated with either vehicle (DMSO), **(A)** GW501515 (500nM) or **(B)** GW501516 (800 nM) for 24 h prior exposure to 10 ng/ml IL-1 β (*upper panel*) or TNF- α (*lower panel*). At indicated time points, total cell lysates were extracted. Equal amounts of total protein (50 μ g) were resolved, electrotransferred and probed for phosphorylated TAK1 (Thr184/187), total TAK1 and β -tubulin. Values below each band represent the mean fold differences ($n = 3$) in expression level with respect to vehicle-treated F_{CTRL} at 5 min, which was assigned the value of one.

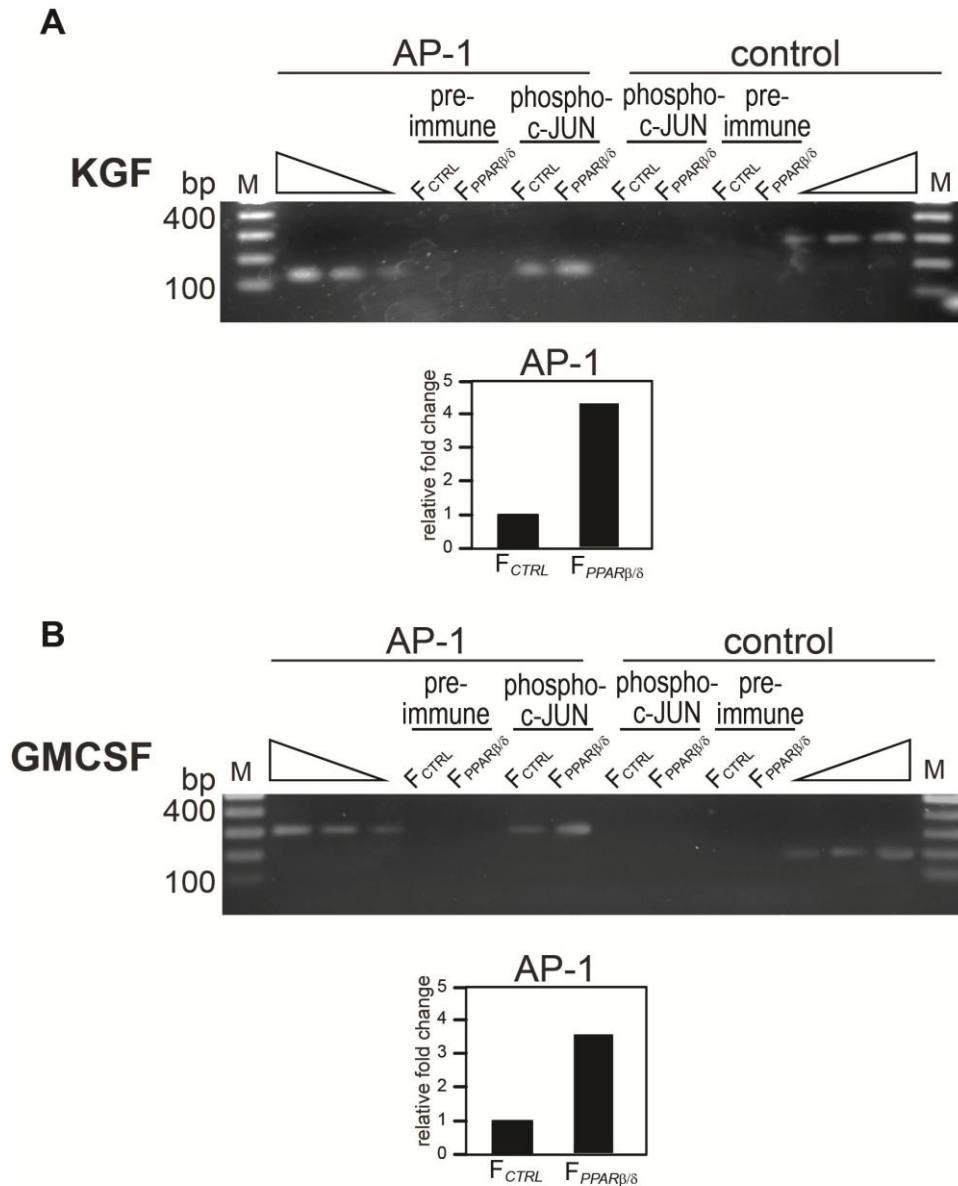


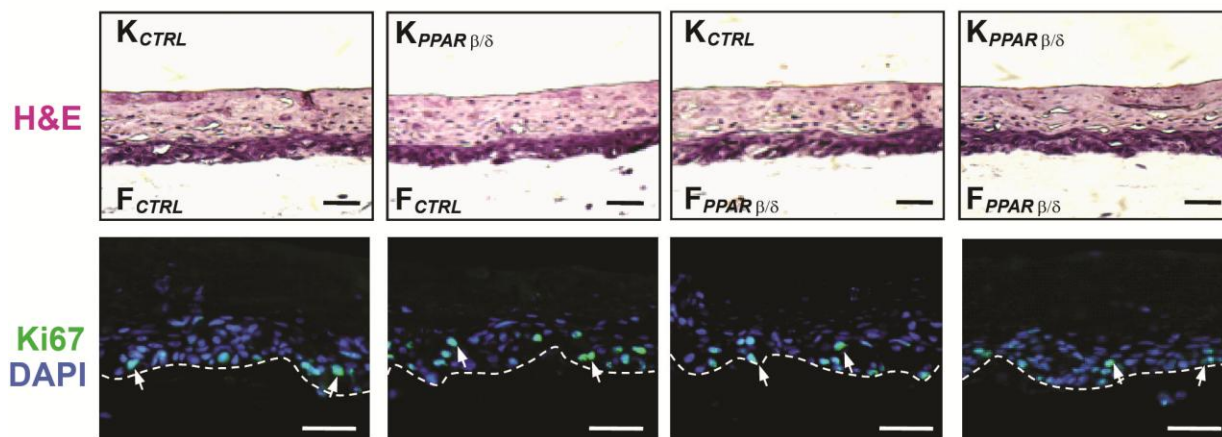
Figure 9. Increased c-Jun binding to AP-1 site of human KGF and GM-CSF gene in $F_{PPAR\beta/\delta}$.

ChIP of AP-1 binding site of human **(A)** KGF and **(B)** GMCSF genes using phospho-c-JUN antibodies. The gene sequence spanning the AP-1 site and a random control sequence were analyzed by PCR in the immunoprecipitated chromatin of F_{CTRL} and $F_{PPAR\beta/\delta}$ fibroblasts extracted from K/ F_{CTRL} and K/ $F_{PPAR\beta/\delta}$ OTC, respectively. Preimmune serum was used as a control. qPCR was performed on immunoprecipitates of phospho-c-JUN antibodies and normalized to input (chromatin before immunoprecipitation). Results are represented in fold change as compared with F_{CTRL} fibroblasts extracted from K/ F_{CTRL} OTC. No immunoprecipitation was observed with preimmune serum, and no amplification was observed for a control sequence. M, 100 bp DNA molecular weight ladder.

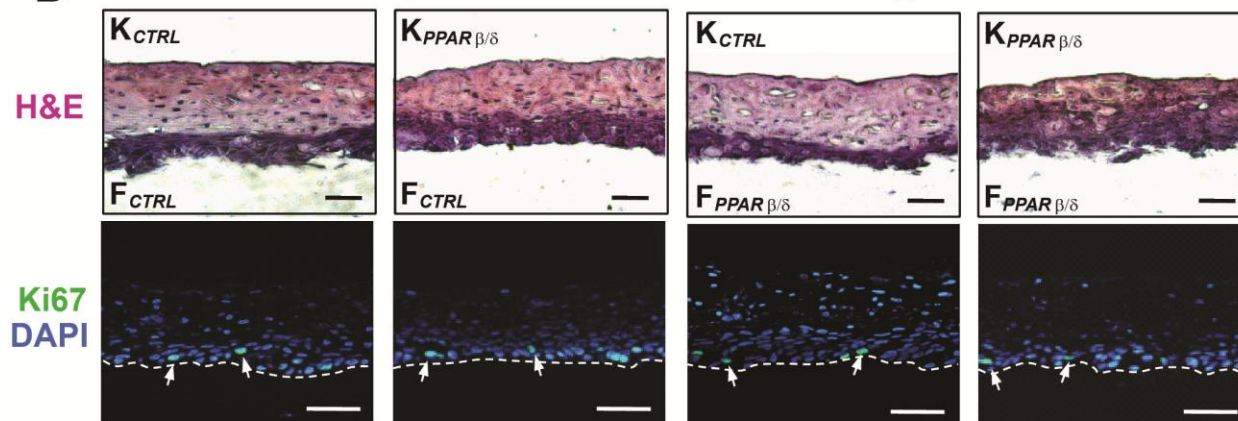
1.4.4 Neutralization of IL-1 α / β signalling abolishes the mitogenic action of $F_{PPAR\beta/\delta}$

Our results showed that IL-1 β -mediated, but not TNF- α -mediated, TAK1 activation and AP-1-dependent expression of mitogenic factors were increased in $F_{PPAR\beta/\delta}$. This result suggested that the IL-1 α / β pathway is responsible for the mitogenic effect of PPAR β / δ -knockdown in fibroblasts. If this was the case, negating the effect of IL-1 α / β with neutralizing antibodies against IL-1 α / β would counteract the effect of PPAR β / δ -knockdown in $F_{PPAR\beta/\delta}$. As anticipated, OTCs exposed to anti-IL-1 α and β antibodies displayed a reduction in Ki67-positive keratinocytes, and the mitogenic action of $F_{PPAR\beta/\delta}$ was completely abolished (compare Fig. 10A & 10C), indicating that IL-1 α / β signaling is a major pathway in the control of keratinocyte proliferation. This was further confirmed by immunoblot analysis of cyclin D1 and PCNA (compare Fig. 11A & 11C). Similarly, inhibiting the action of the mitogenic factors should replicate the neutralizing effect of anti-IL-1 α / β antibodies. To test this possibility, we treated the OTCs with neutralizing antibodies against KGF, GMCSF and IL-6, the three most abundant mitogenic factors in our model. To avoid possible compensatory effects, we neutralized all three growth factors simultaneously. Consistent with the results reported so far, all OTCs showed thinner epidermis and reduced keratinocyte proliferation when compared to the corresponding OTC treated with pre-immune IgG (Fig. 11B & 11C and 10B & 10C). Altogether, our observations indicated that the mitogenic action of the $F_{PPAR\beta/\delta}$ was due to an increase in IL-1 α / β mediated expression of mitogenic factors via TAK1 and AP-1.

A IL-1 α & β neutralizing antibodies



B KGF, GMCSF and IL-6 neutralizing antibodies



C Pre-immune IgG control

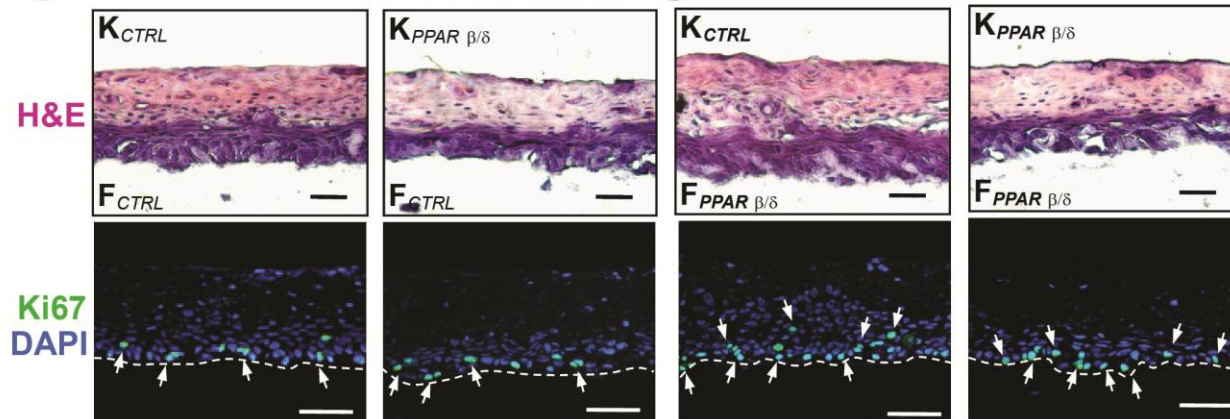


Figure 10. Neutralizing antibodies against IL-1 α / β or against KGF, GMCSF and IL-6 abolished the mitogenic effect of F_{PPAR β / δ}

(A-C) Indicated OTCs were constructed and set at air interface for 3 d prior adding to **(A)** IL-1 α and β , **(B)** KGF, GM-CSF, and IL-6 neutralizing antibodies or **(C)** preimmune IgG control. Neutralizing antibodies or preimmune IgG, each at 400 ng/ml, were added to serum-free OTC medium at each change of medium. The epidermis thickness in OTCs treated with 10 μ g/ml neutralizing anti-IL-1 α / β antibodies was K_{CTRL}/F_{CTRL}, 89.84 \pm 2.11 μ m; K_{PPAR β / δ} /F_{CTRL}, 82.69 \pm 1.06 μ m; K_{CTRL}/F_{PPAR β / δ} , 90.86 \pm 2.54 μ m; and K_{PPAR β / δ} /F_{PPAR β / δ} , 80.18 \pm 2.77 μ m, whereas that in OTCs treated with anti-KGF, GM-CSF, and IL-6 (0.8 μ g/ml each) was K_{CTRL}/F_{CTRL}, 112.42 \pm 3.57 μ m; K_{PPAR β / δ} /F_{CTRL}, 81.46 \pm 2.03 μ m; K_{CTRL}/F_{PPAR β / δ} , 88.94 \pm 4.32 μ m; and K_{PPAR β / δ} /F_{PPAR β / δ} , 85.15 \pm 1.69 μ m. All values lower (epidermis thinner) than those of the corresponding OTCs were treated with a preimmune IgG (K_{CTRL}/F_{CTRL}, 139.08 \pm 3.39 μ m; K_{PPAR β / δ} /F_{CTRL}, 113.69 \pm 2.70 μ m; K_{CTRL}/F_{PPAR β / δ} , 165.71 \pm 3.14 μ m; K_{PPAR β / δ} /F_{PPAR β / δ} , 114.86 \pm 4.23 μ m). Data are mean \pm SEM, n = 4. No difference in Ki67-stained (arrows) proliferating cells were observed among the different OTCs except for the OTCs F_{PPAR β / δ} , treated with preimmune IgG in which the number of proliferating keratinocytes was higher, as expected. Mean Ki67-positive cells per microscopic field were as listed subsequently (neutralizing antibodies against IL-1 α / β : K_{CTRL}/F_{CTRL}, 6 \pm 1.9; K_{PPAR β / δ} /F_{CTRL}, 7 \pm 1.3; K_{CTRL}/F_{PPAR β / δ} , 8 \pm 2.0; and K_{PPAR β / δ} /F_{PPAR β / δ} , 8 \pm 2.3; neutralizing antibodies against KGF, GMSF, and Il-6: K_{CTRL}/F_{CTRL}, 9 \pm 3.4; K_{PPAR β / δ} /F_{CTRL}, 6 \pm 1.9; K_{CTRL}/F_{PPAR β / δ} , 8 \pm 2.7; and K_{PPAR β / δ} /F_{PPAR β / δ} , 7 \pm 2.6; preimmune IgG control treatment: K_{CTRL}/F_{CTRL}, 10 \pm 3.2; K_{PPAR β / δ} /F_{CTRL}, 9 \pm 1.7; K_{CTRL}/F_{PPAR β / δ} , 34 \pm 4.1; and K_{PPAR β / δ} /F_{PPAR β / δ} , 35 \pm 2.2). Picture from representative immunostained sections are shown. H&E, haematoxylin and eosin staining. Dashed white lines denote epidermal-dermal junction. Bars, 40 μ m.

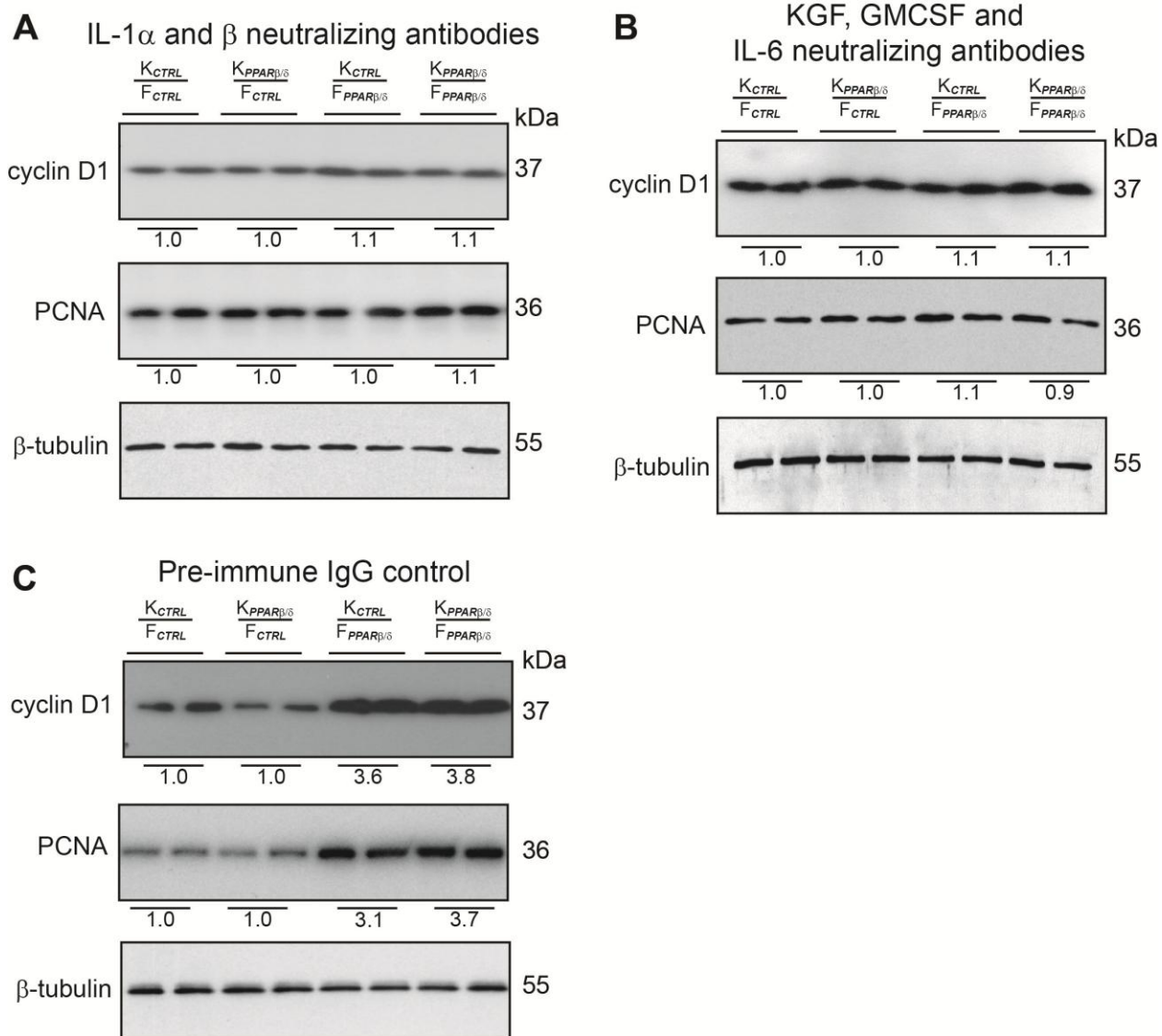


Figure 11. Neutralizing antibodies against IL-1 α/β or against KGF, GMCSF and IL-6 abolished the mitogenic effect of $F_{PPAR\beta/\delta}$

Immunoblot analysis of epidermis from indicated OTCs treated with **(A)** IL-1 α/β (400 ng/ml) **(B)** KGF, GMCSF and IL-6 neutralizing antibodies (each at 400 ng/ml) or **(C)** pre-immune IgG (400 ng/ml). Antibodies were added to OTC medium at each change of medium. Cell proliferation was measured using cyclin D1 and PCNA. Values below each band represent the mean fold differences in expression level with respect to K_{CTRL} from K_{CTRL}/F_{CTRL} OTC, which was assigned the value of one. β -tubulin served as a loading control. Representative immunoblots of epidermis from 2 indicated OTCs are shown.

1.4.5 Human sIL-1ra gene is a direct target of PPAR β/δ in fibroblasts

In vivo, the release of IL-1 α/β by basal keratinocytes is sufficient to maintain tissue homeostasis and to initiate cutaneous inflammation^{133,165}. While we did not detect a change in the expression of IL-1 α/β in the protein array (Table 2), we clearly showed that PPAR β/δ specifically attenuated IL-1 β response, including the activation of TAK1. This suggested that the attenuation of IL-1 β signaling by PPAR β/δ occurs upstream of TAK1 activation. To examine whether PPAR β/δ has a regulatory effect in IL-1 α/β signaling cascade, we measured the mRNA levels of IL-1 α , IL-1 β , IL-1R1, IL-1R2, icIL-1ra, sIL-1ra and IRAK (IL-1 receptor-associated kinase) - all key players of IL-1 signaling – in OTC epidermal keratinocytes (K_{CTRL} and K_{PPAR β/δ}) and dermal fibroblasts (F_{CTRL} and F_{PPAR β/δ}). With the exception of higher level of sIL-1ra in the OTC F_{CTRL}, we detected no change in the expression of the other mediators of IL-1 α/β signaling (Fig.129A). Consistently, elevated sIL-1ra was detected in the medium of OTC with F_{CTRL} as compared to F_{PPAR β/δ} , but no difference was observed in icIL-1ra protein within the fibroblasts (Fig. 12B).

To determine whether the sIL-1ra promoter is directly regulated by PPAR β/δ in the fibroblasts, a 4.4 kb fragment of the promoter region was subcloned into a luciferase reporter vector and analyzed in transactivation assays. Three putative PPRE sequences were identified in the sIL-1ra promoter (Genbank no. X64532), PPRE1 at position -1038/-1050, PPRE2 at -1072/-1084 and PPRE3 at -4067/-4079, using NUBIScan¹⁵⁸ (Fig. 13A). Transfected primary fibroblasts treated with the PPAR β/δ ligand GW501516 alone showed only a modest ~3-fold increase in reporter activity (Fig. 13A). As expected,

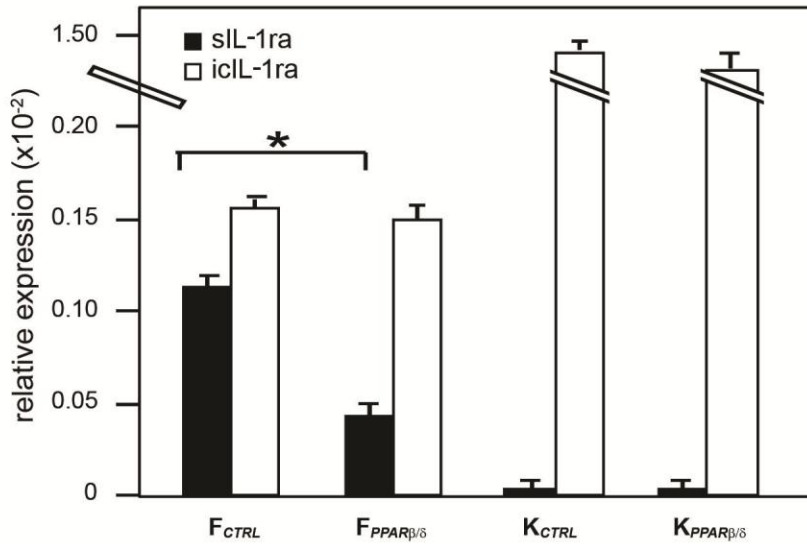
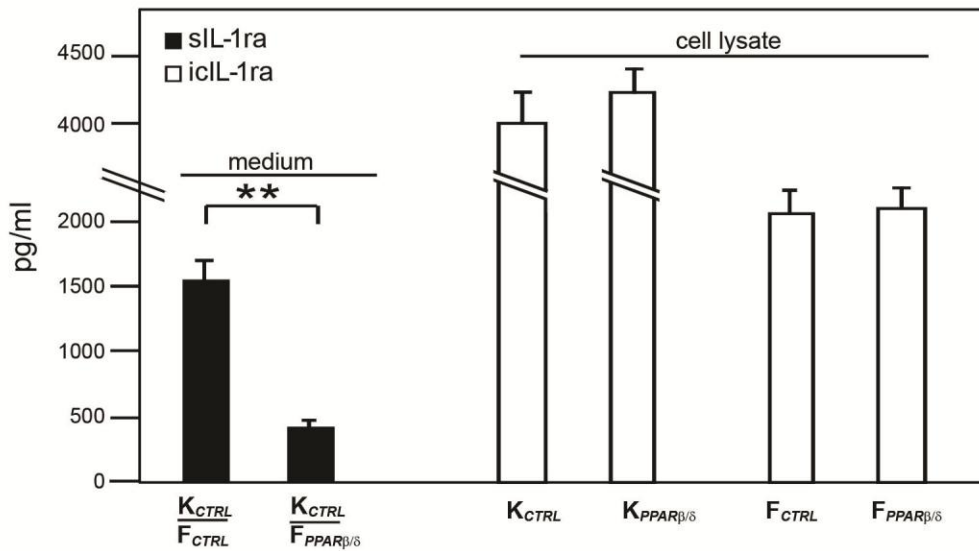
A**B**

Figure 12. Reduced sIL-1ra in PPARβ/δ deficient fibroblasts.

Expression of sIL-1ra and icIL-1ra mRNA (**A**) and protein (**B**) in OTC keratinocytes (K_{CTRL} and K_{PPARβ/δ}) and fibroblasts (F_{CTRL} and F_{PPARβ/δ}). sIL-1ra and icIL-1ra mRNA were analyzed by qPCR and normalized to ribosomal protein P0. sIL-1ra level was determined by ELISA from medium of K_{CTRL}/F_{CTRL} and K_{CTRL}/F_{PPARβ/δ} OTCs. The icIL-1ra levels were measured by ELISA from cell lysates. Data are mean ± SEM, *n* = 4. * denotes *p* < 0.05, ** *p* < 0.01.

treatment with IL-1 β increased the reporter activity by ~20-fold, consistent with earlier studies¹⁶⁶. Importantly, this IL-1 β -mediated transactivation was further enhanced by treatment with GW501516 to ~50-fold (Fig. 13A). To identify the functional PPRES responsible for the PPAR-mediated up-regulation, site-directed mutagenesis of the PPRES was performed. Transactivation assays with the various mutated promoters clearly showed that the stimulatory effects of PPAR β/δ were mediated by two PPRES, i.e. PPRES1 and PPRES3. To investigate if PPAR β/δ was truly bound to these identified PPRES in the sIL-1ra promoter, electrophoretic mobility shift assay (EMSA) and chromatin immunoprecipitation (ChIP) were performed. As expected from the above results, specific protein-DNA complexes were detected in EMSA for PPRES1 and PPRES3, which were effectively competed by a consensus PPRE oligonucleotide (Fig. 13B). As positive control, the consensus PPRE oligonucleotide was used as a probe, which was specifically competed by the unlabelled consensus PPRE but not by a non-specific competitor containing a non-functional MED DR1 element from the malic enzyme promoter¹⁶⁷ (Fig. 13B). Similarly, ChIP done on OTC F_{CTRL} using a monoclonal anti-PPAR β/δ antibody showed the binding of PPAR β/δ to both PPRES1 and PPRES3 (Fig. 13C). As expected, this effect was not observed in the F_{PPAR β/δ} and no signal was seen with pre-immune serum either. In addition, no binding was detected to a control sequence residing between PPRES1 and PPRES3. These data clearly showed that PPAR β/δ specifically binds to the identified functional PPRES in the human sIL-1ra promoter in OTC F_{CTRL}. Together, they indicated that the human sIL-1ra promoter is a direct PPAR β/δ target in primary human dermal fibroblasts.

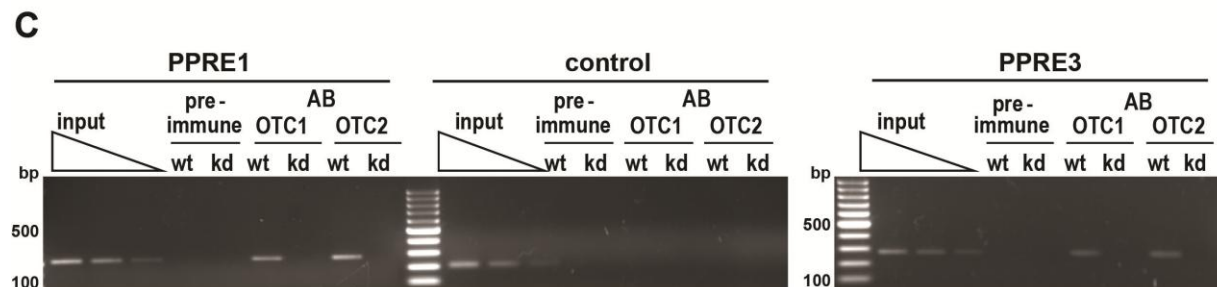
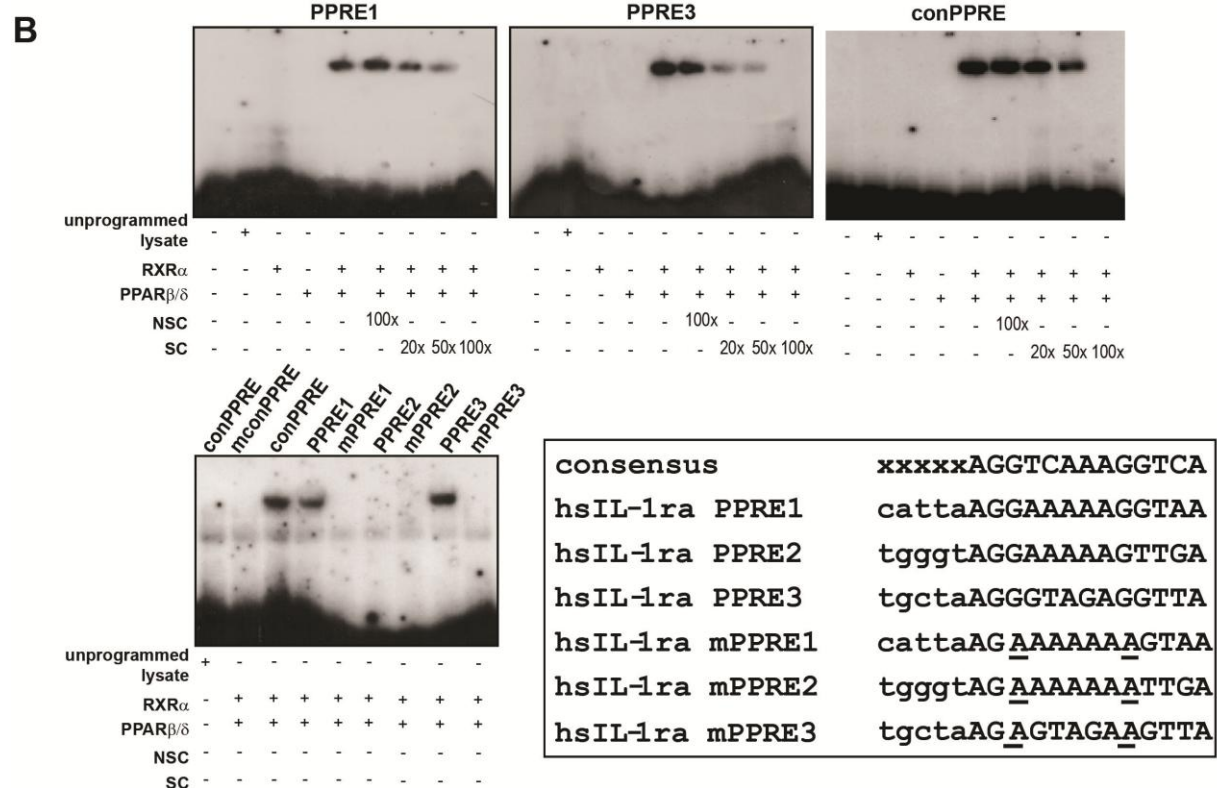
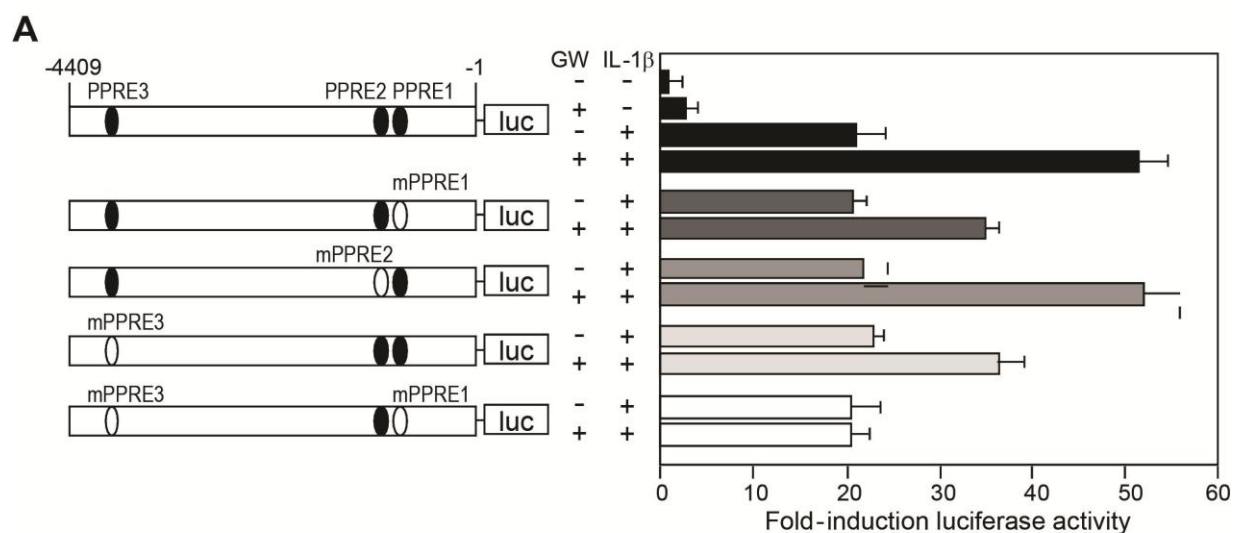


Figure 13. Human sIL-1ra is encoded in a direct PPAR β/δ target gene in fibroblasts.

(A) PPRE1 and PPRE3 of the human sIL-1ra gene are functional. Transactivation assay in fibroblasts co-transfected with a luciferase (luc) promoter driven by the human sIL-1ra promoter and pEF1- β -galactosidase as control of transfection efficiency. Relative positions of the 3 putative PPREs (PPRE 1-3) and their mutants (mPPRE 1-3) are represented in solid and open ovals, respectively. Cells were treated with either GW501516 (500 nM) and/or IL-1 β (10 ng/ml) for 24 h. Luciferase activity was measured and normalised reporter activity is shown as fold induction as compared to untreated fibroblasts. Data are mean \pm SEM, n=4. **(B)** EMSA of human sIL-1ra PPRE1, PPRE3 and consensus PPRE (conPPRE). Radiolabelled PPRE1 (*Top left panel*), PPRE3 (*Top middle panel*) and conPPRE (*Top right panel*) were incubated either with RXR α , PPAR β/δ or both. NSC denotes non-specific competitor, the non-functional MEd DR1 element in the malic enzyme promoter. SC denotes non-radiolabelled conPPRE. As positive control, conPPRE was used. Mutated consensus PPRE is denoted by mconPPRE. PPAR β/δ did not bind to PPRE2 and mutated PPRE probes (mconPPRE, mPPRE1, 2, 3) (*bottom left panel*). Alignment of the PPREs (hsIL-1ra PPRE 1-3) in the promoter of human sIL-1ra gene with the consensus PPRE. Site-directed mutations are indicated as underlined nucleotides (hsIL-1ra mPPRE 1-3) (*bottom right panel*). **(C)** PPAR β/δ binds to PPRE1 and PPRE3 of the human sIL-1ra gene in fibroblasts. ChIP assays were conducted using pre-immune IgG or antibodies against PPAR β/δ (AB) in F_{CTRL} (wt) and F_{PPAR β/δ} (kd) fibroblasts extracted from 2 independent OTCs (OTC1 and OTC2). The regions spanning PPRE1 and 2 of the sIL-1ra gene were amplified using appropriate primers (Table 1). A control region between PPRE1 and 2 served as negative control.

Altogether, these results revealed interplay between two neighboring cell types in normal skin, the keratinocytes and the fibroblasts. We showed that IL-1 α/β secreted by the keratinocytes activates TAK1/AP-1 signaling, which up-regulates the expression of mitogenic factors in the fibroblasts and thus, enhances epidermal proliferation. We also showed that PPAR β/δ in the fibroblasts plays a homeostatic role where it stimulates the expression of the sIL-1ra, modulates IL-1 α/β -mediated mitogenic factors gene expression and thus, attenuates epidermal proliferation.

1.4.6 sIL-1ra knockdown fibroblasts increase keratinocytes proliferation

As a natural antagonist of IL-1 α/β signaling, sIL-1ra attenuates IL-1 α/β action by competitive binding to the type 1 IL-1 receptor. So far herein, we have demonstrated that the sIL-1ra gene in fibroblasts is a direct target of PPAR β/δ , and that accordingly PPAR β/δ knockdown result in a reduced production of sIL-1ra. To test if the reduced production of sIL-1ra by $F_{PPAR\beta/\delta}$ triggers keratinocyte proliferation, we examined the effect of exogenous IL-1ra supplemented into the medium of various OTCs, in particular those with $F_{PPAR\beta/\delta}$. Importantly, exogenous IL-1ra abolished the mitogenic effect of $F_{PPAR\beta/\delta}$ (Fig. 14A, top panel). This was further confirmed by immunoblot analysis of cyclin D1 and PCNA on the epidermis from the various OTCs (Fig. 14A, bottom panel). Thus, inhibition of IL-1 α/β signaling using IL-1ra can rescue the pro-proliferating effect that PPAR β/δ deficiency in the fibroblasts has on keratinocyte proliferation.

To strengthen these results, we examined the role of sIL-1ra on epidermal proliferation using RNA interference. A siRNA designed to target sIL-1ra was introduced

into the human primary fibroblasts. qPCR and ELISA analyses revealed >95% reduction in sIL-1ra mRNA and protein in the transduced fibroblasts (Fig. 14B). The knockdown showed high specificity for the targeted sIL-1ra mRNA as the level of ic-IL-1ra mRNA was not altered (Fig. 14B, left panel). The sIL-1ra-knockdown fibroblasts ($F_{sIL-1ra}$), together with wildtype keratinocytes, were used in OTC. Consistent with the above results, reducing the sIL-1ra production in fibroblasts resulted in increased keratinocyte proliferation as indicated by the large increase in Ki67-positive cells, and cyclin D1 and PCNA expression (Fig. 15A & 15B, left panel). This marked increase in epidermal cell proliferation is accompanied by enhanced activation of TAK1 and c-JUN in the $F_{sIL-1ra}$ when compared to F_{CTRL} (Fig. 15B, right panel).

To provide further evidence that reduced sIL-1ra in fibroblasts results in the increased expression of mitogenic factors, protein arrays were used to compare conditioned media from OTCs using wildtype keratinocytes with either F_{CTRL} or $F_{sIL-1ra}$

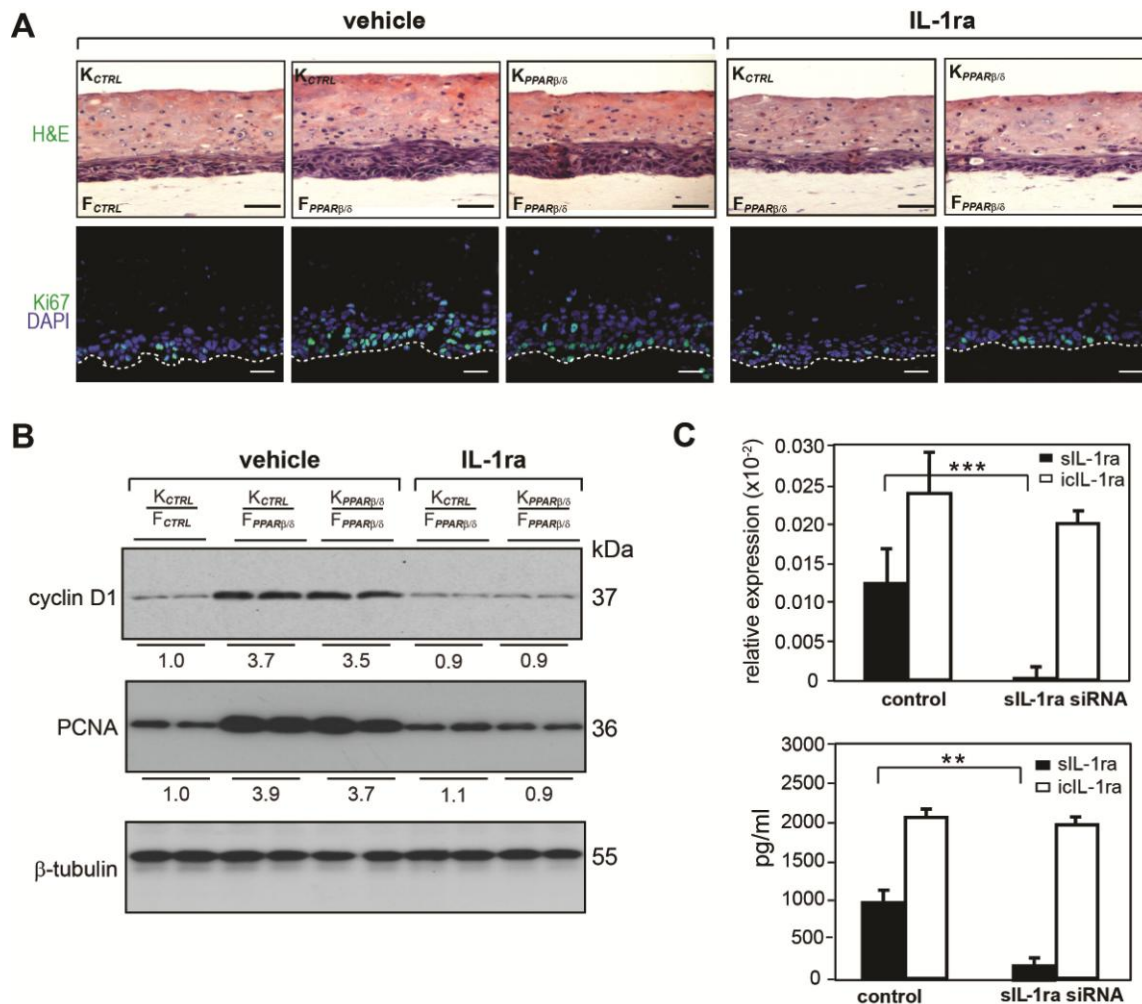


Figure 14. Reduced sIL-1ra in fibroblasts potentiates epidermal keratinocyte proliferation.

(A) Indicated OTCs were constructed as described in Material and methods and treated with either vehicle (PBS) or 10 μ g/ml IL-1ra from day 3 after air interface setting. Fresh medium containing either vehicle or IL-1ra were changed every 3 d for 2 wk. As control for comparison, vehicle-treated K_{CTRL}/F_{CTRL} was shown. Pictures from representative sections immunostained with the denoted markers are shown. Ki67, cell proliferation; DAPI, nuclear staining. Dashed white lines represent epidermal-dermal junction. Mean numbers of proliferating cells were determined as described in Fig. 7. Vehicle (PBS) treatment: K_{CTRL}/F_{CTRL}, 8.5 ± 1.7 ; K_{CTRL}/F_{PPAR β/δ} , 30.5 ± 4.1 ; K_{PPAR β/δ} /F_{PPAR β/δ} , 29 ± 3.6 ; exogenous IL-1ra treatment: K_{CTRL}/F_{CTRL}, 8 ± 2.26 ; K_{PPAR β/δ} /F_{PPAR β/δ} , 7 ± 2.04 . Bars: (top) 40 μ m; (bottom) 20 μ m. **(B)** Immunoblot analysis of epidermis from indicated OTCs treated with either vehicle (PBS) or exogenous IL-1ra (50 ng/ml). Cell proliferation was measured using PCNA and cyclin D1. Pictures and values below each band were as derived as described in Figure 8C. **(C)** Specific knockdown of sIL-1ra in human fibroblasts. *Left*: Knockdown efficiency was monitored by qPCR and normalized with control ribosomal protein P0. Specificity of knockdown was assessed by the relative expression level of icIL-1ra. *Right*: protein expression of sIL-1ra and icIL-1ra as determined by ELISA. ** denotes $p < 0.01$; ***, $p < 0.001$. Data are mean \pm SD, $n = 3$.

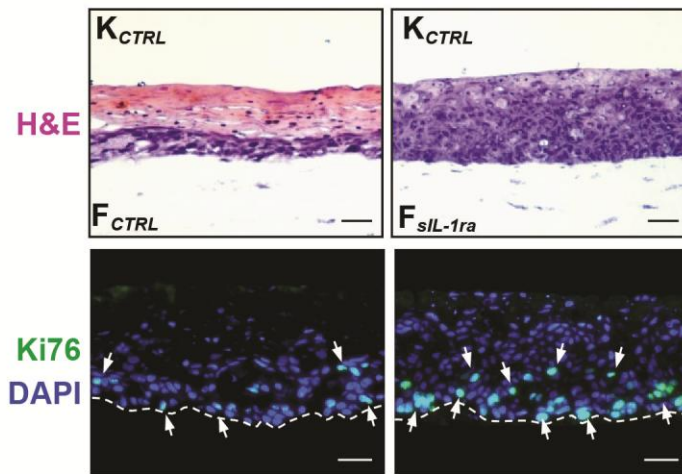
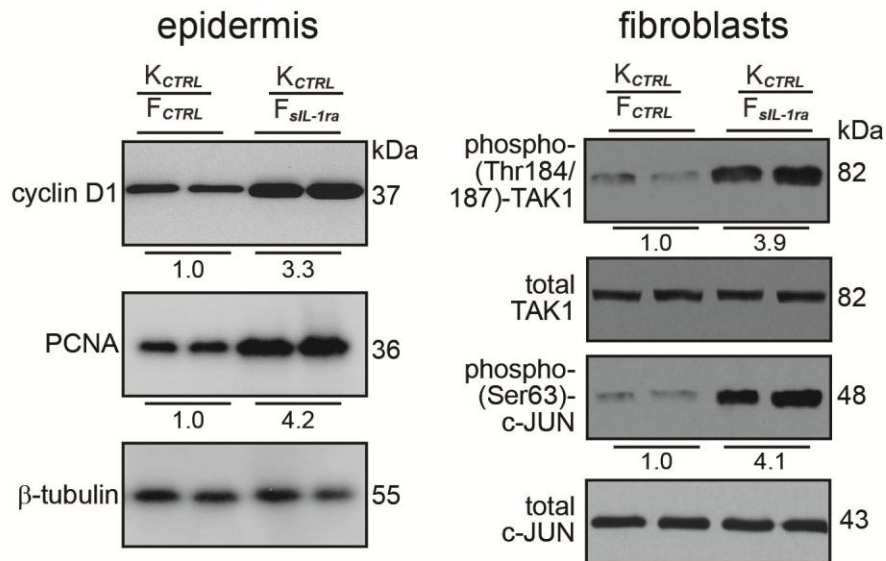
A**B**

Figure 15. Reduced fibroblasts sIL-1ra increases epidermal proliferation.

(A) OTCs were constructed using K_{CTRL} with either control (F_{CTRL}) or sIL-1ra-knockdown ($F_{sIL-1ra}$) fibroblasts. H&E: Hematoxylin and eosin staining (*top panel*); Bar: 40 μ m. Ki67: cell proliferation (white arrows); DAPI: nuclear staining. Bar: 20 μ m. Mean numbers of proliferating cells were derived as described in Figure 3. Broken lines denote epidermal-dermal junction. **(B)** Immunoblot analysis of keratinocytes and fibroblasts extracted from two independent indicated OTCs. Equal amounts of total protein (50 μ g) were resolved, electrotransferred and probed for indicated proteins. Values below each band represent the mean fold differences in expression level with respect to K_{CTRL} or F_{CTRL} extracted from K_{CTRL}/F_{CTRL} OTC.

(Table 3). In addition to those listed in Table 1, the expression of two additional factors, chemokine ligand 1/growth-related oncogene (CXCL1 or GRO- α) and stromal-derived growth factor (SDF-1), were increased in OTC $F_{sIL-1ra}$ compared to F_{CTRL} . The expression of CXCL1 and SDF-1 is c-JUN-dependent and their expression increased keratinocyte proliferation^{134,163}. Similarly, when comparing OTCs with F_{CTRL} and $F_{PPAR\beta/\delta}$, there was a trend for higher CXCL1 and SDF-1 expression in OTCs $F_{PPAR\beta/\delta}$, although the fold increase was not significant.

Finally, we also performed ChIP using phospho-c-JUN antibodies on the KGF, GMCSF and IL-6 gene promoters in fibroblasts extracted from K_{CTRL}/F_{CTRL} and $K_{CTRL}/F_{sIL-1ra}$ OTCs. The sequences spanning the AP-1 binding site were significantly enriched in the immunoprecipitates obtained from $F_{sIL-1ra}$ compared to F_{CTRL} (Fig. 16, left panel). This was further confirmed by qPCR normalized to chromatin before immunoprecipitation i.e. input (Fig. 16, right panel). Altogether, we concluded that reduced sIL-1ra production in the fibroblasts, as observed in $F_{PPAR\beta/\delta}$, had a pronounced mitogenic effect on the epidermis.

Table 3: Relative fold change of protein expression in OTCs with F_{siL1ra} compared to F_{CTRL}.

Cytokines /Growth Factors	^a Fold increase
^b KGF	5.47±0.22**
^b IL-6	6.11±0.31**
IL-8	3.47±0.06**
IL-10	3.88±0.15**
IL-16	3.78±0.41**
^b GMCSF	7.74±0.31**
Chemokine ligand 1 (CXCL1) / Growth-related oncogene (GRO- α)	2.67±0.16*
Stromal-derived growth factor 1 (SDF-1)	2.33±0.07*
I-309	4.57±0.20**
Eotaxin-2	6.19±0.62**
VEGF	0.22±0.030*
PIGF	0.25±0.021*

^aThe intensities of signals were quantified by densitometry. Positive control in the array blot, as provided manufacturer, was used to normalise the results from different membranes being compared. Values obtained from the control OTC derived using WT keratinocytes and fibroblasts were arbitrarily assigned a value of 1. Values represent the mean fold increase as compared to control OTC (n=3).

^bChIP was performed on these genes using phospho-c-JUN antibody.

* denotes p<0.1

** p<0.01.

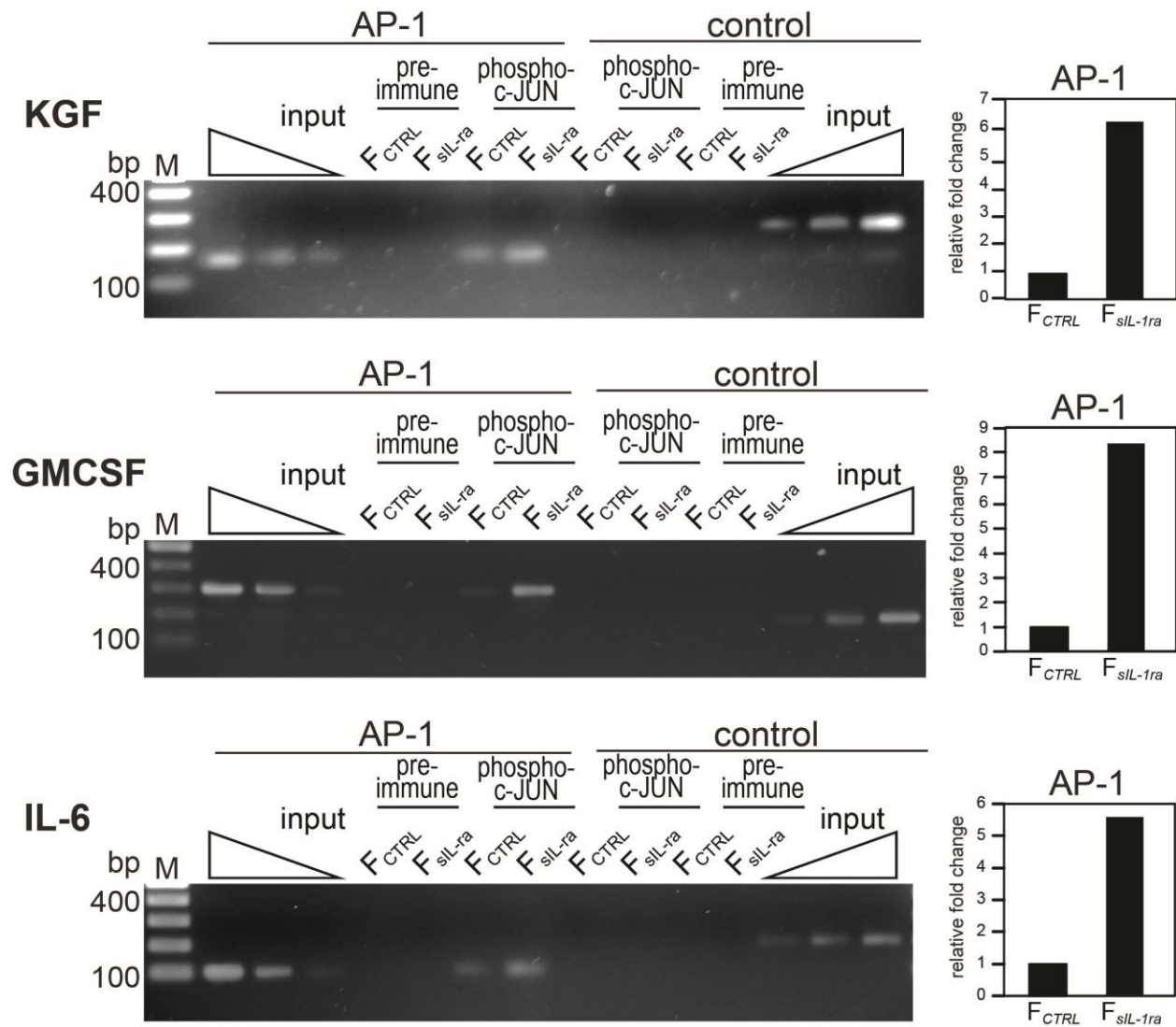


Figure 16. Increased c-JUN binding to AP-1 site of human KGF, GMCSF and IL-6 gene promoter in F_{sIL-1ra}.

ChIP of AP-1 binding site of human KGF (*top*), GMCSF (*middle*) and IL-6 (*bottom*) genes using phospho-c-JUN antibodies. The gene sequence spanning the AP-1 site and a random control sequence were analyzed by PCR in the immunoprecipitated chromatin of F_{CTRL} and F_{sIL-1ra} fibroblasts extracted from K/F_{CTRL} and K/F_{sIL-1ra} OTC, respectively. Pre-immune serum was used as a control. qPCR was done on immunoprecipitates of phospho-c-JUN antibodies and normalised to input (chromatin before immunoprecipitation). Results are represented in fold change as compared to F_{CTRL} extracted from K/F_{CTRL} OTC. M: 100 bp DNA molecular weight ladder.

1.4.7 PPAR β/δ KO mice show reduced sIL-1ra expression during early wound healing

Next, we evaluated the relevance of our findings during mouse skin wound healing, an *in vivo* model that involves the IL-1 α/β pathway. We first demonstrated that, consistent with our observations in human cells, activated PPAR β/δ increased the IL-1 α -induced sIL-1ra expression in WT but not in PPAR β/δ -KO primary fibroblasts (Fig. 17A & B). Next, we examined the *in vivo* expression of IL-1ra in skin wound biopsies collected during early wound healing. Quantitative PCR analysis of early wound biopsies (Day 1 to Day 3) showed a significantly lower sIL-1ra expression in PPAR β/δ -KO tissue when compared to its WT counterpart (Fig. 17C), consistent with the enhanced cell proliferation previously reported during early wound healing¹⁴². Notably, this difference in sIL-1ra expression was no longer detected in later wound biopsy specimens (Day 7) (Fig. 17C). Consistently, analysis of wound fluids collected from Day 2 and 3 wound beds showed reduced sIL-1ra protein in PPAR β/δ -KO mice, when compared to WT mice (Fig. 17C). The expression of icIL-1ra in early and late wound biopsies was unchanged between WT and PPAR β/δ -KO mice (data not shown). Because keratinocytes only produced icIL-1ra, the change in sIL-1ra expression was attributed to the fibroblasts, a hypothesis which was verified by performing qPCR analysis of laser microdissected epithelium and dermis sections from Day 4 wound biopsies of WT and KO mice (Fig. 18). Consistent with our above results, wound PPAR β/δ -KO dermis had reduced sIL-1ra expression, and concomitantly increased levels of IL-6, GM-CSF and KGF when compared to wound WT dermis (Fig. 17D). These results confirmed that the expression of sIL-1ra was also modulated by PPAR β/δ in mouse fibroblasts. We next

examined the effect of topical application of exogenous IL-1ra on the expression of IL-6, GMCSF and KC (also known as CXCL1, GRO α , another c-JUN target gene) in early wound biopsies. As expected, exogenous IL-1ra reduced the expression of the IL-6, GMCSF and KC in PPAR β / δ -KO wounds (Fig. 17E). In summary, *in vivo* wound biopsy and fluid analyses also revealed lower sIL-1ra mRNA and protein in the PPAR β / δ -KO mice. Taken together our observations from two different species, and from both OTC and *in vivo* experiments indicated that PPAR β / δ -deficient fibroblasts had reduced sIL-ra expression compared to wildtype cells, and that this reduced sIL-1ra production increased epidermal proliferation.

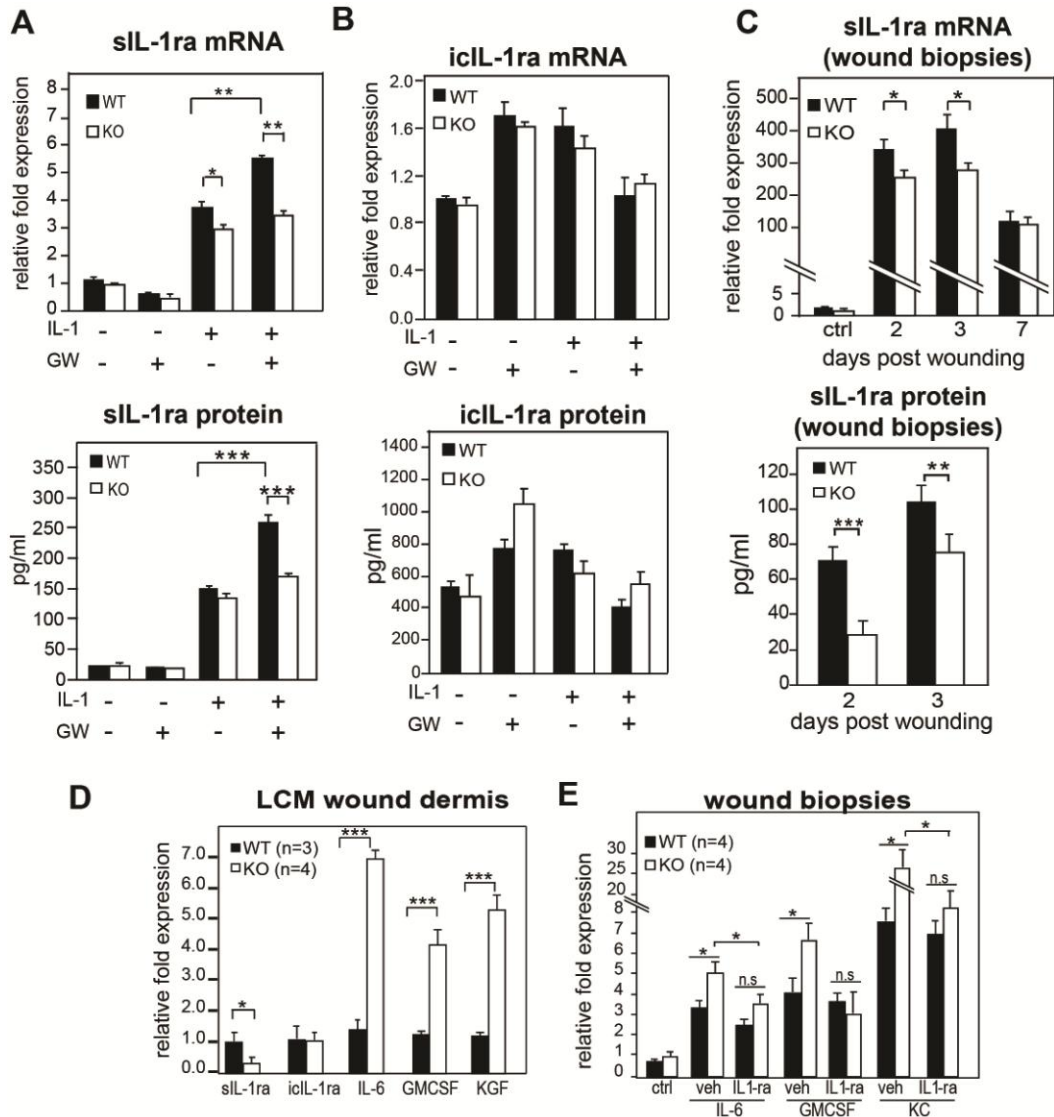


Figure 17. Regulation of IL-1 β signaling via PPAR β/δ during wound repair in PPAR β/δ -null mice.

Expression level of (A) sIL-1ra and of (B) icIL-1ra in wildtype (WT) and PPAR β/δ -null (KO) fibroblasts. WT and KO primary fibroblasts were treated with PPAR β/δ ligand (GW: GW501516, 100 nM) and/or IL-1 β (10 ng/ml). The mRNA (*left panel*) and protein (*right panel*) expression levels were measured by qPCR and ELISA, respectively. Values are mean \pm SEM, $n = 4$. (C) Expression level of sIL-1ra in early wound biopsies of KO mice. Wound fluids and biopsies were collected at the indicated day post-wounding (Day 1-3, $n = 7$ and Day 7, $n = 4$). Unwounded skin was used as control (ctrl, $n = 4$). sIL-1ra mRNA and protein levels were determined by qPCR and ELISA, respectively. * denotes $p < 0.05$; **, $p < 0.01$; ***, $p < 0.001$. (D) Expression of sIL-1ra, icIL-1ra, KGF, IL-6 and GMCSF mRNAs from microdissected dermis of WT ($n = 3$) and KO ($n = 4$) wound biopsies. Indicated mitogenic factors mRNA levels were analyzed by qPCR and normalized to control ribosomal protein P0. Data are mean \pm SEM, $n = 4$. (E) Expression levels of indicated factors mRNAs in vehicle (veh; carboxymethylcellulose)- and IL-1ra-treated (3 \times 2.5 μ g) wounds of KO and WT mice as compared to corresponding unwounded (ctrl) skin. Data are mean \pm SEM, $n = 4$.

Laser Capture Microdissection (LCM)

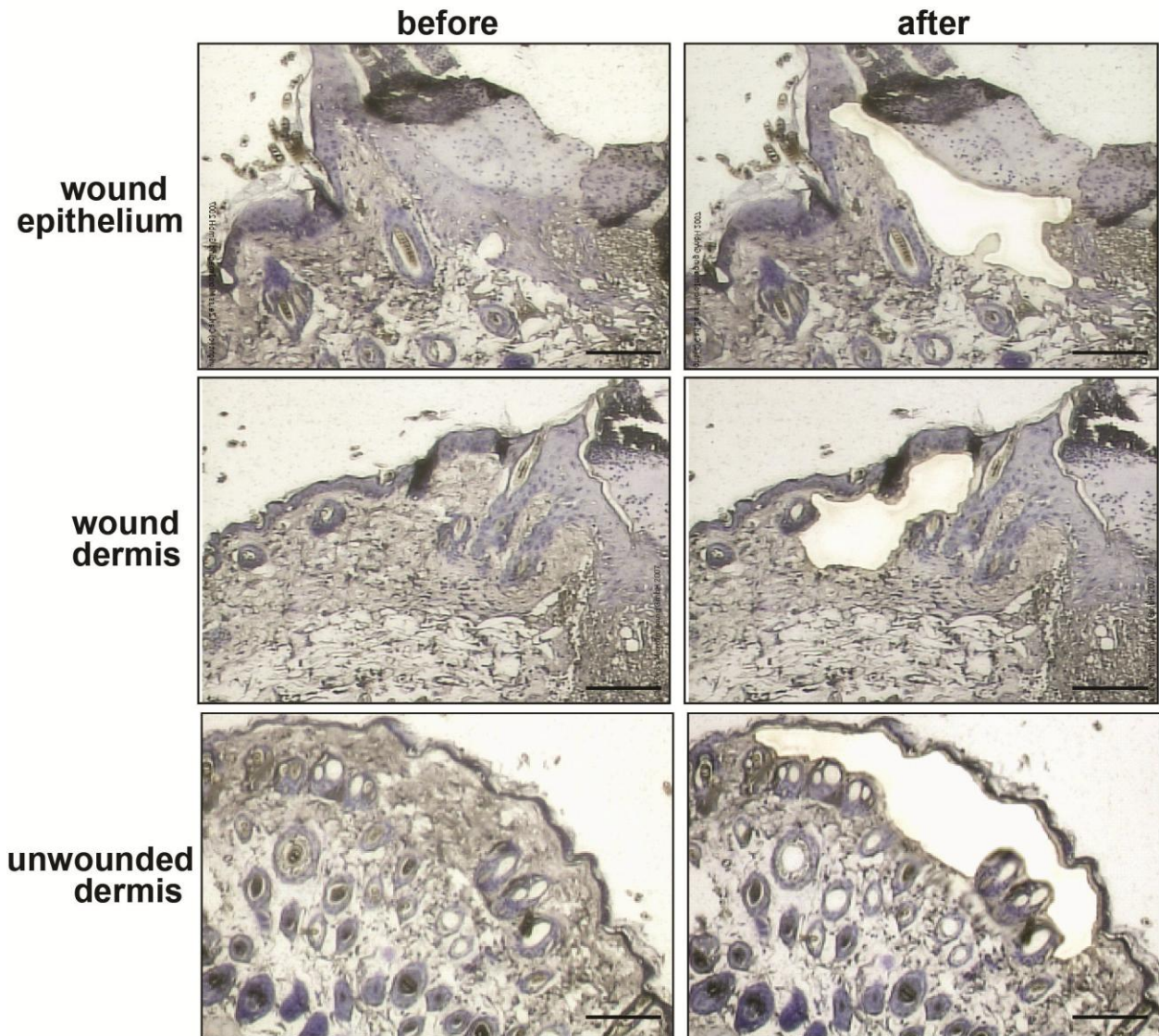


Figure 18. Laser capture microdissection (LCM) of normal and wound biopsies.

Hematoxylin and eosin (H&E) stained of normal skin and Day 4 wound biopsies from wildtype and PPAR β/δ -knockout mice before and after laser capture microdissection using PALM Microbeam Axio Observer Z1 (Carl Zeiss, Inc.) with a long distance Plan-Neofluar 20x/0.40 NA objective. The acquisition software used was PALM RoboSoftware 4.2 (Carl Zeiss, Inc.). Pictures were taken with a charge-coupled device camera system (3-Chip; Hitachi), and representative H&E stained sections are shown. Microdissected tissues were subsequently processed for real-time PCR analysis. Bars, 20 μ m.

1.5 DISCUSSION

Wound healing is a complex process that consists of a cascade of overlapping events, including inflammation, re-epithelialization, and remodeling, directed at restoring the epidermal barrier. During the healing process, interactions between different cell types provide coordination between individual events, allowing for temporal and spatial control. Re-epithelialization is accomplished through increased keratinocyte proliferation and the guided migration of keratinocytes over the granulation tissue. Such processes require ordered changes in the behavior and phenotype of the keratinocytes; such changes are modulated by the interplay of keratinocytes with dermal fibroblasts, i.e., epithelial-mesenchymal communication and the ability to integrate diverse signals from the wound microenvironment through a network of autocrine- and paracrine-acting factors. The results presented here suggest a novel unsuspected role of PPAR β/δ in fibroblasts, as it appears to ensure a balanced functional interaction between the dermis and epidermis. We show that keratinocyte proliferation is controlled by the same dermal fibroblasts that produce AP-1-dependent mitogenic factors under the control of the IL-1/TAK1 signaling cascade, whose activity level is modulated by PPAR β/δ via the direct control of the secreted IL-1 antagonist (sIL-1ra) (Fig. 19).

The development and maintenance of normal epidermal tissue requires a continuous exchange of signals with the underlying dermal compartment. Fibroblasts are a major cell type in the dermis, and their function in regulating extracellular matrix deposition and growth factor expression helps determine the differentiation state of the epidermis. Previous studies have shown that gene expression changes in the dermal fibroblasts significantly influence epithelial cell fate¹⁶⁸. In the presence of

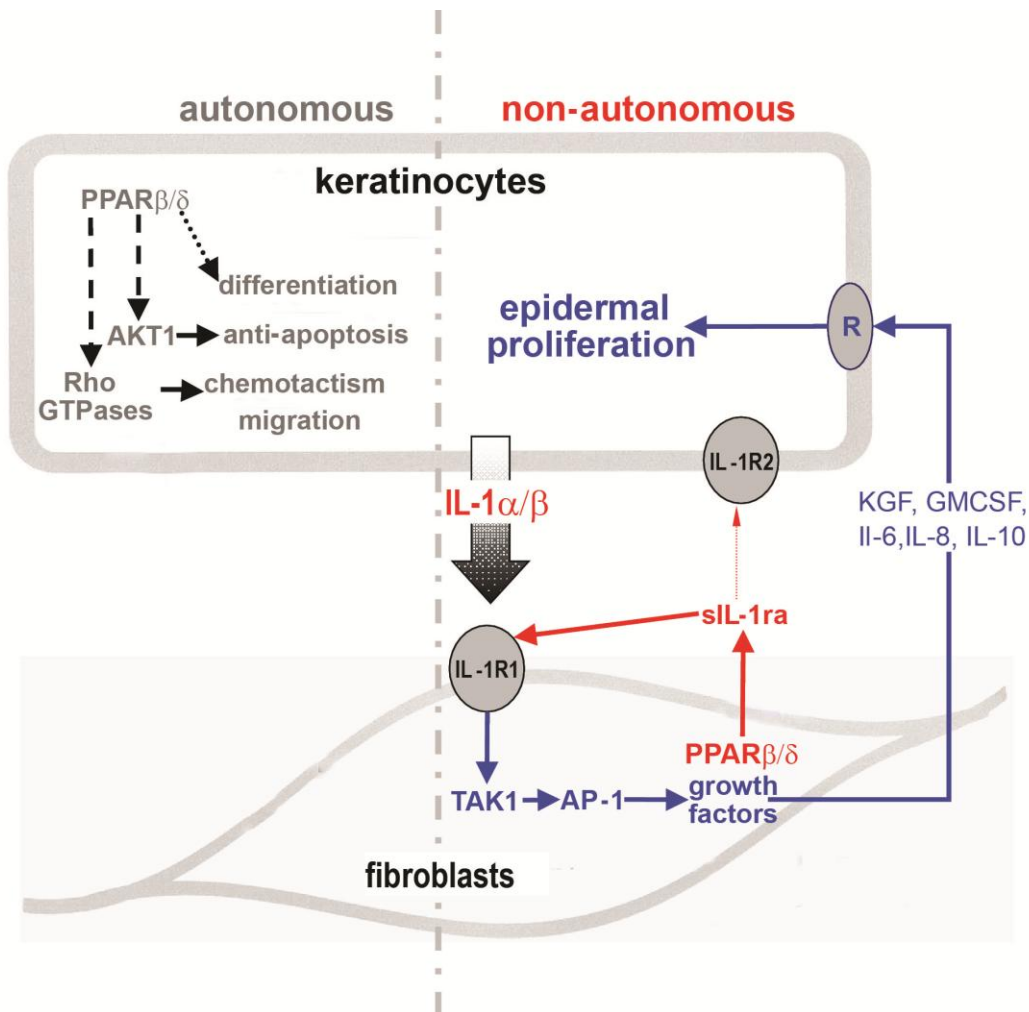


Figure 19. The autonomous and non-autonomous actions of PPAR β/δ .

PPAR β/δ confers anti-apoptotic properties to keratinocytes and potentiates their migration via AKT1 and Rho GTPases, respectively, in a cell-autonomous manner^{169,170}. PPAR β/δ also influences keratinocyte differentiation in a yet unknown mechanism. PPAR β/δ regulates epidermal proliferation in a non-autonomous fashion via a paracrine mechanism. Interleukin-1 (IL-1) constitutively produced by the adjacent keratinocytes activates c-JUN, an obligate partner of AP-1 transcription factor via the transforming growth factor kinase-1 (TAK1), and consequently increases the production of several mitogenic factors. The expression of PPAR β/δ in the underlying fibroblasts attenuates this IL-1 signaling via the production of secreted IL-1 receptor antagonist (sIL-1ra). sIL-1ra has little affinity for type 2 IL-1 receptor (IL-1R2), which is highly expressed in keratinocytes. Thus, sIL-1ra acts in an autocrine fashion onto the fibroblasts, which expressed the predominant functional type 1 IL-1 receptor (IL-1R1). The binding of sIL-1ra to IL-1R1 modulates the IL-1-mediated signalling events and consequently decreases the production of several AP-1-mediated mitogenic factors. The mitogenic factors exert a reduced paracrine effect on the epithelial proliferation via their cognate receptors (R). Therefore, PPAR β/δ in the fibroblasts plays an important homeostatic role in maintaining epidermal homeostasis, the absence of PPAR β/δ resulting in significant epidermal proliferation.

IL-1-producing keratinocytes, PPAR β/δ was found to be the predominant PPAR isotype in fibroblasts. Interestingly, PPAR β/δ directly increased the expression of sIL-1ra in the fibroblasts, acting in an autocrine manner to modulate the expression of several IL-1-dependent mitogenic factors (Fig. 16). This autocrine action is possible because IL-1R1 is the predominant IL-1 receptor subtype in fibroblasts, whereas keratinocytes express IL-1R2, which has a very low affinity for sIL-1ra and protects them from an exacerbated autocrine action of the IL-1 α/β that they constitutively produce. Importantly, this study highlights the fact that PPAR β/δ has a homeostatic role during epidermal formation in the dermal fibroblasts, balancing cell proliferation by controlling IL-1 α/β signaling.

It was reported that the enhanced TPA-induced hyperplasia in KO mice was due to reduced ubiquitin C, whose expression is regulated by PPAR β/δ ¹³³. The impaired ubiquitin-dependent proteasome-mediated protein turnover in KO mice resulted in a higher PKC α level and increased Raf1 and MAPK/ERK activities, which in turn, led to an increase in the level of cell proliferation¹⁷¹. Other reports from two different model systems have shown that PKC α overexpression does not affect the proliferation of primary human keratinocytes and the proliferation of PKC α -transgenic mouse keratinocytes^{172,173}. In fact, PKC α -transgenic mouse keratinocytes treated with TPA underwent apoptosis¹⁷². This is in apparent discrepancy with the delayed wound healing kinetics observed in KO mice. Enhanced keratinocyte proliferation has also been observed in many situations that do not involve TPA exposure, such as in the skin of untreated KO mice compared with their wildtype (WT) counterparts, in the early stages of wound healing and following hair plucking^{136,142,174}. Furthermore, no difference was observed in the expression of phosphorylated MEK-1/2 and ERK-1/2 between the

untreated (i.e., no TPA treatment) KO and WT mice¹⁷¹. This raises the question of how epidermal hyperproliferation occurs at wound edges in the early stages following injury in KO mice in the absence of TPA¹³⁶. These observations point to a complex role of PPAR β/δ in cell proliferation. Indeed, our results showing that PPAR β/δ deficiency in fibroblasts increases their mitogenic effect on epithelial cells highlights this complexity. The underlying mechanism involves reduced sIL-1ra production by fibroblasts, allowing for stronger IL-1 signaling, resulting in increased TAK1 activity with a consequent rise in mitogenic growth factor production. The *in vivo* relevance of this mechanism was observed during early wound repair in KO mice, with reduced levels of sIL-1ra in early wound biopsies (Day 1 to 3) but not in late biopsies (Day 7). This pattern is consistent with the early epidermal hyperproliferation reported in KO mice during the inflammatory phase of wound healing¹⁴².

This study and earlier reports suggest different roles of PPAR β/δ in the dermis and the adjacent epidermis. The activation of PPAR β/δ conferred anti-apoptotic properties to the keratinocytes, mediated in part by the increased activation of the PKB α /Akt1 survival pathway¹³⁹. This anti-apoptotic role was similarly observed in mouse tubular renal epithelial cells¹⁷⁵ and in human keratinocyte HaCaT cells¹⁷⁶. Our data now clearly show that PPAR β/δ signaling in fibroblasts has a pronounced effect on the growth potential of adjacent epithelia. Such differential roles were previously observed for TGF- β 1 signaling in wound repair¹⁷⁷. Interestingly, an *in vivo* crosstalk between TGF- β 1/Smad3 and PPAR β/δ signaling in keratinocytes has been reported during wound repair¹⁵⁴. The development of a vascular supply is important for wound healing. Of note, we also observed a reduced expression of VEGF and PlGF in OTC with F_{PPAR β/δ} . While

it is tempting to speculate that both VEGF and PlGF may be target genes of PPAR β/δ , their regulation is complex and context-dependent and involves numerous factors, such as von Hippel-Lindau tumor suppressor (pVHL), Sp-1, NF- κ B, HIF- α and AP-1, among others^{178,179}. Importantly, epithelial-mesenchymal interactions can also modulate VEGF expression. During wound repair, impaired angiogenesis is consistent with the delayed wound healing observed in KO mice¹³⁶.

1.6 FUTURE STUDIES

The tissue microenvironment plays a pivotal role in modulating gene expression and cellular behavior, including the communication between the epithelium and the mesenchyme. Likewise, the microenvironment milieu is comprised of factors that are produced and released by these various cell types as communication signals. Of interest, the activation of IL-1 signaling has been reported to promote tumor growth, while its repression by IL-1ra has likewise been reported to have an anti-tumor effect¹⁸⁰. The role of PPAR β/δ in tumorigenesis remains debatable because there is evidence that this PPAR isotype both potentiates and attenuates epithelial cancers¹⁸¹⁻¹⁸³. Although this question is not directly addressed in my previous study, the data clearly demonstrated that $F_{PPAR\beta/\delta}$ can increase the proliferation of human squamous carcinoma cells, which may significantly impact the carcinogenic process.

1.6.1 Tumor-stroma interaction during cancer progression: effect of nuclear receptors including PPAR β/δ in Cancer-associated fibroblasts (CAFs)

Skin cancers are the most frequently diagnosed cancer worldwide. There are two major types of skin cancer namely the most serious case of malignant melanoma and the

common non-melanoma such as basal cell carcinoma (BCC) and squamous cell carcinoma (SCC). Patients having malignant melanoma often succumb to poor prognosis and mortality if left untreated. Although patients infrequently die from SCC and BCC, these tumours can cause skin disfigurement resulting in social isolation. While earlier studies on cancer were primarily focused on the epithelial carcinoma cells, the contributing role of the tumor stroma is gradually gaining research importance in recent years. Cancer cells often secrete cytokines and growth factors that alter the normal physiological functions of fibroblasts and thus affect nearly every aspect of stroma remodelling and tumor growth^{122,123,184}. On the other hand, the tumor microenvironment not only serves as a passive soil for the seeding and growth of tumor cells ('the seed'), but also plays an active role in influencing the behaviour of tumor cells. As such, a more realistic representation of in vivo conditions would require the analysis of the tumour-stroma interaction.

The complex, dynamic interactions between tumor cells and the surrounding tumor microenvironment play a key role in promoting tumor growth and metastatic progression. The tumor stroma comprises most of the tumor mass in many carcinomas and is characterized by the increased deposition of extracellular matrix^{124,185}. Its volume and composition are partly governed by the response of stromal fibroblasts (also known as cancer-associated fibroblasts, CAF) to the cytokines/signals that are released by the cancer cells. As a major component of the tumor stroma, CAFs are recognized as prominent modifiers of cancer progression. CAFs are large spindle shaped mesenchymal cells that can be identified based on the combination of different markers such as the expression of α -smooth muscle actin, fibroblast activation protein, fibroblast-

specific protein-1, neuron-glia antigen-2 and PDGF β -receptor¹²³. Previous studies comparing CAFs with normal fibroblasts showed that CAFs promote carcinogenesis in non-tumorigenic epithelial cell and support in vivo tumor growth^{184,186,187}. This effect was only observed with CAFs but not with normal fibroblasts suggests an exclusive role of CAFs in promoting tumor growth¹⁸⁴. In addition, CAFs dissected from human tumor biopsies revealed a contrasting microarray transcriptional profile from isolated cultured CAFs and normal fibroblasts. This suggests that CAFs should not be studied in isolation, given the indispensable paracrine influence from their counterpart tumor cells¹⁸⁸.

Cancer-associated fibroblasts are an established source of classical growth factors known to possess a tumor-promoting role, for example epidermal growth factor, transforming growth factor- β and hepatocyte growth factor¹²³. In fact, majority of current research on CAFs has been focused on the secretion of pro-tumorigenic signals^{185,189}. Recent works showed that targeting platelet-derived growth factor (PDGF) signalling in CAFs can delay the progression and decrease growth of invasive carcinomas^{190,191}. Using a PDGF receptor tyrosine kinase inhibitor to block PDGF signalling also decrease the expression of fibroblast growth factor-2, a potent angiogenic factor and keratinocyte growth factor¹⁹². A similar paracrine signalling was also demonstrated in CXCL12 chemokine expressing CAFs, where binding of CXCL12 to receptor on epithelial cancer cells enhanced their proliferation¹⁹³. A direct pro-metastatic effect of CAFs was also been shown in experiments where different fibroblasts were co-injected with tumor cells^{125,194}. By contrast, very little is known about the transcription factors that are important for CAF phenotype. In addition, the signalling pathways that result in gene expression changes and coordinated tumor-promoting responses are also unclear. To develop therapeutic

approaches that focus on containing cancer as a chronic and innocuous disease, both tumor cells and CAFs need to be targeted. A better understanding of the role of nuclear receptors (NRs) in CAFs, which feed tumor growth, may identify specific NRs as potential pharmacological targets against this deadly biological event.

1.6.1.1 Reduced expression of PPAR β/δ in fibroblast results in increased A5RT3 proliferation

Most of these studies have been restricted to the cancerous epithelial cells and the expression profile of NRs in CAFs is unknown. Using organotypic co-culture (OTCs) of human metastatic skin squamous cell carcinoma (A5RT3) with either CAFs or normal dermal fibroblasts (NFs), we first compared the NRs expression profiling of CAFs from NFs. In line with the above-mentioned objective, gene expression of 48 NRs was determined with qPCR analyses performed on mechanically separated dermis equivalents of OTCs. The result revealed that 24 NRs including 12 orphan receptors (eg. PPAR γ , RAR β and RXR) were up-regulated in CAFs comparing to NF. Three NRs namely PPAR β/δ , VDR and GR were down-regulated while the remaining 21 NRs were neither detected nor changed (Fig. 20). These data suggested a unique NRs profiling in CAFs.

To provide supporting evidence that the epithelial tumor-CAFs interactions are operative in the OTC and can reliably preserves the CAFs phenotype. The expression of few NRs was verified by performing qPCR analysis of laser microdissected stromal fibroblasts from the peri-normal tissue (PNFs) and squamous cell carcinoma (CAFs) (Fig. 21A). Consistent with our above results, CAFs had reduced PPAR β/δ expression, increased PPAR β/δ expression and no significant change in PPAR β/δ expression when

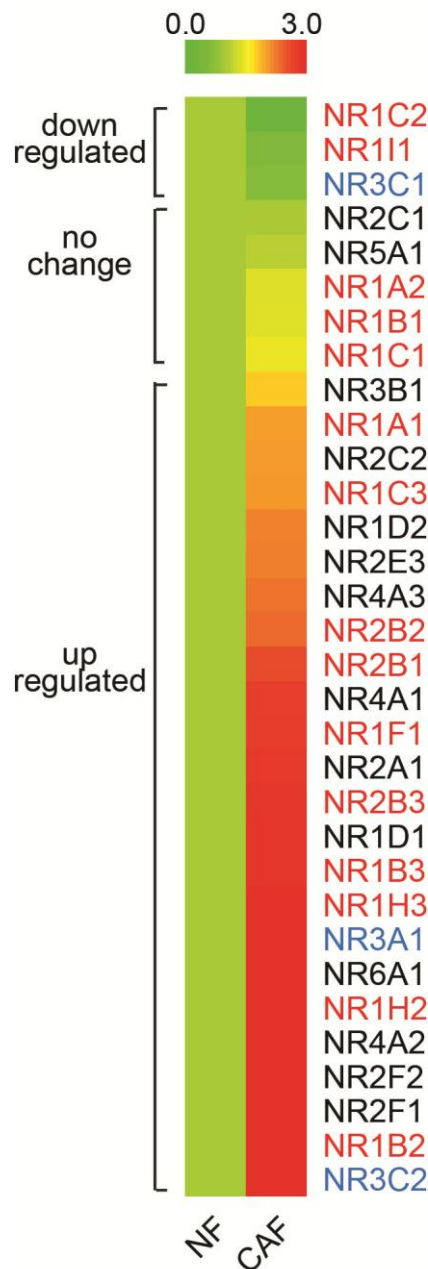


Figure 20. Heatmap shows changes in gene expression of 48 nuclear receptor (NRs) in normal skin fibroblasts (NF) or cancer-associated fibroblasts (CAFs).

NFs and CAFs were isolated from normal human skin and skin squamous cell carcinoma biopsies, respectively, via the explant method. Following organotypic co-culture with HaCaT-ras A5RT3, a human metastatic skin squamous cell carcinoma (Muller et al, 2001; kindly provided by German Cancer Research Center), we examined the expression profile of 48 NRs in these two types of fibroblasts. This organotypic culture allows for the epithelial tumor-CAF communication and fibroblasts of <3 passages were used. NRs that functions as homodimers (blue) and those that partners with retinoid X receptor (NR2B1-3) are indicated in red. Orphan receptors are denoted in black. Data are mean \pm SD, $n = 3$

compared to PNF (Fig. 21B). Our previous data showed that sIL-1ra is a direct PPAR β/δ target gene in the fibroblasts. To this end, we examined the expression of sIL-1ra in CAF. Consistent with the role of PPAR β/δ in regulating epithelial-mesenchymal via IL-1 signaling, we observe a reduced expression of sIL-1ra in CAF when compared with PNF.

To provide further evidence that reduced PPAR β/δ in fibroblasts results in increased tumor epithelial proliferation, two OTCs were constructed using A5RT3 keratinocyte with either control (F_{CTRL}) or PPAR β/δ -knockdown ($F_{PPAR\beta/\delta}$) fibroblasts. We accessed the knockdown efficiency of PPAR β/δ expression in normal human dermal fibroblasts by lentivirus-mediated siRNAs using qPCR and immunoblot analyses. qPCR revealed a >90% reduction of PPAR β/δ expression in cells transduced with the siRNA PPAR β/δ 11 sequence as designed in table 1 (Fig. 19A, left panel). Consistent with this result, immunoblot analysis showed negligible levels of PPAR β/δ protein in the transduced cells (Fig. 22A, right panel) The A5RT3/ $F_{PPAR\beta/\delta}$ OTCs with reduced levels of PPAR β/δ displayed a higher mean number of Ki67-positive cells with respect to the control OTC (Fig. 22B) and increased cyclin D1, PCNA expressions (Fig. 22C). Altogether, these results revealed a potential proliferation stimulatory effect of reduced PPAR β/δ in CAFs on the tumour epithelial growth.

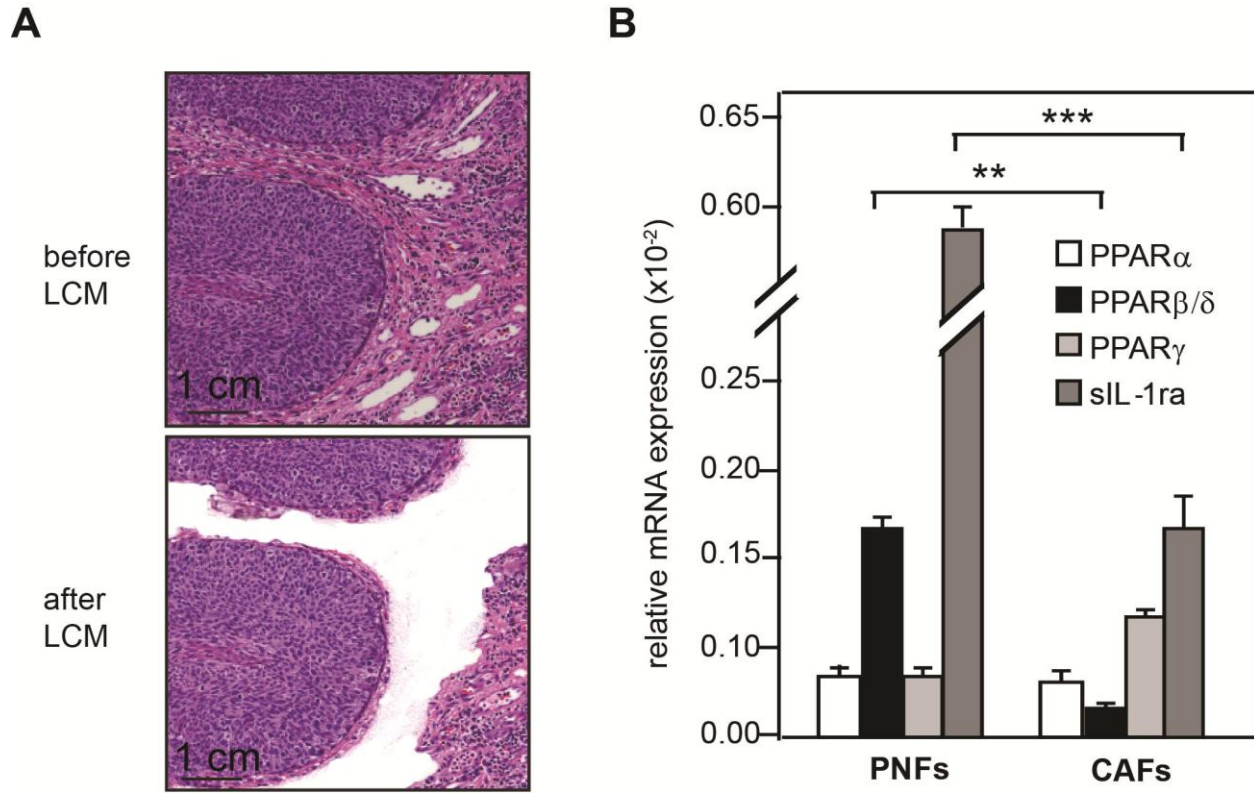


Figure 21. Reduced PPAR β/δ and sIL-1ra in cancer-associated fibroblasts.

(A) H&E images of squamous cell carcinoma before and after laser capture microdissection (LCM) using PALM Microbeam (Carl Zeiss). (B) Relative expression of PPAR α , PPAR β/δ , PPAR γ and sIL-1ra in stromal fibroblasts from peri-normal tissue (PNFs) and squamous cell carcinoma (CAFs). Expression levels were normalized with control ribosomal protein P0 mRNA. ** denotes $p < 0.01$; ***, $p < 0.001$. Data are mean \pm SD, $n = 3$

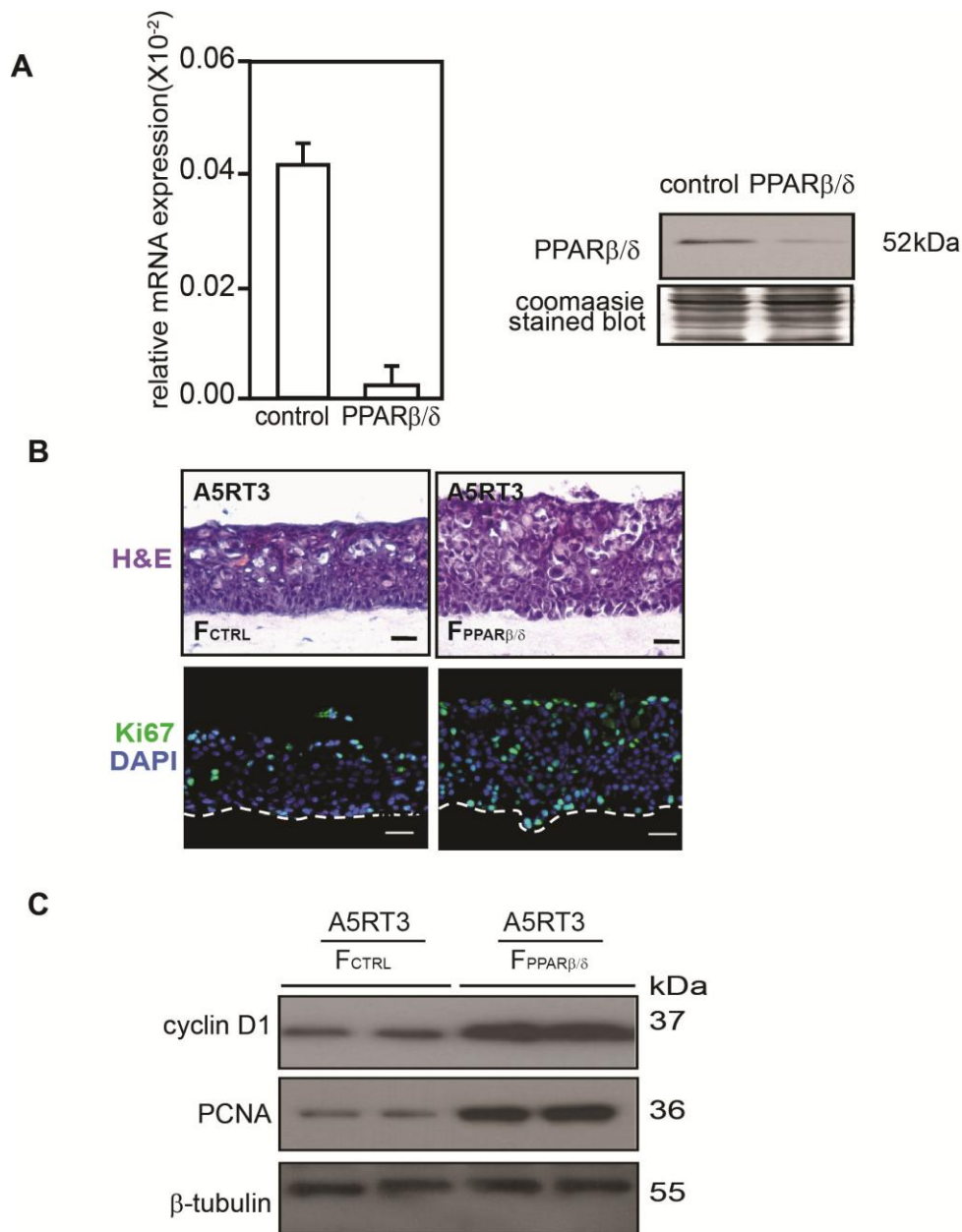


Figure 22. PPAR β/δ -deficient fibroblasts increase epithelial tumor cell proliferation.

(A) Normal human fibroblasts were transduced with a lentiviral vector harboring a control (F_{CTRL}) or PPAR β/δ (F_{PPAR β/δ}) siRNA. Efficiency in suppressing PPAR β/δ mRNA (left) and protein (right) expression were determined by qPCR and immunoblot, respectively. **(B)** F_{PPAR β/δ} potentiates the growth of human squamous cell carcinoma cell line (HaCat-A5RT3) in organotypic coculture (OTC). H&E staining revealed a thicker epithelial layer associated with a higher number of Ki67-positive proliferating cells. Scale bar denotes 20 μ m. **(C)** Immunoblot analysis of the tumor epithelia from OTC with proliferation markers, PCNA and cyclin D1. β -tubulin showed equal loading and transfer.

1.6.1.2 Organotypic culture with $F_{PPAR\beta/\delta}$ show increased expression of mitogenic factors

Earlier studies have shown that ligand-activated PPAR β/δ stimulated the differentiation of human keratinocytes in monolayer cultures. In this study, the autocrine and paracrine consequences of PPAR β/δ deficiency during human epidermis formation using the organotypic skin culture (OTC) model were examined. In this skin reconstruction assay, keratinocytes were cultured on a collagen matrix containing dermal fibroblasts

The paracrine effect of $F_{PPAR\beta/\delta}$ on epidermal proliferation is likely mediated by changes in the production and secretion of mitogenic or anti-mitogenic factors by the fibroblasts. To understand the mechanism underlying the enhanced epidermal proliferation in OTC with $F_{PPAR\beta/\delta}$, an unbiased protein array was done. Inflammatory cytokine and growth factor arrays were used to compare conditioned media from OTCs reconstructed using wildtype keratinocytes with either F_{CTRL} or $F_{PPAR\beta/\delta}$. A total of 76 distinct proteins were screened and the results showed that the protein expression of several mitogenic factors and cytokines were increased in OTC with $F_{PPAR\beta/\delta}$ (Table 4). Notably, most of the proteins whose expression was increased have a known mitogenic action on keratinocytes. The expression of transforming growth factor- β 1 (TGF- β 1), which exerts a pronounced anti-proliferative effect on keratinocytes, and the highly abundant IL-1 α , constitutively produced by keratinocytes, remained unchanged. The expression of two pro-angiogenic factors, namely vascular endothelial growth factor (VEGF) and placental growth factor (PIGF), were reduced in OTC with $F_{PPAR\beta/\delta}$ when compared to F_{CTRL} .

Table 4: Relative fold change in growth factors/ cytokines expression in HaCaT-A5RT3 OTCs with $F_{sIL-1\alpha}$ compared to HaCat-A5RT3 OTCs with F_{CTRL} .

Growth Factors/Cytokines	relative fold increase ^A
IL-6	1.60*
IL-8	1.69**
FGF-4	1.67**
PDGF-AA	1.76**
NT-4	1.78*
MCP-1	1.86**
GDNF	1.89*
TIMP-2	1.91**
SCF	2.00**
bFGF	2.01**
VEGF	2.04**
IGFBP-1	2.13**
HGF	2.24**
IL-6aR	2.39**
M-CSF	2.66**
GMCSF	2.69*
FGF7	2.96*
HB-EGF	2.97**
TGF-b1	3.04**
PDGF-BB	3.04**
I-309	3.23**
TNF-a	3.49**
IP-10 ^B	0**
IL-15 ^B	0**

Growth Factors/Cytokines	relative fold decrease
IL-12 p70	0.46*
MIP-1d	0.46*
IL-17	0.38**
IL-16	0.35**
MIP-1a	0.32**
IL-3	0.28**
Eotaxin	0.09**
IL-2 ^C	0**
IL-4 ^C	0**

^AThe intensities of signals were quantified by densitometry. Positive control in the array blot, as provided manufacturer, was used to normalise the results from different membranes being compared. Values obtained from the control OTC derived using HaCaT-RT3 (RT3) squamous cell carcinoma and F_{CTRL} fibroblasts were arbitrarily assigned a value of 1. Values represent the mean fold increase as compared to control OTC (n=4). ^B and ^C denote not detected in RT3/ F_{CTRL} and RT3/ $F_{sIL-1\alpha}$ OTC, respectively. * denotes $p < 0.01$ and ** $p < 0.001$.

To further investigate the effect of reduced PPAR β/δ in the fibroblasts on epithelial growth *in vivo*, the Cre-Lox technology in mice can be employed to conditionally knockout PPAR β/δ in the fibroblasts. This mice model will clarify the impact of PPAR β/δ knockout fibroblasts or CAF, which was shown to have reduced PPAR β/δ expression, on the adjacent epithelial growth. It is hypothesized that these conditional knockout mice will be more susceptible to proliferative effect in the epithelial layer upon chemical inductions.

1.6.1.3 Expression Profiles of Nuclear Receptor in CAFs from Squamous Cell Carcinoma.

The NRs expression profiling of CAFs has revealed unique changes in their expression. We will extend our expression profiling of all 48 nuclear receptor to at least 4 more CAFs using quantitative real-time PCR (qPCR). This will allow a firm conclusion about their expression levels in CAFs in skin SCCs and importantly provide pertinent information of specific NRs as potential targets. Human skin SCCs will be procured by dermatologists in National Skin Centre, Singapore and we will isolate the CAFs as previously described¹⁹⁵. CAFs isolated from patient biopsies will also be obtained from asterand. These CAFs will be co-culture with A5RT3 to establish the essential epithelial-mesenchyme communication. After one week of co-culture, we will perform NR expression profiling of CAFs. To underscore the relevance of the NR expression profile, qPCR will be performed on stromal fibroblast micro dissected from at least 3 archived SSCs. These findings aim to reveal a detail and relevant expression profile of nuclear receptors in cancer-associated fibroblasts.

1.6.1.4 Effect of Modified CAFs on the Adjacent Tumour Growth using Organotypic Co-culture.

To unravel the functional roles of NRs, we can perform either over-expression or knock-down of nuclear receptors in CAFs. We hypothesized that the ectopic expression of the gene, if it was down-regulated in CAFs, can attenuate epithelial tumour growth. Similarly, a RNA interference (RNAi) approach could be adopted to shut down the expression of the highly expressed NRs. As a proof of concept, our studies showed that the deficiency of PPAR β/δ in the fibroblasts can modulate the adjacent tumour cell proliferation. Herein, we refer to these CAFs, either over-expressing a specific NR or whose endogenous expression of NR is suppressed by RNAi, as modified CAFs. We will either over-express or knockdown the expression of NRs using a lentiviral method. The efficiency of over-expression and suppression will be verified by qPCR and Immunoblot analysis. These modified CAFs will be used to construct OTC with A5RT3 tumour cell. The apoptotic and proliferation indexes will be determined by immunofluorescence analysis using TUNEL and anti-Ki67, respectively. We will also perform growth factors and phosphoprotein arrays to map out the underlying mechanism for the paracrine tumour-promoting or anti-tumor effects, as a consequence of overexpression or deficiency in a specific NR in CAFs. A better understanding of the role of NRs in CAFs, which feed tumour growth, may identify specific NRs as potential pharmacological targets against this deadly biological event.

1.6.2.4 Orthotropic Surface Transplantation Assay in Nude Mice

The transplantation model is considered the most reliable test to identify normal epithelia physiology as well as alterations in growth and differentiation associated with malignant transformation *in vivo* condition. The particular technique exploits hat-shaped silicone transplantation chambers that protects the graft from desiccation and isolate it from contiguous host epidermis. This transplantation method offers several advantages when compared with the subcutaneous injection of a mixture of tumour cells and CAFs. Among others, early mesenchymal events, such as granulation tissue formation and angiogenesis can be studied in detail. In general, the graft consists of a preformed monolayer of tumour cells on a CAFs-embedded collagen matrix that separates it from

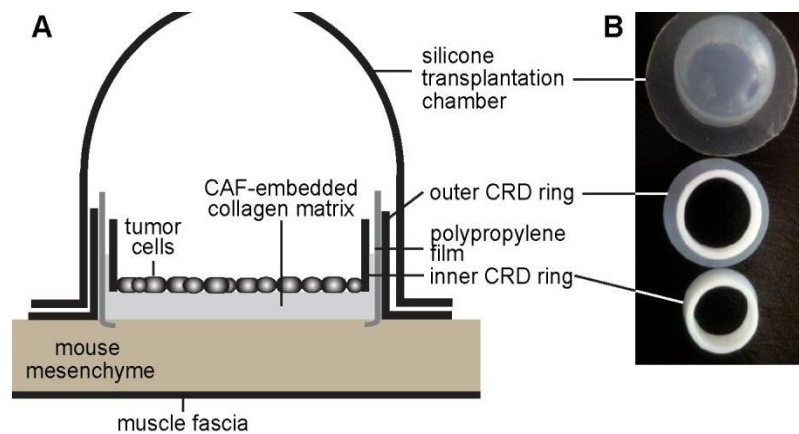


Figure 23. Graft transplantation assay.

(A) Schematic cross sections through a transplantation system of tumor cells implanted as an early organotypic culture on a cancer-associated fibroblast (CAF) embedded collagen matrix that separates the tumor epithelia and the mesenchyme. (B) Components of the Combi-Ring-Dish (CRD) transplantation chamber. The Teflon inner (8.5mm inner diameter, thickness 2 mm) rings are indicated. Silicone transplantation chamber (inner diameter: 12mm; outer diameter: 24mm; height: 10.7 mm).

the mouse mesenchyme (Fig. 23). After 4-6 weeks post-transplantation, focused gene expression profile of a panel of genes relevant to tumourigenesis will be performed.

The long term objective of this project is to identify nuclear receptors in cancer-associated fibroblasts (CAFs) that can elicit tumour-promoting or anti-tumour paracrine effects, and whose expression patterns correlates with those seen in human disease. The expected benefit is to target specific NRs in the CAFs, aiming to prevent or reverse the behaviour and functions of CAFs in order to contain the early transformation of cancer cells or to cause them to regress.

CHAPTER 2: REGULATION OF EPITHELIAL-MESENCHYMAL NITRIC OXIDE SIGNALING BY ANGIOPOIETIN-LIKE 4 ACCELERATE CUTANEOUS WOUND HEALING IN DIABETIC MICE

Publication:

Chong, H.C., Chan J. S., Goh, C.Q., Gounko, N.V., Luo, B.W., Wang, X.L., Foo, S., Wong, M.T.C., Choong, C., Kersten, S. and Tan, N.S. (2014) Angiopoietin-like 4 stimulates STAT3-mediated iNOS expression and enhances angiogenesis to accelerate wound healing in diabetic mice. *Mol. Ther.* 2014 Jun 6. Doi: 10.1038/my.2014.102 [Epub ahead of print]

HCC designed, performed, and analysed the experiments in this study, with intellectual input from NST. XW and SF performed some animal studies and provided technical help. CQG, NVG, and BL performed electron microscopy. MTCW and CC contributed patient material for analysis and provided intellectual input. NST provided overall coordination with respect to the conception, design, and supervision of the study. **HCC** and NST wrote the manuscript with comments from co-authors

Supporting Publications:

Goh, Y.Y., Pal, M., **Chong, H.C.**, Zhu, P.C., Tan, M.J., Punugu, L., Lam, C.R.I., Yau, Y.H., Tan, C.K., Huang, R.L., Tan, S.M., Tang, M.B.Y., Ding, J.L., Kersten, S. and Tan, N.S. (2010). Angiopoietin-like 4 interacts with integrins $\beta 1$ and $\beta 5$ to modulate keratinocyte migration. *Am. J. Pathol.* 177(6):2791-2803.(IF: 5.224).

Goh, Y.Y., Pal, M., **Chong, H.C.**, Zhu, P., Tan, M.J., Punugu, L., Tan, C.K., Huang, R.L., Sze, S.K., Tang, M.B., Ding, J.L., Kersten, S. and Tan, N.S. (2010). Angiopoietin-like 4 interacts with matrix proteins to modulate wound healing. *J. Biol. Chem.* 285(43): 32999-33009. (IF: 5.328)

Sections contributed by the candidate: **HCC** performed all the animal experiments inclusive of all wound biopsies analysis, laser capture microdissections and proximity ligation assay in these two studies. **HCC** also performed molecular cloning and purification of all the ANGPTL4 proteins which are used for interaction studies.

A review paper had also been published in an open access journal, Journal of Oncology by Hindawi Publishing Corporation in year 2012.

Chong, H.C., Tan, C.K., Huang, R.L. and Tan, N.S. (2012). Matricellular Proteins: A Sticky Affair with Cancers. *J. Oncol.* doi:10.1155/2012/351089.

HCC, CKT and RLH wrote the manuscript and prepared the figures. NST revised the manuscripts.

2.1 ABSTRACT

Poor healing diabetic wounds are prone for infections and effective therapies have been lacking. Recent identified matricellular protein, Angiopoietin-like 4 (ANGPTL4), is up-regulated during normal wound healing and has been implicated in angiogenesis and vascular permeability. ANGPTL4 can interact with specific matrix proteins preventing their degradation, and affects cell-matrix communication by altering the availability of intact matrix proteins. ANGPTL4-null mice have delayed wound re-epithelialization, reduced matrix proteins expression, increased inflammation and impaired wound-related angiogenesis, which are characteristics of diabetic wounds. However, its expression and role in diabetic wound repair remains unclear. Here we examined the impact of ANGPTL4 on diabetic wound healing and identified possible regulation of ANGPTL4 expression. Using diabetic mouse model, we found that diabetic wound has altered expression of ANGPTL4 as compared to normal wound. Furthermore, topical application of recombinant ANGPTL4 enhanced diabetic wound closure, re-epithelialization, wound angiogenesis and tissue granulation. Importantly, focused gene expression profiling revealed that treatment with ANGPTL4 can restore majority of the dysregulated temporal and expression levels of cytokines, growth factors and transcription factors observed in diabetic mice wounds. Our study suggested that replacement of ANGPTL4 provide adjunctive or new therapeutics avenues in diabetes-associated complications, such as diabetic foot ulcers.

2.2 INTRODUCTION

2.2.1 Diabetes wound repair

Type 2 diabetes mellitus (DM) is a chronic metabolic disorder, and its global prevalence has been steadily increasing. DM is most likely one of the oldest diseases known to mankind. The first reported case of diabetes is found in an Egyptian manuscript from approximately 3000 years ago¹⁹⁶. The first distinction between type 1 and type 2 DM was made in 1936¹⁹⁷. Type 2 DM (formerly known as non-insulin dependent DM) is characterized by insulin insensitivity due to insulin resistance, declining insulin production, and the failure of pancreatic beta-cells¹⁹⁸. This leads to a decrease in glucose transport into the liver, muscle cells, and fat cells accompanied by an increase in fat breakdown and hyperglycemia. The involvement of impaired alpha-cell function has recently been recognized as an important component of the pathophysiology of type 2 DM¹⁹⁸. Due to this dysfunction, the glucagon and hepatic glucose levels that rise during fasting are not suppressed with a meal¹⁹⁹. The inadequate insulin levels and increased insulin resistance combine to produce hyperglycemia¹⁹⁹. The majority of individuals suffering from type 2 DM are obese, with central visceral adiposity. Therefore, adipose tissue is also believed to play a crucial role in the pathogenesis of type 2 DM because elevated non-esterified fatty acid concentrations or ectopic fat storage syndrome (deposition of triglycerides in muscle, liver and pancreatic cells) can produce insulin resistance and beta-cell dysfunction¹⁹⁹. Type 2 DM can result from interactions among genetic, environmental and behavioral risk factors^{200,201}. People with type 2 DM are more vulnerable to a variety of short- and long-term complications that often lead to their premature death. The increased morbidity and mortality in patients with type 2 DM are caused by its insidious onset and late diagnosis. As a result of this

tendency, it is fast becoming an epidemic in some countries, and the number of affected people is expected to double in the next decade. This will further add to the already existing burden on healthcare providers, especially in poorly developed countries.

Chronic, non-healing foot ulcers are a significant problem for patients with diabetes. A quarter of the patients suffering from this low extremity ulcers will eventually undergo amputation. Neuropathy (mainly the loss of cutaneous sensory nerves) combined with the association of uncontrolled hyperglycemia is a major predictor of diabetic ulcer formation²⁰². Blood lipid abnormalities associated with insulin resistance can also lead to severe vasculopathy in foot ulcers²⁰². These can affect the immune response against any infection when the skin barrier is breached and the healing response is adversely affected. The healing of an acute wound follows a predictable chain of events (refer to section 1.2.2). This chain of events occurs in a carefully regulated fashion that is reproducible from wound to wound. The phases of wound healing are overlapping, but are described in a linear fashion for the purpose of clarity. The phases that characterize wound healing include the inflammatory phase, the cellular migration and proliferation phase, and the wound contraction and remodeling phase¹¹. Diabetic wounds are characterized by the accumulation of devitalized tissue, increased/prolonged inflammation, poor wound-related angiogenesis and deficiencies in the ECM components²⁰². Diabetic wounds show elevated levels of matrix metalloproteinases (MMPs), increased proteolytic degradation of ECM components, and the inactivation of growth factors. Together, these characteristics culminate in a corrupt ECM that cannot support healing. Abnormal nitric oxide (NO) production also contributes to the pathogenesis of impaired healing. Cells such as keratinocytes,

fibroblasts and macrophages display dysfunctional expression and responses to many growth factors and cytokines. Thus, these wounds typically are non-responsive to most treatments.

Without question, tissue biopsy or excision is considered the most appropriate sampling method for the collection of clinical samples for research. However, it is difficult to study diabetic wounds in humans because of ethical issue associated with obtaining the diabetic skin biopsies. This procedure is restricted because non-healing wounds may require long term care, making the sampling itself potentially traumatic to the patient. For this reason, many of the diabetic wound studies completed to date have been carried out in diabetic mouse models with characteristics that are somewhat similar to humans.

2.2.2 Mouse models of diabetes

Ideally, more than one mouse model should be used to represent the diversity seen in human diabetic patients. Mouse models for type 1 diabetes are derived from animals with either spontaneously developing autoimmune diabetes or chemical deletion of the pancreatic beta cells²⁰³. Type 2 diabetes models can be derived from mice that are either obese or non-obese with varying degrees of insulin resistance and functional failure of the Beta islet cell²⁰⁴. These mice exhibit syndrome of insulin resistance and type 2 diabetes with characteristics somewhat similar to humans. However, no single animal model of type 2 diabetes can recapitulate the full range of clinical features. Further research was needed to develop an extremely useful model to study the pathogenesis of type 2 diabetes and test potential therapeutic strategies.

2.2.2.1 Mutant genes causing diabetes-obesity syndromes in mice

Most of the current mice models of type 2 diabetes are obese due to the closely related link between obesity and diabetes. Obesity can be the result of genetic manipulation or induced by high fat feeding. Although obesity in humans is rarely caused by a single gene mutation, single gene mutation mice models of obesity are commonly used in type 2 diabetes researches. The commonly used single gene mutation models of obesity are defective in leptin signalling. Leptin induces the sensation for one to experience satiety, and thus, a lack of functional leptin in these animals causes increased appetite resulting in obesity. These models include the Lep^{ob/ob} mouse, which is deficient in leptin and the Lepr^{db/db} mouse, which is deficient in the leptin receptor. These models are often used to test new therapies for type 2 diabetes^{205,206}.

The Lep^{ob/ob} mouse is a model of severe obesity. It was first discovered as a spontaneous mutation in an outbred colony at Jackson Laboratory in 1949. This phenotype was bred into C57BL/6 mice and the mutated protein was identified as leptin²⁰⁷. The weight increase starts at early age, and the mice will eventually develop hyperinsulinaemia. By 4 weeks, hyperglycaemia is apparent, with blood glucose concentrations continuing to rise²⁰⁸. Other metabolic aberrations include hyperlipidaemia, a disturbance in temperature regulation and lower physical activity²⁰⁸. In addition, these mice are infertile and thus mutant mice strain can only be obtained by crossing two heterozygous mice²⁰⁹. The pancreatic islet volume is dramatically increased in these mice. Although there are some abnormalities in insulin release, islets maintain the production of insulin²¹⁰. However this model is not completely representative of human

type 2 diabetes due to the lack of complete beta islet cell failure. The diabetes phenotype in this model is not particularly severe. It should be noted that much more severe diabetes can be developed with regression of islets and can lead to early mortality²¹¹.

The $\text{Lepr}^{\text{db/db}}$ mouse originated from the Jackson Laboratory and is due to an autosomal recessive mutation in the leptin receptor^{212,213}. These animals shared similar phenotype and characteristics as the $\text{Lep}^{\text{ob/ob}}$. They are obese due to increase in appetite, hyperinsulinaemic and hyperglycaemic. Obesity is apparent from 3–4 weeks of age with hyperinsulinaemia and hyperglycaemia developing at 4–8 weeks. These mice develop ketosis after a few months of age and have a relative short lifespan²⁰⁴.

2.2.2.2 Streptozotocin induced diabetic mice

In chemically induced models of type 1 diabetes, the endogenous beta cells are mostly destroyed, and thus, there is little or no production of endogenous insulin. These will eventually lead to hyperglycaemia and weight loss. Chemically induced diabetes provides a simple and relatively cheap model of diabetes in mice. Diabetes is usually induced around a week with a stable hyperglycaemia prior to the start of the experiment. Two main compounds are used to induce diabetes are Streptozotocin (STZ) (2-deoxy-2-(3-(methyl-3-nitrosoureido)-d-glucopyranose) or alloxan^{214,215}. Glucose can compete with alloxan and STZ, due to the similarity in structure to glucose and thus, the mice need to be fasted to increase the efficiency of the chemical^{214,215}. Both alloxan and STZ are relatively unstable for prolonged storage, and thus the chemical solutions should be made fresh prior to injection.

STZ is synthesized by *Streptomyces achromogenes* and can be administered by i.p. or i.v. to mouse to induce diabetes²¹⁵. Once in the bloodstream, STZ enters the pancreatic beta cell through the Glut-2 transporter and causes alkylation of the DNA^{215,216}. Subsequently, the activation of PARP will lead to NAD⁺ depletion, a reduction in cellular ATP and finally ceases the insulin production²¹⁷. In addition, STZ can be a source of free radicals which can contribute to DNA damage and cell death. STZ can be administered as a single high dose or as multiple low doses depends on the type and age of the mouse.

2.2.2.3 Diabetes induced by diabetogens such as alloxan monohydrate

The diabetic inducing effect of alloxan (2,4,5,6-tetraoxypyrimidine; 5,6-dioxyuracil) is mainly attributed to rapid uptake of this chemical by the beta cells and the formation of free radicals, which beta cells have poor defence mechanisms against²¹⁸. Alloxan is reduced to dialuric acid and then re-oxidized back to alloxan, creating a redox cycle for the generation of superoxide radicals and highly reactive hydroxyl radicals that cause DNA fragmentation of beta cell²¹⁶. Alloxan can also be taken up by the liver, but it has better protection to reactive oxygen species and thus not as susceptible as the beta cells^{219,220}. Doses used in mice range from 50 to 200 mg/kg, depending on the strain and the route of administration with i.p and s.c. administration requiring up to three times as high a dose as the i.v. route²¹⁶. It should be noted that alloxan has a narrow diabetogenic dose, and even light overdosing can cause general toxicity, especially to the kidney²¹⁶.

2.2.2.4 Type 2 diabetes mellitus in mouse model induced by high fed diet

The model of high fat feeding to C57BL/6 mice was first described in the early 80s²²¹. High fat feeding can lead to obesity, hyperinsulinaemia and altered glucose homeostasis due to insufficient compensation by the islets²²². Normal chow (on a caloric basis usually around 26% protein, 63% carbohydrate and 11% fat) is exchanged for a diet where the number of calories from fat is increased significantly (around 58% of energy derived from fat). The amount of food intake by the mice should be monitored to ensure that they do not compensate by eating less. It has been shown that high-fat-fed mice can weigh more than normal chow fed controls within a week after introducing the diet²²². The weight gain is associated with insulin resistance and lack of insulin production by the beta cell for compensation leads to impaired glucose tolerance.

Since the obesity is contributed by environmental factors rather than genes, it is believe to model the human situation more accurately in this high fed induction than genetic models of obesity-induced diabetes. High fat feeding is often used in transgenic or knock-out models, which may not show an overt diabetic phenotype under normal conditions, but when the beta cells are forced to work harder, the gene may be shown to be of importance. It should be noted that the background strain of the mice can determine the susceptibility to diet-induced metabolic changes, and thus, effects could be missed if a more resistant strain is used²²³. It has been reported that there is even heterogeneity of response to high fat feeding within the inbred C57BL/6 strain, indicating that differential responses to a high-fat diet are not purely due to the mice genetic background²²⁴.

2.2.3 Topical therapeutic strategies for treating diabetic wound

Diabetes is a multisystem disorder that affects the wound healing process. Physiological changes in tissues and cells may delay healing, and diabetes can also produce a range of complications, including neuropathy and ischaemia, which may lead to foot ulceration²⁰². Patients with unhealed ulcers have an increased risk of infection, and lower-limb amputation is usually preceded by foot ulceration. A diabetic foot ulcer (DFU) is defined as a full thickness wound occurring below the ankle in a diabetic patient, regardless of its duration. It is characterized by a loss of epithelium extending into or through the dermis and into deeper tissues. These chronic ulcers fail to progress through an orderly and timely sequence of repair and are thus slow to heal²⁰². They commonly develop at pressure points on the plantar surfaces, over the metatarsal heads, on the big toe, and on the heels.

To effectively manage these problems and to create a healthy physical and biochemical environment for the promotion of healing, one must understand the disease complications and healing process. Standard wound care management includes surgical debridement, the treatment of infections and local wound care²²⁵. Wound care typically involves cleansing with saline and the use of wound dressings that promote a moist environment. Consideration should be given to revascularization, if necessary, and to controlling the serum glucose levels and arterial risk factors, such as hypertension and dyslipidemia²²⁵. Although topical treatment is an important aspect of wound care, it is considered secondary to surgical and systemic care. Much effort has focused on discovering effective recombinant growth factors for the topical treatment of DFUs. Given that the targets of members of the EGF, FGF, PDGF, and TGF- β families

participate in the dermal wound repair process, it is logical to use these growth factors in the drug development strategies for treating DFUs. With one notable exception (PDGF-BB or becaplermin), the drug development effort can be considered a failure for several reasons²²⁶. Perhaps the most significant reason is that these growth factors typically target a single biological process that is essential for wound healing. To date, the only growth factor approved by the US Food and Drug Administration for the treatment of diabetic foot ulcers is recombinant PDGF-BB (becaplermin), which comes as a topical cream. PDGF-B is known to be a potent mitogen and chemotactic agent for stromal cells and may increase the wound vascularization by stimulating angiogenesis²²⁶. Thus, there is an urgent need for better, new or adjunctive treatments.

2.2.4 Nitric oxide and wound healing

Nitric oxide is a free radical that is formed from the terminal guanidino nitrogen atom of arginine²²⁷. The guanidino nitrogen accepts five electrons in an oxidation process requiring molecular oxygen, resulting in formation of NO and citrulline²²⁷. Nitric oxide synthases are homodimeric enzymes responsible for this conversion. Tetrahydrobiopterin, flavine mononucleotide (FMN), flavine adenine dinucleotide (FAD), nicotinamide-adenine-dinucleotide phosphate (NADPH), and oxygen are required as co-factors for full nitric oxide synthase activity^{227,228}. NO synthases exist in three distinct isoforms: two constitutive (endothelial and neuronal) isoforms and one inducible isoform. The constitutive isoforms are permanently active, generating low concentrations of NO, and they are regulated by intracellular calcium fluxes or exogenous calmodulin. The expression, transcription, and function of the inducible isoform (iNOS) are induced by a

variety of cytokines, growth factors, and inflammatory stimuli on target cells. iNOS activity leads to the release of NO levels that are greater than those generated by the constitutive isoforms. Excessively high amounts of NO formed by the inducible isoform can contribute to the detrimental effects in inflammatory situations²²⁹. The inducible isoform of NO synthase is also expressed during wound healing^{230,231}.

As NO is unstable and difficult to measure directly, stable metabolites are used as substitutes for NO formation. Nitrite and nitrate are two widely used stable end products that can be measured in wound fluid. However, non-enzymatic NO formation can still occur; therefore, these measurements may not translate to the equimolar formation of NO. Several other direct or indirect detection methods can also be performed, such as immunohistochemistry, direct measurements of the enzyme content and/or activity, assessment of the peroxynitrite formation in tissue, and gene expression studies.

NO production or iNOS expression is high during the early phases of wound healing. It is conceivable that the majority of NO synthesis is due to the inflammatory cells present during the early phase of healing, especially macrophages^{232,233}. Other cell types, such as fibroblasts, keratinocytes, and endothelial cells, may also contribute to NO synthesis²³⁴⁻²³⁷. The overall time course of iNOS activity and NO generation during wound healing has to be viewed as a decreasing curve over time^{235,238}. Presumably, iNOS activity can be downregulated by the resolution of the inflammatory response or by cytokine signaling. It is likely that bacterial infected wounds with continued inflammatory responses could continue the production of NO, but this has not been studied directly²³². The *in vitro* signals of iNOS induction have been well studied;

however, little is known of the *in vivo* signals during wound healing. Of the numerous cytokines and growth factors secreted and released into the wound environment, interleukin-1, tumor necrosis factor-alpha (TNF- α), and INF- γ are the most likely iNOS inducers²³⁹. TGF- β 1 is one of the strongest iNOS inhibitors during wound healing²³³. However during wound healing there is negative regulation of NO synthesis where the presence of unknown factors reduces iNOS activity, and not by the depletion of substrate²⁴⁰.

Nitric oxide has been shown to inhibit activation of caspases and thereby prevent apoptosis²⁴¹. At high concentration, NO is cytostatic to multiple cell types such as endothelial and fibroblasts²³⁴. Conversely, recent evidence suggests that NO can stimulate cell proliferation at low concentration^{242,243}. The mechanism of action by which NO influences wound healing remains unclear. However, there are data suggesting that at least some effects of NO on wound healing might be systemically mediated. For examples, studies have shown that arginine-free nutrition inhibits LPS-induced NO synthesis at the wound site²⁴⁴. Nitric oxide mediates inflammation induced edema formation and inhibits cell invasion into tissue^{245,246}. The effect of NO on wound healing is not necessary iNOS-mediated as it is also demonstrated that eNOS knock-out mice present an impaired healing phenotype too²⁴⁷. High concentration of iNOS inhibitors can have a lethality effect on the cells²⁴⁸.

Studies of fibroblasts derived from keloids and hypertrophic scars demonstrate low constitutive NOS expression, thus stimulating higher cell proliferation, which is responsible for the high cellularity that is characteristic of these disorders. Keratinocyte proliferation is iNOS-dependent²⁴⁹, and wound reepithelialization is also NO-dependent,

likely mediated indirectly through vascular endothelial growth factor (VEGF) signaling²⁵⁰. Interestingly, the induction of iNOS in keratinocytes is paralleled by the induction of GTP-cyclohydrolase I, the rate-limiting enzyme for tetrahydrobiopterin formation, which is essential for full iNOS activity²³⁵. Nitric oxide has been shown to increase angiogenesis in ischemic murine tissues, whereas eNOS inhibitors impair angiogenesis in granulation tissues. Vascular endothelial growth factor, a potent angiogenic growth factor, is closely linked to NO; VEGF increases NO production at the gene expression level^{251,252}, and the angiogenic effect of VEGF appears to be dependent on NO^{253,254}. It has also been shown that NOS blockade prevents VEGF production, VEGF-induced endothelial cell proliferation, and VEGF-mediated activation of mitogen-activating protein kinase²⁵⁵. Endothelial cell migration, endothelial cell adhesion, and endothelial organization are all dependent on NO via VEGF^{237,256-258}, which is produced by keratinocytes during wound healing²⁵⁹. Feedback mechanisms act by downregulating PKC-induced VEGF expression²⁶⁰. Collagen synthesis during wound healing can be correlated with NO synthesis. Matrix synthesis is impaired by iNOS inhibition, whereas NO administration and iNOS transfection enhance matrix synthesis²⁶¹⁻²⁶³. Furthermore, wound-derived fibroblasts are characterized by a distinct phenotype, where the endogenous iNOS expression correlates with an increased level of collagen synthesis²³⁰. Excisional wound closure can be delayed by iNOS inhibition in which NO induces keratinocytes migration²⁴⁵. Wound healing is characterized by the organized secretion of growth factors. NOS-KO mice showed delay excisional wound healing and alterations in wound healing related cytokines, such as basic fibroblast growth factor (bFGF), TGF- β 1, TNF- α VEGF and IL-4²⁶⁴. Thus, the depletion of iNOS gene expression can alter wound

cytokine expression; however, little is known about whether NO can directly affect growth factor and cytokine secretion, activation, and time of action.

2.2.5 The role of matricellular proteins in wound healing

Matricellular proteins form a group of extracellular matrix (ECM) proteins that do not serve a primary structural role but function rather as modulators of cell-matrix interactions²⁶⁵. Members of the group, including thrombospondin (TSP) -1, TSP-2²⁶⁶, SPARC²⁶⁷, tenascin (TN)-C²⁶⁸, osteopontin (OPN)²⁶⁹, CCN-1 (cyr 61)²⁶⁵ and the recently discovered angiopoietin-like protein 4 (ANGPTL4)^{270,271}, have been shown to participate in a number of processes related to tissue repair. The major ECM constituents include collagen and fibronectins, which serve primarily a structural role in the matrix through the maintenance of structural integrity²⁶⁵. These molecules bind to cytokines, proteases, protease inhibitors and proteins through the bridging from those matricellular proteins²⁶⁵. This forms an ECM reservoir with extensive networks of cytokines that can influence cell migration to the wounded region or direct cell proliferation during wound healing²⁷². Matricellular proteins are usually up-regulated during wound healing, where they modulate interactions between cells and the extracellular matrix to exert control over events that are essential for efficient tissue repair^{272,273}. Studies in knockout mice have indicated that a deficiency in one or more of these matricellular proteins can alter the course of wound healing^{266,267,269,271,274}. Detailed mechanisms regarding individual roles of each matricellular protein, with the exception of ANGPTL4, will not be covered in this thesis (Figure 24) (Instead, please refer to my review article titled “Matricellular proteins: a sticky affair with cancer²⁷⁵,” which is attached for further reading).

There are currently no known clinical applications for matricellular protein-derived treatments in tissue repair. Many matricellular proteins bind to and act synergistically with each other and with ECM proteins. Efficient therapies, therefore, may require the synergistic use of cytokines, matricellular proteins and matrices such fibronectin. With a better understanding of matricellular protein action, we can generate more efficient therapies to improve wound healing and other related diseases

3-3 mediated pathway which modulate cell migration via integrin internalization. **(C)** ANGPTL4 binds specific matrix proteins and delays their degradation by proteases. However, this association does not interfere with integrin-matrix protein recognition unlike TNC. **(D)** ANGPTL4 interacting with integrin activates Rac1 and NADPH oxidase, which generate high level of O_2^- . This will further activating the Src machinery and stimulates its downstream PI3K/PKB mediated cell proliferation and survival pathway. **(E)** ANGPTL4 can trigger vascular disruption by binding to and dispersing vascular-endothelial cadherin (VE-Cad) and claudin-5 at endothelial junctions, via the activation of integrin $\alpha 5\beta 1$ **(F)** Cyr61 can promote cell proliferation and survival through the activation of integrin mediated signaling pathway either by direct binding with integrin or integrin-syndecan4. The downstream intracellular events may be mediated through the FAK/PI3K/PKB signaling pathway, resulting in either activation of the NF- κ B survival pathway or phosphorylation of GSK3 β and nuclear translocation of β -catenin for cell proliferation. **(G)** OPN can interact with several integrins and also CD44 family of receptors. These complexes are able to mediate cell proliferation and survival through PI3k/PKB pathway activation and motility of cell through the activation of AP-1-dependent gene expression via the MEK/Erk pathway.

2.2.5.1 Angiopoietin like protein 4

Angiopoietin-like protein 4 (ANGPTL4) is a secreted protein mainly expressed in the liver that regulates triglyceride metabolism by inhibiting the lipolysis of triglyceride-rich lipoproteins (Figure 25). Experimental results show that ANGPTL4 functions to regulate circulating triglyceride levels during different nutritional states and therefore plays a role in lipid metabolism during feeding/fasting through the differential inhibition of lipoprotein lipase (LPL). The N-terminal domain of angiopoietin-like proteins has been shown to play an active role in lipid metabolism. Using deletion mutants, it was demonstrated that the N-terminal domain containing fragment (17-207) and not the C-terminal fibrinogen-like domain containing fragment (207—460) increased the plasma triglyceride levels in mice^{276,277}. ANGPTL4 has been identified as a novel paracrine and, possibly, endocrine regulator of lipid metabolism and a target of peroxisome proliferators-activated receptors (PPARs)²⁷⁸. It is expressed in numerous cell types, such as adipocytes and hepatocytes, and is upregulated after fasting and hypoxia²⁷⁹. Importantly, ANGPTL4 undergoes proteolytic processing to release its C-terminal fibrinogen-like domain (cANGPTL4), which circulates as a monomer of unknown function. The N-terminal coiled-coil domain of ANGPTL4 (nANGPTL4) mediates the oligomerization of ANGPTL4 and binds to lipoprotein lipase to modulate lipoprotein metabolism, mediating oligomerization and lipoprotein metabolism²⁷⁷. In contrast, cANGPTL4 exists as a monomer, and its function remains unknown. ANGPTL4 has been shown to play a context-dependent role in angiogenesis and vascular permeability²⁸⁰. ANGPTL4 can disrupt the tight junctions of the endothelial tissue by directly interacting with three novel binding partners: integrin $\alpha 5\beta 1$, VE-cadherin (vascular endothelial cadherin) and

claudin-5. It disrupts these interactions in a temporally sequential manner, thus increasing the overall vascular permeability²⁸⁰.

ANGPTL4, was a recently shown to be a matricellular protein involved in the regulation of wound healing^{270,271}. ANGPTL4 expression in wound keratinocytes is up-regulated by PPAR β/δ in response to inflammation during wound healing²⁷⁸. ANGPTL4 can independently interact with specific matrix proteins and integrin to co-ordinate cell-matrix communication during the proliferative phase of wound healing^{270,271}. Briefly, ANGPTL4 can interact with vitronectin and fibronectin in the wound matrix by delaying the protease-based degradation of these local ECM proteins²⁷¹. Concurrently, ANGPTL4 can specifically interact with the $\beta 1$ and $\beta 5$ integrins that reside on the surface of wound keratinocytes²⁷⁰. These activate integrin-mediated intracellular signaling and enhance cell migration²⁷⁰. Altogether, the delayed degradation of vitronectin and fibronectin has a direct impact on integrin-mediated signaling in wound keratinocytes because their interaction does not interfere with integrin–matrix protein recognition necessary for cellular migration. ANGPTL4 can activate several integrin mediated intracellular signaling pathways, including focal adhesion kinase (FAK), Rho GTPase and 14-3-3 σ -dependent signaling cascades to modulate cell migration²⁷⁰. In addition, a recent study showed that PPAR β/δ mediated ANGPTL4 can regulate PKC (protein kinase Cs) and AP-1 (activator protein 1) transcription factors to promote epidermal differentiation, which is important for the maturation of the epidermis during the remodeling phase of wound healing²⁸¹. ANGPTL4 stimulates the increased activation of c-Jun and JUNB and is transcriptionally regulated by the expression of PKCs²⁸¹. The expression of epidermal differentiation markers, such as transglutaminase

1 and involucrin, can be induced by ligand activated-PPAR β/δ and ANGPTL4, which is associated with increased AP-1 binding to the cognate promoter²⁸¹. The deficiency in ANGPTL4 in mice (ANGPTL4^{-/-}) results in delayed wound re-epithelialization, reduced matrix protein expression, an increased inflammation and an impaired wound-related angiogenesis^{270,271,281}. However, the expression of ANGPTL4 and its role in cases of chronic wound repair, such as those observed commonly in diabetic patients, remains unclear.

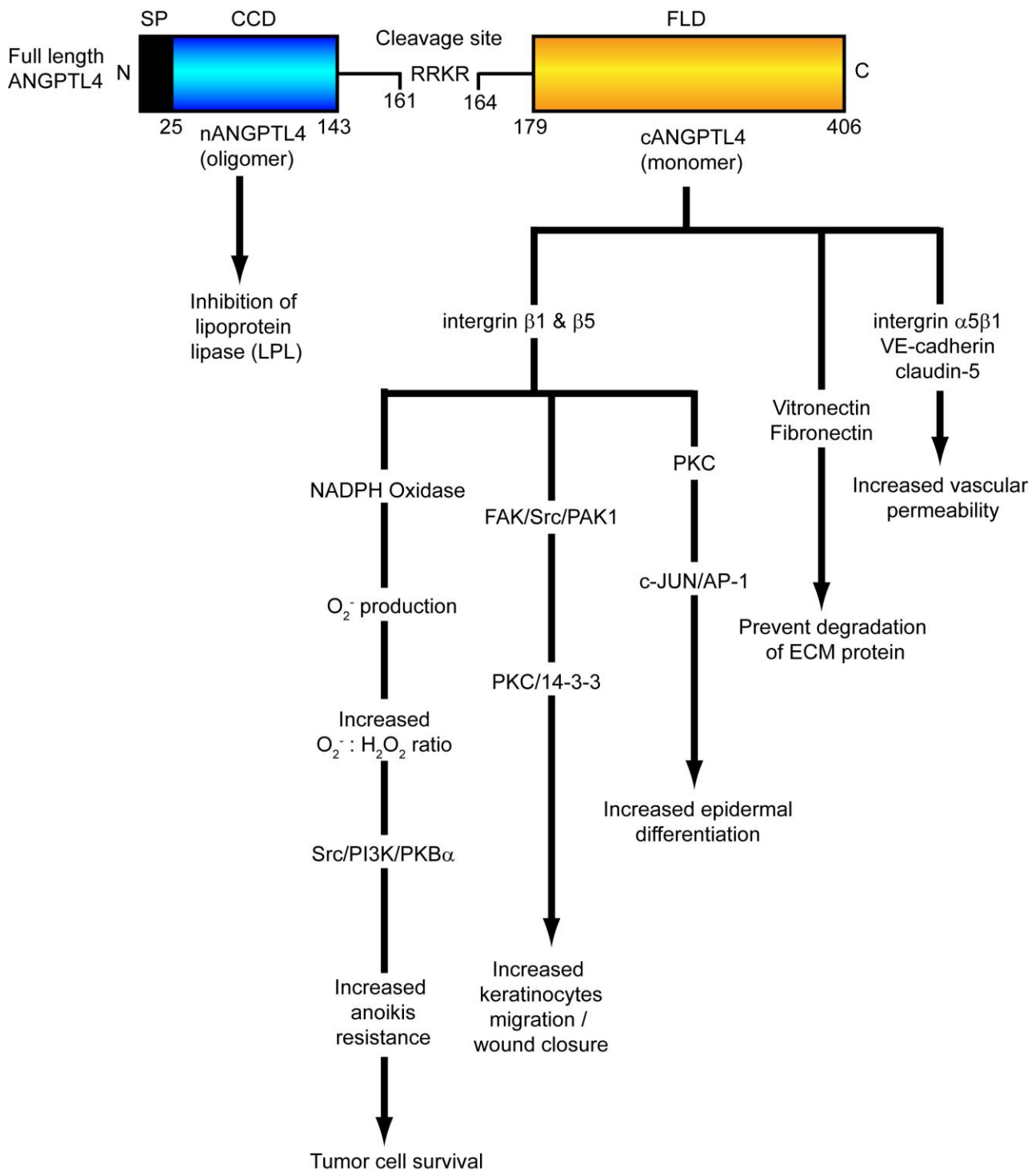


Figure 25. Structure and biological functions of ANGPTL4.

Full length ANGPTL4 (65 kDa) comprises a highly hydrophobic signal peptide (SP), an N-terminal coiled-coil domain (CCD), and a COOH-terminal fibrinogen-like domain (FLD). ANGPTL4 protein oligomerizes prior to secretion and cleavage. The N- and COOH-terminal domains are separated by a short linker that, after being secreted from the cell, can be cleaved into the nANGPTL4 (26 kDa) and cANGPTL4 (47 kDa)

fragments. Cleavage is at a conserved basic sequence (-RRKR-). The nANGPTL4 remains oligomeric, whereas cANGPTL4 will dissociate into monomers. Both fANGPTL4 and nANGPTL4 are involved in the modulation of triglyceride disposition via their inhibitory effect on LPL. However, this inhibitory effect on LPL seems to be weaker in the case of fANGPTL4 inhibition. cANGPTL4 binds to integrin $\beta 1$ or $\beta 5$ and activates 2 downstream processes. One process involves the stimulation of NADPH oxidase leading to the production of O_2^- . A high ratio of O_2^- to H_2O_2 has been found to activate the Src/ERK/PKB α prosurvival pathway, thereby conferring anoikis resistance and promoting tumor growth. Alternatively, cANGPTL4-bound $\beta 1$ -integrin can activate the FAK/Src/PAK1 cascade to trigger the PKC-mediated signaling pathways that are crucial for effective wound healing. It is also interesting to note that cANGPTL4 has been found to trigger vascular disruption by binding to and dispersing vascular-endothelial cadherin (VE-Cad) and claudin-5 at endothelial junctions, via the activation of integrin $\alpha 5\beta 1$. ANGPTL4 can binds vitronectin and fibronectin to delays their degradation by proteases. ANGPTL4 activates PKC and AP-1 dependent signaling pathways to increase cell differentiation.

2.3 MATERIALS AND METHODS

2.3.1 Reagents

Antibodies used: Ki67 and keratin 6 (NCL-Ki67p and NCL-CK6 from NovoCastra, Leica Biosystem, Germany); β -tubulin(H-235), PCNA (PC10) and α SMA (alpha-SM1) (sc-9104, sc-56 and sc-130617 from Santa Cruz Biotechnology, USA); CD31 (BD Pharmingen, USA); CD68 (FA-11) (Biolegend); F4/80 (AbD Serotec, UK); STAT3, pSTAT1 (Y701) and STAT1 (ab7966, ab30645 and ab2415 from Abcam, UK); iNOS/NOS II, NT (06-573, Merck Millipore, USA); pStat3 (Tyr705) and pStat1 (Tyr701) (#9145 and #9171 from Cell Signaling Technology, USA); ID3 (2B11) (MA1-23242, Thermo Scientific, USA) cANGPTL4: monoclonal antibodies against the C-terminal mouse (190-410 amino acids) of ANGPTL4 were produced by ProSci, respectively; goat anti-rabbit and anti-mouse IgG-HRP (Santa Cruz Biotechnology, USA); Alexa Fluor 488 or 594 goat anti-mouse IgG, anti-rat IgG and anti-rabbit IgG (Molecular probes, USA). DAB peroxidase substrate kit (Vector Laboratories, UK). Unless mentioned otherwise, all chemicals were from Sigma-Aldrich and molecular biology enzymes from Fermentas. All oligonucleotides were synthesized by Sigma-Proligo.

2.3.2 Recombinant cANGPTL4 expression, purification and endotoxin removal

The cDNAs encoding c-terminal end of human ANGPTL4 (185 - 406) were isolated by PCR, subcloned into pET-30a (+) vector and transformed into E. coli Rosetta-gami™ bacteria (Novagen). Protein expression was induced by 1 mM IPTG at 28°C for 3 hour and the bacteria pellets was sonicated for 60 min on ice in lysis buffer (50mM Tris pH

8.0, 300mM NaCl, 0.1% Triton X). Total protein lysate obtained was allowed to pass through an affinity nickel-Sepharose column and the purified recombinant cANGPTL4 was retrieved with elute solution (50mM Tris, 300mM NaCl, 100mM imidazole, pH 8.0). The imidazole was removed from the purified cANGPTL4 solution by passing through a desalt column. The endotoxin contamination of the purified cANGPTL4 was reduced by a phase separation technique using 1% of detergent, Triton X-114. The mixture was incubated at 4° C for 30 min with stirring to ensure homogeneity. The sample was then transferred to a 37° C water bath, incubated for 10 min, and centrifuged (20,000 x g, 10 min) at room temperature. The upper aqueous phase containing the recombinant cANGPTL4 was carefully removed and subjected to Triton X-114 phase separation for at least two more cycles.

2.3.3 Genotyping of diabetic mice

Heterozygous BKS.Cg-DOCK7^m +/+ *Lep^{db}*/J (ob/+) were purchased from The Jackson Laboratory (Bar Harbor, ME, USA). Age- and sex-matched homozygous ob/ob and wildtype (+/+) were obtained by interbreeding the ob/+ littermates. At 3-wk old, offsprings were separated from their parents and genotyped. All mice used in this study were individually caged housed in a temperature-controlled room (23 °C) on a 12 h light-dark cycle, and allowed *ad libitum* access to standard mouse chow diet and water. The mutant mice exhibit severe diabetic conditions from 8 weeks on age and blood glucose level of diabetic mice was 473±14.6 mg/dL and non-diabetic mice was 122.5±5.21 mg/dL as determined by Accu-Chek Advantage glucometer (Roche Diagnostic, Switzerland).

A small ear biopsy (<0.5 cm) was collected from each mouse for genotyping and ear tagged after anesthetized with an intraperitoneal injection of ketamine/xylazine (100 mg/kg + 10 mg/kg). To extract genomic DNA, ear biopsies were digested in 300 µL of genotyping lysis buffer pH 8.0 (10 mM Tris-HCl, 100 mM ethylenediaminetetraacetic acid (EDTA) and 0.5% sodium dodecyl sulfate (SDS)) for 2 h at 56 °C with agitation in the presence of 0.2 mg/mL RNaseA and 1 mg/mL Proteinase K. The lysate was then centrifuged at 13 000 rpm for 10 min at room temperature (RT) to remove debris. The supernatant was transferred to a tube containing 500 µL isopropanol. 1 mL of ice-cold 70% ethanol was added and the solution was mixed by inversion. Precipitated genomic DNA was visible and pelleted at 13 000 rpm for 10 min at RT. The supernatant was decanted and the DNA was allowed to air-dry. The air-dried pellet was resuspended in 100 µL Tris-EDTA buffer for 5 min at 70 °C. Genomic DNA was then genotyped using a customized TaqMan® SNP genotyping Assay (Applied Biosystems, USA). Genotyping was performed on extracted DNA using. Primer sequences were (5'-CCA ACT TCC CAA CAG TCC ATA CAA T-3') and (5'-CTC ATC AAA TGT TAT TTC TTA GTC ATT CAA ACC A-3'). 6FAM™ dye-MGB-labeled probe for mutant allele sequence (TTG ATG GAG GTA AAC AA) and VIC® dye-MGB-labeled probe for wild type allele sequence (TGA TGG AGG GAA ACA A).The assay was performed with TaqMan Universal PCR Master Mix (Applied Biosystems, USA) and 80 nM of the respective customized dye labeled probes using CFX96™ real-time PCR detection system (Bio-Rad laboratories, USA). Using this assay, +/+ mice show an end point detection of VIC-dye fluorescence only, homozygous mutant ob/ob show FAM-dye fluorescence only and heterozygous ob/+ show both VIC- and FAM-dye fluorescence.

2.3.4 Full excisional splinted wounding

Mice were anesthetized prior surgery by a single intraperitoneal anaesthetized with of ketamine/xylazine (80 mg/kg + 10mg/kg). Two circular 5 mm full-thickness excisional wounds were created on the dorso-medial back of each mouse and silicon donut-shaped splints of 10mm diameter were centered over the wounds. The silicon splint was adhered to the skin with cyanoacrylate glue. On the day of surgery (day 0), 50 μ L of recombinant human ANGPTL4 (rhANGPTL4) protein of 1 mg/mL or 2 mg/mL or PBS mixed with 1% carboxyl methylcellulose (CMC) was applied topically to their respective cutaneous wound and protected with an occlusive dressing, Tegaderm™ (3M, USA) throughout the duration of the study. Mice were euthanized by CO₂ inhalation at Day 1, 3, 5, 7 and 10 post wounding. At the indicated time, photo imaging, histomorphometric and other biological analysis of wound biopsies were done.

2.3.5 Tissue preparation and sectioning

Wound biopsies were fixed in 4% paraformaldehyde-PBS (PFA) overnight at 4 °C. Tissues were either embedded in OCT tissue freezing medium (Leica Microsystems, USA) to be frozen immediately with liquid nitrogen or embedded in paraffin. For paraffin embedding procedure, the tissues were dehydrated over a series of increasing graded ethanol followed by xylene. Dehydrated tissues were submerged in molten paraffin wax prior to paraffin embedding using the tissue embedding System Leica EG1160 (Leica Microsystems, USA). Cryosections of 8 μ m thickness or paraffin section of 5 μ m thickness were used for histological or immunofluorescence staining.

2.3.6 Assessment of wound healing

Images of wounds were captured at Day 1, 3, 5, 7 and 10 post-wounding using a Canon G12 digital camera. A ruler was included in each image to allow standard calibration of measurements. Surface wound area was quantified using Image-Pro® Plus version 5.1.0.20 software (Media Cybernetics, USA). Surface wound area at each time point were standardized and expressed as a percentage of initial wound area at Day 1 (100%). Histomorphometric measurement was made from sections through the center of the wound to obtain the actual wound representation. Sections of wound biopsies over the indicated time were stained by haematoxylin-eosin staining. Histological images were visualized with Nikon Eclipse 90i brightfield microscope using a Plan Fluor, 10 x/0.30 objective and taken with QCapture Pro version 5.0.1.26 software (QImaging, Canada). The measurements were performed three times from random sections using Adobe Photoshop CS5.1 and image pixel was calibrated to μm using the scale bar.

2.3.7 Van gieson elastic stain

Tissue sections from mice wound biopsies were deparaffinized and rehydrated in PBS. These sections were stained in Weigert's iron heamatoxylin (Merck Millipore, USA) for 8 min at RT followed by staining in Van Gieson's picrofuchsin solution (Merck Millipore, USA) for 1 min at RT. Images were visualized with Nikon Eclipse 90i brightfield microscope using a Plan Fluor, 10 x/0.30 objective and taken with QCapture Pro version 5.0.1.26 software (QImaging, Canada).

2.3.8 Focused real-time PCR array

Real-time PCR arrays were used to analyze the expression of a focused panel of genes. qPCR was performed with KAPA[™] SYBR qPCR Universal Master Mix (KAPABiosystems) using CFX96[™] real-time PCR detection system (Bio-Rad laboratories, USA). Melt curve analysis was included to assure that only one PCR product was formed. Primers were designed to generate a PCR amplification product of 100 to 250 bp. Only primer pairs yielding unique amplification products without primer dimer formation were subsequently used for real-time PCR assays. Expression was related to the control gene ribosomal protein P0 (RPLP0), which did not change under any of the experimental conditions studied. The sequences of qPCR primers are available in Table 5.

Table 5: List of primer pairs sequences.

Genes	Forward Sequence (5' to 3')	Reverse Sequence (5' to 3')
ADAM metalloproteinase domain 9 (ADAM9)	GGACGGAACCAAGTCTGCTG	CCACTGAACAAAGTTGCCCA
Adiponectin (ADIPOQ)	AGCCGCTTATATGTATCGCTCA	TGCCGTCATAATGATTCTGTTGG
AKT1	CCAAGGCCCAACACCTTTATC	TTCTGCCTCTTGAGTCCATC
ANGPT1	TGCACTAAAGAAGGTGTTTGTCT	CCTCCCCATTACATCCATATT
ANGPT2	CGAGGCGCATTCGCTGTAT	GGCTGATGCTACTTATTTTGCCC
ANGPTL4	TCCAACGCCACCCACTTAC	TGAAGTCATCTCACAGTTGACCA
CCL2	TTAAAAACCTGGATCGGAACCAA	GCATTAGCTTCAGATTACGGGT
CCL11	GAATCACCAACAACAGATGCAC	ATCCTGGACCCACTTCTTCTT
Cyclin-dependent kinase 4 (CDK4)	CCAATGTGTACGGCTGATGG	TGTCCAGGTATGTCTCAGGT
Cyclin-dependent kinase inhibitor 2B (CDKN2B)	CCCTGCCACCTTACCAGA	CAGATACCTCGCAATGTCACG
cystatin A (CSTA)	TACGGAGGTGTTTCAGAGGC	CAGCGACGGCTTGAGTTTT
CXCL1	CTGGGATTACCTCAAGAACATC	CAGGGTCAAGGCAAGCCTC
CXCL5	TGCGTTGTGTTTGTCTTAACCG	AGCTATGCTTCCACCTGAGG
CXCL9	GAACGGAGATCAAACTGCCT	TGTAGTCTTCTTGAACGACGA
CXCL10	CCAAGTGCTGCCGTCATTTTC	GGCTCGCAGGGATGATTTCAA
Epidermal growth factor receptor (EGFR)	GGGAGCATTTGGCACAGTGTA	GCCATCACATAGGCTTCGTCAA
EPHA3	TTCTGGTCGGGAGGTTTGTG	ACTGCTTGAGTAGGGTCTTCA
EPHB3	ACCGTAAGAGACTGTAAACAGCA	GTCCACTTTCACGTAGGGGTT
Fatty acid synthase (FAS)	AGAGATCCCGAGACGCTTCT	GCCTGGTAGGCATTCTGTAGT
Fibroblast growth factor 1 (FGF1)	CAGCTCAGTGCAGAAAGTG	TGTCTGCGAGCCGTATAAAAG
FGF2	GCGACCCACACGTCAAACCTA	TCCATCTTCTTCATAGCAAGGT
FBJ osteosarcoma oncogene B (FOSB)	GCCACTGCGGACCAACAATT	TTATTGGCGCAGGTGACGAACC
Fos related antigen 2 (FRA2)	AGCCTCCCGAAGAGGACAG	AGGACATTGGGGTAGGTGAA
Growth differentiation factor 3 (GDF3)	TAAGGTGGGACAGATTGCTTTT	CTGGACAGTTACCTGAGGTA
GLI-Kruppel family member GLI1 (GLI1)	GAGCCCTTCTTTAGGATTCCCA	ACCCCGAGTAGAGTCATGTGG
GM-CSF	TCGTCTCTAAGAGTCTCTCTT	GCAGTATGCTGTGATGAGTGG
Hepatocyte growth factor (HGF)	CTGTCTCATGTGCGCCATCC	TGGGTCTTCTTGGTAAGAGTAG
HIF1 α	GGTCATCGCAGTTGGAACCTCC	CGCTTGTGTCTTGGAAAGGCTG
Baculoviral IAP repeat-containing 2 (IAP2)	AGGGACCATCAAGGGCACAG	TTTGTGTGTTTGGCGGTGTCTC
Insulin-like growth factor binding protein 4 (IGFBP4)	AGAAGCCCTGCGTACATTG	TGTCCTCCACGATCTTCACTT
IL1R1	GCCAAGGTGGAGGACTCAG	CCAGGGTCAATCTTCAACAGT
IL-6	TAGTCTTCTTACCCCAATTTCC	TTGGTCTTACGCACTCTTCTC
IL-10	AGAAGCATGGCCAGAAATCA	GGCCTTGTAACACCTTGGT
IL-18	TGGAACCCAGACCAAGACTG	CCTGGAACACGTTTCTGAAAGA
Inhibin, beta A (INHBA)	ATAGAGGACGACATTGGCAGG	ATAGAGGACGACATTGGCAGG
Integrin, alpha V (ITGAV)	CCTGTGCTCCATTGTACCACT	AGCATACTCAACGGTCTTTGTG
Jun B proto-oncogene (JUN-B)	GACCTGCACAAGATGAACCAC	AGGCTGGAGAGTAAGTGTGA
Keratinocyte growth factor (KGF)	CCGTGGCAGTTGGAATTGTG	CCTCCGCTGTGTGTCCATTT
Kl67	CTGCCCTCAGATGGCTCAAAGA	GAAGACTTCGGTTCCCTGTAAC
Kruppel-like factor 9 (KLF9)	GCCGCCTACATGGACTTCG	GCCGTTACCTGTATGCAC
Mitogen-activated protein kinase 3 (MAPK3 (1B))	ACCACATTCTAGGTATCTTGGGT	GATGCGCTTGTTTGGGTTGAA
Mitogen-activated protein kinase kinase kinase 1 (MAP4K1)	CTCACAGCTCGCTCAGATCC	GAGGGGACAGCCGTTGAAT
Melan-a (MLANA)	TGGATACAGAACCTTGATGGACA	GGGCTGATGGGATTCTCTTGT
MMP9	AAACCACCTCTCCGACTCCAG	AGCTCGGTGGTGTCTCCAATG
MMP13	ACCTCCACAGTTGACAGGCT	AGGCACTCCACATCTTGGTTT
OPN	ATCTCACCATTCGGATGAGTCT	TCAGTCCATAAGCCAAGCTATCA
PAI1	GTGCATCACTCCACAAACCTGC	TAACGTGGGTGCCCAAGCATC
PDGFA	CGCTGCACTGGCTGTTGTA	TTCCCTACGCCTTCTGTCTC
PDGFB	CGAGCCAAGACGCTCAAG	CATGGGTGTGCTTAAACTTTCG
Platelet and Endothelial Cell Adhesion Molecule 1 (PECAM1)	TGCACCCCATCACTTACCACC	TAAACACGCGTCTGTTCCTC
PPAR α	TCGGCGAACTATTTCGGCTG	GCATTGTGAAAACGGCAGT
PPAR β/δ	TTGAGCCCAAGTTTCGAGTTTG	CGGTCTCCACACAGAATGATG
PPAR γ	TGTGGGGATAAAGCATCAGGC	CCGGCAGTTAAGATCACACCTAT
Ras homolog gene family, member A (RHOA)	AGCCTTCTTCACCTGGACTGC	CACCACTGCTCAGCAAGTAAAG
Rpl27	CAAGGGGATATCCACAGAGTACCTT	CTGGTGGCTGGAATTGACCGCTA
SKI-like oncogene (SKIL)	AGGCAGAGACAAAGTAAGTCCA	CGTCTGGGTAAGACACTGTTTTT
SMAD3	CCCCCACTGGATGACTACAG	TCCATCTTCACTCAGGTAGCC
SOCs1	CTGCGGCTTCTATTGGGGAC	AAAAGGACGTCGAAGGTCTCG
SOCs3	CAAGAACCCTACGCATCCAGTG	CCAGCTTGAGTACACAGTCGAA
SPARC	ACTACATCGGACCATGCAAAATAC	GTACAAGGTGACCAGGACATTTT
STAT1	GGAGCACGCTGCCTATGATG	CTCCAGAGAAAAGCGGCTGTA
STAT3	CAATACCATTGACCTGCCGAT	GAGCGACTCAAACCTGCCCT
STAT5A	AGTGGTTTCGACGGGGTGAT	ATGGCTTCAGATTCCAGAGGT
TGF α	CACTCTGGGTACGTGGGTG	CACAGGTGATAATGAGGACAGC

TGFβ1	CCGCAACAACGCCATCTATG	CTCTGCACGGGACAGCAAT
TGFβ2	TCGACATGGATCAGTTTATGCG	CCCTGGTACTGTTGTAGATGGA
TGFβ receptor 1 (TGFβR1)	TCCCAACTACAGGACCTTTTCA	GCAGTGGTAAACCTGATCCAGA
TIMP1	CTTGGTTCCCTGGCGTACTC	ACCTGATCCGTCCACAAACAG
TIMP2	CTGGACGTTGGAGGAAAGAAG	GGTGATGCTAAGCGTGTCCC
TIMP3	GCGCAAGGGCCTCAATTAC	AGAGACACTCATTCTTGGAGGT
TLR2	CCAGACACTGGGGGTAAACATC	CGGATCGACTTTAGACTTTGGG
TLR4	AAAGTGGCCCTACCAAGTCTC	TCAGGCTGTTTGTTCCTCAAATC
TNC	GCTACCGACGGGATCTTCG	TAGCCGTGGTACTGATGGTTT
TNFα	GGCTTTCCGAATTCCTGGAG	CCCCGGCCTTCCAAATAAA
TNFα interacting protein 2 (TNFαIP2)	AAAGGGATACCTACTTGCTGCT	CAAGCCCGACACCTTGAAG
TSP-1	GAAGCAACAAGTGGTGTCAGT	ACAGTCTATGTAGAGTTGAGCCC
VEGFA	GCACATAGAGAGAATGAGCTTCC	CTCCGCTCTGAACAAGGCT
VG1 related sequence (VGR)	TCCTTGAACCGCAAGAGTCTC	CTCACCCTCAGGAATCTGGG
VHL	AAAGAGCGGTGCCTTCAGG	CACTTGGGTAGTCTCCTCAAATC
X-ray repair complementing defective repair in Chinese hamster cells 1 (XRCC1)	TCTTCAGTCGTATCAACAAGACG	GTTTGCTGGGAGGTTTCTCTG
ID3		
Primers for ChIP	Forward Sequence (5' to 3')	Reverse Sequence (5' to 3')
STAT binding site	CATGCGAAGATGAGTGGACC	CCAATAAAGCATTACACATGG
Control	AGCCCTGGACCTGCTGATAGAG	AATGAGGACCACGGTGGCAC

2.3.9 Hydroxyproline assay

Wound biopsies were frozen in liquid nitrogen, and then homogenized thoroughly in distilled water. The net weight of the wound biopsies was predetermined for normalization. In addition, trans-4-hydroxy-L-proline (0-300 µg/mL) was included as standards. Aliquots of samples (50 µL) were hydrolyzed in 2 N NaOH at 120°C for 2 hours, and then oxidized with chloramine-T reagent (0.0127 g/mL) for 25 min at RT. The chromophore was then developed with the addition of p-dimethylaminobenzaldehyde (DMAB) reagent (0.3 g/mL dissolved in methanol/hydrochloric acid solution (2:1 v/v)). The absorbance of reddish hue complex formed was measured at 550 nm using SpectraMax® M2e Multi-Mode Microplate Reader and SoftMax® Pro Microplate Data Acquisition & Analysis Software (Molecular Devices, USA). Absorbance values were plotted against the concentration of standard hydroxyproline, and the value of unknown hydroxyproline were then determined from the standard curve.

2.3.10 Nitric oxide determination

Intracellular level of NO from wound biopsies were measured using cell-permeable 4,5-diamino-fluorescein (DAF-FM diacetate) (D23844, Molecular probes, Invitrogen, USA). Wound biopsies were lysed in Krebs buffer, and incubated with 10 μ M DAF-FM diacetate for 30 min at 37 °C in darkness. The fluorophore signal was recorded immediately at 495 nm excitation and 515 nm emission wavelengths using a GloMax 20/20 Luminometer (Promega, USA). Fluorescence was expressed as arbitrary fluorescence units (AU), and was measured with the same instrument settings for all experiments.

2.3.11 Immunofluorescence staining

Tissue sections were fixed in 4% PFA at RT for 10 min and washed in 1X PBS. Sections intended for staining of α SMA, ANGPTL4, iNOS and pSTAT3 were subjected to heated antigen retrieval in citrate buffer (pH 6.0). Blocking was performed either using 2% bovine serum albumin (BSA) containing 0.1% Triton X-100 (α SMA staining) or using 3% normal goat serum (NGS) (ANGPTL4, iNOS and pSTAT3 staining) for an hour at RT. The sections were then incubated with their respective primary antibodies for overnight at 4 °C, followed by incubation with Alexa 488- or Alexa594- conjugated secondary antibodies (Invitrogen, USA) for 60 min in the dark. Negative controls were carried out in the absence of the primary antibody. The slides were counterstained with DAPI (Vectashield) and images capture using the LSM 710 confocal microscope (Carl Zeiss, Germany) with the Plan-Apochromat 20x/0.8 NA objective. Analyses were performed with the ZEN 2012 Light Edition software (Carl Zeiss, Germany).

2.3.12 Immunohistochemistry for CD31

Tissue sections were fixed in 4% PFA at RT for 10 min and washed in 1X PBS. Sections were subjected to heated antigen retrieval in citrate buffer (pH 6.0). Blocking was performed using 2% bovine serum albumin (BSA) containing 0.1% Triton X-100 for an hour at RT. The sections were then incubated with rat Anti-mouse CD31 (PECAM-1) Antibody (BD pharmingen, USA) for overnight at 4 °C, followed by incubation with biotinylated goat anti rat IgG antibody (Vector laboratories, USA). Next, sections were incubated in Avidin:Biotinylated enzyme Complex (ABC; Vector Laboratories, USA) for 30 minutes after incubation with secondary antibodies. Sections were developed with 3,3'-diaminobenzidine (DAB) substrate (Vector Laboratories, USA) to give a brown colour stain. Slides were mounted with Fluka Eukitt® quick-hardening mounting medium (Sigma-Aldrich, USA). Negative controls were carried out in the absence of the primary antibody. Images were taken using Carl Zeiss MIRAX MIDI using a Plan-Apochromat 20x/0.8 NA objective and Marlin F146.C camera, and MIRAX Viewer Version 1.11.49.0 software.

2.3.13 Proximity ligation assay

PLA experiments were performed in accordance to the manufacturer's protocol (Olink Biosciences, Sweden) using pairs of antibodies probing for the protein interactions that are of interest. Mouse monoclonal anti-integrin β [clone JB1A] (1:50; Merck Millipore, USA) paired with rabbit polyclonal anti-Rac1 [ab97732] (1:20; Abcam, USA) and rabbit monoclonal anti-active integrin β 1 [CD29, clone EP1041Y] (1:50; Abcam, USA) paired with mouse monoclonal anti-cANGPTL4, 4A11H5 were used. Following the primary

antibodies incubation, a pair of secondary proximity probes: Duolink[®] in situ PLA[®] probe anti rabbit plus with Duolink[®] in situ PLA[®] probe anti mouse minus (Olink Biosciences, Sweden) were diluted 1:5 and mixed in the antibody diluent buffer. Sections were then incubated for 60 min at 37 °C in a pre-heated humidified chamber. Duolink[®] *In Situ* Detection Reagents Orange kit (Olink Biosciences, Sweden) was used for the subsequent assay. The sections were washed twice with Duolink[®] wash buffer A (0.01 M Tris, 0.15 M NaCl and 0.05% Tween 20, pH 7.4) for 5 min and incubated with prepared hybridization-ligation mix from the kit for 30 min at 37 °C in a pre-heated humidified chamber. Next, the sections were washed twice with Duolink[®] wash buffer A and incubated with prepared amplification-detection mix from the kit for 100 min at 37 °C in the same chamber but away from light. After incubation, sections were washed twice with Duolink[®] wash buffer B (0.2 M Tris and 0.1 M NaCl, pH 7.4) for 10 min followed with 0.01x Duolink[®] wash buffer B for 2 min. Sections were counterstained and mounted in Vectorshield[®] mounting media with DAPI (Vector Laboratories, USA). Negative controls were carried out in the absence of the primary antibody. PLA images were taken using the LSM 710 confocal microscope (Carl Zeiss, Germany) with the Plan-Apochromat 40x/1.4 oil differential interference contrast objective. Analyses were performed with the ZEN 2012 Light Edition software (Carl Zeiss, Germany) and PLA signals were quantified using Blobfinder software (Centre for image Analysis, Uppsala University).

2.3.14 *In vitro* diabetic wound assay

Human skin biopsies were provided by Dr. Marcus Wong from Plastic, Reconstructive and Aesthetic Surgery of TTSH, Singapore (NHG DSRB Ref: 2012/00071). Human skin

specimen were placed in sterile cultured medium, DMEM supplemented with 10% fetal bovine serum (FBS) containing penicillin (1000 U/mL) and streptomycin (1000 µg/mL), and the subcutaneous fats were removed with surgical scissors. All the trimming and procedure were performed in a sterile biological safety cabinet. The remaining skin specimen was cut precisely into 1.0 cm² full thickness pieces. Each skin biopsies were washed thrice with antibiotic containing 1x PBS and placed on the dry base of the in a 6 well cell culture microplates. The skin explants were either cultured in medium containing 5.5 mM glucose and 1 nM insulin (normal condition) or 25 mM glucose and 10 nM insulin (diabetic condition) in a humidified atmosphere of 5% CO₂ at 37 °C. The top of the skin explants were not fully covered by the cultured medium, but were exposed to air and moisture.

2.3.15 Chromatin Immunoprecipitation (ChIP)

Briefly, biopsies from saline- and cANGPT4-treated ob/ob wounds at day 7 post injury were cut into small pieces prior to digestion with 0.5% collagenase I at 37 °C. Cells were retrieved and crosslinked using 0.5% formaldehyde for 10 min at 37°C, followed by sonication in SDS lysis buffer (1% SDS, 10mM EDTA, and 50mM Tris-HCl, pH 8.1) to obtain crosslinked DNA that measure 200-500bp in length. 10% of the supernatant was used as input, while the remaining amount was subjected to pSTAT3(Y705) specific antibody (Cell Signaling Technology, USA) or pre-immune IgG to form complexes. Complexes were pulled down by Protein A/G (Santa Cruz, USA) and were eluted with elution buffer (1% SDS, 0.1M NaHCO₃). DNA fragments were reverse crosslinked at 65°C for 6 hr. PCR was performed with 5-10 µL of the eluate and using primers flanking

either the stat binding site of iNOS gene (-942 to -934) or an unrelated control sequence (>2kbp away from the binding site). The primer pairs used were given in Table 5.

2.3.16 Transmission Electron Microscopy

Skin tissue biopsies were fixed with 4% PFA, 2.5% glutaraldehyde and 0.2% picric acid in 0.1 M sodium cacodylate buffer, pH 7.6, and incubated for 2 weeks at 4°C. The fixed sample blocks were incubated in 1% OsO₄ and 1.5% potassium hexacyanoferrate in cacodylate buffer for 1hr, then dehydrated in a graded series of ethanol concentrations, and embedded in Spurr's resin. Semi-thin sections stained with toluidine blue were used for orientation. Ultrathin sections of the skin were counterstained with 7% uranyl acetate and Reynold's lead citrate before examination under JEM-1010 electron microscope operating at 80 kV or JEM-2200FS.

2.3.17 Scanning Electron Microscopy

Tissue preparation for scanning electron microscopy of collagen fibers was performed as previously described with minor modifications^{18–19}. Wound biopsies were immersed in 0.1 N NaOH at 80°C for 1 hour to decellularize the tissue, after which they were successively transferred into 0.1 N NaOH at room temperature for 5 min, into distilled water at room temperature for 5 min. Elastic fibers were removed from the decellularized tissue by elastase treatment at 37°C for 30 minutes at a concentration of 9.5 U/mL in 100 mmol/L Tris buffer (pH 7.4) containing 1 mmol/L CaCl₂ and 0.02% NaN₃. The decellularised tissue is then fixed in 2% glutaraldehyde and 1% paraformaldehyde in 0.1 mol/L PBS (pH 7.4) overnight at 4°C. Following fixation, the

tissues were washed twice with PBS and postfixed in 1% osmium tetroxide for 1 hour. The specimens were then dehydrated in graded concentration of ethanol ranging from 50% to 100% and dried in a critical-point drying apparatus using liquid CO₂ as immersion medium. The samples were then mounted onto a metal stub with double-sided carbon tape. After this, the specimens were sputter-coated with a thin layer of gold using SPI-Module Sputter Coater System (Structure Probe) and examined with a JSM-5410LV scanning electron microscope (JEOL).

2.3.18 Laser capture microdissection (LCM).

Paraffin-embedded sections were mounted onto MembraneSlides 1.0 PEN (Carl Zeiss) that was pre-treated with UV for 30 min. Hematoxylin- and eosin-stained sections were then subjected to LCM using Arcturus® XT laser capture microdissection system according to the manufacturer's instructions (Life technologies). LCM tissues were collected onto an adhesive CapSure® Macro LCM Caps (Life technologies). The LCM caps with the captured samples were capped onto 500 µL centrifuging tubes containing 15 µL of lysis buffer and process as previously described. Total RNA was isolated using RecoverAll™ total nucleic acid isolation (Ambion) according to the manufacturer protocol. Fifty ng of RNA was subjected to Full Spectrum™ Complete Transcriptome RNA Amplification (System Biosciences) according to manufacturer's recommendation prior qPCR.

2.3.19 Immunoblotting

Wound biopsies were homogenized with ice-cold protein lysis buffer pH 8.0 (20 mM

Na₂H₂PO₄, 250 mM NaCl, 1% Triton X-100, 0.1% SDS and 1 mM PMSF). Total protein lysates were precipitated by a chloroform/methanol solvent method prior been resolved on 10% SDS-PAGE. The proteins were electrotransferred onto a onto immobilon-FL polyvinylidene fluoride membrane (IPFL00010 from Merck Millipore,USA). The membranes were blocked with Odyssey Blocking buffer (#927-40000 from LI-COR Biotechnology, USA) for 1 h at RT. The membrane was incubated with indicated primary antibodies overnight at 4 °C in 1:1 proportion of blocking buffer to TBS (50 mM Tris.HCl, pH 7.6, 150 mM NaCl) containing 0.05% Tween-20. Appropriate IRDye® 680 or 800 conjugated anti IgG secondary antibodies (#926-68071, #926-68070, #926-32210 and #926-32211, LI-COR Biotechnology, USA) (1:10000) for 1 h at RT. The protein bands were revealed using Odyssey® CLx Infrared Imaging System (LI-COR Biotechnology, USA) and signals were quantified by densitometry with the aid of Image Studio Software (LI-COR Biotechnology, USA). For cANGPTL4 specific mouse monoclonal antibody (4A11H5) immunoblotting procedure, membrane was blocked with 1x Odyssey Blocking buffer overnight at 4 °C. The membrane was incubated with anti-cANGPTL4 (4A11H5) at 4 °C overnight using 0.6 µg/cm² of the membrane in 1:1 proportion of blocking buffer to TBS (50 mM Tris.HCl, pH 7.6, 150 mM NaCl) containing 0.1% Tween-20.

2.3.20 RNA extraction and reverse transcription

At indicated time skin wound biopsies were excised and total RNA was extracted using TRIzol® Reagent (Invitrogen, USA) followed by PureLink™ Micro-to-Midi Total RNA Purification System (Invitrogen, USA) accordingly to the manufacturer's protocol. Total

RNA was quantified at A260/A280 absorbance using Nanodrop ND1000 (Thermo scientific, USA). Five µg of total RNA was reversed transcribed using 200 U of Moloney Murine Leukemia Virus Reverse Transcriptase, RNase H Minus (M-MLV RT) (Promega, USA) in the presence of 5 µl of its corresponding 5X reaction buffer, 1 µg of oligo dT, 1.25 µl of 10 mM dNTP and 3 U of RiboLock™ RNase Inhibitor (Fermentas, Canada) using iCycler thermal PCR System (Bio-Rad laboratories, USA). Subsequently, RNA was digested with 2.5 U of RNase H (New England BioLabs, USA).

2.3.21 Isolation of cells.

Post wounding skin biopsies were minced by scissors and immersed in 500 µL of digestion solution (250 U/mL type I collagenase in DMEM with 10% FBS) for 2 hour at 37°C with continue shaking. The tissue mixture was filtered through cell strainer (pore size 100 µm) followed by spinning through another cell strainer (pore size 70 µm) at 200 x g. Isolated cells were inspected under microscope before performing further analysis.

2.3.22 Intracellular staining and Flow cytometry.

For determination of proliferative endothelial cells, intracellular staining for CD31 and Ki67 was carried out on the cells isolated from fresh wound biopsy. Cells were fixed and permeabilized in 300 µL of cytoperm buffer (0.01% paraformaldehyde with 0.1% NP40 in PBS) for 20 min on ice and blocked with 10% normal goat serum in PBS for 30 min at room temperature. Following that the cells were incubated with staining buffer (3% NGS in PBS) containing the rat anti-CD31 (1:200) and rabbit anti-Ki67 (1:200) for 30 minutes on ice, followed by incubation with FITC conjugated goat anti-rat IgG and PE

conjugated goat anti-rabbit IgG secondary antibody for another 30 minutes on ice before flow cytometric analysis. For determination of nitric oxide, intracellular staining with cell-permeable 4,5-diamino-fluorescein (DAF-FM diacetate) (D23844, Molecular probes, Invitrogen, USA) was carried out on the transfected keratinocytes. Cells were incubated with in DMEM alone phenol red free containing 2mM of DAF-FM diacetate for 30 min in a humidified incubator with 5% CO₂ at 37°C. Cells were then trypsinized and resuspended with DMEM supplemented with 10% FBS phenol red free before flow cytometric analysis. Flow cytometry was carried out using BD Accuri C6 flow cytometer (BD Biosciences, USA) and data analysis was performed using Flowjo software version 7.6.5 (Tree Star Inc, USA).

2.3.23 Transient suppression of STAT3 in keratinocytes.

Keratinocytes were seeded at 5×10^4 cells in 6 well culture plates and were incubated overnight in a humidified incubator with 5% CO₂ at 37°C prior to the transfection assay. The experimental setups include untreated cells, non-targeting scrambled siRNA and ON-TARGETplus SMARTpool STAT3 siRNA (L-003544-00-0005) (Thermo scientific, USA). A final concentration of 5 μ M of siRNA and 4 μ L DharmaFECT transfection reagent with serum free medium was added to each seeded well according to the manufacture protocol. Transfection medium was replaced with fresh media 16 hours after the transfection and analysis were performed within 24 to 96 hour post transfection.

2.3.24 Statistical analysis

Statistical analysis was performed using two tailed Mann-Whitney tests with GraphPad Prism software (version 4.00) (GraphPad Software Inc, USA) or two way ANOVA using SPSS v.19 software (IBM Corporation, USA). All statistical tests were 2-sided. A *p* value of < 0.05 is considered significant.

2.4 RESULTS

2.4.1 Reduced ANGPTL4 expression in impaired diabetic wound healing.

First, we characterized the spatiotemporal expression profile of ANGPTL4 mRNA and protein in wound healing of full-thickness excisional splint wounds between ob/+ (normal) and ob/ob (diabetic) mice. Macroscopic observation revealed that wounds of ob/ob mice were closed by only 40% when compared with ob/+ mice, whose wounds were completely closed by day 7-10 post-injury (Figure 26A and B). Haematoxylin and eosin staining of day 3, 5, 7 and 10 post-wound sections showed impaired epithelial regeneration and granulation tissue formation in ob/ob when compared with ob/+ mice. Histomorphometric analysis of centrally dissected ob/ob wound sections revealed significantly delayed re-epithelialization between day 3-10 post-wounding (Figures 26C). The epidermal wound area above the wound bed of the ob/ob mice remained larger compared with ob/+ mice on day 10 post-injury, suggesting delayed resolution of the wound re-epithelialization in ob/ob mice (Figure 26D). Quantitative real-time PCR (qPCR) analyses revealed reduced mRNA level of ANGPTL4 from day 3 post-wounding in ob/ob mice compared with ob/+ mice (Figure 27A). Consistent with qPCR data, the immunoblot analysis showed a ~5-fold reduction in the protein level of cANGPTL4 at day 5 post-wounding in ob/ob wounds (Figure 27B). Similarly, the immunofluorescence

staining of ANGPTL4 revealed a lower signal in the wound epithelia and wound bed when compared with ob/+ wounds (Figure 27C). The specificity of antibody was determined by infrared western blot analysis using skin biopsies from wildtype (ANGPTL4^{+/+}) and ANGPTL4-knockout (ANGPTL4^{-/-}) mice (Figure 28).

2.4.2 Topical application of cANGPTL4 improves the healing rate of diabetic wounds.

Next, we examined the effect of a single topical application of recombinant cANGPTL4 on the diabetic wound healing rate. We inflicted two full-thickness excisional splint wounds on the dorsal skin of ob/ob mice: one to be treated with saline and the other with cANGPTL4 (Figure 29A). Wound images at days 7 and 10 post-injury showed improved wound closure with cANGPTL4 treatment compared with saline treatment (Figure 29B). Histomorphological examination of wound sections showed that cANGPTL4 significantly accelerated re-epithelialisation compared with saline controls, as indicated by the reduced epithelial gap (Figure 29C and D). Similarly, the length of neo-epithelia from human skin biopsies was significantly dose-dependently increased in the diabetic-like condition with cANGPTL4 treatment compared to in normal or diabetic conditions without cANGPTL4 (Figures 29E and F).

Aberrant growth factor production and activation of cognate signalling cascades contribute to poor diabetic wound healing. To investigate if treatment of diabetic wounds with cANGPTL4 affected their expression profiles, we performed focused qPCR arrays on wound biopsies from control ob/+, and saline- and cANGPTL4-treated ob/ob wounds. We analysed 77 genes clustered according to the biological functions of proliferation, angiogenesis, cell migration, ECM matrix, cell apoptosis, and inflammation. Heat maps

revealed significant expression changes in many genes associated with angiogenesis, ECM remodelling, and inflammation (Figure 30A; Table 6, 7, and 8). cANGPTL4-treated ob/ob wounds exhibited a 61.1% change in overall differential gene profile compared to saline-treated ob/ob wounds, suggesting an altered wound healing signature (Figure 30B).

2.4.3 ANGPTL4 induces angiogenesis in diabetic wounds

Next, we examined expressions of markers of specific cell types, including endothelial cells (CD31), myofibroblasts (α SMA), proliferating cells (PCNA), and macrophages (F4/80). Saline-treated ob/ob wounds displayed reduced CD31 and α SMA expressions from day 3 post-wounding compared with ob/+ wounds. F4/80 and PCNA expressions were elevated until day 10 post-wounding in saline-treated ob/ob wounds compared with ob/+ wounds, consistent with prolonged inflammation and delayed resolution of wound re-epithelialisation (Figures 31A and B). Although the F4/80 and PCNA expression pattern remained unchanged in cANGPTL4-treated ob/ob wounds, the overall expression levels were significantly reduced compared to in saline-treated ob/ob wounds (Figure 31B). Notably, the CD31 and α SMA expression profiles in cANGPTL4-treated ob/ob wounds had reverted to those observed in ob/+ wounds (Figure 31B). To further strengthen our finding, immunofluorescence staining of Ki67, α SMA and CD31 were performed on day 5 and day 7 post-wounding biopsies from ob/+, saline- and cANGPTL4-treated ob/ob mice. No difference was observed in number of Ki67-positive proliferating cells among ob/+, saline- and cANGPTL4-treated ob/ob wounds (Figure 32). Consistent with the finding from western blots, immunostaining of

CD31 and α SMA in cANGPTL4-treated ob/ob wounds have reverted to those observed in ob/+ wounds (Figure 32).

To determine if ANGPTL4 improves wound angiogenesis, we performed immunofluorescence staining of CD31 and quantitative analysis of CD31-positive isolated cells from various treated day-5 wound biopsies. The Chalkley counting method was applied for analysing the extent of endothelial tube formation wherein a higher Chalkley count represents better angiogenesis. Chalkley counting method is a morphometric point counting systems using microscope eyepiece graticule and has been recommended as a standard in international consensus reports on the quantification of angiogenesis. cANGPTL4 treatment increased CD31 immunohistochemistry staining in ob/ob wounds compared with saline-treated ob/ob wounds (Figure 33A, top), indicating increased wound vasculature. The mean Chalkley counts of the cANGPTL4-treated ob/ob wounds was significantly 2-fold higher compared to saline-treated ob/ob wounds (Figure 33A, bottom). Our FACS analysis showed approximately 53% increase in CD31+ endothelial cells in cANGPTL4-treated ob/ob wounds compared with saline-treated ob/ob wounds, approaching to the level detected in ob/+ wounds (Figure 33B). Furthermore, 72.9% of the CD31+ endothelial cell population in cANGPTL4-treated ob/ob wounds also stained positive for proliferation marker Ki67, compared with only 30.7% and 52.4% (CD31+Ki67+) for saline-treated ob/ob and ob/+ wounds, respectively. Altogether, these observations indicate that cANGPTL4 improves wound angiogenesis.

To check if ANGPTL4 have any direct effect on the endothelial cells (ECs) survival, we have performed FACS analysis for both apoptosis (annexin and PI staining)

and proliferation (incorporation of BrdU) assay on attached ECs in the presence and absence of cANGPTL4. Our results did not show any significant difference on apoptosis and proliferation of cANGPTL4-treated ECs compared with saline-treated ECs (Figure 34)

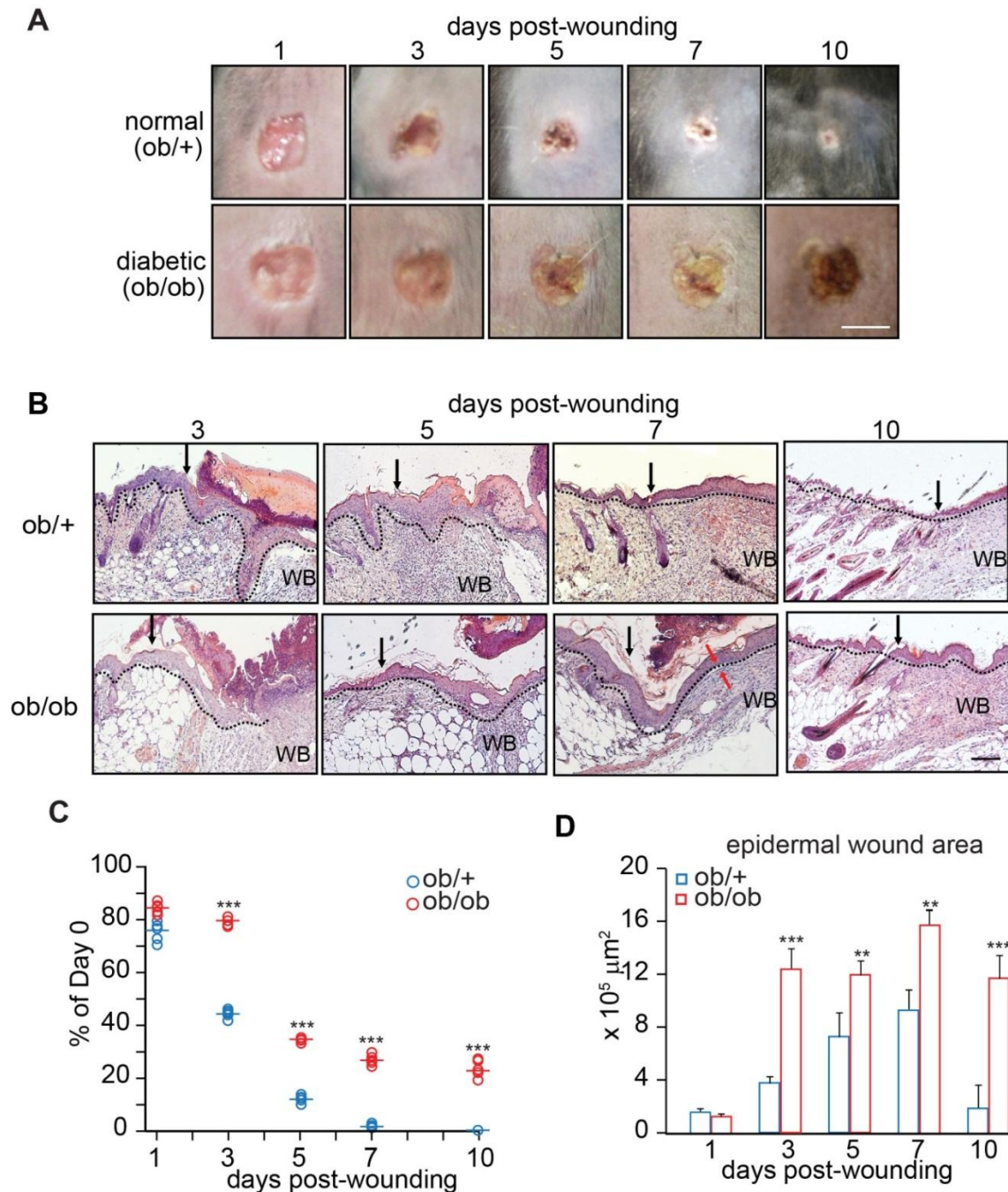


Figure 26. Analysis of centrally dissected ob/+ and ob/ob wound sections.

(A) Photos of normal (ob/+) and diabetic (ob/ob) wound biopsies taken at days 1, 3, 5, 7, and 10 post-wounding. Scale bar: 5 mm. **(B)** Representative haematoxylin and eosin images of wound biopsy sections from ob/+ and ob/ob mice at indicated days post-wounding. Arrows indicate the wound edge. Dotted lines delineate the epidermis–dermis interface. WB, wound bed. Scale bar: 100 μm. **(C)** Wound closure kinetics of ob/+ and ob/ob mice, with wound surface areas plotted as percentage of day 0 (100%). **(D)** Measurements of the epidermal wound area of ob/+ and ob/ob wound biopsies sections. Data are mean ± SEM, $n = 9$. * $p < 0.05$; ** $p < 0.01$; *** $p < 0.001$.

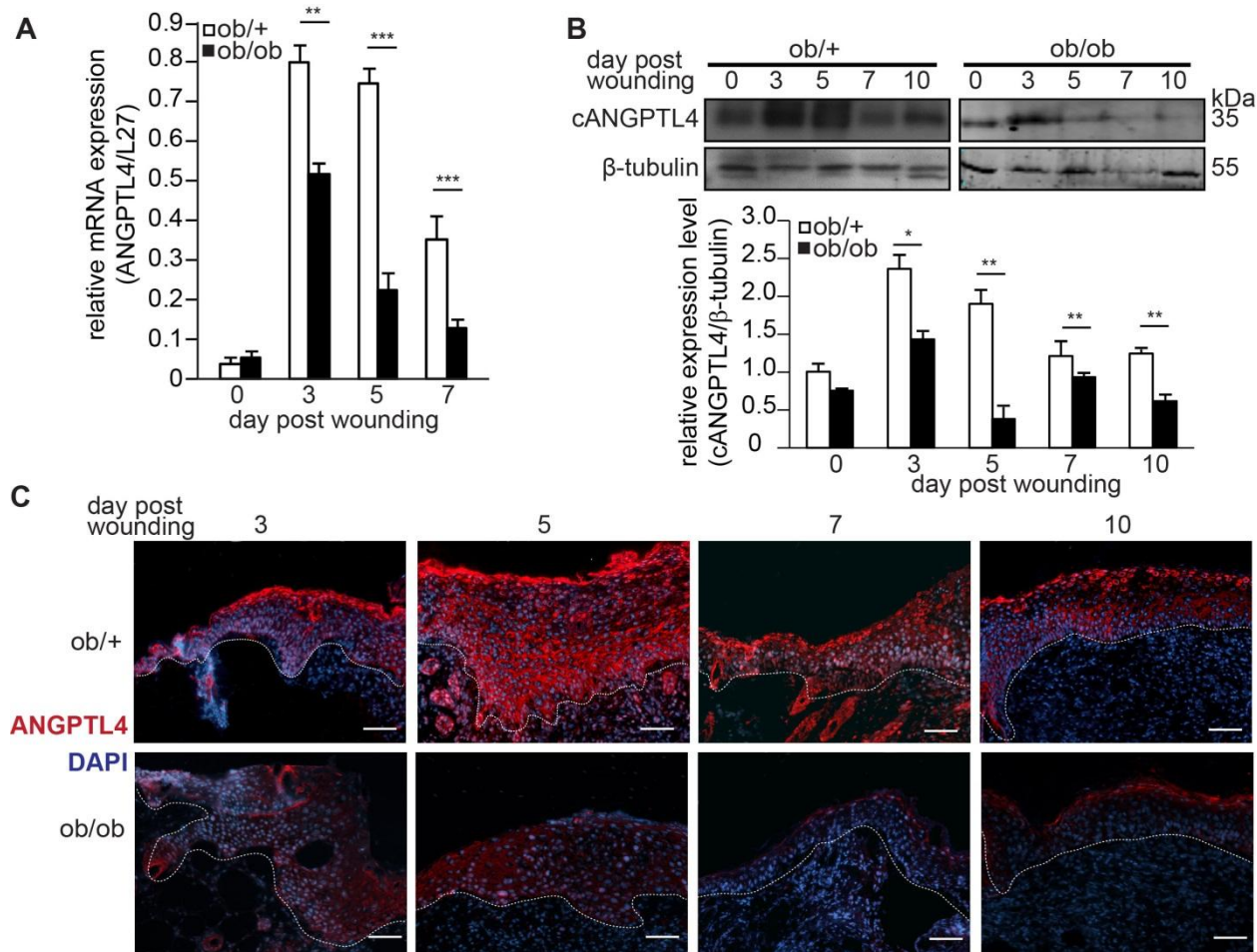


Figure 27. Expression of ANGPTL4 was reduced in diabetic wounds.

(A-B) Relative ANGPTL4 mRNA **(A)** and protein **(B)** levels in ob/+ and ob/ob wound biopsies as analysed by qPCR and immunoblotting, respectively. Graph shows the relative cANGPTL4 protein level compared to in the day 0 wound in ob/+ mice. qPCR values were normalized to the housekeeping gene ribosomal protein L27. β-tubulin served as a loading and transfer control for immunoblotting. **(C)** Immunofluorescence staining of ANGPTL4 (red) in ob/+ and ob/ob wound biopsies. Sections were counterstained with DAPI (blue). Dotted lines delineate the epidermis-dermis interface. Scale bar: 40 μm. Data are mean ± SEM, $n = 9$. * $p < 0.05$, ** $p < 0.01$, *** $p < 0.001$.

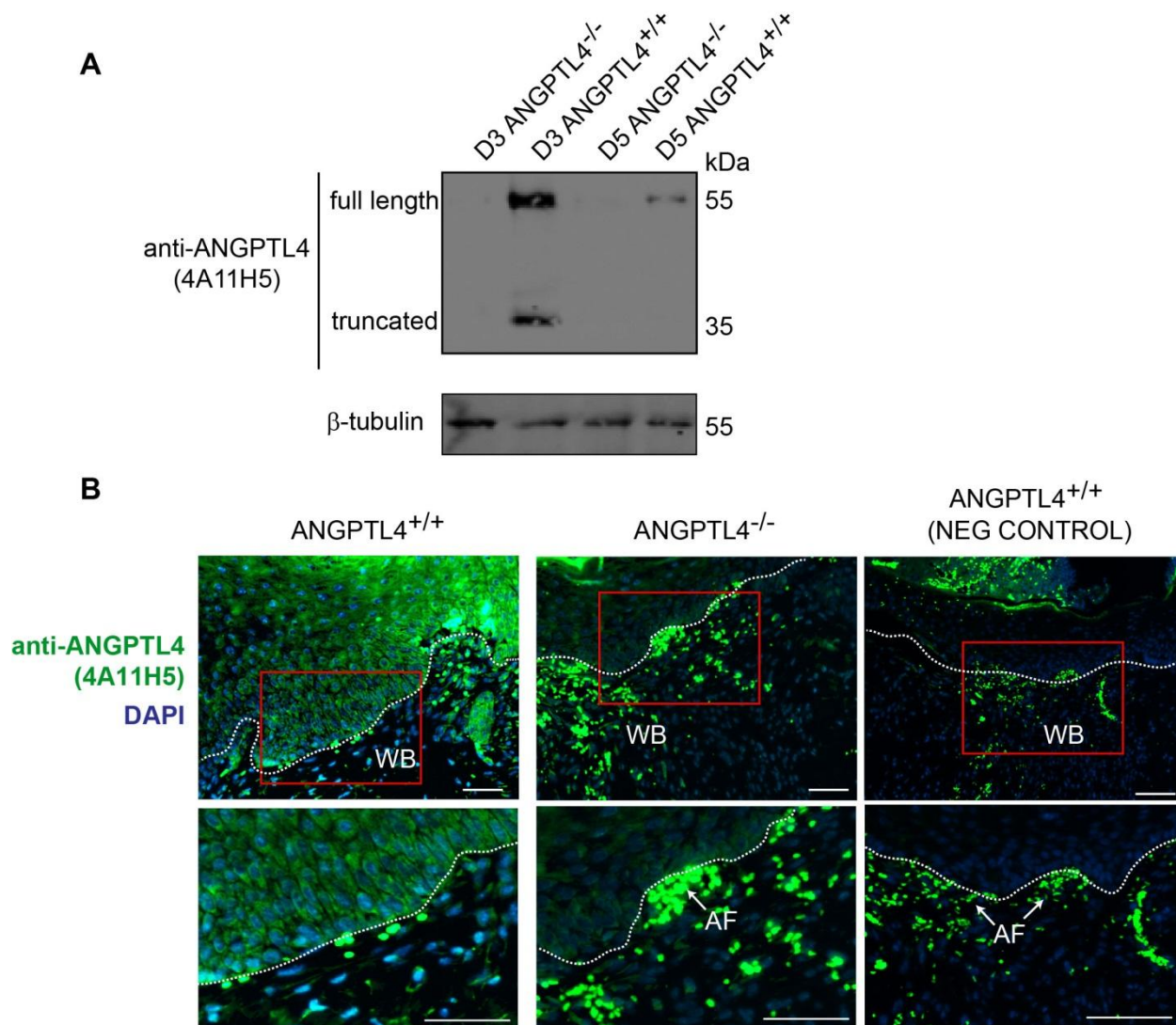


Figure 28. Specificity of monoclonal antibodies against mouse ANGPTL4.

Specificity of monoclonal antibodies against mouse ANGPTL4. **(A)** Immunoblot detection using monoclonal antibodies against cANGPTL4 (clone 4A11H5). Total wound biopsy lysates of wild-type (ANGPTL4^{+/+}) and ANGPTL4-knockout (ANGPTL4^{-/-}) mice were used. β -tubulin served as a loading and transfer control. **(B)** Immunofluorescence staining of cANGPTL4 (green) in day-5 post-wound biopsies from ANGPTL4^{+/+} and ANGPTL4^{-/-} mice using monoclonal antibodies against cANGPTL4 (clone 3F4F5). Nuclei were counterstained with DAPI (blue). Dotted lines delineate the epidermis-dermis interface. Scale bar: 20 μ m. AF: auto fluorescence. WB: wound bed.

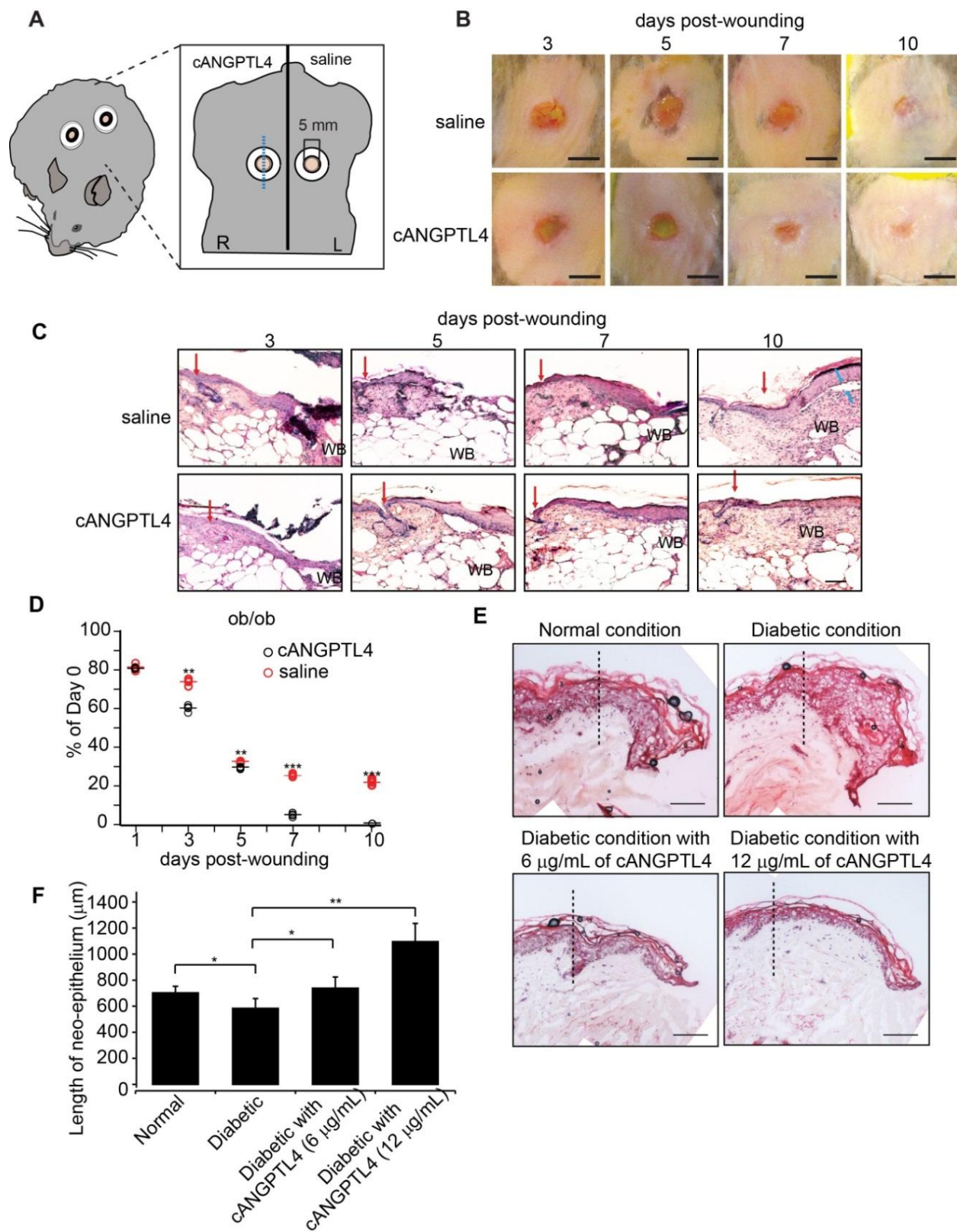


Figure 29. Topical application of ANGPTL4 improves diabetic wound healing.

(A) A schematic diagram illustrating the location and dimensions of full-thickness excision splint wounds on the dorsal skin of ob/ob mice. Single topical application of cANGPTL4 and control saline were both performed on each mouse. The blue dotted line indicates the centrally dissected region histological sections. **(B)** Representative photographs of saline- and cANGPTL4-treated ob/ob wound biopsies taken at day 3, 5, 7, and 10 post-wounding. Scale bar: 5 mm. **(C)** Representative haematoxylin and eosin images of saline- and cANGPTL4-treated wound sections. Arrows indicate the wound edge. Dotted lines delineate the epidermis–dermis interface. WB, wound bed. Scale bar: 100 μ m. **(D)** Wound closure kinetics of saline- and cANGPTL4-treated ob/ob wounds, with wound surface areas plotted as percentage of day 0 (100%). Data are mean \pm SEM, $n = 3$. * $p < 0.05$, ** $p < 0.01$. (b) Average lengths of neo-epithelium from human skin biopsies cultured for five days under normal and diabetic conditions with various cANGPTL4 concentrations. Data are mean \pm SEM, $n = 9$. * $p < 0.05$, ** $p < 0.01$, *** $p < 0.001$. **(E)** Representative haematoxylin and eosin-stained images of day-5 post-culturing human skin biopsies in normal conditions, diabetic conditions, and diabetic conditions with various concentrations of cANGPTL4. Black dotted lines mark the edge of the wound biopsy at day 0. Scale bar: 100 μ m. **(F)** Histomorphometric measurements of the neo epithelium from day-5 post-culturing human skin biopsies in normal conditions, diabetic conditions, and diabetic conditions with various concentrations of cANGPTL4. Data are mean \pm SEM, $n = 9$. * $p < 0.05$; ** $p < 0.01$.

Table 6. Gene expression in ob/+ wound

GenBank Accession No.	Symbol	Day 0	Day 3	Day 5	Day 7	Day 10
PROLIFERATION						
NM_008416	JUN-B	0.156725	6.554231	0.686169	0.588833	0.740001
NM_008108	GDF3	0.229432	6.458987	2.496683	1.688878	1.227741
NM_001033239	CSTA	0.188826	4.410111	19.62685	8.619888	4.364321
NM_011577.1	TGFB1	0.208501	2.552748	0.930714	0.573895	0.537032
NM_009532	XRCC1	0.409888	4.198295	1.129176	0.977582	2.504406
NM_001081117.2	Ki67	0.588614	5.438939	2.334188	2.623753	3.532172
NM_008037	FOSL2 (FRA2)	0.304307	2.714392	0.578645	1.197301	1.043532
NM_011386.2	SKIL (SnoN)	0.933885	6.077622	5.291099	2.839864	2.465658
NM_009652.3	AKT1	0.594666	3.446702	1.482059	1.238363	0.856369
NM_010427.4	HGF	0.291696	1.172812	1.299929	0.499510	0.523416
NM_011952	MAPK3 (1b)	0.351700	1.105140	0.604718	0.490997	0.420572
NM_009870	CDK4	0.637520	1.941299	1.289818	1.329348	1.012852
NM_009896	SOCS1	0.751820	2.015070	2.614084	0.911380	1.054464
NM_008008.4	KGF (FGF7)	0.514706	1.121522	0.805334	0.382475	0.653387
NM_031199.3	TGFA	1.109040	1.833541	2.902839	2.059449	1.384412
NM_007670.4	p15 (CDKN2B)	0.868720	1.674337	1.066530	0.908250	2.178165
AF016189.1	Smad3	0.661817	1.268314	1.040053	0.544876	0.578266
NM_008006.2	FGF2	0.424226	0.758342	0.404547	0.205858	0.116904
NM_009283	STAT 1	0.762617	1.081457	1.543661	0.645053	0.284173
NM_008279.2	MAP4K1	0.520385	0.904445	1.013113	0.508003	0.336498
NM_207655	EGFR	0.664681	1.006642	0.765933	0.649277	1.052040
NM_011145.3	PPAR β/δ	0.858071	0.412738	1.301343	0.497965	0.009220
NM_007987.2	FAS	0.208006	0.226172	0.034424	0.294469	0.434092
NM_009370.2	TGFBR1 (ALK5)	0.968227	0.932627	0.914630	0.872759	1.227945
NM_010927.3	iNOS (NOS2)	0.367154	0.203582	1.026928	0.830821	0.697027
NM_009969.4	GM-CSF	1.305664	2.057592	2.319032	0.914727	1.289411
NM_011144.6	PPAR α	1.376648	0.632694	0.504220	0.400709	0.522342
ANGIOGENESIS						
NM_007426.3	ANGPT2	0.110251	0.611290	1.771250	0.254272	0.542262
NM_009505	VEGFA	1.256536	4.690086	2.205454	0.880261	1.104457
BC003806	STAT 3	0.704101	1.526852	1.145983	0.678334	0.527540
NM_011057.3	PDGFB	0.938039	1.825587	1.793180	0.767349	0.703514
AF016189.1	Smad3	0.661817	1.268314	1.040053	0.544876	0.578266
NM_008808.3	PDGFA	1.034881	1.018791	2.165501	1.084197	0.596449
NM_009370.2	TGFBR1 (ALK5)	0.968227	0.932627	0.914630	0.872759	1.227945
NM_009640.3	ANGPT1	0.312981	0.223352	0.185313	0.106564	0.354713
NM_010197.3	FGF1	1.506516	0.845095	0.630055	0.433178	0.586736

NM_010927.3	iNOS (NOS2)	0.367154	0.203582	1.026928	0.830821	0.697027
NM_008816.2	PECAM1	1.588275	0.808740	0.777321	0.556189	0.528869
NM_009605	Adipoq	0.257089	0.063623	0.025200	0.058030	0.196103
MIGRATION						
NM_010140	EPHA3	0.171504	1.410735	1.281664	0.973647	0.495663
NM_011952	MAPK3 (1b)	0.351700	1.105140	0.604718	0.490997	0.420572
BC003806	STAT 3	0.704101	1.526852	1.145983	0.678334	0.527540
NM_008036	FOSB	0.844083	1.618836	0.867265	0.668838	0.237066
NM_008402	ITGAV	0.846653	1.623685	1.197204	0.841523	1.464738
AF016189.1	Smad3	0.661817	1.268314	1.040053	0.544876	0.578266
NM_010143	EPHB3	0.529828	0.904733	1.098044	1.000996	1.697639
NM_008279.2	MAP4K1	0.520385	0.904445	1.013113	0.508003	0.336498
NM_016802	RHOA	0.981261	0.993775	0.959051	0.838295	0.292791
NM_009370.2	TGFBR1 (ALK5)	0.968227	0.932627	0.914630	0.872759	1.227945
NM_009396.2	TNFAIP2	0.906535	0.835809	0.654888	0.223550	0.280186
NM_001127330.1	PPAR γ	1.202532	0.414603	0.380897	0.343301	0.282584
ECM						
NM_011593	TIMP1	0.097499	4.779940	0.615597	0.958408	0.450441
NM_009263	OPN (Spp1)	0.159337	3.386260	4.407381	0.672715	0.059469
NM_011607	TNC	0.338232	4.641325	7.723610	5.793988	5.375437
NM_013599	MMP9	0.531998	4.645245	6.016101	1.933875	0.820979
NM_008607	MMP13	0.232440	1.656137	0.666829	0.157788	0.147205
NM_011580	TSP-1	0.476082	2.211606	1.336181	1.194293	1.231223
NM_007404	ADAM9	0.395403	1.213515	0.922171	0.342360	0.502758
NM_009242	SPARC	0.480204	0.790912	1.807140	1.017414	0.620502
NM_011594	TIMP2	0.497669	1.036548	1.227695	0.723035	0.989423
NM_011595.2	TIMP3	0.896732	0.560416	0.344548	0.200935	0.748156
NM_008871	PAI1 (Serpine1)	1.717840	0.884620	0.889975	0.807652	0.147766
NM_009367.3	TGFB2	1.284430	0.576548	0.736159	0.456816	0.430501
NM_010296.2	GLI1	1.502637	0.463211	0.562287	0.830497	0.324001
APOPTOSIS						
NM_007464	IAP2	0.665846	1.511230	1.138860	0.771053	0.395123
NM_009283	STAT 1	0.762617	1.081457	1.543661	0.645053	0.284173
NM_010517	IGFBP4	0.614106	0.888844	0.794956	0.303044	0.749203
INFLAMMATION						
NM_013693	TNFA	0.037312	10.2316	0.468858	0.422693	0.096479
NM_008176	CXCL1	0.083437	11.05786	0.793785	0.764558	0.222295
NM_010548.2	IL-10	0.020473	1.212068	1.264306	0.646134	0.441396
NM_009141.2	CXCL5	0.149996	3.711946	0.489938	0.408244	0.097458

NM_021274.1	CXCL10	0.091558	2.402611	0.894154	0.391871	0.335992
NM_011333.3	CCL2	0.086708	1.764824	1.228643	0.346389	0.110375
NM_008380	INHBA	0.182848	3.492547	1.071480	0.740565	0.810593
NM_007707	SOCS3	0.526876	4.127815	1.742194	0.789632	0.430064
NM_011905	TLR2	0.503839	2.670658	0.809051	0.389091	0.302130
NM_031168.1	IL-6	0.366964	1.705026	2.175877	0.605557	0.571960
BC109135	IL1R1	0.496046	1.924439	1.098497	0.653671	1.475758
NM_010431	HIF1A	0.752800	2.806556	1.038764	0.756955	0.682358
NM_021297	TLR4	0.503916	1.382422	1.054945	0.475487	0.424482
NM_008599.4	CXCL9	0.345309	0.727598	1.372522	0.565455	0.459662
NM_011488	STAT 5A	0.453144	0.918977	0.756884	0.581519	0.459055
NM_009507.3	VHL	1.001643	1.742515	1.298497	0.814256	0.597035
NM_009283	STAT 1	0.762617	1.081457	1.543661	0.645053	0.284173
NM_008360.1	IL-18	0.366857	0.203418	1.026099	0.830150	0.696464
NM_010638	KLF-9	0.685050	0.862250	0.386243	0.336787	0.280775
NM_011330.3	CCL11	0.529826	0.320064	0.593788	0.206036	0.217236
NM_010927.3	iNOS (NOS2)	0.367154	0.203582	1.026928	0.830821	0.697027

Table 7. Gene expression in Saline-treated ob/ob wound.

GenBank Accession No.	Symbol	Day 0	Day 3	Day 5	Day 7	Day 10
PROLIFERATION						
NM_008416	JUN-B	0.152556	3.172094	1.526778	4.484403	0.287089
NM_008108	GDF3	0.136515	4.965691	6.243470	3.966791	1.550918
NM_001033239	CSTA	0.508856	27.13025	12.53943	23.37949	0.406501
NM_011577.1	TGFB1	0.549678	1.355657	3.658518	3.642923	0.660413
NM_009532	XRCC1	3.868010	0.530499	1.031126	1.409277	1.518873
NM_001081117.2	Ki67	1.853563	3.629809	4.337301	4.743085	1.651986
NM_008037	FOSL2 (FRA2)	0.389147	1.190892	0.566979	0.741474	0.302783
NM_011386.2	SKIL (SnoN)	2.759996	8.323164	7.297358	9.664507	2.415079
NM_009652.3	AKT1	1.134636	1.321611	2.016966	1.711165	0.510856
NM_010427.4	HGF	0.160628	1.743398	2.166984	0.647157	0.904471
NM_011952	MAPK3 (1b)	0.597765	0.716862	0.944315	0.734004	0.394860
NM_009870	CDK4	0.813738	1.337735	1.360731	1.560888	1.018518
NM_009896	SOCS1	1.497767	4.148567	3.142511	2.844695	0.437668
NM_008008.4	KGF (FGF7)	0.595196	1.110988	0.991840	0.742551	0.623343
NM_031199.3	TGFA	2.332045	5.168670	4.421783	2.873906	2.726296
NM_007670.4	p15 (CDKN2B)	1.499122	0.705773	1.415514	1.818516	1.478039
AF016189.1	Smad3	0.742435	0.750201	0.441932	0.598625	0.186970
NM_008006.2	FGF2	1.317701	0.766727	0.713610	0.360296	0.185439
NM_009283	STAT 1	1.007855	1.307954	2.155304	1.825283	0.473602
NM_008279.2	MAP4K1	0.278249	0.832453	0.819214	0.807961	0.291905
NM_207655	EGFR	1.023921	0.713711	1.000820	0.444678	0.714879
NM_011145.3	PPAR β/δ	0.514494	2.530547	2.382542	2.280499	1.296668
NM_007987.2	FAS	0.439816	0.099373	0.224529	0.135704	0.263693
NM_009370.2	TGFBR1 (ALK5)	2.250052	2.189751	1.554899	1.455078	1.831485
NM_010927.3	iNOS (NOS2)	0.102444	0.035823	0.001465	0.000879	0.000051
NM_009969.4	GM-CSF	0.532663	1.575585	0.216542	5.371917	2.828046
NM_011144.6	PPAR α	1.358423	0.585544	0.716725	0.508685	0.755341
ANGIOGENESIS						
NM_007426.3	ANGPT2	2.597985	0.522414	1.412809	1.019220	0.291111
NM_009505	VEGFA	1.317539	1.372430	1.666211	0.969143	0.441270
BC003806	STAT 3	0.838114	1.418559	0.857724	0.339311	0.172353
NM_011057.3	PDGFB	0.669607	1.105467	1.523259	2.128962	0.947266
AF016189.1	Smad3	0.742435	0.750201	0.441932	0.598625	0.186970
NM_008808.3	PDGFA	0.300793	0.745053	1.267399	1.203785	0.673345
NM_009370.2	TGFBR1 (ALK5)	2.250052	2.189751	1.554899	1.455078	1.831485

NM_009640.3	ANGPT1	0.271623	0.541881	0.486119	0.361020	0.208196
NM_010197.3	FGF1	1.809058	1.298661	1.220293	0.873766	0.791780
NM_010927.3	iNOS (NOS2)	0.102444	0.035823	0.001465	0.000879	0.000051
NM_008816.2	PECAM1	1.026536	1.012497	1.271402	1.030997	0.486843
NM_009605	Adipoq	0.525416	0.118814	0.081237	0.043210	0.059965

MIGRATION

NM_010140	EPHA3	0.856996	0.323590	2.581308	0.504820	0.444591
NM_011952	MAPK3 (1b)	0.597765	0.716862	0.944315	0.734004	0.394860
BC003806	STAT 3	0.838114	1.418559	0.857724	0.339311	0.172353
NM_008036	FOSB	0.474459	2.473119	0.902717	1.233993	0.129576
NM_008402	ITGAV	1.486966	2.218466	3.554344	2.428998	0.618679
AF016189.1	Smad3	0.742435	0.750201	0.441932	0.598625	0.186970
NM_010143	EPHB3	0.389309	1.173355	0.966125	0.878085	0.871821
NM_008279.2	MAP4K1	0.278249	0.832453	0.819214	0.807961	0.291905
NM_016802	RHOA	0.656541	1.501634	1.183005	1.251562	0.693547
NM_009370.2	TGFBR1 (ALK5)	2.250052	2.189751	1.554899	1.455078	1.831485
NM_009396.2	TNFAIP2	1.334465	0.900658	0.394656	0.916066	0.434364
NM_001127330.1	PPAR γ	1.476165	0.923280	0.820091	0.499319	0.464317

ECM

NM_011593	TIMP1	0.092007	0.675698	0.641478	0.466803	0.346310
NM_009263	OPN (Spp1)	0.321897	11.29194	9.796510	6.725629	0.642136
NM_011607	TNC	0.196003	9.033474	22.59936	16.33259	3.236137
NM_013599	MMP9	0.486960	9.389738	5.523574	11.41316	0.324407
NM_008607	MMP13	0.196111	1.485535	1.072455	2.229062	0.556222
NM_011580	TSP-1	0.178282	2.934585	1.655054	5.159779	0.417450
NM_007404	ADAM9	1.481524	1.773434	1.590105	1.043663	0.435286
NM_009242	SPARC	0.766017	0.643615	1.251748	1.260813	0.512365
NM_011594	TIMP2	0.615494	0.690985	1.270724	0.802109	0.397484
NM_011595.2	TIMP3	1.082271	0.327056	0.547626	0.502637	0.409326
NM_008871	PAI1 (Serpine1)	0.827940	0.504290	0.910365	2.138120	0.777036
NM_009367.3	TGFB2	1.267494	1.106269	0.693061	1.008982	0.465939
NM_010296.2	GLI1	0.777933	0.523369	0.833232	0.636208	0.621880

APOPTOSIS

NM_007464	IAP2	0.881733	0.995298	0.952775	1.001650	0.451337
NM_009283	STAT 1	1.007855	1.307954	2.155304	1.825283	0.473602
NM_010517	IGFBP4	0.847077	0.400526	1.231736	0.543980	0.370002

INFLAMMATION

NM_013693	TNFA	0.058466	1.534815	0.864856	6.997037	0.097500
NM_008176	CXCL1	0.103358	7.129337	4.410788	6.082674	0.036343

NM_010548.2	IL-10	0.297165	1.451524	1.288575	0.515189	0.264587
NM_009141.2	CXCL5	0.501839	40.88581	49.65191	5.464767	0.372129
NM_021274.1	CXCL10	0.250498	1.126345	1.284465	0.890984	0.680621
NM_011333.3	CCL2	0.214683	8.392496	5.935198	1.128045	0.200589
NM_008380	INHBA	0.919534	2.784224	5.537288	2.269734	1.586482
NM_007707	SOCS3	1.077089	5.065714	2.008733	2.584182	0.374945
NM_011905	TLR2	0.489705	2.922228	2.985972	3.031845	0.281524
NM_031168.1	IL-6	0.195309	8.340513	5.607855	3.060826	1.208423
BC109135	IL1R1	0.921124	1.726157	3.633038	1.147471	0.455597
NM_010431	HIF1A	0.895448	1.387657	0.906589	0.592514	0.778827
NM_021297	TLR4	0.713236	2.706313	2.601621	1.873377	0.369483
NM_008599.4	CXCL9	1.157953	2.190138	2.601004	2.702952	3.172733
NM_011488	STAT 5A	0.852498	0.754894	1.008012	0.649486	0.236424
NM_009507.3	VHL	1.440808	2.150269	2.576122	2.349019	0.933073
NM_009283	STAT 1	1.007855	1.307954	2.155304	1.825283	0.473602
NM_008360.1	IL-18	0.599095	0.486806	0.888455	0.557822	0.345020
NM_010638	KLF-9	1.401337	0.431655	0.642859	0.516679	0.310364
NM_011330.3	CCL11	0.969593	0.610924	0.957601	0.370957	0.464304
NM_010927.3	iNOS (NOS2)	0.102444	0.035823	0.001465	0.000879	0.000051

Table 8. Gene expression in cANGPTL4-treated ob/ob wound.

GenBank Accession No.	Symbol	Day 0	Day 3	Day 5	Day 7	Day 10
PROLIFERATION						
NM_008416	JUN-B	0.152556	0.290977	0.208893	0.766593	0.167475
NM_008108	GDF3	0.136515	0.846272	0.296635	2.639181	0.218525
NM_001033239	CSTA	0.508856	0.436876	0.892908	1.389773	0.808699
NM_011577.1	TGFB1	0.549678	1.010338	0.871393	0.986599	0.762965
NM_009532	XRCC1	3.868010	1.213521	3.451768	6.807802	1.314453
NM_001081117.2	Ki67	1.853563	2.490830	1.048289	1.563181	1.089726
NM_008037	FOSL2 (FRA2)	0.389147	0.374920	0.292734	1.037806	0.536654
NM_011386.2	SKIL (SnoN)	2.759996	4.644625	0.958261	0.205126	1.329661
NM_009652.3	AKT1	1.134636	1.186596	2.733216	2.781050	1.233187
NM_010427.4	HGF	0.160628	0.700922	2.321898	3.635397	0.980706
NM_011952	MAPK3 (1b)	0.597765	0.989835	0.468527	0.504593	0.557869
NM_009870	CDK4	0.813738	1.063913	0.873984	0.929762	0.879897
NM_009896	SOCS1	1.497767	0.871649	0.263218	2.390392	0.576740
NM_008008.4	KGF (FGF7)	0.595196	0.771334	1.472135	0.915021	1.124630
NM_031199.3	TGFA	2.332045	4.677648	3.229010	0.035038	2.678183
NM_007670.4	p15 (CDKN2B)	1.499122	2.126865	1.404709	0.795709	1.176000
AF016189.1	Smad3	0.742435	0.462236	0.015755	0.383951	0.649618
NM_008006.2	FGF2	1.317701	0.443933	2.333738	0.177052	0.132299
NM_009283	STAT 1	1.007855	0.997653	0.980602	0.980859	1.000369
NM_008279.2	MAP4K1	0.278249	0.750923	0.598703	0.496168	0.784413
NM_207655	EGFR	1.023921	1.435695	0.308265	0.587702	1.157887
NM_011145.3	PPAR β/δ	0.514494	0.711088	15.66685	1.811131	0.064872
NM_007987.2	FAS	0.439816	0.872716	0.952662	0.286981	0.595842
NM_009370.2	TGFBR1 (ALK5)	2.250052	1.049709	1.250868	21.28802	2.680332
NM_010927.3	iNOS (NOS2)	0.232430	0.215077	0.262108	0.834560	0.500736
NM_009969.4	GM-CSF	0.532663	0.538789	0.140713	1.251679	0.869274
NM_011144.6	PPAR α	1.358423	0.797189	1.360061	1.655384	1.062509
ANGIOGENESIS						
NM_007426.3	ANGPT2	2.597985	0.591592	1.246518	0.070762	0.001531
NM_009505	VEGFA	1.317539	0.892290	1.269733	1.239880	0.761824
BC003806	STAT 3	0.838114	1.024890	0.508845	0.824855	0.561319
NM_011057.3	PDGFB	0.669607	0.862382	0.718599	2.285251	0.846454
AF016189.1	Smad3	0.742435	0.462236	0.015755	0.383951	0.649618
NM_008808.3	PDGFA	0.300793	0.527603	0.540157	2.009957	0.718748
NM_009370.2	TGFBR1 (ALK5)	2.250052	1.049709	1.250868	21.28802	2.680332

NM_009640.3	ANGPT1	0.271623	0.523158	0.789467	0.373875	0.353373
NM_010197.3	FGF1	1.809058	0.675523	0.911098	2.808195	1.058101
NM_010927.3	iNOS (NOS2)	0.232430	0.215077	0.262108	0.834560	0.500736
NM_008816.2	PECAM1	1.026536	9.734563	40.79655	80.68790	0.175586
NM_009605	Adipoq	0.525416	0.893195	1.281693	0.295419	0.358659

MIGRATION

NM_010140	EPHA3	0.856996	0.988881	0.775695	1.061996	0.677151
NM_011952	MAPK3 (1b)	0.597765	0.989835	0.468527	0.504593	0.557869
BC003806	STAT 3	0.838114	1.024890	0.508845	0.824855	0.561319
NM_008036	FOSB	0.474459	0.444920	0.514906	0.554858	0.313006
NM_008402	ITGAV	1.486966	1.653031	0.324666	0.099062	1.032131
AF016189.1	Smad3	0.742435	0.462236	0.015755	0.383951	0.649618
NM_010143	EPHB3	0.389309	0.401851	0.933636	3.133712	0.720600
NM_008279.2	MAP4K1	0.278249	0.750923	0.598703	0.496168	0.784413
NM_016802	RHOA	0.656541	0.648247	1.623903	5.220673	0.848715
NM_009370.2	TGFBR1 (ALK5)	2.250052	1.049709	1.250868	21.28802	2.680332
NM_009396.2	TNFAIP2	1.334465	0.831268	0.974859	1.426047	0.863158
NM_001127330.1	PPAR γ	1.476165	5.312032	0.077685	0.085928	1.257537

ECM

NM_011593	TIMP1	0.092007	0.428043	0.322566	0.423165	0.171270
NM_009263	OPN (Spp1)	0.321897	0.338047	0.659040	0.730737	0.434753
NM_011607	TNC	0.196003	0.688293	0.605825	1.365889	0.858515
NM_013599	MMP9	0.486960	0.325888	0.769769	1.277531	0.611197
NM_008607	MMP13	0.196111	0.242981	0.258511	1.746660	0.218456
NM_011580	TSP-1	0.178282	0.682218	0.493199	2.000362	0.278808
NM_007404	ADAM9	1.481524	2.147589	0.467171	2.137471	11.81901
NM_009242	SPARC	0.766017	0.957468	0.796479	0.809897	0.692813
NM_011594	TIMP2	0.615494	0.972705	1.119709	0.942139	0.439807
NM_011595.2	TIMP3	1.082271	0.877912	0.952572	1.509514	2.262474
NM_008871	PAI1 (Serpine1)	0.827940	0.504427	0.910143	1.296887	0.629588
NM_009367.3	TGFB2	1.267494	1.179050	0.774397	1.370055	0.683359
NM_010296.2	GLI1	0.777933	2.061107	0.423950	0.490343	1.332113

APOPTOSIS

NM_007464	IAP2	0.881733	0.888382	1.288717	1.131918	0.734564
NM_009283	STAT 1	1.007855	0.997653	0.980602	0.980859	1.000369
NM_010517	IGFBP4	0.847077	1.034808	0.868898	0.782863	0.960491

INFLAMMATION

NM_013693	TNFA	0.058466	0.293317	0.079136	0.504884	0.132312
NM_008176	CXCL1	0.103358	0.353159	0.165312	0.652480	0.127210

NM_010548.2	IL-10	0.297165	0.909327	0.899593	0.829194	0.320147
NM_009141.2	CXCL5	0.501839	0.501839	0.585031	0.997935	0.266491
NM_021274.1	CXCL10	0.250498	0.685454	0.563339	1.024823	0.476465
NM_011333.3	CCL2	0.214683	0.705153	0.839760	0.526328	0.290852
NM_008380	INHBA	0.919534	0.912952	0.866716	0.977302	0.924911
NM_007707	SOCS3	1.077089	1.087759	1.090964	0.963710	1.126733
NM_011905	TLR2	0.489705	0.924216	0.755532	1.526709	0.526428
NM_031168.1	IL-6	0.195309	0.224720	0.507640	0.711335	0.196630
BC109135	IL1R1	0.921124	0.934476	1.074441	1.026327	0.973915
NM_010431	HIF1A	0.895448	1.136411	0.792758	0.750116	1.253959
NM_021297	TLR4	0.713236	0.922546	1.072581	1.115380	0.944624
NM_008599.4	CXCL9	1.157953	1.052630	1.006731	0.955921	1.009809
NM_011488	STAT 5A	0.852498	1.027928	0.950384	0.832105	0.879752
NM_009507.3	VHL	1.440808	1.480614	0.966011	0.768630	1.196276
NM_009283	STAT 1	1.007855	0.997653	0.980602	0.980859	1.000369
NM_008360.1	IL-18	0.599095	0.831837	1.030033	1.007655	0.873737
NM_010638	KLF-9	1.401337	1.351285	0.209858	0.106323	0.293995
NM_011330.3	CCL11	0.969593	1.001181	1.038671	0.967775	0.930282
NM_010927.3	iNOS (NOS2)	0.232430	0.215077	0.262108	0.834560	0.500736

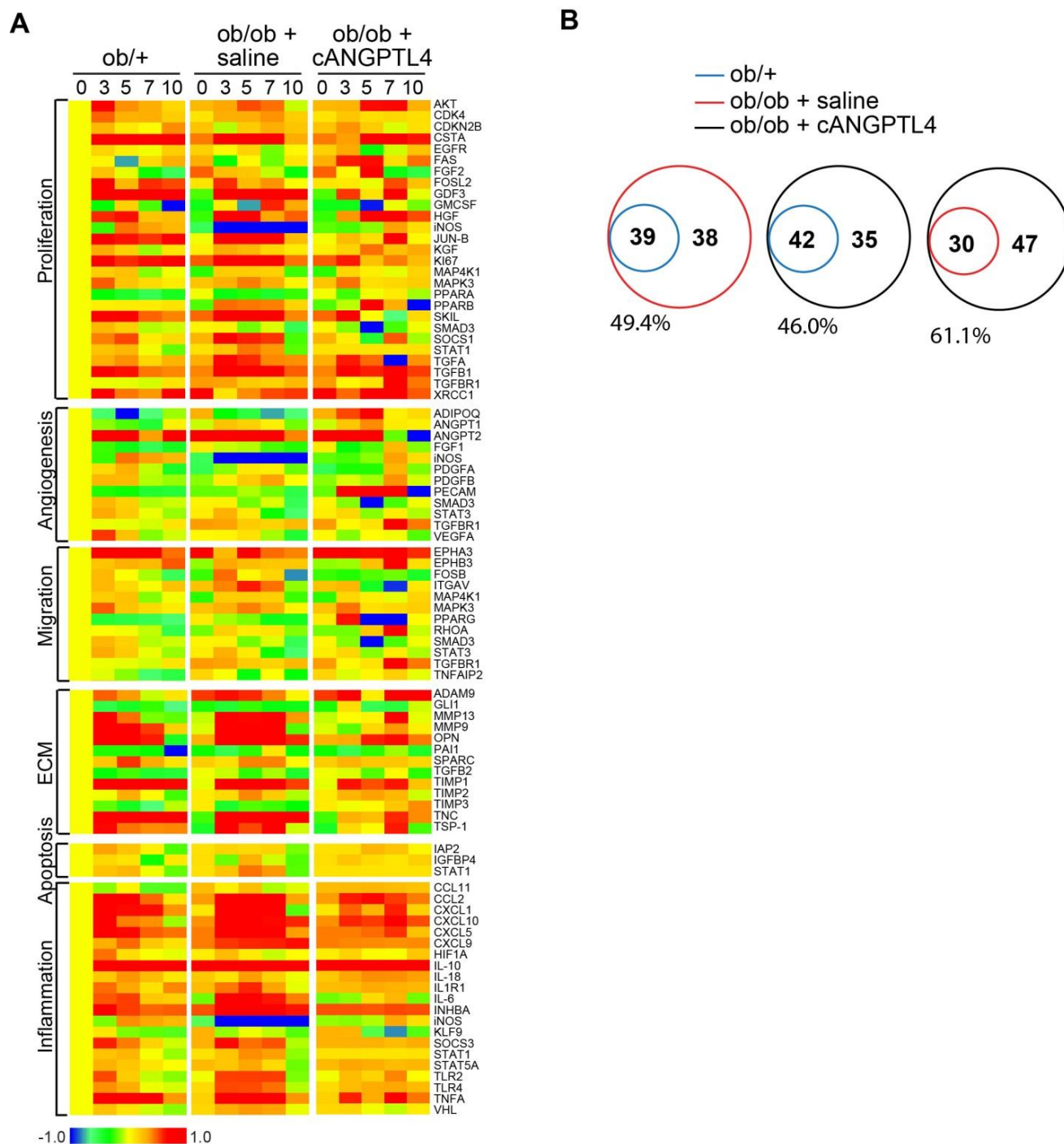


Figure 30. ANGPTL4 implications on several biological gene functions.

(A) Heat maps show gene expression profiles of ob/+, and saline- and cANGPTL4-treated ob/ob wounds. Genes are clustered according to the following biological gene functions: proliferation, angiogenesis, migration, ECM, apoptosis, and inflammation. The colour spectrum from blue to red depicts the fold-change in LOG form from -1.0 to 1.0 . **(B)** Venn diagram comparing total number of genes from ob/+ (blue), and saline- (red) and cANGPTL4-treated (black) ob/ob wounds. Comparisons of the percentages of total numbers of genes changed.

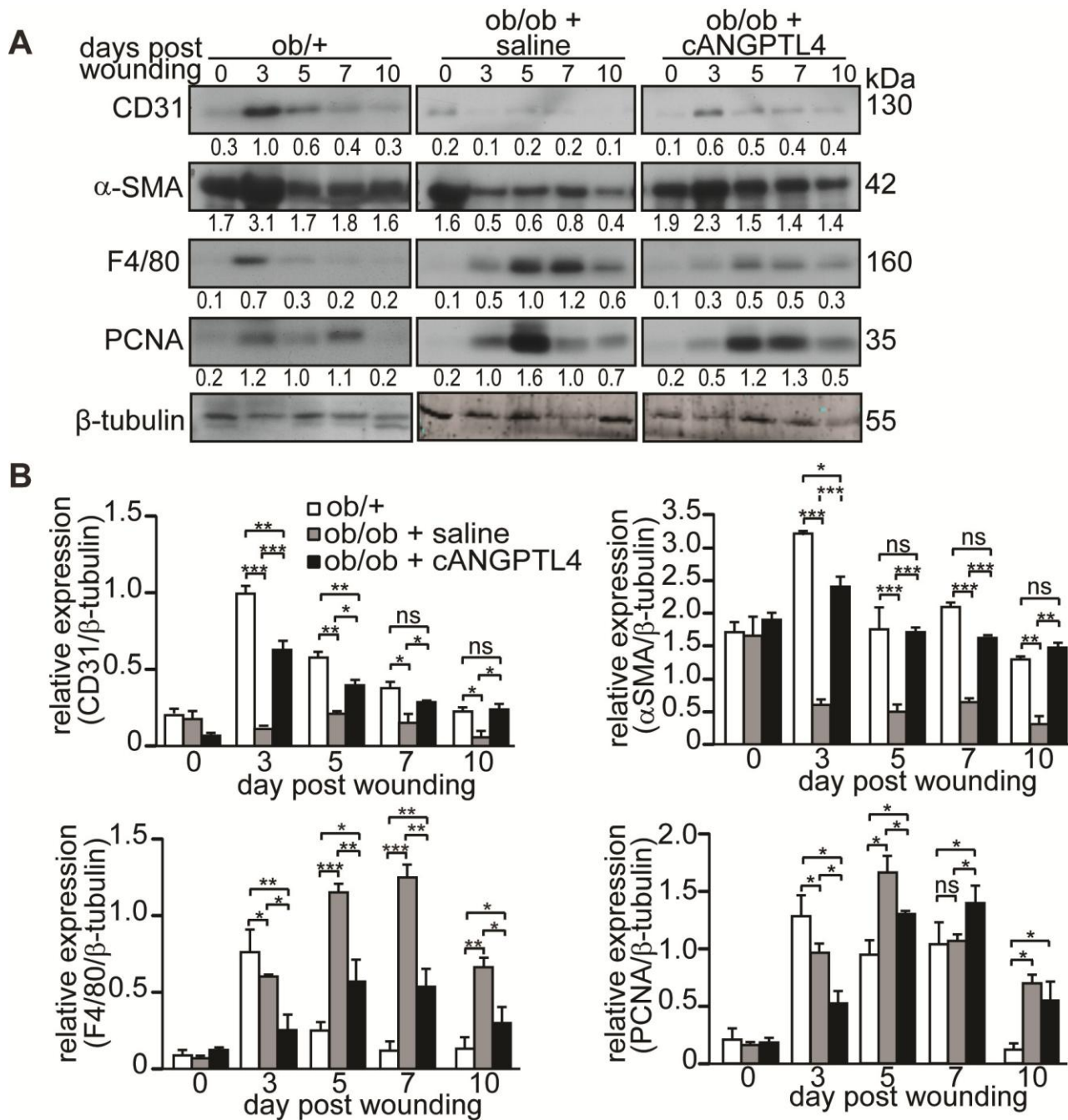


Figure 31. ANGPTL4 improves wound-related angiogenesis.

(A) Representative immunoblots and **(B)** graph showing relative protein levels of indicated proteins from ob/+, and saline- and cANGPTL4-treated ob/ob wound biopsies. The graph was determined based on the mean densitometry value of the immunoblot obtained from 3 independent set of mice wounding experiments. The data was normalized against the densitometry value of β -tubulin, which served as a loading and transfer control. Data are mean \pm SEM, $n = 12$ mice per set. * $p < 0.05$; ** $p < 0.01$, *** $p < 0.001$ by unpaired Student's t-test.

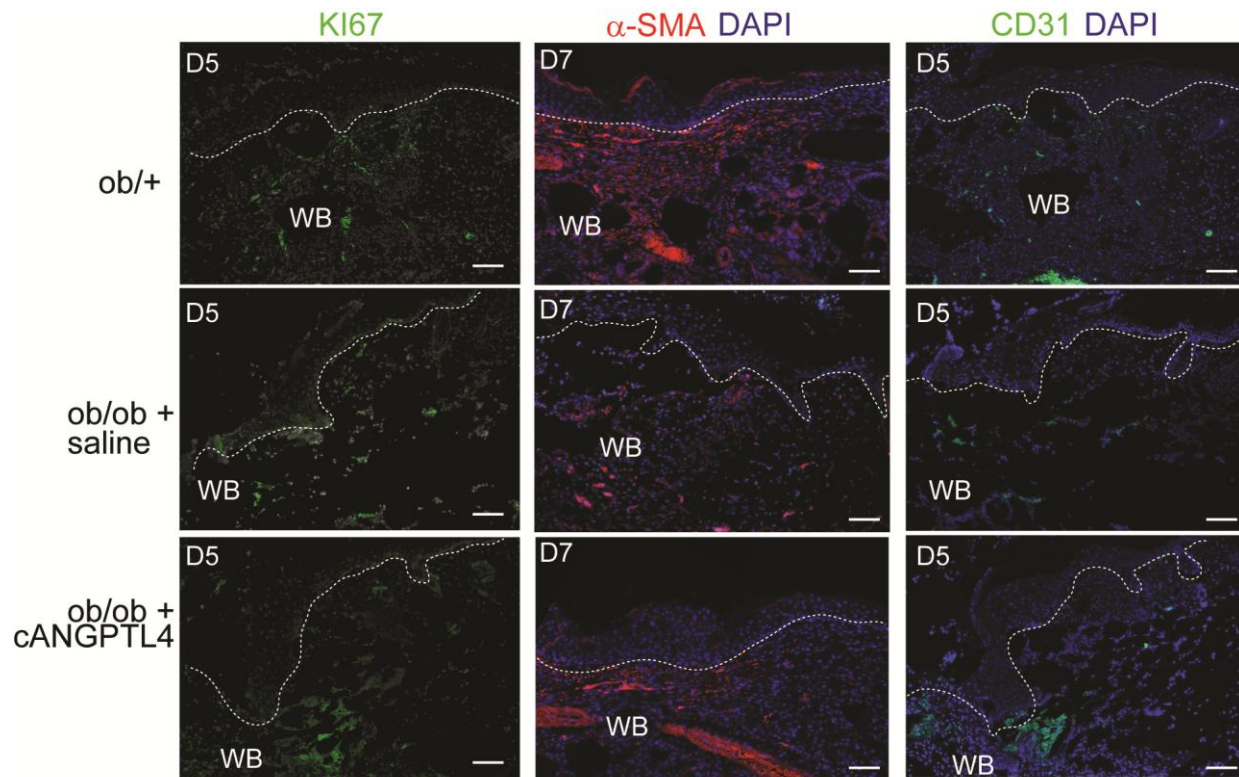


Figure 32. Immunofluorescence staining of wound biopsies

Immunofluorescence staining for Ki67 (green), α SMA (red) and CD31 (green) on *ob/+*, and saline- and cANGPTL4-treated *ob/ob* wound biopsies. Nuclei are counterstained with DAPI (blue). Dotted lines delineate the epidermis–dermis interface. WB: wound bed. Scale bar: 20 μ m.

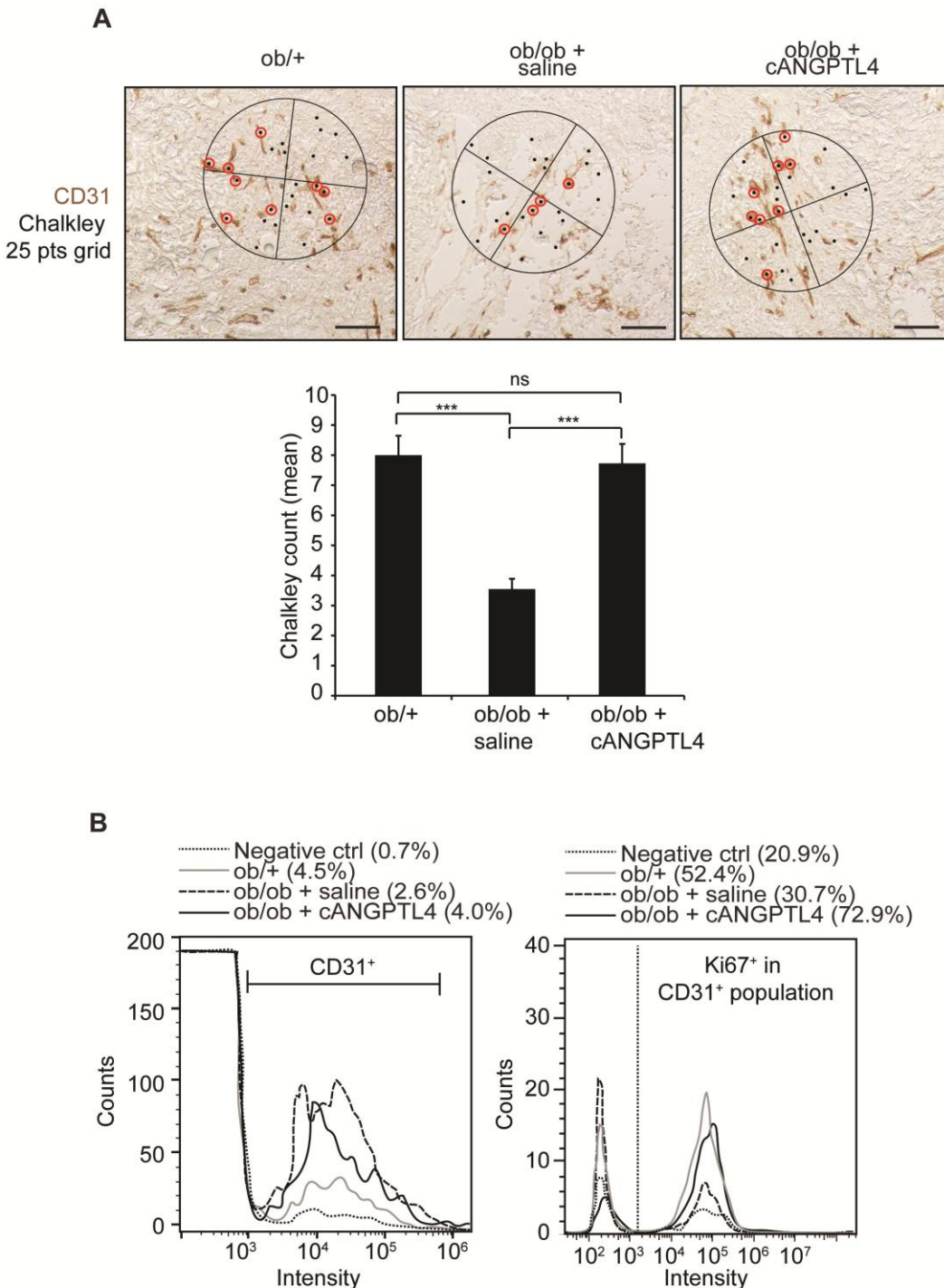


Figure 33 ANGPTL4 induced angiogenesis in ob/ob wound.

(A) Representative immunostaining for CD31 (brown) on ob/+, and saline- and cANGPTL4-treated ob/ob wound biopsies. Scale bar: 40 μ m. Chalkley's 25 points grids were used to determine the mean chalkley counts shown in the graph for at least 3 microscopic fields from 3 independent experiments. Data are mean \pm SEM, $n = 9$. *** $p < 0.001$; **(B)** Representative histograms generated from flow cytometry showing percentage of CD31⁺ endothelial cells population from total cells isolated from ob/+, saline treated ob/ob and cANGPTL4 treated ob/ob wound biopsies (left panel). Histograms gated from CD31⁺ endothelial cells population showing percentage of Ki67⁺ proliferative cells (right panel).

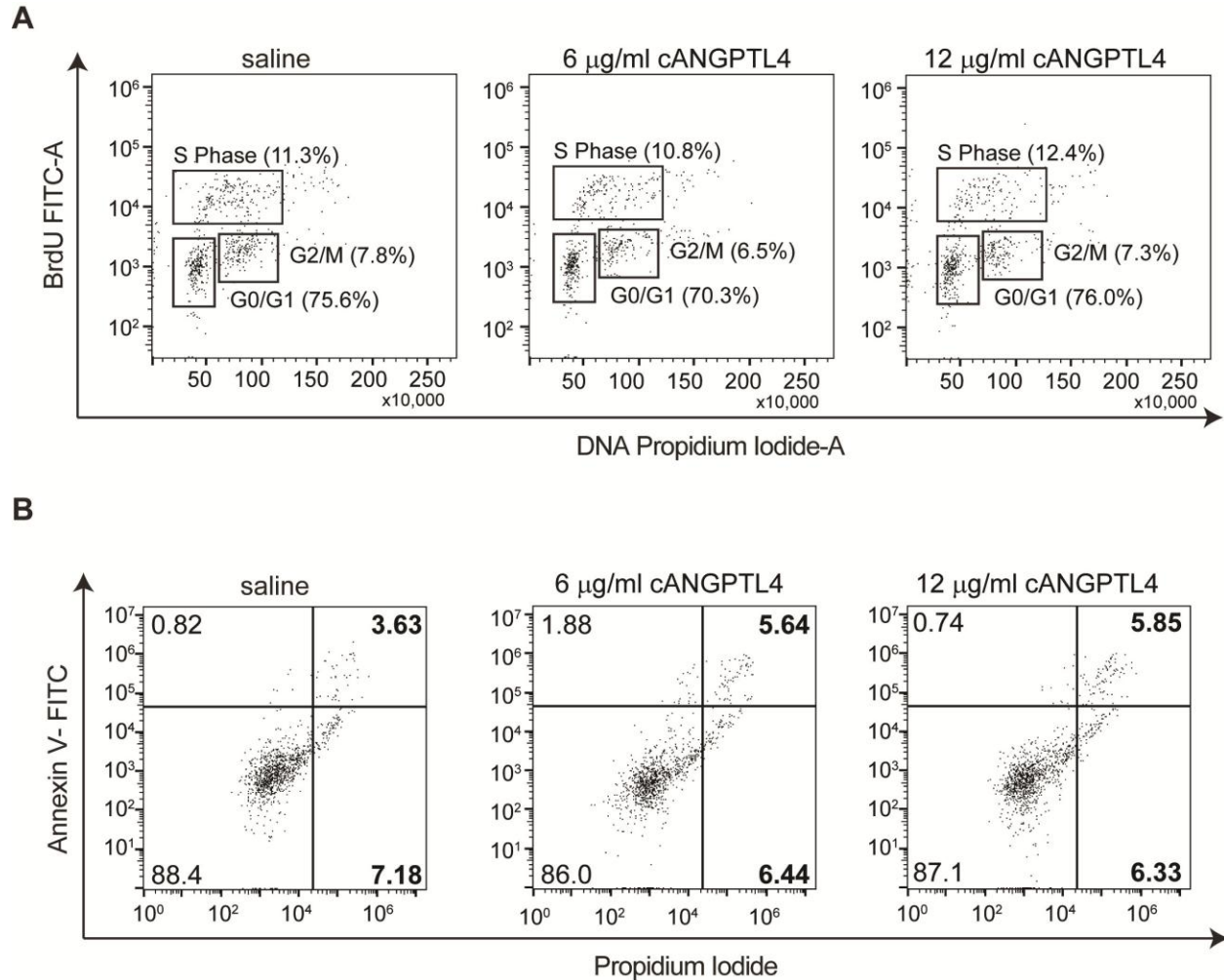


Figure 34 ANGPTL4 has no direct effect on endothelial cells survival and proliferation.

(A-B) Percentage of apoptotic **(A)** and proliferative **(B)** cells of saline- or cANGPTL4-treated endothelial cells as analyzed by FACS. Apoptotic and proliferating cells were determined by Annexin V-FITC: propidium iodide (PI) and BrdU staining, respectively. The total percentage counts of Annexin V⁺/PI⁻ (early apoptosis) and Annexin V⁺/PI⁺ cells (late apoptosis) populations were considered apoptotic (bold). Data are mean \pm SEM from six independent experiments.

2.4.4 ANGPTL4 increases nitric oxide (NO) production as an angiogenic mediator in diabetic wounds.

Our focused gene array analysis revealed that iNOS expression was dramatically increased in ob/ob wounds treated with cANGPTL4 compared with saline. To understand how ANGPTL4 modulates angiogenesis, we first examined the level of nitric oxide (NO), which is a potent angiogenesis mediator in various time points of our wound biopsies. Using a DAF-FM diacetate-based assay, we detected an overall NO reduction in ob/ob compared with ob/+ wounds (Figure 35A). Furthermore, cANGPTL4-treated ob/ob wounds showed significantly increased NO production from day 3 post-wounding compared to those with saline treatment, suggesting that cANGPTL4 may mediate NO production (Figure 35A).

We further found that, in contrast to ob/+ wounds in which eNOS expression peaked at day 5 post-wounding, eNOS expression in ob/ob wounds transiently peaked at day 3 post-wounding (Figure 35B). cANGPTL4 treatment of ob/ob wounds resulted in an increase in eNOS expression from day 5 post-wounding, more closely resembling the expression pattern of ob/+ wounds. The maximal fold-change in eNOS expression was similar between ob/+ and cANGPTL4 treated ob/ob wounds. These observations suggest that the elevation of eNOS in wounds may be a secondary effect. cANGPTL4 also did not modulate eNOS expression in primary human dermal microvascular endothelial cells (Figure 35C). Our results showed that ob/ob wounds expressed little iNOS mRNA compared to normal ob/+ wounds, in which iNOS expression peaked at day 3 post-injury. cANGPTL4 treatment in ob/ob wounds increased iNOS expression, which peaked at day 7 post-injury (Figure 35D). Consistently, our immunofluorescence

staining for iNOS showed increased intensity in day-7 cANGPTL4-treated wounds compared with saline controls (Figure 35E). To further strengthen our findings, we examined the NO level of ANGPTL4-knockout (KO) mice. Post wounding biopsies from KO mice have significantly lower level of NO detected in the wound epithelium by DAF staining when compared to wild type (WT) mice (Figure 35F). In addition, we separately examined the mRNA expression of iNOS in laser capture microdissected wound epithelia and dermis from the day 7 post-wound biopsies of ob/ob mice (Figure 36). The iNOS mRNA level in the epithelia of cANGPTL4-treated wounds was 10-fold higher than in saline-treated controls. cANGPTL4 treatment of ob/ob wounds did not affect dermal fibroblast iNOS mRNA expression, indicating a cell type-specific response.

To confirm the roles of iNOS and NO inducing angiogenesis and improve wound healing in diabetic wound healing, we co-treated ob/ob wounds with cANGPTL4 and aminoguanidine (AG), a selective iNOS inhibitor. As expected, ob/ob wound treated with cANGPTL4 in the presence of AG displayed a delay in wound healing comparable with the saline treated ob/ob wounds (Figure 37A). Histomorphometric analysis of saline treated, cANGPTL4 treated and cANGPTL4 plus AG treated ob/ob wound sections revealed significantly delayed in the percentage of wound closure for both saline treated and cANGPTL4 plus AG treated ob/ob wound when compared to cANGPTL4 treated ob/ob wound (Figure 37B and C). Altogether, these observations suggested that ANGPTL4 stimulates the expression of iNOS in the wound keratinocytes, elevated NO at the wound site to enhance diabetic wound closure rate.

To further strengthen our findings, we have performed in-vitro tube formation assay using endothelial cells alone or cocultured with keratinocytes in the presence and

absence of cANGPTL4. Aminoguanidine (AG), an iNOS inhibitor, was also used in the assay. The tube formation assays were performed under normal and diabetic conditions. Our observation showed that tubule formation was impaired in diabetic conditions, albeit only slightly. Tube formation was not affected by cANGPTL4, regarding of culture conditions. As expected, AG only has little effect. Notably, our result showed that cANGPTL4 accelerated tubule formation only in the presence of keratinocytes which was inhibited by AG (Figure 38). Thus, the tubule-promoting effect of cANGPTL4 works via a keratinocyte-endothelial cells interaction. (Figure 38).

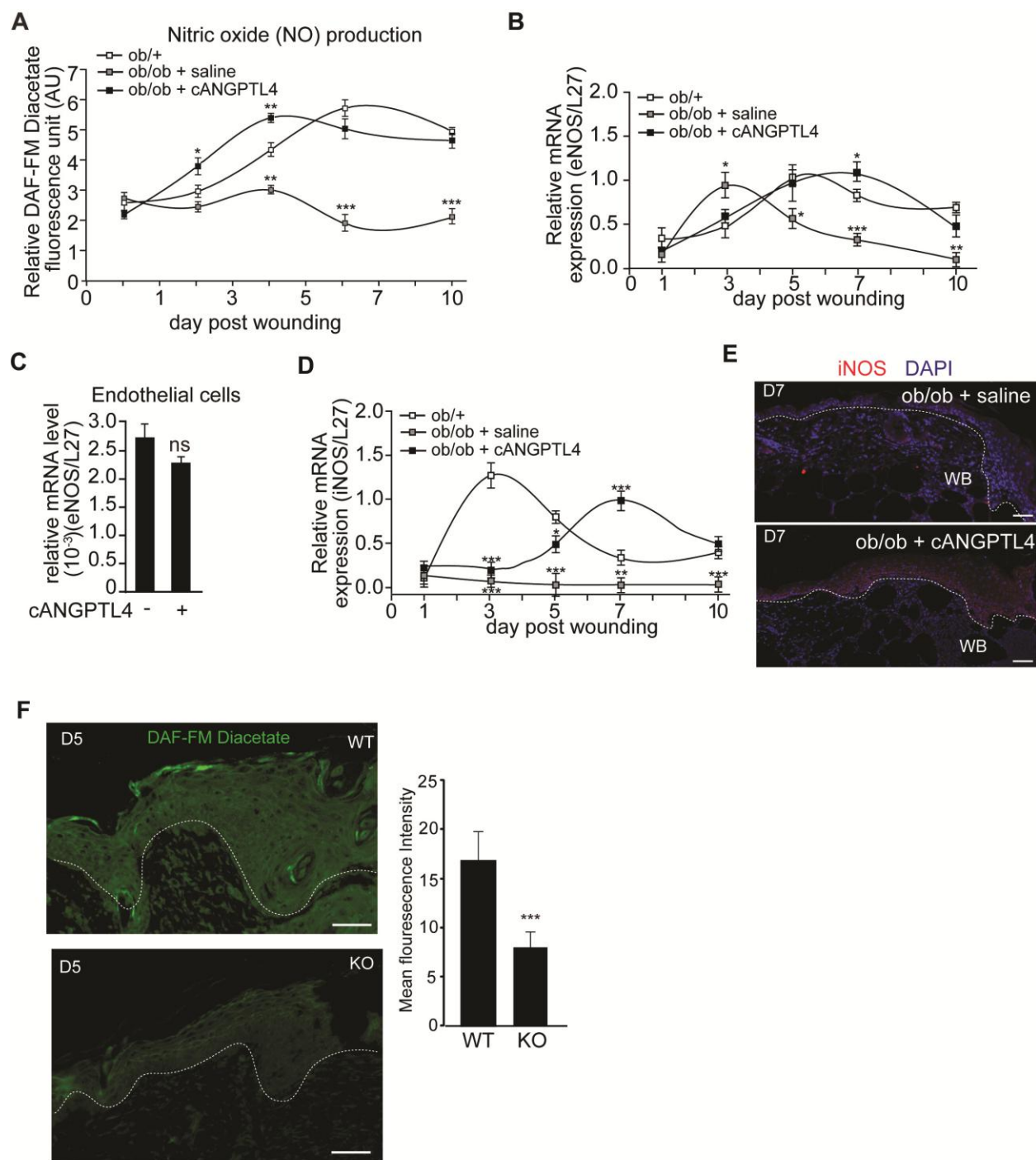


Figure 35. ANGPTL4 regulates NO production in wound epithelium.

(A) Nitric oxide production in ob/+, and saline- and cANGPTL4-treated ob/ob at indicated post-wounding days, determined by measuring the relative DAF-FM diacetate fluorescence level (arbitrary unit, AU). Values were normalized to total protein. **(B–D)**

Relative mRNA levels of eNOS **(B)** and iNOS **(D)** from indicated wound biopsies, and from primary human dermal microvascular endothelial cells (c), as analysed by qPCR. Values were normalized to the housekeeping gene ribosomal protein L27. **(E)** Immunofluorescence staining of iNOS (red) in day 7 wound biopsies of saline- and cANGPTL4-treated ob/ob mice. Dotted lines delineate the epidermis–dermis interface, scale bar: 50 μ m. WB: wound bed. **(F)** DAF-FM diacetate fluorescence (green) staining of day 5 post wounding WT and KO mice. Graph shows the mean fluorescence intensity from at least 3 microscopic fields of 3 independent mice. Value are mean \pm SEM, $n = 12$. *** $p < 0.001$ compared to WT mice.

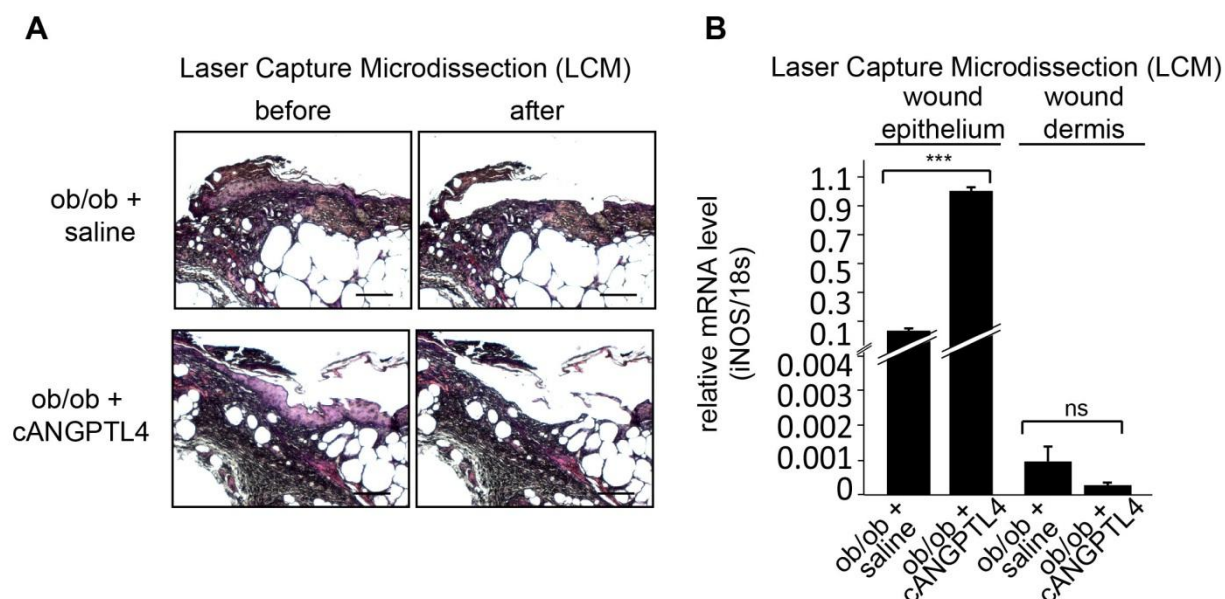


Figure 36. Laser capture microdissection (LCM) of saline- and cANGPTL4-treated ob/ob.

(A) Representative before and after LCM images of wound biopsies from saline and cANGPTL4 treated ob/ob mice, Scale bar: 150 μ m. **(B)** Expression of iNOS mRNA from laser capture microdissected wound epithelium and wound dermis of saline treated ob/ob mice and cANGPTL4 treated ob/ob mice. mRNA level were normalized to 18s ribosomal RNA. Data are mean \pm SEM, $n = 3$. *** $p < 0.001$ compared to saline treated ob/ob mice.

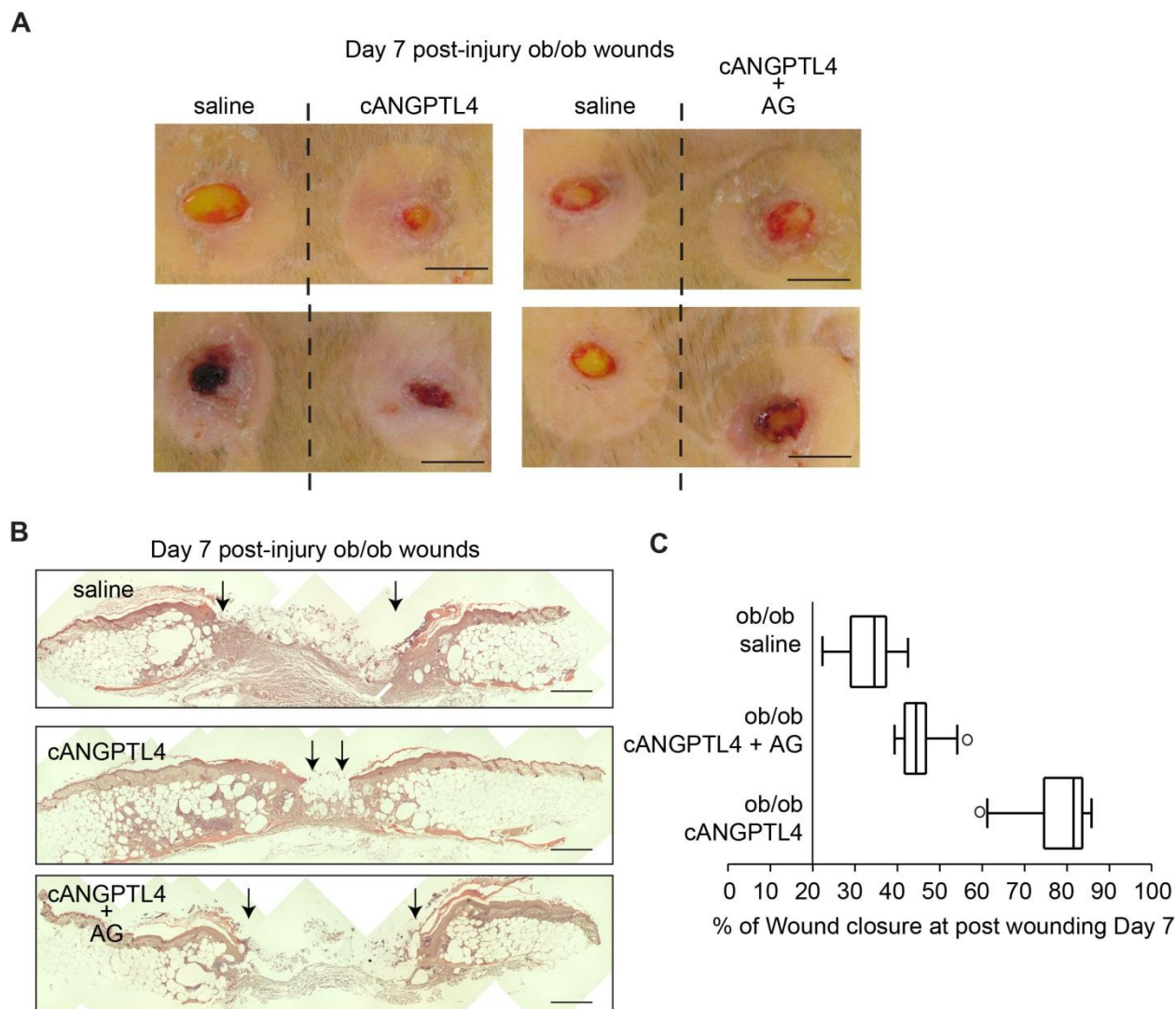


Figure 37. ANGPTL4 regulates iNOS expression.

(A) Photographs of ob/ob wounds treated with either saline, cANGPTL4 alone, or cANGPTL4 and aminoguanidine (AG). Representative pictures from three independent experiments from are shown. Scale bar: 5 mm. **(B)** Haematoxylin and eosin-stained images of wound sections. Arrows point to the epithelial wound edge. Scale bar: 500 μ m. **(C)** Box and whisker plot of the percentage of wound closure in saline treated, cANGPTL4 treated and cANGPTL4 plus AG treated ob/ob day 7 post wounds biopsies sections. Histomorphometric measurements were determined from 10 independent sections from the various wound biopsies. Middle bar = median, box = interquartile range, whiskers = full value range, * = possible outlier.

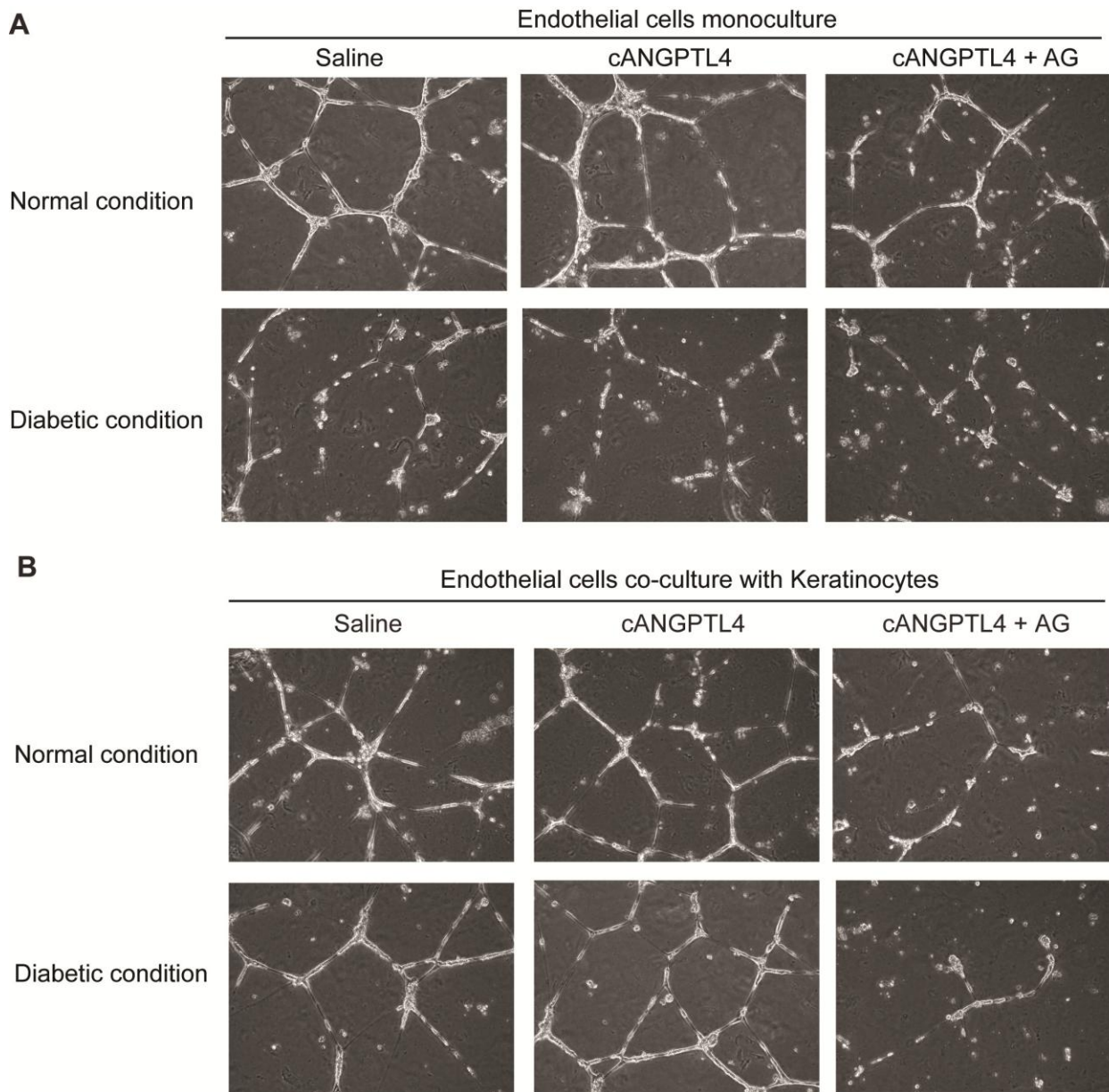


Figure 38. Effect of ANGPTL4 on *in vitro* endothelial tubule formations.

Representative images of *in vitro* endothelial tubule formation from **(A)** endothelial cells monoculture or **(B)** endothelial cells co-cultured with keratinocytes under normal or diabetic condition with indicated treatments. n=3.

2.4.5 ANGPTL4 regulates iNOS expression via STAT3 activation in keratinocytes.

To decipher the underlying mechanism, we first examine the interaction between exogenous cANGPTL4 and integrins in ob/ob wounds using proximity ligation assay (PLA). cANGPTL4 binds to integrin and subsequently activating downstream mediators such as FAK, Src and ERK to modulate gene expression²⁸². PLA signals, visualized as red spots, were increased in cANGPTL4-treated ob/ob wounds compared to saline-treated wounds, suggesting that cANGPTL4 bound and activated integrin β 1 (Figure 39A and C). This was confirmed using PLA for active integrin β 1 and active Rac1 interactions, which showed increased PLA signals per cell in cANGPTL4-treated compared with saline-treated ob/ob wounds (Figure 39B and D). PLA performed with single specific antibody served as negative controls (Figure 39E). Immunoprecipitation using anti-cANGPTL4 followed by immunoblot analysis also showed that the activation of downstream mediators such as phosphorylated FAK and Src (Figure 40A).

In silico analysis of mouse *iNOS* gene promoter revealed a putative STAT binding site. Immunofluorescence staining showed more wound keratinocytes were stained positive for phosphorylated STAT3 in cANGPTL4-treated ob/ob wounds compared with saline controls (Figure 40B). Keratin 6 identifies hyperproliferative wound keratinocytes. We also examined the JAK/STAT3 activation in day 5 and 7 post-wound biopsies from ANGPTL4 KO and WT mice. Interestingly, the expression of both phosphorylated STAT3 and JAK1 proteins, i.e. activated proteins, was significantly reduced in KO when compared with WT (Figure 40C). In addition, immunoblotting of phosphorylated STAT3 and JAK1 proteins from laser microdissected wound epithelia of saline- and cANGPTL4-treated ob/ob wounds clearly showed that cANGPTL4 can

activate JAK1/STAT3 signalling in the wound keratinocytes (Figure 40D). As expected, this activation of JAK1/STAT3 signalling was also observed in laser microdissected wound epithelium of normal human skin compared to diabetic human skin (Figure 40D). To determine whether cANGPTL4 regulates iNOS expression via STAT3 signalling in keratinocytes, we measured iNOS mRNA by qPCR and NO production using DAF-FM in STAT3-knockdown keratinocytes (Ker_{STAT3}) treated with cANGPTL4. Our result showed reduced iNOS mRNA and NO levels in Ker_{STAT3} compared with Ker_{CTRL} (Figure 40E and 40F).

Finally, *in vivo* chromatin immunoprecipitation (ChIP) showed that phospho-STAT3 specifically bound to the cognate responsive elements in the promoter of the mouse *iNOS* gene in ANGPTL4-treated but not saline-treated ob/ob wounds (Figure 40G, left panel). No immunoprecipitation or amplification was seen with pre-immune IgG or with a control sequence upstream of the responsive elements in the promoter *iNOS* gene (Figure 40G, left panel). Quantitative ChIP showed ~15-fold enrichment in STAT-binding region (SBE) when compared with cognate controls (Figure 40G, right panel). Altogether, these observations indicate that ANGPTL4 stimulates NO generation in wound keratinocytes through direct transcriptional regulation of the *iNOS* gene by pSTAT3.

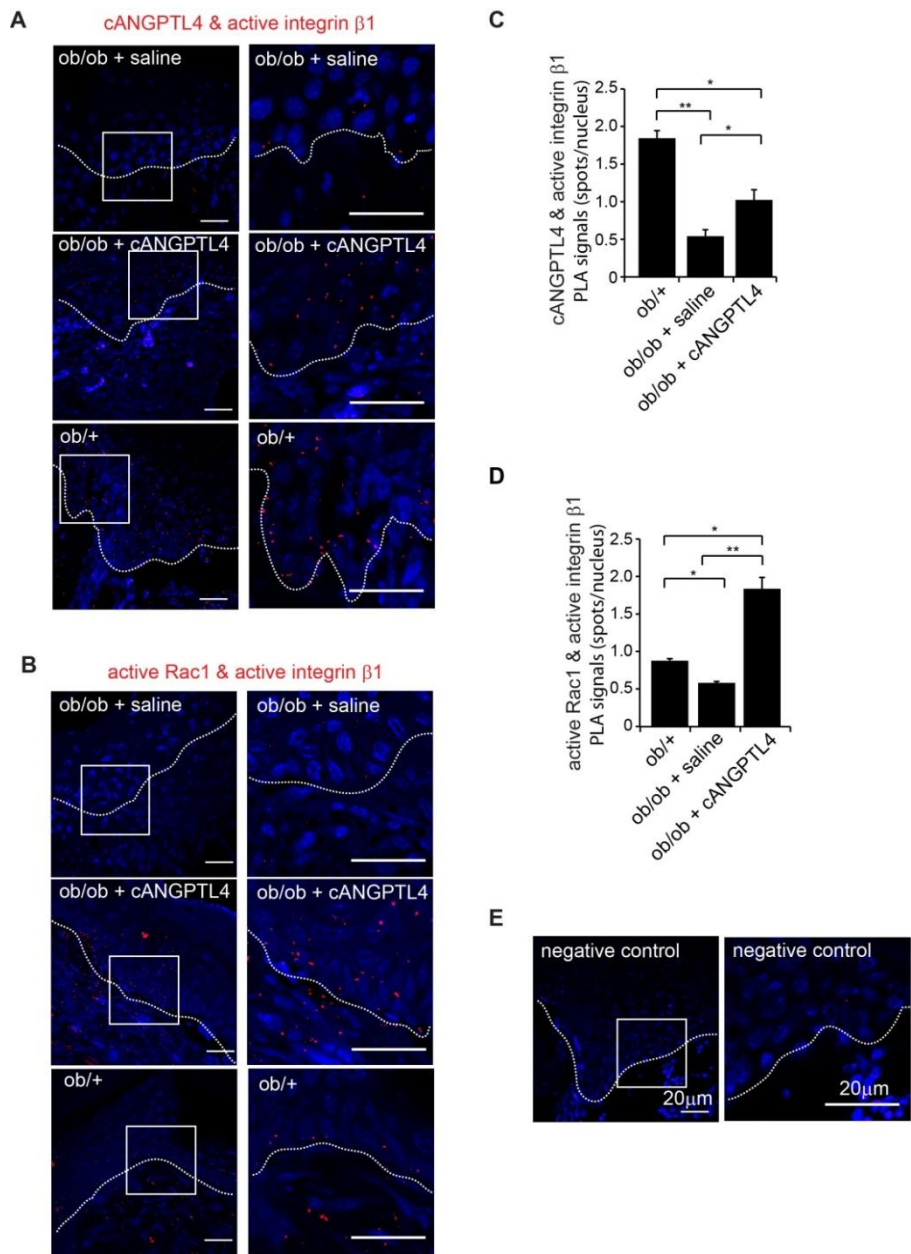


Figure 39. ANGPTL4 activates the integrin signaling pathway.

Detection of **(A)** cANGPTL4:active integrin $\beta 1$ and **(B)** active integrin $\beta 1$:active Rac1 complexes using proximity ligation assay (PLA). Higher magnification images are shown on the left panel in a white box. Each PLA signal (red) indicates one detected interaction event. Nuclei were counterstained with DAPI (blue). Images were acquired in a one z-plane using LSM710 META confocal laser-scanning microscope (Carl Zeiss). Scale bar: 20 μm . Dotted white lines denote the epidermal–dermal junction. **(C–D)** Quantification of PLA signals of cANGPTL4:active integrin $\beta 1$ **(C)** and active integrin $\beta 1$:active Rac1 **(D)**. Each PLA signal indicates one detected interaction event. Number of PLA signals per nucleus was determined using Blobfinder software. Data are mean \pm SEM, $n = 3$. * $p < 0.05$, ** $p < 0.01$. **(E)** The negative control included no primary antibodies. Representative pictures from three independent experiments are shown.

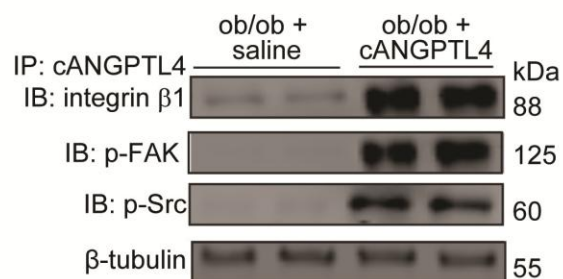
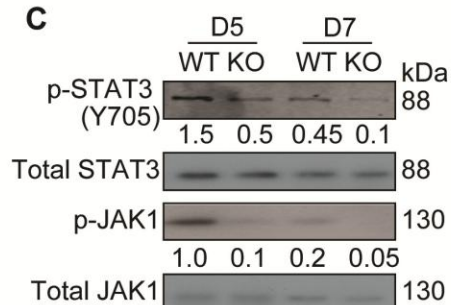
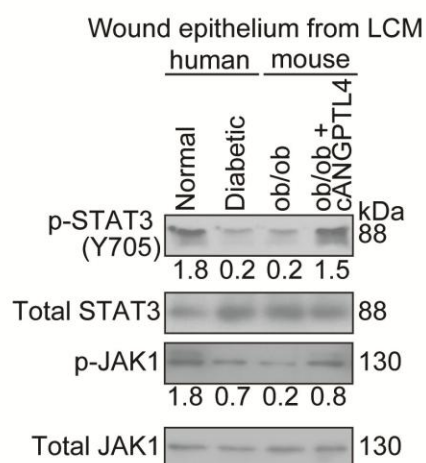
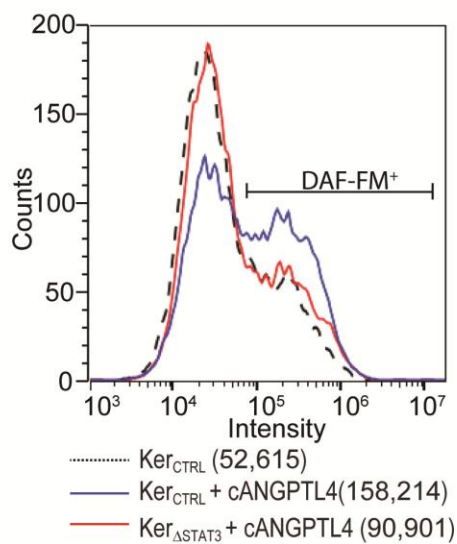
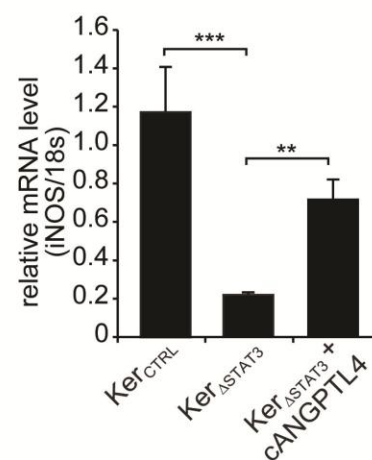
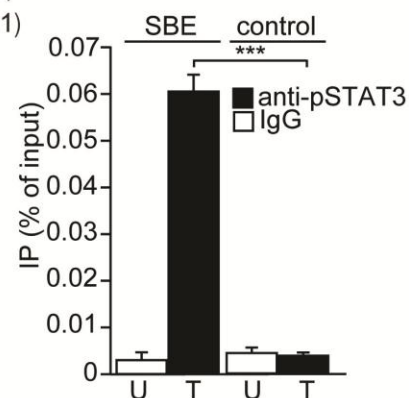
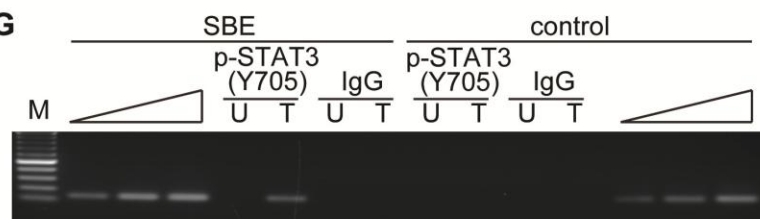
A**B****C****D****E****F****G**

Figure 40. ANGPTL4 activates JAK1/STAT3 signalling to regulate iNOS expression in keratinocytes.

(A) Immunodetection of indicated proteins from anti-cANGPTL4 immunoprecipitates of saline- or cANGPTL4-treated ob/ob wound biopsies. β -tubulin from total tissue lysate was used to verify equal loading. **(B)** Dual immunofluorescence staining of pSTAT3(Y705) (green) and CK6 (red) in saline- and cANGPTL4-treated ob/ob wounds. Dotted lines delineate the epidermis–dermis interface. Nuclei are stained with DAPI (blue) Scale bar: 40 μ m. WB: wound bed. **(C)** immunodetection of pSTAT3(Y705), total STAT3, p-JAK1 and total JAK1 in post wounding D5 and D7 of both KO and WT mice. **(D)** immunoblots of pSTAT3(Y705), total STAT3, pJAK1 and total JAK1 from laser capture microdissected epithelium of normal human skin, diabetic human skin, saline treated ob/ob wound and cANGPTL4 treated ob/ob wound. **(E)** Representative histograms generated from flow cytometry showing the mean intensity of DAF-FM signal from STAT3 knockdown keratinocytes in the absence or presence of cANGPTL4, Data are mean \pm SEM, $n = 3$ **(F)** Relative mRNA expression level of iNOS from STAT3 knockdown keratinocytes in the absence or presence of cANGPTL4, $n = 3$. ** $p < 0.01$, *** $p < 0.001$. **(G)** ChIP assays were conducted using pre-immune IgG or antibodies against pSTAT3(Y705) in saline- (U) and cANGPTL4-treated (T) ob/ob wounds at day 7 post-injury. Graph (right panel) shows quantitative ChIP as percentage of input. Specific regions spanning promoter binding sites of the iNOS gene were amplified using appropriate primers (Table S1). A control region served as a negative control.

2.5 DISCUSSION

Diabetic wounds heal poorly, often resulting in ulceration. Relatively few topical medications are effective for ulcer care, and amputation rates remain high in non-healing diabetic patients. Growing evidence indicates that altered expression levels of cytokines and ECM proteins play a significant role in the delayed healing of diabetic wounds. Experimental evidence shows that vascular-endothelial growth factor (VEGF), platelet-derived growth factor, and epidermal growth factor accelerate diabetic wound healing in animal models²⁸³; however, successful results require high doses of these growth factors. Furthermore, these therapeutic strategies ignore the central coordinating role of the matrix proteins in orchestrating and enhancing the cascade of cellular events in the wound healing response.

Here, we have shown that the topical application of recombinant cANGPTL4 accelerates wound re-epithelialization in diabetic mice by improving wound angiogenesis. The matricellular protein cANGPTL4 expression has been weakly detected in normal intact skin and is markedly elevated upon wound injury. In contrast, cANGPTL4 expression remains low throughout the healing period in diabetic wounds. Topical application of cANGPTL4 modulates several regulatory networks involved in cell migration, angiogenesis and inflammation, as evidenced by an altered wound healing gene expression signature when compared with saline-treated diabetic wounds. Various studies have suggested that the role of ANGPTL4 in angiogenesis may be context-dependent. Conflicting roles for ANGPTL4 in tumor vascularization have been reported²⁸⁴. In a model of oxygen-induced retinopathy, pathological neovascularization was strongly inhibited in angptl4-deficient mice. Recent study showed that ANGPTL4

improves the cerebral vasculature network after brain injury and displays vasculoprotective properties when used as an adjunct to VEGF²⁸⁵. Evidence from ANGPTL4-knockout mice indicates that ANGPTL4 is pro-angiogenic in normal wound healing²⁸². These observations suggest a role for ANGPTL4 in angiogenesis, although the underlying mechanism remains unresolved. Here we showed that ANGPTL4 has a dramatic influence in the expression profile of endothelial-specific CD31 in diabetic wounds, returning its profile to that observed in wild-type wounds. cANGPTL4 induces NO production through an integrin/JAK/STAT3-mediated upregulation of iNOS expression in diabetic skin, thus revealing a hitherto unknown mechanism by which ANGPTL4 regulates angiogenesis via keratinocyte-to-endothelial-cell communication (Figure 41). Interestingly, impaired wound angiogenesis was also observed in mice that lack $\alpha 3\beta 1$ integrin in epidermis, lending support for a keratinocyte-to-endothelial-cell crosstalk that is dependent on epithelial integrin-mediated signalling²⁸⁶. Proximity ligation assay and co-immunoprecipitation analysis revealed that exogenous cANGPTL4 interacted with integrin $\beta 1$. ANGPTL4-bound integrins activated downstream mediators such as Rac1 and JAK. We further showed that ANGPTL4 regulates iNOS expression via STAT3 activation in keratinocytes as evidenced by immunoblot analysis of microdissected wound epithelia, STAT3-knockdown keratinocytes and *in vivo* chromatin immunoprecipitation. VEGF is a potent angiogenic factor that can also modulate NO generation via eNOS upregulation. In contrast to VEGF, cANGPTL4 had little effect on eNOS expression, but clearly induced iNOS expression. We observed that ANGPTL4 treatment shifted the eNOS expression peak to day 7 post-wounding, which is most likely due to the increase in proliferating endothelial cells (Ki67⁺CD31⁺) already detected

in the day-5 wounds. Numerous studies have shown that NO can profoundly impact angiogenesis, and we are only beginning to understand the mechanism for its observed beneficial effect on wound repair.

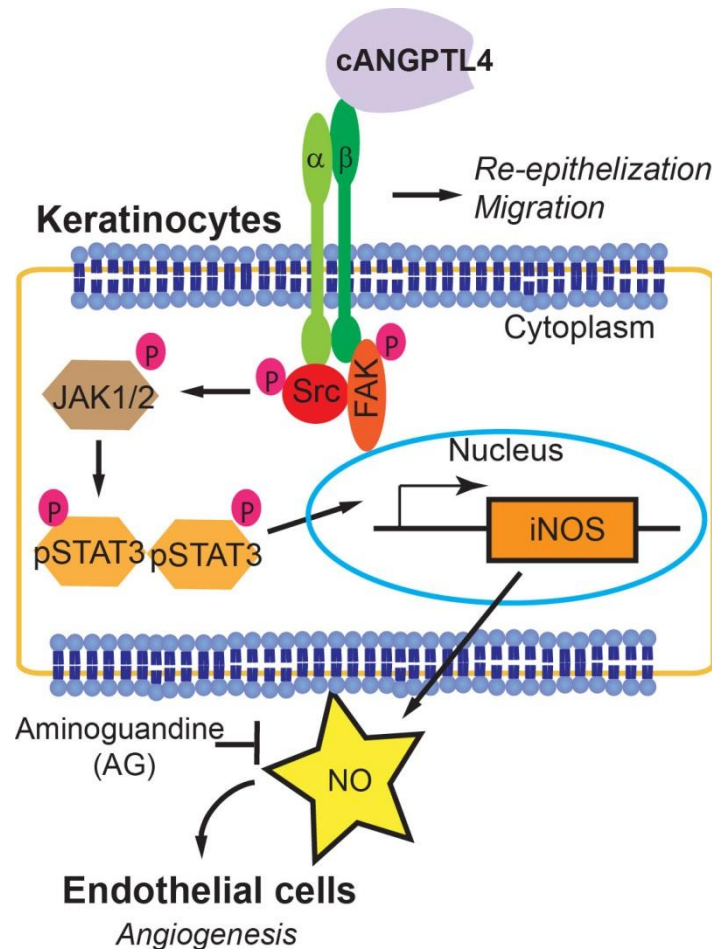


Figure 41. Schematic illustration of the autocrine and paracrine effect of ANGPTL4 on cutaneous wound healing.

cANGPTL4 can interact with integrin $\beta 1$, and activated the Src, ERK, and AKT signalling cascades, leading to subsequent JAK1/STAT3 activation. Activated STAT3 can then mediate the upregulation of iNOS expression by specifically bound to the cognate responsive elements in the promoter of *iNOS* gene. Wound angiogenesis can then be promoted by the increase NO production from the wound keratinocytes in the wound microenvironment.

Inflammation plays both positive and negative roles in cutaneous repair – the level and length of inflammation can dictate both the healing time and quality of repair⁸³. Recapitulating the dampened inflammatory responses found in foetal and adult chronic wounds has proved useful in accelerating repair and reduced scarring^{115,287}. We observed that expression of the macrophage marker F4/80 was reduced upon treatment with cANGPTL4 compared to saline, suggesting that cANGPTL4 may reduce wound inflammation. The relationship between ANGPTL4 and inflammation remains unclear. ANGPTL4 has been implicated in other inflammation-associated pathologies; it plays a protective role against the severe pro-inflammatory effects of saturated fat, as well as in arthritis (particularly in models dependent on adaptive immunity) and in atherosclerosis. The underlying mechanism is unknown and is likely to be highly complex, beyond the scope of this current work.

Our study suggests that the replacement of matricellular protein ANGPTL4 can provide an adjunctive or new therapeutic avenue for treating poorly healing wounds, such as diabetes-associated ulcers. Furthermore, the present results confirm that therapeutic angiogenesis remains an attractive treatment modality for diabetic wound healing.

2.6 FUTURE STUDIES

2.6.1 The effect of cANGPTL4 in tissue remodelling and collagen scar formation

My previous work mentioned on nonhealing wounds involving in persistent and unresolved inflammation, in which case progression of the repair response culminates in diffuse fibrosis and excessive deposition of matrix proteins, particularly collagen. Scarring and wound healing occur within a spectrum ranging from scar-free healing in embryos to scar-forming healing in children and adults. It is believed that the scarring response is the result of rapid replacement of missing tissue and is sub-optimal in terms of appearance and function compared to the tissue, results in a reduction in the likelihood of infection and an increased likelihood of organism survival following injury²⁸⁸⁻

²⁹⁰.

Comparison of the architecture of regenerated scar-free wounds in embryos with scars of adults reveals that the collagen in scar-free wounds is organised in “basket weave” architecture whereas in adult scars the collagen is abnormally organised in parallel bundles of fine fibres²⁹¹. Comparative biochemical analysis of scar tissues and scar-free wounds revealed very few differences, with consistently higher level of collagen type 1 alpha-2 (COL1A2) in the former. Hence, it is the organisation of collagen that is largely responsible for scar formation rather than a biochemical problem relating to an abnormal composition of the scar tissue. Whilst many studies have been directed at understanding the critical factors that influence poorly healing wounds, they have typically not translated to the effective therapeutic approaches for scar management. As such, scar improvement still remains an area of clear medical need.

Currently there are no registered pharmaceuticals for the prophylactic improvement of scarring and no single therapy is universally accepted as the standard of care^{87,88}.

A great deal of research has revealed that the profiles and quantities of growth factors and cytokines associated with scar-free healing are often different to those in adult scar-forming healing, but many of these are not mechanistically causative and only a few of these factors are potential therapeutic targets for scar improvement^{291,292}. Presently, individual cytokine-mediated candidates, such as IL-10 and TGF- β 3 have performed poorly in Phase III clinical trials. Importantly, these therapeutic strategies ignore the central coordinating role of the matricellular proteins in orchestrating cellular events in wound healing and scarring response. Matricellular proteins can associate with the diverse proteins of the extracellular matrix reservoir, bridging them with cognate cell surface receptors and can be a possible medium for paracrine communication during wound healing. They reside at the crossroads of cell–matrix communication, modulating several regulatory networks²⁹³. Presumably, the regulatory pathways consist of complex networks, creating many opportunities for the compensatory adjustments required for wound repair. Hence, it may be more efficacious to target or replace the necessary matricellular proteins involved in multiple cell-cell or cell-matrix communications than individual cytokine-mediated candidates. Thus far, only one matricellular protein cysteine-rich protein 61 (CCN1) has been reported to reduce scar formation by inducing fibroblast senescence. CCN1 also induces DNA damage response pathways, activates p53 and generates reactive oxygen species. However, this is not a desirable solution since as fibroblasts are involved in all phases of wound healing. Periostin, another matricellular protein, is a pro-fibrogenic protein that mediates

fibroblast differentiation and extracellular matrix synthesis. However, it is not a desirable solution since fibroblasts are involved in all phases of wound healing²⁹⁴. In this context, angiopoietin-like 4 (ANGPTL4), a recently identified matricellular protein, could be a prime candidate. Previously, we showed the capabilities of cANGPTL4 facilitates wound re-epithelialisation, involved in cell to matrix interaction and improved wound angiogenesis^{282,295}. Wounds in ANGPTL4-knockout mice exhibit delayed healing, increased inflammation, and impaired wound-related angiogenesis^{282,295}. However, the roles of ANGPTL4 on tissue remodelling are unknown and there is great potential to investigate its impact on fibroblasts and collagen scar formation.

2.6.1.1 Recombinant cANGPTL4 reduces collagen scar deposition in ob/ob diabetic wounds

Delayed diabetic wound healing leads to excessive collagen production and deposition at the wound bed. To examine whether cANGPTL4 influenced the level of scarring, we examined the effect of topically applied recombinant cANGPTL4 on diabetic wound healing. We inflicted two full-thickness excisional splint wounds on the dorsal skin of ob/ob mice: one to be treated with saline and the other with cANGPTL4. At Day-10 post-wounding, we measured the amount of hydroxyproline, a major component of collagen, from biopsies of saline-treated and cANGPTL4-treated ob/ob wounds. We detected reduced hydroxyproline in cANGPTL4-treated wound biopsies when complete wound closure was observed compared with vehicle-treated wounds (Figure 42A). Van Gieson staining of wound sections similarly showed reduced collagen deposition at the wound bed in cANGPTL4-treated compared to saline-treated ob/ob wounds (Figure

34B). We additionally characterized the architectural *arrangement of collagen* fibres in saline- and ANGPTL4-treated ob/ob wounds using scanning and transmission electron microscopy. As expected, collagen fibrils of saline-treated wounds exhibited orderly alignment and were significantly thicker (Figure 43), indicating scar tissue formation. In contrast, collagen fibres in cANGPTL4-treated wounds had a random basket-weave appearance and were thinner (Figure 43). These observations indicate that recombinant cANGPTL4 treatment reduced collagen scar tissue in diabetic wounds.

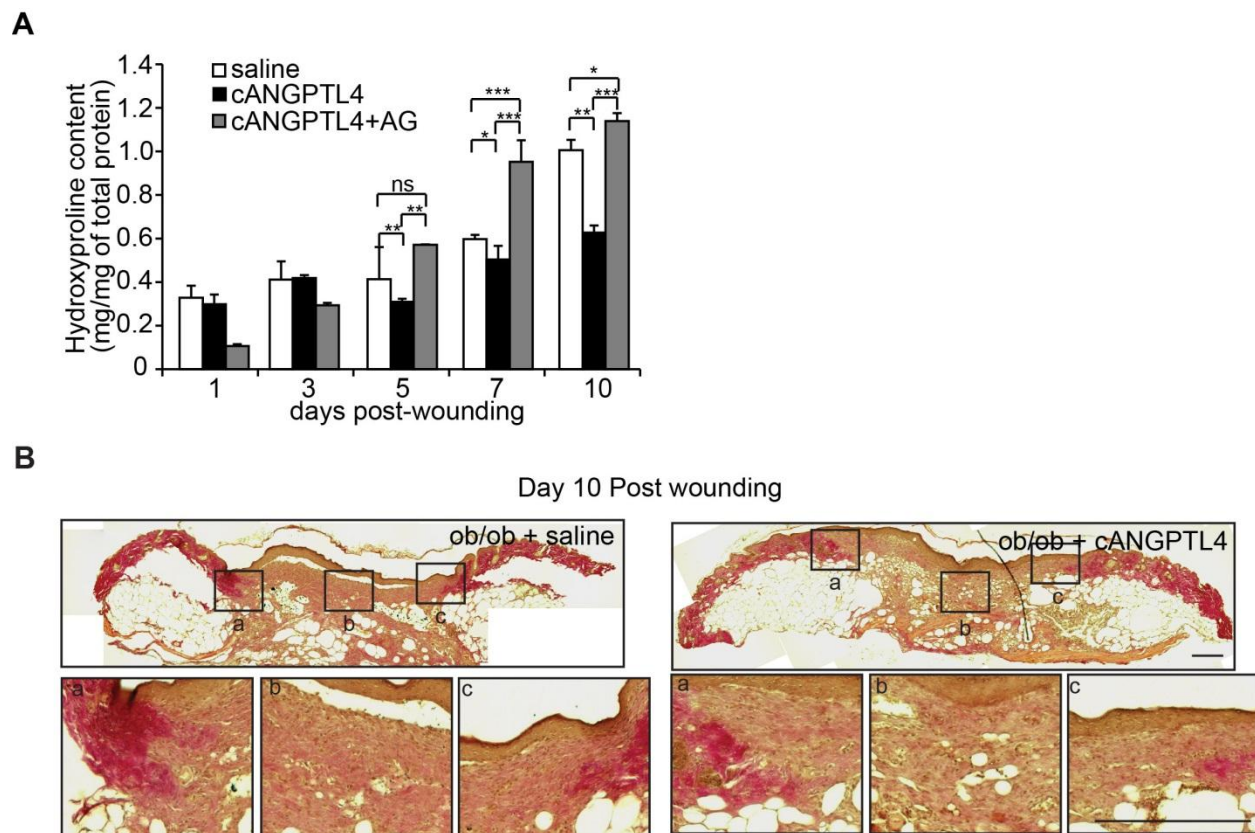


Figure 42. Reduced collagen deposition in cANGPTL4 treated ob/ob wounds

(A) Tissue hydroxyproline level from saline- and cANGPTL4-treated ob/ob wounds. The amounts of hydroxyproline (mg) were determined from a hydroxyproline standard curve and normalized with the total protein concentration. Data are mean \pm SEM, $n = 3$. *** $p < 0.001$. **(B)** Van Gieson's stain of saline- and cANGPTL4-treated ob/ob wounds at day 10 post-injury. Scale bar: 40 μ m.

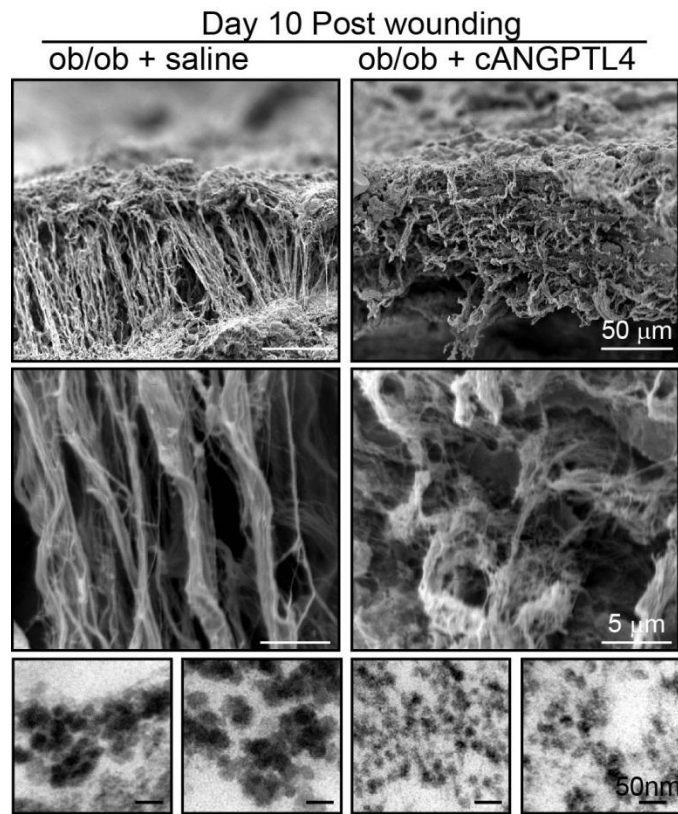


Figure 43. Scanning and transmission electron microscopy imaging of connective tissues

Scanning and transmission electron microscopy imaging of connective tissues near the wound bed region of saline- and cANGPTL4-treated ob/ob wounds at day 10 post-injury. Cross sectional images of collagen fibril sizes were obtained by transmission electron microscopy.

2.6.1.2 Improved biomechanical properties of cANGPTL4-treated wounds.

We next examine if cANGPTL4 treatment improves the quality of the healed wounds. To this end, we performed comparative biomechanical testing of cANGPTL4-treated and vehicle-treated regenerated tissues. Section of skin was carefully removed and cut into constant geometry to avoid inconsistency with the specimen gripping strength (Figure 44A). The stress-strain relationship derived from tensile test provides complete information related to the effect of saline- or cANGPTL4-treatment on the biomechanical properties of a wounded skin. In the tensile test, the skin specimen was subjected to failure and the relationship of force vs extension was determined. The maximal tensile strength is the maximum strength that the wound tissue being stretch before break. A high value represents high fragility of the skin tissue. cANGPTL4-treated wound tissue and unwound skin tissue displayed a higher maximal tensile strength compared to saline-treated wound tissue (0.378 ± 0.037 MPa and 0.429 ± 0.012 MPa vs 0.212 ± 0.025 MPa; Figure 44B). cANGPTL4-treated wound tissue showed no difference in the relaxation properties compared to either unwound tissue or saline-treated wound tissue (Figure 44C). Mature scar tissue has more resistance against breakage upon stretching, thus we also measured the toughness, ultimate elongation and elastic modulus properties based on the stress-strain curve. The toughness is measured by the total area underneath the stress-strain curve. The ultimate elongation is the maximum strain or length that the wound tissue can stretch before breaking and usually expressed as a percentage of its original length. A higher value reflects better elasticity of the skin tissue. The elastic modulus determines the specimen's tendency to be deformed where a stiffer specimen will have a higher elastic modulus. Both cANGPTL4-treated wound

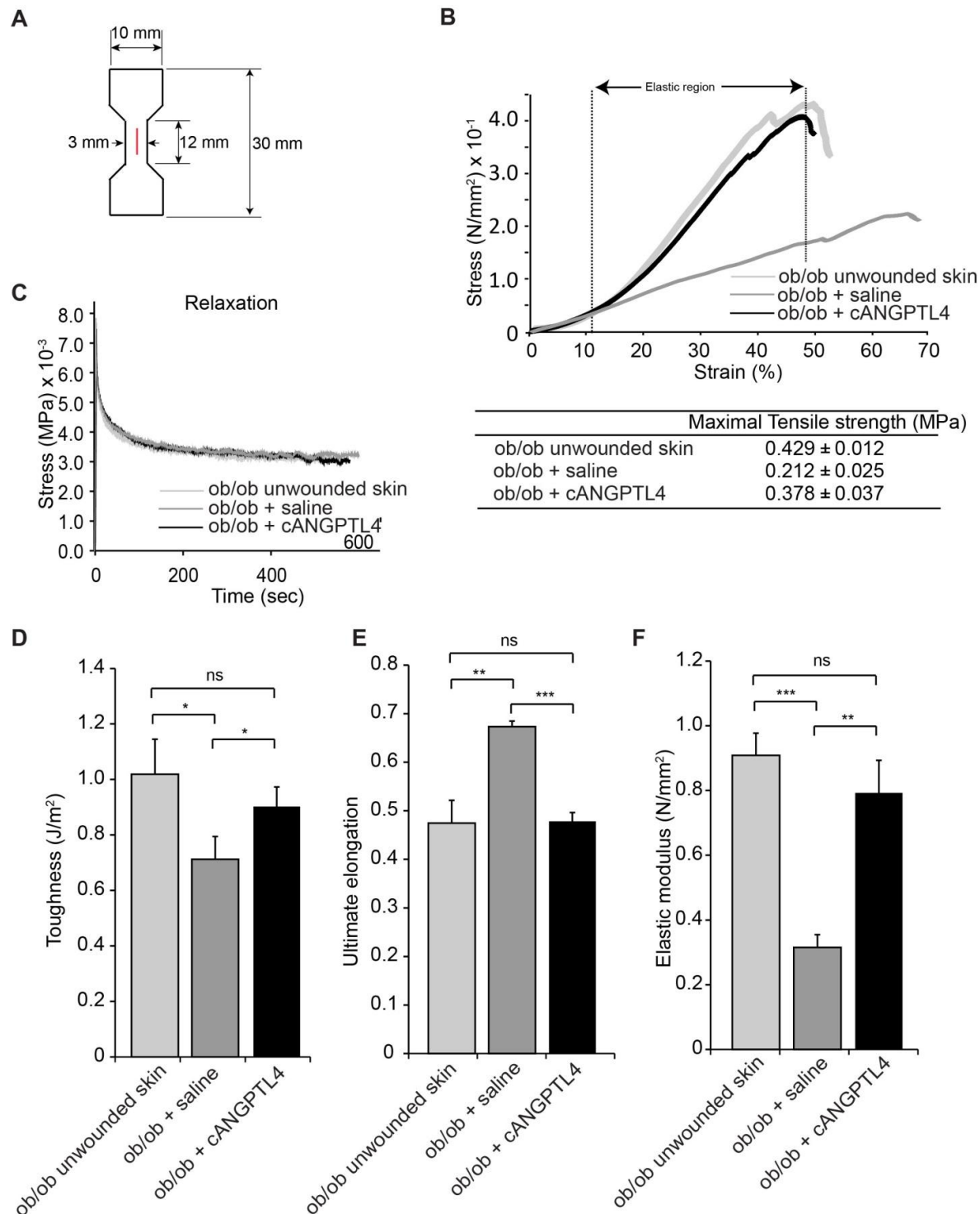


Figure 44. biomechanical properties of cANGPTL4-treated wounds

(A) Geometrisketch of the dimensions used to cut out the biopsies prior to tensile strength test. **(B)** The stress-strain curve **(C)** Relaxation curve **(D)** toughness graph **(E)** Ultimate elongation graph and **(F)** Elastic modulus graph of unwounded skin, saline-treated and cANGPTL4-treated ob/ob wound biopsies. Data are mean ± SEM, $n = 3$. * $p < 0.05$; ** $p < 0.01$, *** $p < 0.001$

tissue and unwound skin tissue displayed non-significant difference in the measurement of three biomechanical properties. On the other hand, the saline-treated wound tissue showed significant reduced in toughness, elevated in ultimate elongation and reduced in elastic modulus when compared to either cANGPTL4-treated wound tissue or unwound skin tissue (Figure 44D-F). Overall, these observations indicate that cANGPTL4 treatment of wound tissue can restore the skin biomechanical properties to a level resembling the status of an unwound skin.

2.6.1.3 ANGPTL4 restores wound fibroblast migration into wound bed

The laying down of connective tissue in the scar involves the migration and proliferation of fibroblasts into the site of injury and the deposition of ECM proteins produced by the activated fibroblasts. Live imaging revealed a dose-dependent effect of cANGPTL4 to accelerate fibroblasts migration (Figure 45A). The *in vitro* fibroblasts migration assay displayed a complete closure after 15 hours of treatment with 12 µg/mL cANGPTL4 while the saline-treated fibroblasts remain at 50% closure (Figure 45B). To examine if ANGPTL4 has any effect on the proliferation of the fibroblasts which may have a contributing effect on the migration, we can performed BrdU cell proliferation assay on saline- and cANGPTL4-treated fibroblasts.

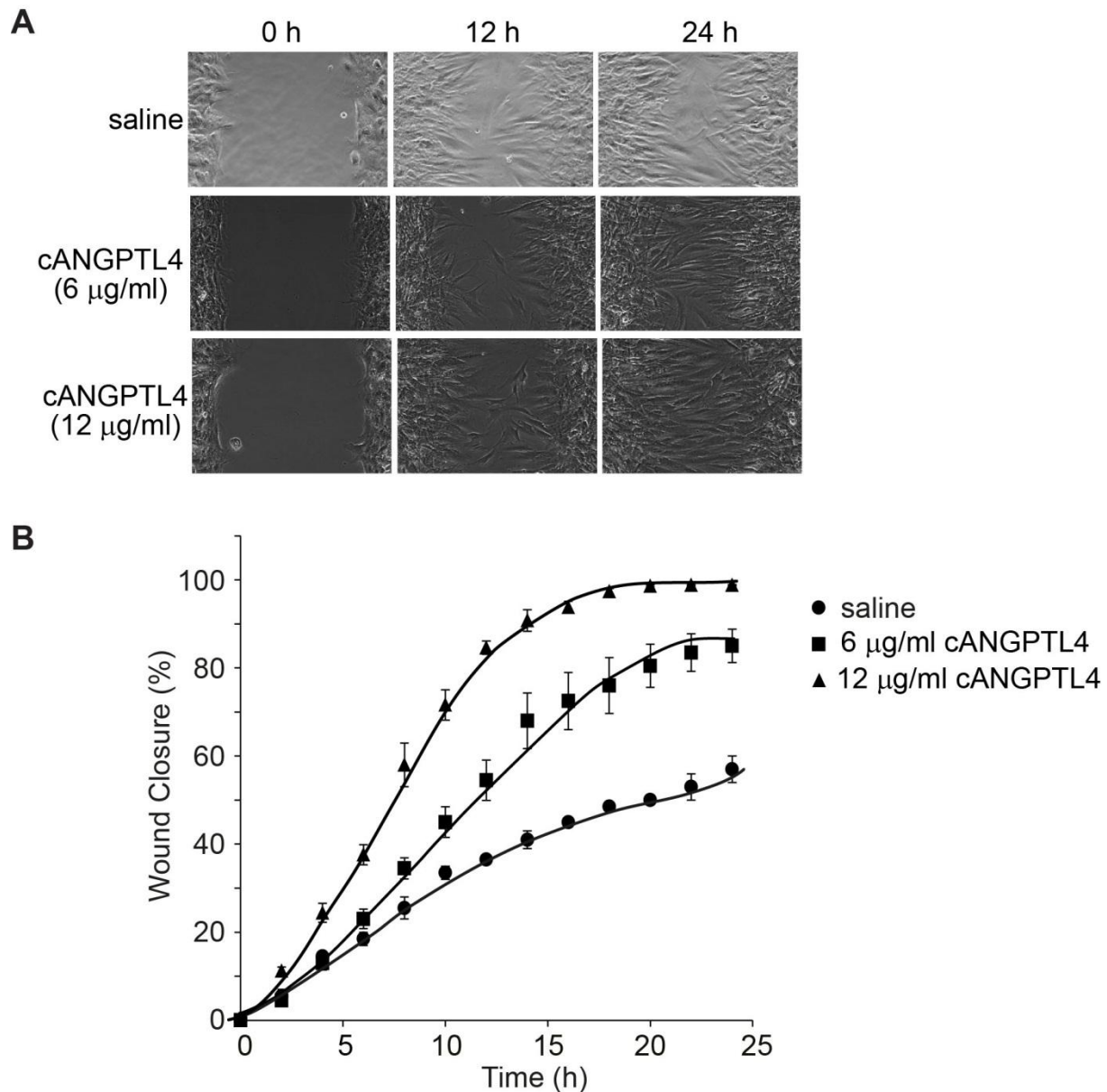


Figure 45. ANGPTL4 restores wound fibroblast migration

(A) Representative time-lapsed images of scratch wound fibroblast culture treated with saline, 6 µg/mL of cANGPTL4 or 12 µg/mL of cANGPTL4. **(B)** Percentage of wound closure is determined by measurement of surface area covered by the migrating fibroblasts. Graph plotted base on measurement from 6 independent time-lapsed images of various scratch wound fibroblasts culture at selected time points. Data are mean \pm SEM, $n = 6$.

2.6.1.4 Potential mechanism for scarring: ANGPTL4 inhibits collagen 1 alpha-2 (COL1A2) expression in a β -catenin-dependent manner

Type I collagen is generated from two strands of COL1A1 and one strand of COL1A2. Evidence shows that reduced COL1A2 expression contributes to smaller scar tissue. To examine if ANGPTL4 has a direct effect on the expression of COL1A2, we examined the mRNA level of COL1A2 in fibroblasts treated with recombinant ANGPTL4 in the presence of either actinomycin D or cycloheximide. The decrease mRNA level of COL1A2 were abolished by both treatments, indicating that *de novo* mRNA and protein synthesis were required (Figure 46A). *In silico* analysis reveals that the human COL1A2 gene proximal promoter contains numerous E-boxes, specific DNA sequences to which bHLH transcription factors bind. Of interest, the bHLH transcriptional factor scleraxis was shown to synergize with Smad3 to regulate fibroblast collagen synthesis^{296,297}. In the first instance, we can examine the protein expression level of smad3 and scleraxis to check if ANGPTL4 treatment can modulate their expressions. Next, we can determine if ANGPTL4 treatment affects smad3 or scleraxis-mediated transactivation of COL1A2 promoter, ChIP can be performed using lysates from TGF β -treated and TGF β -ANGPTL4 co-treated fibroblasts. Interestingly, our preliminary data showed the mRNA expression of ID3 was elevated in cANGPTL4-treated primary fibroblasts (Figure 46B). Inhibitor of DNA-binding/differentiation proteins (ID) comprise a family of proteins that heterodimerize with bHLH transcription factors to inhibit DNA binding of bHLH proteins like scleraxis. Ectopic expression of ID3 decreases COL1A2 promoter activity. This observation raised the question how ANGPTL4 stimulates ID3 expression. ID3 is a transcriptional target of β -catenin-Tcf/LEF in C2C12 myoblasts, but the Tcf/LEF binding site was not identified. It was previously shown that ANGPTL4

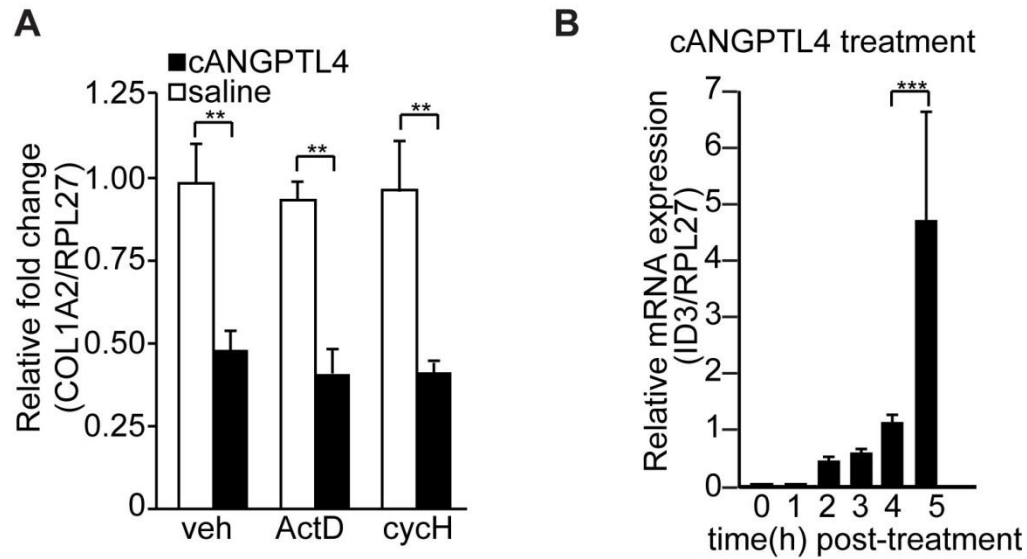


Figure 46. reduced id3 and collagen expression in cANGPTL4 treated fibroblasts

(A) Expression of COL1A2 mRNA from saline treated and cANGPTL4 (6 $\mu\text{g/mL}$) treated fibroblasts in the presence of PBS vehicle, actinomycin D (1 $\mu\text{g/mL}$) or cycloheximide (0.02 $\mu\text{g/mL}$). culture. **(B)** Expression of ID3 mRNA in cANGPTL4 (6 $\mu\text{g/mL}$) treated fibroblasts culture for a timeline of 5 hours. mRNA level were normalized to RPL27.

** $p < 0.01$, *** $p < 0.001$.

interacts with VE-cadherin in endothelial cells and triggers nuclear translocation of β -catenin to stimulate gene transcription, although no target gene was identified. Thus, we portended similar mechanism may be functional in fibroblasts. Firstly, we can investigate if ANGPTL4 can interact with cadherin-11, the predominant cadherin type in fibroblasts and determine the expression level of nuclear β -catenin in TGF β -treated fibroblasts co-treated with either saline (control) or ANGPTL4. Next, we can examine the human ID3 promoter site and reveal all potential Tcf-binding sites (TBE). ChIP β -catenin experiment followed by re-chip LEF can be performed in TGF β -ANGPTL4 co-treated fibroblasts compared with TGF β -treated cells. The result obtained from these experiments should provide strong clues on the potential mechanism of ANGPTL4 on scar formations.

2.7 GENERAL CONCLUSION

Restoration of skin integrity and homeostasis following injury is a vital process. A poor healing wound is an open portal for infections and often results in chronic inflammation. Impaired wound repair results in substantial morbidity, lost productivity, and healthcare expenditures. Despite the enormous impact of these poor healing wounds, current therapeutic approaches are often not sufficient. The development of novel efficient therapies requires a thorough understanding of the interplay among different cell types during wound healing. Such new insights on heterotypic cell communication will also lead to a better understanding of skin biology and aid in the development of better treatment and clinical injury management. The work of my PhD reveals two novel paracrine interactions between keratinocyte-fibroblast²⁹⁸ and keratinocyte-endothelial cells²⁹⁹ (Figure 47).

During wound healing, the increase proliferation of the keratinocytes is a biological event that aims to facilitate wound closure. However, how do the keratinocytes know when to proliferate and at what rate remains unclear. In mice lacking PPAR β/δ , epidermal cells proliferate excessively after wounding. But cultured keratinocytes from these mice do not proliferate any faster than normal cells and, in fact, are more susceptible to apoptosis. This discrepancy was my first indication that PPAR β/δ might regulate crosstalk between layers of the skin—the epidermal hyperproliferation seen in the knockout mice could be due to faulty signals from the dermal cells. My first chapter revealed a novel paracrine effect of fibroblast PPAR β/δ on keratinocyte cell growth. I showed that PPAR β/δ -deficient fibroblasts made wild type keratinocytes hyperproliferative by secreting extra doses of several growth factors. The fibroblasts

were stimulated to produce these growth factors by keratinocyte-released cytokine IL-1 - underscoring the reciprocity between the two cell types. Blocking either the IL-1 signal or any of the growth factors released by the fibroblasts returned the epithelia to normal²⁹⁸. Tumor has been described as wounds that never heal, and numerous studies have shown extensive overlap in gene expression profiles. Therefore, I hypothesized that dysregulation of keratinocyte-fibroblast communication may have contribute to the behaviour of tumorigenic epithelial cells. Indeed, cancer-associated fibroblasts have reduced level of PPAR β/δ , which may result in significant epithelial hyperproliferation of cancer cells.

As a ligand-activated transcription factor, PPAR β/δ directly regulates the expression of numerous target genes in wound keratinocytes. Together with other lab members, we showed that angiopoietin-like 4 (ANGPTL4) is a direct PPAR β/δ target gene^{270,271}. We reported novel functions of ANGPTL4 in the keratinocytes during wound healing by modulating cell migration via the control of integrin-mediated signalling and regulating the cell-matrix communication via the control of matrix protein integrity. We showed that the wound keratinocytes are the major producer of ANGPTL4 at the wound site. Importantly, we identify integrins $\beta 1$ and $\beta 5$ as novel binding partners of ANGPTL4. This interaction activates integrin-FAK-Src-PAK1 signaling and allows for selective integrin internalization to aid cell migration²⁷⁰. We also showed that ANGPTL4 interacts with vitronectin and fibronectin in the wound bed, delays their proteolytic degradation and thus regulate the availability of intact matrix proteins²⁷¹. The binding of ANGPTL4 to matrix proteins does not interfere with the recognition of the matrix protein by cognate integrins. These interactions enhance integrin-mediated signalling. We unravelled how

Figure 47. Schematic Illustration of keratinocyte-fibroblast and keratinocyte-endothelial cell crosstalks during wound healing.

(1) After ligand binding, PPAR β/δ forms heterodimers with the receptor for 9 cis-retinoid (RXR) in the nucleus. PPAR β/δ /RXR heterodimers associate with transcriptional coactivators and bind to sequence specific PPAR response elements (PPRE) located on target ANGPTL4 gene, leading to increase expression and secretion of ANGPTL4 from keratinocytes. (2) On the other hand, the activation of PPAR β/δ in fibroblasts can attenuates IL-1 signaling from keratinocyte via the production of sIL-1ra. sIL-1ra has little affinity for IL-1R2, which is highly expressed in keratinocytes. Thus, sIL-1ra acts in an autocrine fashion onto the fibroblasts, which expressed the predominant functional IL-1R1. The binding of sIL-1ra to IL-1R1 modulates the IL-1-mediated signaling events and consequently decreases the production of several AP-1-mediated mitogenic factors. The mitogenic factors exert a reduced paracrine effect on the epithelial proliferation via their cognate receptors. (3-4) ANGPTL4 interacting with integrin also activates FAK-src-PAK1 signaling and PKC/14-3-3 mediated pathway which modulate cell migration via integrin internalization. ANGPTL4 binds specific matrix proteins and delays their degradation by proteases (5) ANGPTL4 secreted from keratinocytes can interacts with VE-cadherin and claudin-5 expressed on endothelial cells surface to disrupts intercellular contact formation and possible initiation of angiogenesis. (6) ANGPTL4 can interact with integrin β 1, and activate the Src/ERK/AKT signaling cascades, leading to subsequent JAK1/STAT3 activation. Activated STAT3 can then mediate the upregulation of iNOS expression by specifically binding to the cognate responsive elements in the promoter of iNOS gene. Wound angiogenesis can then be promoted by the increase in NO production from the wound keratinocytes in the wound microenvironment. (7) ANGPTL4 can regulate collagen scar formation by binding to an unknown receptor from fibroblasts.

ANGPTL4 modulates the integrity of matrix proteins to directly influence integrin-mediated signalling, and thus lamellipodia formation and cell migration. Our findings underscore the importance of a dynamic integrin-matrix interaction, where communication between cells and environment allows the cells to constantly interrogate and modify the wound environment, modulate their gene expression and behaviour, thereby determining the tissue phenotype.

Thus, ANGPTL4 is a new member of the family of matricellular proteins. Matricellular proteins reside at the crossroads of cell–matrix and cell-cell communication, modulating several key regulatory networks. Presumably, the regulatory pathways consist of complex networks, creating many opportunities for the compensatory adjustments required for wound repair²⁷⁵. In this respect, my second chapter showed that ANGPTL4 is a novel keratinocyte-endothelial cell communication signal. Using two different *in vivo* models based on topical immuno-neutralization of ANGPTL4 and ablation of *ANGPTL4* gene, we showed that wounds in ANGPTL4-knockout mice exhibit delayed healing and share many characteristics of diabetic wounds, including reduced expression of matrix proteins, increased inflammation, and impaired wound-related angiogenesis²⁹⁹. Diabetic wounds are characterized by accumulation of devitalized tissue, increased/prolonged inflammation, poor wound-related angiogenesis, and deficiencies in extracellular matrix (ECM) components. Diabetic wounds show elevated levels of matrix metalloproteinases and increased proteolytic degradation of ECM components, culminating in a corrupt microenvironment that cannot support healing. Cells such as keratinocytes, fibroblasts, and endothelial cells also display dysregulated expressions of and responses to many growth factors and cytokines. I showed that ANGPTL4

expression is markedly elevated upon normal wound injury. In contrast, ANGPTL4 expression in wound epithelia remains low throughout the healing period in diabetic wounds. I showed that the topical application of matricellular protein cANGPTL4 modulated several regulatory networks involved in cell migration, angiogenesis and inflammation, as evidence by an altered gene expression profile signature. Notably, ANGPTL4 has a dramatic influence on the expression of endothelial-specific CD31 in diabetic wounds, returning its profile to that observed in wild type wounds. I further showed that ANGPTL4 induced nitric oxide production through an integrin/JAK/STAT3-mediated upregulation of iNOS expression in wound epithelia, thus revealing a hitherto unknown mechanism by which ANGPTL4 regulated angiogenesis via keratinocyte-to-endothelial cell communications²⁹⁹. My findings show that the replacement of ANGPTL4 can provide an adjunctive or new therapeutic avenue for treating poor healing wounds such as diabetes-associated ulcers. My study also confirms that therapeutic angiogenesis remains an attractive treatment modality for diabetic wound healing.

Wound healing is a complex and dynamic process of replacing devitalized and missing cellular structures and tissue layers. The human adult wound healing process can be divided 3 overlapping phases: inflammatory, proliferative and maturational phases. These biological processes require tightly-coordinated and regulated mechanisms involving autocrine and paracrine signalings. My study has revealed heterotypic communications among different cell types during the proliferative phase. It is conceivable that such intercellular signalling may have significant impact of other phases of wound healing. Indeed, our lab preliminary findings showed that ANGPTL4 interacts with C-reactive protein (CRP) in the wound fluid collected during the inflammatory phase.

The biological consequence of this novel interaction is currently under investigation in the lab. My preliminary finding also implicated a role for ANGPTL4 in tissue remodelling and collagen scar formation that occur during the maturational phase. The precise anti-scarring mechanism of ANGPTL4 is now described in a revised manuscript.

All the references cited in this conclusion are publications with me either as first or co-authorship

REFERENCES

1. Bressler RS, Bressler CH Functional anatomy of the skin. *Clin Podiatr Med Surg* 1989; **6**: 229-246
2. Tay SS, Roediger B, Tong PL, Tikoo S, Weninger W The Skin-Resident Immune Network. *Current dermatology reports* 2014; **3**: 13-22
3. Brenner M, Hearing VJ The protective role of melanin against UV damage in human skin. *Photochem Photobiol* 2008; **84**: 539-549
4. Tagami H, Yoshikuni K Interrelationship between water-barrier and reservoir functions of pathologic stratum corneum. *Arch Dermatol* 1985; **121**: 642-645
5. Wilkes GL, Brown IA, Wildnauer RH The biomechanical properties of skin. *CRC Crit Rev Bioeng* 1973; **1**: 453-495
6. Krafts KP Tissue repair: The hidden drama. *Organogenesis* 2010; **6**: 225-233
7. Enoch S, Leaper D John Basic science of wound healing. *Surgery Oxford External Resources* 2005; **23**: 37-42
8. Monaco JL, Lawrence WT Acute wound healing an overview. *Clin Plast Surg* 2003; **30**: 1-12
9. Martin P Wound healing--aiming for perfect skin regeneration. *Science* 1997; **276**: 75-81
10. Sinno H, Prakash S Complements and the wound healing cascade: an updated review. *Plastic surgery international* 2013; **2013**: 146764
11. Reinke JM, Sorg H Wound repair and regeneration. *Eur Surg Res* 2012; **49**: 35-43

12. Arnold F, West DC Angiogenesis in wound healing. *Pharmacol Ther* 1991; **52**: 407-422
13. Bauer SM, Bauer RJ, Velazquez OC Angiogenesis, vasculogenesis, and induction of healing in chronic wounds. *Vasc Endovascular Surg* 2005; **39**: 293-306
14. Epstein H Cutaneous wound healing. *External Resources* 1999; **341**: 738-746
15. Clark RA Regulation of fibroplasia in cutaneous wound repair. *Am J Med Sci* 1993; **306**: 42-48
16. Sarrazy V, Billet F, Micallef L, Coulomb B, Desmoulière A Mechanisms of pathological scarring: role of myofibroblasts and current developments. *Wound Repair Regen* 2011; **19 Suppl 1**: s10-s15
17. Verhaegen PDHM, van Zuijlen PPM, Pennings NM, van Marle J, Niessen FB, van der Horst CMAM et al Differences in collagen architecture between keloid, hypertrophic scar, normotrophic scar, and normal skin: An objective histopathological analysis. *Wound Repair Regen* 2009; **17**: 649-656
18. Cohen, I., Diegelman, R., Dome, R., Schwartz, S., Shires, G. & Spencer, F. *Wound care and wound healing*. 1999).
19. Kloth, L., McCulloch, J. & Feedar, J. *Wound healing*. 1990).
20. Majno G, Shea SM, Leventhal M Endothelial contraction induced by histamine-type mediators: an electron microscopic study. *J Cell Biol* 1969; **42**: 647-672
21. Cohen, I., Diegelman, R., Dorne, R., Greenfield, L., Mulholland, M. & Oldham, K. et al *Wound healing*. **30**, 1993).
22. Glat, P., Longaker, M., Aston, S., Besley, R. & Thorn, C. *Wound healing*. 1997).

23. Wahl SM, Hunt DA, Wakefield LM, McCartney-Francis N, Wahl LM, Roberts AB et al Transforming growth factor type beta induces monocyte chemotaxis and growth factor production. *Proc Natl Acad Sci U S A* 1987; **84**: 5788-5792
24. Hynes RO Integrins: a family of cell surface receptors. *Cell* 1987; **48**: 549-554
25. Cetinkale O, Ulualp KM, Ayan F, Düren M, Cizmeci O, Pusane A Early wound excision and skin grafting restores cellular immunity after severe burn trauma. *Br J Surg* 1993; **80**: 1296-1298
26. Newman SL, Henson JE, Henson PM Phagocytosis of senescent neutrophils by human monocyte-derived macrophages and rabbit inflammatory macrophages. *J Exp Med* 1982; **156**: 430-442
27. Fauci, A., Haynes, B., Isselbacher, K., Braunwald, E. & Wilson, J. *Cellular and molecular basis of immunity*.
28. Werb Z, Bainton DF, Jones PA Degradation of connective tissue matrices by macrophages. III. Morphological and biochemical studies on extracellular, pericellular, and intracellular events in matrix proteolysis by macrophages in culture. *J Exp Med* 1980; **152**: 1537-1553
29. Malawista SE, Montgomery RR, van Blaricom G Evidence for reactive nitrogen intermediates in killing of staphylococci by human neutrophil cytoplasts. A new microbicidal pathway for polymorphonuclear leukocytes. *J Clin Invest* 1992; **90**: 631-636
30. Madden JW, Peacock EE Studies on the biology of collagen during wound healing. I. Rate of collagen synthesis and deposition in cutaneous wounds of the rat. *Surgery* 1968; **64**: 288-294
31. McCartney-Francis N, Mizel D, Wong H Transforming growth factor-beta (TGF- β) as an immunoregulatory molecule [abstract]. *FASEB J* ;A875. 1988; **2**:
32. Schaffer MR, Tantry U, Gross SS, Wasserburg HL, Barbul A Nitric oxide regulates wound healing. *J Surg Res* 1996; **63**: 237-240

33. Gailit J, Clark RA Wound repair in the context of extracellular matrix. *Curr Opin Cell Biol* 1994; **6**: 717-725
34. Simpson DM, Ross R The neutrophilic leukocyte in wound repair a study with antineutrophil serum. *J Clin Invest* 1972; **51**: 2009-2023
35. Erlich, H. & Hunt, T. *The role of connective tissue matrix in wound healing*. 1988).
36. Circolo A, Welgus HG, Pierce GF, Kramer J, Strunk RC Differential regulation of the expression of proteinases/antiproteinases in fibroblasts. Effects of interleukin-1 and platelet-derived growth factor. *J Biol Chem* 1991; **266**: 12283-12288
37. Fauci AS Resistance to HIV-1 infection: it's in the genes. *Nat Med* 1996; **2**: 966-967
38. Lawrence WT Physiology of the acute wound. *Clin Plast Surg* 1998; **25**: 321-340
39. Minchenko A, Salceda S, Bauer T, Caro J Hypoxia regulatory elements of the human vascular endothelial growth factor gene. *Cell Mol Biol Res* 1994; **40**: 35-39
40. Patel B, Khaliq A, Jarvis-Evans J, McLeod D, Mackness M, Boulton M Oxygen regulation of TGF-beta 1 mRNA in human hepatoma (Hep G2) cells. *Biochem Mol Biol Int* 1994; **34**: 639-644
41. Scannell G, Waxman K, Kaml GJ, Ioli G, Gatanaga T, Yamamoto R et al Hypoxia induces a human macrophage cell line to release tumor necrosis factor-alpha and its soluble receptors in vitro. *J Surg Res* 1993; **54**: 281-285
42. Gharaee-Kermani M, Phan SH Role of cytokines and cytokine therapy in wound healing and fibrotic diseases. *Curr Pharm Des* 2001; **7**: 1083-1103
43. Ross R Platelet-derived growth factor. *Annu Rev Med* 1987; **38**: 71-79

44. Roberts AB, Anzano MA, Wakefield LM, Roche NS, Stern DF, Sporn MB Type beta transforming growth factor: a bifunctional regulator of cellular growth. *Proc Natl Acad Sci U S A* 1985; **82**: 119-123
45. Postlethwaite AE, Keski-Oja J, Moses HL, Kang AH Stimulation of the chemotactic migration of human fibroblasts by transforming growth factor beta. *J Exp Med* 1987; **165**: 251-256
46. Postlethwaite AE, Keski-Oja J, Balian G, Kang AH Induction of fibroblast chemotaxis by fibronectin. Localization of the chemotactic region to a 140,000-molecular weight non-gelatin-binding fragment. *J Exp Med* 1981; **153**: 494-499
47. Grotendorst G, Seppa H, Seppa S, Platelet-derived growth factor in chemotactic for fibroblasts. *Biol* 1982; **92**: 584-588
48. Westermarck B, Blomquist E Stimulation of fibroblast migration by epidermal growth factor. *Cell Biol Int Rep* 1980; **4**: 649-654
49. Grzesiak JJ, Pierschbacher MD Shifts in the concentrations of magnesium and calcium in early porcine and rat wound fluids activate the cell migratory response. *J Clin Invest* 1995; **95**: 227-233
50. Reed MJ, Puolakkainen P, Lane TF, Dickerson D, Bornstein P, Sage EH Differential expression of SPARC and thrombospondin 1 in wound repair: immunolocalization and in situ hybridization. *The journal of histochemistry and cytochemistry : official journal of the Histochemistry Society* 1993; **41**: 1467-1477
51. Parks WC Matrix metalloproteinases in repair. *Wound Repair Regen* 1999; **7**: 423-432
52. Parsons SL, Watson SA, Brown PD, Collins HM, Steele RJ Matrix metalloproteinases. *Br J Surg* 1997; **84**: 160-166
53. Assoian RK, Sporn MB Type beta transforming growth factor in human platelets: release during platelet degranulation and action on vascular smooth muscle cells. *J Cell Biol* 1986; **102**: 1217-1223

54. Werb Z, Tremble P, Damsky CH Regulation of extracellular matrix degradation by cell-extracellular matrix interactions. *Cell Differ Dev* 1990; **32**: 299-306
55. Finlay GA, Thannickal VJ, Fanburg BL, Paulson KE Transforming growth factor-beta 1-induced activation of the ERK pathway/activator protein-1 in human lung fibroblasts requires the autocrine induction of basic fibroblast growth factor. *J Biol Chem* 2000; **275**: 27650-27656
56. Nanney LB, Magid M, Stoscheck CM, King LE Comparison of epidermal growth factor binding and receptor distribution in normal human epidermis and epidermal appendages. *J Invest Dermatol* 1984; **83**: 385-393
57. Niall M, Ryan GB, O'Brien BM The effect of epidermal growth factor on wound healing in mice. *J Surg Res* 1982; **33**: 164-169
58. Werner S, Peters KG, Longaker MT, Fuller-Pace F, Banda MJ, Williams LT Large induction of keratinocyte growth factor expression in the dermis during wound healing. *Proc Natl Acad Sci U S A* 1992; **89**: 6896-6900
59. Cavani A, Zambruno G, Marconi A, Manca V, Marchetti M, Giannetti A Distinctive integrin expression in the newly forming epidermis during wound healing in humans. *J Invest Dermatol* 1993; **101**: 600-604
60. Clark RA, Lanigan JM, DellaPelle P, Manseau E, Dvorak HF, Colvin RB Fibronectin and fibrin provide a provisional matrix for epidermal cell migration during wound reepithelialization. *J Invest Dermatol* 1982; **79**: 264-269
61. Wysocki AB, Grinnell F Fibronectin profiles in normal and chronic wound fluid. *Lab Invest* 1990; **63**: 825-831
62. Mackie EJ, Halfter W, Liverani D Induction of tenascin in healing wounds. *J Cell Biol* 1988; **107**: 2757-2767
63. Blanco-Mezquita JT, Hutcheon AEK, Stepp MA, Zieske JD α V β 6 integrin promotes corneal wound healing. *Invest Ophthalmol Vis Sci* 2011; **52**: 8505-8513

64. Tsuruta D, Hashimoto T, Hamill KJ, Jones JCR Hemidesmosomes and focal contact proteins: functions and cross-talk in keratinocytes, bullous diseases and wound healing. *J Dermatol Sci* 2011; **62**: 1-7
65. Odland G, Ross R Human wound repair. I. Epidermal regeneration. *J Cell Biol* 1968; **39**: 135-151
66. Grotendorst, G., Pincev, D., Martin, G., Hunt, T., Heppenstall, R. & Pines, E. *Molecular mediators of tissue repair*. 1984).
67. Witte MB, Barbul A General principles of wound healing. *Surg Clin North Am* 1997; **77**: 509-528
68. Folkman J, Klagsbrun M Angiogenic factors. *Science* 1987; **235**: 442-447
69. Gailit J, Bueller H, Clark R Platelet-derived growth factor and inflammatory cytokines have differential effects on the expression of integrins alpha1b1 and alpha.
70. Gospodarowicz D, Neufeld G, Schweigerer L Fibroblast growth factor: structural and biological properties. *J Cell Physiol Suppl* 1987; **Suppl 5**: 15-26
71. Gospodarowicz D, Abraham JA, Schilling J Isolation and characterization of a vascular endothelial cell mitogen produced by pituitary-derived folliculo stellate cells. *Proc Natl Acad Sci U S A* 1989; **86**: 7311-7315
72. Strodbeck F Physiology of wound healing. *Newborn Infant Nurs Rev External Resources* 2001; **1**: 43-52
73. Robson MC, Steed DL, Franz MG Wound healing: biologic features and approaches to maximize healing trajectories. *Curr Probl Surg* 2001; **38**: 72-140
74. Gurtner GC, Werner S, Barrandon Y, Longaker MT Wound repair and regeneration. *Nature* 2008; **453**: 314-321

75. Eckes B, Nischt R, Krieg T Cell-matrix interactions in dermal repair and scarring. *Fibrogenesis & tissue repair* 2010; **3**: 4
76. Barker TH The role of ECM proteins and protein fragments in guiding cell behavior in regenerative medicine. *Biomaterials* 2011; **32**: 4211-4214
77. Jacinto A, Martinez-Arias A, Martin P Mechanisms of epithelial fusion and repair. *Nat Cell Biol* 2001; **3**: E117-E123
78. Hinz B Formation and function of the myofibroblast during tissue repair. *J Invest Dermatol* 2007; **127**: 526-537
79. Gurtner GC, Evans GR Advances in head and neck reconstruction. *Plast Reconstr Surg* 2000; **106**: 672-82; quiz 683
80. Bullard KM, Longaker MT, Lorenz HP Fetal wound healing: current biology. *World J Surg* 2003; **27**: 54-61
81. Lorenz HP, Whitby DJ, Longaker MT, Adzick NS Fetal wound healing. The ontogeny of scar formation in the non-human primate. *Ann Surg* 1993; **217**: 391-396
82. Ashcroft GS, Mills SJ, Lei K, Gibbons L, Jeong MJ, Taniguchi M et al Estrogen modulates cutaneous wound healing by downregulating macrophage migration inhibitory factor. *J Clin Invest* 2003; **111**: 1309-1318
83. Eming SA, Krieg T, Davidson JM Inflammation in wound repair: molecular and cellular mechanisms. *J Invest Dermatol* 2007; **127**: 514-525
84. Akaishi S, Ogawa R, Hyakusoku H Keloid and hypertrophic scar: neurogenic inflammation hypotheses. *Med Hypotheses* 2008; **71**: 32-38
85. Profyris C, Tziotziou C, Do Vale I Cutaneous scarring: Pathophysiology, molecular mechanisms, and scar reduction therapeutics Part I. The molecular basis of scar formation. *J Am Acad Dermatol* 2012; **66**: 1-10; quiz 11

86. Tziotzios C, Profyris C, Sterling J Cutaneous scarring: Pathophysiology, molecular mechanisms, and scar reduction therapeutics Part II. Strategies to reduce scar formation after dermatologic procedures. *J Am Acad Dermatol* 2012; **66**: 13-24; quiz 25
87. Meier K, Nanney LB Emerging new drugs for scar reduction. *Expert Opin Emerg Drugs* 2006; **11**: 39-47
88. Reish RG, Eriksson E Scar treatments: preclinical and clinical studies. *J Am Coll Surg* 2008; **206**: 719-730
89. Habif, T. P. *Clinical Dermatology*. (Elsevier Health Sciences:2009).
90. Fuchs E Keratins and the skin. *Annu Rev Cell Dev Biol* 1995; **11**: 123-153
91. Michel M, Török N, Godbout MJ, Lussier M, Gaudreau P, Royal A et al Keratin 19 as a biochemical marker of skin stem cells in vivo and in vitro: keratin 19 expressing cells are differentially localized in function of anatomic sites, and their number varies with donor age and culture stage. *J Cell Sci* 1996; **109 (Pt 5)**: 1017-1028
92. Loots MA, Lamme EN, Zeegelaar J, Mekkes JR, Bos JD, Middelkoop E Differences in cellular infiltrate and extracellular matrix of chronic diabetic and venous ulcers versus acute wounds. *J Invest Dermatol* 1998; **111**: 850-857
93. Klechevsky E Human dendritic cells - stars in the skin. *Eur J Immunol* 2013; **43**: 3147-3155
94. de Panfilis G Langerhans cells, dendritic cells, 'dendrocytes' and macrophages in normal human dermis. *Br J Dermatol* 1996; **135**: 652-653
95. Guironnet G, Dezutter-Dambuyant C, Gaudillère A, Maréchal S, Schmitt D, Péguet-Navarro J Phenotypic and functional outcome of human monocytes or monocyte-derived dendritic cells in a dermal equivalent. *J Invest Dermatol* 2001; **116**: 933-939
96. Cichorek M, Wachulska M, Stasiewicz A, Tymińska A Skin melanocytes: biology and development. *Postepy dermatologii i alergologii* 2013; **30**: 30-41

97. Cormack, D. H., Ham, A. W. & Cormack, D. H. *Ham's histology*. (Lippincott Williams & Wilkins:1987).
98. Dupasquier M, Stoitzner P, van Oudenaren A, Romani N, Leenen PJM
Macrophages and dendritic cells constitute a major subpopulation of cells in the mouse dermis. *J Invest Dermatol* 2004; **123**: 876-879
99. Willenborg S, Eming SA Macrophages - sensors and effectors coordinating skin damage and repair. *J Dtsch Dermatol Ges* 2014; **12**: 214-221
100. Boyce DE Dermal cellular inflammation in burns: an insight into the function of dermal microvascular anatomy. *Burns* 2002; **28**: 206; author reply 207
101. Ansel JC, Kaynard AH, Armstrong CA, Olerud J, Bunnett N, Payan D Skin-nervous system interactions. *J Invest Dermatol* 1996; **106**: 198-204
102. Detmar M Molecular regulation of angiogenesis in the skin. *J Invest Dermatol* 1996; **106**: 207-208
103. Werner S, Smola H Paracrine regulation of keratinocyte proliferation and differentiation. *Trends Cell Biol* 2001; **11**: 143-146
104. Chang HY, Chi JT, Dudoit S, Bondre C, van de Rijn M, Botstein D et al Diversity, topographic differentiation, and positional memory in human fibroblasts. *Proc Natl Acad Sci U S A* 2002; **99**: 12877-12882
105. Gosiewska A, Yi CF, Brown LJ, Cullen B, Silcock D, Geesin JC Differential expression and regulation of extracellular matrix-associated genes in fetal and neonatal fibroblasts. *Wound Repair Regen* 2001; **9**: 213-222
106. Grinnell F Fibroblasts, myofibroblasts, and wound contraction. *J Cell Biol* 1994; **124**: 401-404
107. Grotendorst GR Connective tissue growth factor: a mediator of TGF-beta action on fibroblasts. *Cytokine Growth Factor Rev* 1997; **8**: 171-179

108. Azzarone B, Macieira-Coelho A Heterogeneity of the kinetics of proliferation within human skin fibroblastic cell populations. *J Cell Sci* 1982; **57**: 177-187
109. Sorrell JM, Caplan AI Fibroblast heterogeneity: more than skin deep. *J Cell Sci* 2004; **117**: 667-675
110. Sappino AP, Schürch W, Gabbiani G Differentiation repertoire of fibroblastic cells: expression of cytoskeletal proteins as marker of phenotypic modulations. *Lab Invest* 1990; **63**: 144-161
111. Clark RA Fibronectin matrix deposition and fibronectin receptor expression in healing and normal skin. *J Invest Dermatol* 1990; **94**: 128S-134S
112. Singer AJ, Clark RA Cutaneous wound healing. *N Engl J Med* 1999; **341**: 738-746
113. Grinnell F, Zhu M, Carlson MA, Abrams JM Release of mechanical tension triggers apoptosis of human fibroblasts in a model of regressing granulation tissue. *Exp Cell Res* 1999; **248**: 608-619
114. Adzick NS, Lorenz HP Cells, matrix, growth factors, and the surgeon. The biology of scarless fetal wound repair. *Ann Surg* 1994; **220**: 10-18
115. Liechty KW, Kim HB, Adzick NS, Crombleholme TM Fetal wound repair results in scar formation in interleukin-10-deficient mice in a syngeneic murine model of scarless fetal wound repair. *J Pediatr Surg* 2000; **35**: 866-72; discussion 872
116. Cullen B, Silcock D, Brown LJ, Gosiewska A, Geesin JC The differential regulation and secretion of proteinases from fetal and neonatal fibroblasts by growth factors. *Int J Biochem Cell Biol* 1997; **29**: 241-250
117. Eckes B, Zigrino P, Kessler D, Holtkötter O, Shephard P, Mauch C et al Fibroblast-matrix interactions in wound healing and fibrosis. *Matrix Biol* 2000; **19**: 325-332

118. Shah M, Foreman DM, Ferguson MW Neutralisation of TGF-beta 1 and TGF-beta 2 or exogenous addition of TGF-beta 3 to cutaneous rat wounds reduces scarring. *J Cell Sci* 1995; **108 (Pt 3)**: 985-1002
119. Shah M, Foreman D, Ferguson M Neutralising antibody to TGF- β 2 reduces cutaneous scarring in adult rodents. *J Cell Sci* 1994; **107**: 1137-1157
120. Garner WL, Karmioli S, Rodriguez JL, Smith DJ, Phan SH Phenotypic differences in cytokine responsiveness of hypertrophic scar versus normal dermal fibroblasts. *J Invest Dermatol* 1993; **101**: 875-879
121. Ghahary A, Shen YJ, Nedelec B, Wang R, Scott PG, Tredget EE Collagenase production is lower in post-burn hypertrophic scar fibroblasts than in normal fibroblasts and is reduced by insulin-like growth factor-1. *J Invest Dermatol* 1996; **106**: 476-481
122. Bhowmick NA, Neilson EG, Moses HL Stromal fibroblasts in cancer initiation and progression. *Nature* 2004; **432**: 332-337
123. Kalluri R, Zeisberg M Fibroblasts in cancer. *Nat Rev Cancer* 2006; **6**: 392-401
124. Nakagawa H, Liyanarachchi S, Davuluri RV, Auer H, Martin EW, de la Chapelle A et al Role of cancer-associated stromal fibroblasts in metastatic colon cancer to the liver and their expression profiles. *Oncogene* 2004; **23**: 7366-7377
125. Hwang RF, Moore T, Arumugam T, Ramachandran V, Amos KD, Rivera A et al Cancer-associated stromal fibroblasts promote pancreatic tumor progression. *Cancer research* 2008; **68**: 918-926
126. Miles FL, Sikes RA Insidious Changes in Stromal Matrix Fuel Cancer Progression. *Mol Cancer Res* 2014;
127. Boxman I, Löwik C, Aarden L, Ponc M Modulation of IL-6 production and IL-1 activity by keratinocyte-fibroblast interaction. *J Invest Dermatol* 1993; **101**: 316-324
128. Smola H, Thiekötter G, Fusenig NE Mutual induction of growth factor gene expression by epidermal-dermal cell interaction. *J Cell Biol* 1993; **122**: 417-429

129. Kupper TS, Groves RW The interleukin-1 axis and cutaneous inflammation. *J Invest Dermatol* 1995; **105**: 62S-66S
130. Gilchrest BA, Karassik RL, Wilkins LM, Vrabel MA, Maciag T Autocrine and paracrine growth stimulation of cells derived from human skin. *J Cell Physiol* 1983; **117**: 235-240
131. Smith RS, Smith TJ, Blieden TM, Phipps RP Fibroblasts as sentinel cells. Synthesis of chemokines and regulation of inflammation. *Am J Pathol* 1997; **151**: 317-322
132. Maas-Szabowski N, Shimotoyodome A, Fusenig NE Keratinocyte growth regulation in fibroblast cocultures via a double paracrine mechanism. *J Cell Sci* 1999; **112 (Pt 12)**: 1843-1853
133. Maas-Szabowski N, Stark HJ, Fusenig NE Keratinocyte growth regulation in defined organotypic cultures through IL-1-induced keratinocyte growth factor expression in resting fibroblasts. *J Invest Dermatol* 2000; **114**: 1075-1084
134. Szabowski A, Maas-Szabowski N, Andrecht S, Kolbus A, Schorpp-Kistner M, Fusenig NE et al c-Jun and JunB antagonistically control cytokine-regulated mesenchymal-epidermal interaction in skin. *Cell* 2000; **103**: 745-755
135. Angel P, Szabowski A Function of AP-1 target genes in mesenchymal-epithelial cross-talk in skin. *Biochem Pharmacol* 2002; **64**: 949-956
136. Michalik L, Desvergne B, Tan NS, Basu-Modak S, Escher P, Rieusset J et al Impaired skin wound healing in peroxisome proliferator-activated receptor (PPAR)alpha and PPARbeta mutant mice. *The Journal of cell biology* 2001; **154**: 799-814
137. Michalik L, Wahli W Involvement of PPAR nuclear receptors in tissue injury and wound repair. *J Clin Invest* 2006; **116**: 598-606

138. Schmuth M, Haqq CM, Cairns WJ, Holder JC, Dorsam S, Chang S et al Peroxisome proliferator-activated receptor (PPAR)-beta/delta stimulates differentiation and lipid accumulation in keratinocytes. *J Invest Dermatol* 2004; **122**: 971-983
139. Di-Poï N, Tan NS, Michalik L, Wahli W, Desvergne B Antiapoptotic role of PPARbeta in keratinocytes via transcriptional control of the Akt1 signaling pathway. *Mol Cell* 2002; **10**: 721-733
140. Michalik L, Auwerx J, Berger JP, Chatterjee VK, Glass CK, Gonzalez FJ et al International Union of Pharmacology. LXI. Peroxisome proliferator-activated receptors. *Pharmacol Rev* 2006; **58**: 726-741
141. Michalik L, Wahli W PPARs Mediate Lipid Signaling in Inflammation and Cancer. *PPAR research* 2008; **2008**: 134059
142. Tan NS, Michalik L, Noy N, Yasmin R, Pacot C, Heim M et al Critical roles of PPAR beta/delta in keratinocyte response to inflammation. *Genes Dev* 2001; **15**: 3263-3277
143. Steinkasserer A, Spurr NK, Cox S, Jeggo P, Sim RB The human IL-1 receptor antagonist gene (IL1RN) maps to chromosome 2q14-q21, in the region of the IL-1 alpha and IL-1 beta loci. *Genomics* 1992; **13**: 654-657
144. Patterson D, Jones C, Hart I, Bleskan J, Berger R, Geyer D et al The human interleukin-1 receptor antagonist (IL1RN) gene is located in the chromosome 2q14 region. *Genomics* 1993; **15**: 173-176
145. Nicklin MJ, Weith A, Duff GW A physical map of the region encompassing the human interleukin-1 alpha, interleukin-1 beta, and interleukin-1 receptor antagonist genes. *Genomics* 1994; **19**: 382-384
146. Haskill S, Martin G, Van Le L, Morris J, Peace A, Bigler CF et al cDNA cloning of an intracellular form of the human interleukin 1 receptor antagonist associated with epithelium. *Proc Natl Acad Sci U S A* 1991; **88**: 3681-3685

147. Muzio M, Polentarutti N, Facchetti F, Peri G, Doni A, Sironi M et al Characterization of type II intracellular IL-1 receptor antagonist (IL-1ra3): a depot IL-1ra. *Eur J Immunol* 1999; **29**: 781-788
148. Muzio M, Polentarutti N, Sironi M, Poli G, De Gioia L, Introna M et al Cloning and characterization of a new isoform of the interleukin 1 receptor antagonist. *J Exp Med* 1995; **182**: 623-628
149. Malyak M, Guthridge JM, Hance KR, Dower SK, Freed JH, Arend WP Characterization of a low molecular weight isoform of IL-1 receptor antagonist. *J Immunol* 1998; **161**: 1997-2003
150. Malyak M, Smith MF, Abel AA, Hance KR, Arend WP The differential production of three forms of IL-1 receptor antagonist by human neutrophils and monocytes. *J Immunol* 1998; **161**: 2004-2010
151. Arend WP, Malyak M, Guthridge CJ, Gabay C Interleukin-1 receptor antagonist: role in biology. *Annu Rev Immunol* 1998; **16**: 27-55
152. Corradi A, Franzi AT, Rubartelli A Synthesis and secretion of interleukin-1 alpha and interleukin-1 receptor antagonist during differentiation of cultured keratinocytes. *Exp Cell Res* 1995; **217**: 355-362
153. Groves RW, Giri J, Sims J, Dower SK, Kupper TS Inducible expression of type 2 IL-1 receptors by cultured human keratinocytes. Implications for IL-1-mediated processes in epidermis. *J Immunol* 1995; **154**: 4065-4072
154. Tan NS, Michalik L, Di-Poi N, Ng CY, Mermoud N, Roberts AB et al Essential role of Smad3 in the inhibition of inflammation-induced PPARbeta/delta expression. *EMBO J* 2004; **23**: 4211-4221
155. Tan NS, Michalik L, Desvergne B, Wahli W Genetic- or transforming growth factor-beta 1-induced changes in epidermal peroxisome proliferator-activated receptor beta/delta expression dictate wound repair kinetics. *J Biol Chem* 2005; **280**: 18163-18170

156. Schroder J, Schug T, Berry N, Shaw S Cytokine networks in the skin. *J Invest Dermatol* 2007; **119**: 20S-224
157. Steude J, Kulke R, Christophers E Interleukin-1-stimulated secretion of interleukin-8 and growth-related oncogene- α demonstrates greatly enhanced keratinocyte growth in human raft cultured epidermis. *J Invest Dermatol* 2002; **119**: 1254-1260
158. Podvinec M, Kaufmann MR, Handschin C, Meyer UA NUBIScan, an in silico approach for prediction of nuclear receptor response elements. *Mol Endocrinol* 2002; **16**: 1269-1279
159. Florin L, Hummerich L, Dittrich BT, Kokocinski F, Wrobel G, Gack S et al Identification of novel AP-1 target genes in fibroblasts regulated during cutaneous wound healing. *Oncogene* 2004; **23**: 7005-7017
160. Watanabe K, Jose PJ, Rankin SM Eotaxin-2 generation is differentially regulated by lipopolysaccharide and IL-4 in monocytes and macrophages. *J Immunol* 2002; **168**: 1911-1918
161. Heiman AS, Abonyo BO, Darling-Reed SF, Alexander MS Cytokine-stimulated human lung alveolar epithelial cells release eotaxin-2 (CCL24) and eotaxin-3 (CCL26). *J Interferon Cytokine Res* 2005; **25**: 82-91
162. Wiener Z, Pocza P, Racz M, Nagy G, Tolgyesi G, Molnar V et al IL-18 induces a marked gene expression profile change and increased Ccl1 (I-309) production in mouse mucosal mast cell homologs. *Int Immunol* 2008; **20**: 1565-1573
163. Florin L, Maas-Szabowski N, Werner S, Szabowski A, Angel P Increased keratinocyte proliferation by JUN-dependent expression of PTN and SDF-1 in fibroblasts. *J Cell Sci* 2005; **118**: 1981-1989
164. Shim JH, Xiao C, Paschal AE, Bailey ST, Rao P, Hayden MS et al TAK1, but not TAB1 or TAB2, plays an essential role in multiple signaling pathways in vivo. *Genes Dev* 2005; **19**: 2668-2681

165. Groves RW, Rauschmayr T, Nakamura K, Sarkar S, Williams IR, Kupper TS Inflammatory and hyperproliferative skin disease in mice that express elevated levels of the IL-1 receptor (type I) on epidermal keratinocytes. Evidence that IL-1-inducible secondary cytokines produced by keratinocytes in vivo can cause skin disease. *J Clin Invest* 1996; **98**: 336-344
166. Smith MF, Eidlen D, Arend WP, Gutierrez-Hartmann A LPS-induced expression of the human IL-1 receptor antagonist gene is controlled by multiple interacting promoter elements. *J Immunol* 1994; **153**: 3584-3593
167. IJpenberg A, Tan NS, Gelman L, Kersten S, Seydoux J, Xu J et al In vivo activation of PPAR target genes by RXR homodimers. *EMBO J* 2004; **23**: 2083-2091
168. Cheng N, Bhowmick NA, Chytil A, Gorksa AE, Brown KA, Muraoka R et al Loss of TGF-beta type II receptor in fibroblasts promotes mammary carcinoma growth and invasion through upregulation of TGF-alpha-, MSP- and HGF-mediated signaling networks. *Oncogene* 2005; **24**: 5053-5068
169. Di Poi N, Tan N, Michalik L, Wahli W, Desvergne B Antiapoptotic role of PPARbeta in keratinocytes via transcriptional control of the Akt1 signaling pathway. *Journal of biochemistry* 2002; **10**: 721-733
170. Tan N, Icre G, Montagner A, Bordier-ten-Heggeler B, Wahli W, Michalik L The nuclear hormone receptor peroxisome proliferator-activated receptor beta/delta potentiates cell chemotactism, polarization, and migration. *Journal of biochemistry* 2007; **27**: 7161-7175
171. Kim DJ, Murray IA, Burns AM, Gonzalez FJ, Perdew GH, Peters JM Peroxisome proliferator-activated receptor-beta/delta inhibits epidermal cell proliferation by down-regulation of kinase activity. *The Journal of biological chemistry* 2005; **280**: 9519-9527
172. Cataisson C, Joseloff E, Murillas R, Wang A, Atwell C, Torgerson S et al Activation of cutaneous protein kinase C alpha induces keratinocyte apoptosis and intraepidermal inflammation by independent signaling pathways. *J Immunol* 2003; **171**: 2703-2713
173. Wang HQ, Smart RC Overexpression of protein kinase C-alpha in the epidermis of transgenic mice results in striking alterations in phorbol ester-induced inflammation and

COX-2, MIP-2 and TNF-alpha expression but not tumor promotion. *J Cell Sci* 1999; **112** (Pt 20): 3497-3506

174. Man MQ, Barish GD, Schmutz M, Crumrine D, Barak Y, Chang S et al Deficiency of PPARbeta/delta in the epidermis results in defective cutaneous permeability barrier homeostasis and increased inflammation. *J Invest Dermatol* 2008; **128**: 370-377

175. Letavernier E, Perez J, Joye E, Bellocq A, Fouqueray B, Haymann JP et al Peroxisome proliferator-activated receptor beta/delta exerts a strong protection from ischemic acute renal failure. *J Am Soc Nephrol* 2005; **16**: 2395-2402

176. Schug TT, Berry DC, Shaw NS, Travis SN, Noy N Opposing effects of retinoic acid on cell growth result from alternate activation of two different nuclear receptors. *Cell* 2007; **129**: 723-733

177. Beanes SR, Dang C, Soo C, Ting K Skin repair and scar formation: the central role of TGF-beta. *Expert Rev Mol Med* 2003; **5**: 1-22

178. Mukhopadhyay D, Knebelmann B, Cohen HT, Ananth S, Sukhatme VP The von Hippel-Lindau tumor suppressor gene product interacts with Sp1 to repress vascular endothelial growth factor promoter activity. *Mol Cell Biol* 1997; **17**: 5629-5639

179. Green CJ, Lichtlen P, Huynh NT, Yanovsky M, Laderoute KR, Schaffner W et al Placenta growth factor gene expression is induced by hypoxia in fibroblasts: a central role for metal transcription factor-1. *Cancer Res* 2001; **61**: 2696-2703

180. Lewis AM, Varghese S, Xu H, Alexander HR Interleukin-1 and cancer progression: the emerging role of interleukin-1 receptor antagonist as a novel therapeutic agent in cancer treatment. *J Transl Med* 2006; **4**: 48

181. Barak Y, Liao D, He W, Ong ES, Nelson MC, Olefsky JM et al Effects of peroxisome proliferator-activated receptor delta on placentation, adiposity, and colorectal cancer. *Proc Natl Acad Sci U S A* 2002; **99**: 303-308

182. Gupta RA, Tan J, Krause WF, Geraci MW, Willson TM, Dey SK et al Prostacyclin-mediated activation of peroxisome proliferator-activated receptor delta in colorectal cancer. *Proc Natl Acad Sci U S A* 2000; **97**: 13275-13280

183. Harman FS, Nicol CJ, Marin HE, Ward JM, Gonzalez FJ, Peters JM Peroxisome proliferator-activated receptor-delta attenuates colon carcinogenesis. *Nature medicine* 2004; **10**: 481-483

184. Olumi AF, Grossfeld GD, Hayward SW, Carroll PR, Tlsty TD, Cunha GR Carcinoma-associated fibroblasts direct tumor progression of initiated human prostatic epithelium. *Cancer Res* 1999; **59**: 5002-5011

185. Casey T, Bond J, Tighe S, Hunter T, Lintault L, Patel O et al Molecular signatures suggest a major role for stromal cells in development of invasive breast cancer. *Breast Cancer Res Treat* 2009; **114**: 47-62

186. Hayward SW, Wang Y, Cao M, Hom YK, Zhang B, Grossfeld GD et al Malignant transformation in a nontumorigenic human prostatic epithelial cell line. *Cancer Res* 2001; **61**: 8135-8142

187. Tuxhorn JA, Ayala GE, Smith MJ, Smith VC, Dang TD, Rowley DR Reactive stroma in human prostate cancer: induction of myofibroblast phenotype and extracellular matrix remodeling. *Clin Cancer Res* 2002; **8**: 2912-2923

188. Micke P, Kappert K, Ohshima M, Sundquist C, Scheidl S, Lindahl P et al In situ identification of genes regulated specifically in fibroblasts of human basal cell carcinoma. *J Invest Dermatol* 2007; **127**: 1516-1523

189. Ostman A, Augsten M Cancer-associated fibroblasts and tumor growth--bystanders turning into key players. *Curr Opin Genet Dev* 2009; **19**: 67-73

190. Pietras K, Pahler J, Bergers G, Hanahan D Functions of paracrine PDGF signaling in the proangiogenic tumor stroma revealed by pharmacological targeting. *PLoS Med* 2008; **5**: e19

191. Crawford Y, Kasman I, Yu L, Zhong C, Wu X, Modrusan Z et al PDGF-C mediates the angiogenic and tumorigenic properties of fibroblasts associated with tumors refractory to anti-VEGF treatment. *Cancer Cell* 2009; **15**: 21-34

192. Pietras K, Rubin K, Sjöblom T, Buchdunger E, Sjöquist M, Heldin CH et al Inhibition of PDGF receptor signaling in tumor stroma enhances antitumor effect of chemotherapy. *Cancer Res* 2002; **62**: 5476-5484
193. Orimo A, Gupta PB, SgROI DC, Arenzana-Seisdedos F, Delaunay T, Naeem R et al Stromal fibroblasts present in invasive human breast carcinomas promote tumor growth and angiogenesis through elevated SDF-1/CXCL12 secretion. *Cell* 2005; **121**: 335-348
194. Karnoub AE, Dash AB, Vo AP, Sullivan A, Brooks MW, Bell GW et al Mesenchymal stem cells within tumour stroma promote breast cancer metastasis. *Nature* 2007; **449**: 557-563
195. Huschtscha LI, Napier CE, Noble JR, Bower K, Au AYM, Campbell HG et al Enhanced isolation of fibroblasts from human skin explants. *Biotechniques* 2012; **53**: 239-244
196. Ahmed AM History of diabetes mellitus. *Saudi Med J* 2002; **23**: 373-378
197. *Diabetes mellitus history-from ancient to modern times*. 2011).
198. Maitra, A., Abbas, A., Kumar, V. & Fausto, N. *Endocrine system*. 2005).
199. Santoro N, Caprio S, Giannini C, Kim G, Kursawe R, Pierpont B et al Oxidized fatty acids: A potential pathogenic link between fatty liver and type 2 diabetes in obese adolescents? *Antioxid Redox Signal* 2014; **20**: 383-389
200. Ripsin CM, Kang H, Urban RJ Management of blood glucose in type 2 diabetes mellitus. *Am Fam Physician* 2009; **79**: 29-36
201. Yach D, Hawkes C, Gould CL, Hofman KJ The global burden of chronic diseases: overcoming impediments to prevention and control. *JAMA* 2004; **291**: 2616-2622
202. Cavanagh PR, Ulbrecht JS, Caputo GM The non-healing diabetic foot wound: fact or fiction? *Ostomy Wound Manage* 1998; **44**: 6S-12S; discussion 13S

203. Mathews CE Utility of murine models for the study of spontaneous autoimmune type 1 diabetes. *Pediatr Diabetes* 2005; **6**: 165-177
204. Srinivasan K, Ramarao P Animal models in type 2 diabetes research: an overview. *Indian J Med Res* 2007; **125**: 451-472
205. Park JS, Rhee SD, Kang NS, Jung WH, Kim HY, Kim JH et al Anti-diabetic and anti-adipogenic effects of a novel selective 11 β -hydroxysteroid dehydrogenase type 1 inhibitor, 2-(3-benzoyl)-4-hydroxy-1,1-dioxo-2H-1,2-benzothiazine-2-yl-1-phenylethanone (KR-66344). *Biochem Pharmacol* 2011; **81**: 1028-1035
206. Yoshida S, Tanaka H, Oshima H, Yamazaki T, Yonetoku Y, Ohishi T et al AS1907417, a novel GPR119 agonist, as an insulinotropic and β -cell preservative agent for the treatment of type 2 diabetes. *Biochem Biophys Res Commun* 2010; **400**: 745-751
207. Zhang Y, Proenca R, Maffei M, Barone M, Leopold L, Friedman JM Positional cloning of the mouse obese gene and its human homologue. *Nature* 1994; **372**: 425-432
208. Lindstrom P The physiology of obese-hyperglycemic mice [ob/ob mice]. *Scientificworldjournal* . 2007; **7**: 666-685
209. Chehab FF, Lim ME, Lu R Correction of the sterility defect in homozygous obese female mice by treatment with the human recombinant leptin. *Nat Genet* 1996; **12**: 318-320
210. Lavine RL, Voyles N, Perrino PV, Recant L Functional abnormalities of islets of Langerhans of obese hyperglycemic mouse. *Am J Physiol* 1977; **233**: E86-E90
211. Coleman DL Obese and diabetes: two mutant genes causing diabetes-obesity syndromes in mice. *Diabetologia* 1978; **14**: 141-148
212. Chen H, Charlat O, Tartaglia LA, Woolf EA, Weng X, Ellis SJ et al Evidence that the diabetes gene encodes the leptin receptor: identification of a mutation in the leptin receptor gene in db/db mice. *Cell* 1996; **84**: 491-495

213. Hummel KP, Dickie MM, Coleman DL Diabetes, a new mutation in the mouse. *Science* 1966; **153**: 1127-1128
214. Bansal R, Ahmad N, Kidwai JR Alloxan-glucose interaction: effect on incorporation of ¹⁴C-leucine into pancreatic islets of rat. *Acta Diabetol Lat* 1980; **17**: 135-143
215. Dufrane D, van Steenberghe M, Guiot Y, Goebbels RM, Saliez A, Gianello P Streptozotocin-induced diabetes in large animals (pigs/primates): role of GLUT2 transporter and beta-cell plasticity. *Transplantation* 2006; **81**: 36-45
216. Szkudelski T The mechanism of alloxan and streptozotocin action in B cells of the rat pancreas. *Physiol Res* 2001; **50**: 537-546
217. Sandler S, Swenne I Streptozotocin, but not alloxan, induces DNA repair synthesis in mouse pancreatic islets in vitro. *Diabetologia* 1983; **25**: 444-447
218. Nerup J, Mandrup-Poulsen T, Helqvist S, Andersen HU, Pociot F, Reimers JI et al On the pathogenesis of IDDM. *Diabetologia* 1994; **37 Suppl 2**: S82-S89
219. Mathews CE, Leiter EH Constitutive differences in antioxidant defense status distinguish alloxan-resistant and alloxan-susceptible mice. *Free Radic Biol Med* 1999; **27**: 449-455
220. Malaisse WJ, Malaisse-Lagae F, Sener A, Pipeleers DG Determinants of the selective toxicity of alloxan to the pancreatic B cell. *Proc Natl Acad Sci U S A* 1982; **79**: 927-930
221. Surwit RS, Kuhn CM, Cochrane C, McCubbin JA, Feinglos MN Diet-induced type II diabetes in C57BL/6J mice. *Diabetes* 1988; **37**: 1163-1167
222. Winzell MS, Ahrén B The high-fat diet-fed mouse: a model for studying mechanisms and treatment of impaired glucose tolerance and type 2 diabetes. *Diabetes* 2004; **53 Suppl 3**: S215-S219

223. Surwit RS, Feinglos MN, Rodin J, Sutherland A, Petro AE, Opara EC et al Differential effects of fat and sucrose on the development of obesity and diabetes in C57BL/6J and A/J mice. *Metabolism* 1995; **44**: 645-651
224. Burcelin R, Crivelli V, Dacosta A, Roy-Tirelli A, Thorens B Heterogeneous metabolic adaptation of C57BL/6J mice to high-fat diet. *Am J Physiol Endocrinol Metab* 2002; **282**: E834-E842
225. Greer N, Foman NA, MacDonald R, Dorrian J, Fitzgerald P, Rutks I et al Advanced wound care therapies for nonhealing diabetic, venous, and arterial ulcers: a systematic review. *Ann Intern Med* 2013; **159**: 532-542
226. Li H, Fu X, Zhang L, Huang Q, Wu Z, Sun T Research of PDGF-BB gel on the wound healing of diabetic rats and its pharmacodynamics. *J Surg Res* 2008; **145**: 41-48
227. Stamler JS, Singel DJ, Loscalzo J Biochemistry of nitric oxide and its redox-activated forms. *Science* 1992; **258**: 1898-1902
228. Knowles RG, Moncada S Nitric oxide synthases in mammals. *Biochem J* 1994; **298 (Pt 2)**: 249-258
229. Tsukahara Y, Morisaki T, Horita Y, Torisu M, Tanaka M Expression of inducible nitric oxide synthase in circulating neutrophils of the systemic inflammatory response syndrome and septic patients. *World J Surg* 1998; **22**: 771-777
230. Paulsen SM, Wurster SH, Nanney LB Expression of inducible nitric oxide synthase in human burn wounds. *Wound Repair Regen* 1998; **6**: 142-148
231. Reichner JS, Meszaros AJ, Louis CA, Henry WL, Mastrofrancesco B, Martin BA et al Molecular and metabolic evidence for the restricted expression of inducible nitric oxide synthase in healing wounds. *Am J Pathol* 1999; **154**: 1097-1104
232. Mahoney E, Reichner J, Bostom LR, Mastrofrancesco B, Henry W, Albina J Bacterial colonization and the expression of inducible nitric oxide synthase in murine wounds. *Am J Pathol* 2002; **161**: 2143-2152

233. Vodovotz Y, Bogdan C, Paik J, Xie QW, Nathan C Mechanisms of suppression of macrophage nitric oxide release by transforming growth factor beta. *J Exp Med* 1993; **178**: 605-613
234. Garg UC, Hassid A Nitric oxide-generating vasodilators inhibit mitogenesis and proliferation of BALB/C 3T3 fibroblasts by a cyclic GMP-independent mechanism. *Biochem Biophys Res Commun* 1990; **171**: 474-479
235. Frank S, Kolb N, Werner ER, Pfeilschifter J Coordinated induction of inducible nitric oxide synthase and GTP-cyclohydrolase I is dependent on inflammatory cytokines and interferon-gamma in HaCaT keratinocytes: implications for the model of cutaneous wound repair. *J Invest Dermatol* 1998; **111**: 1065-1071
236. Heck DE, Laskin DL, Gardner CR, Laskin JD Epidermal growth factor suppresses nitric oxide and hydrogen peroxide production by keratinocytes. Potential role for nitric oxide in the regulation of wound healing. *J Biol Chem* 1992; **267**: 21277-21280
237. Papapetropoulos A, García-Cardena G, Madri JA, Sessa WC Nitric oxide production contributes to the angiogenic properties of vascular endothelial growth factor in human endothelial cells. *J Clin Invest* 1997; **100**: 3131-3139
238. Frank S, Madlener M, Pfeilschifter J, Werner S Induction of inducible nitric oxide synthase and its corresponding tetrahydrobiopterin-cofactor-synthesizing enzyme GTP-cyclohydrolase I during cutaneous wound repair. *J Invest Dermatol* 1998; **111**: 1058-1064
239. Frank S, Stallmeyer B, Kämpfer H, Kolb N, Pfeilschifter J Nitric oxide triggers enhanced induction of vascular endothelial growth factor expression in cultured keratinocytes (HaCaT) and during cutaneous wound repair. *FASEB journal : official publication of the Federation of American Societies for Experimental Biology* 1999; **13**: 2002-2014
240. Schaffer M, Efron P, Thornton F Nitric oxide, and autocrine regulator of wound fibroblast synthetic function. *J Immunol* 1997; **158**: 2375-2381

241. Wang X, Zalcenstein A, Oren M Nitric oxide promotes p53 nuclear retention and sensitizes neuroblastoma cells to apoptosis by ionizing radiation. *Cell Death Differ* 2003; **10**: 468-476
242. Du M, Islam MM, Lin L, Ohmura Y, Moriyama Y, Fujimura S Promotion of proliferation of murine BALB/C3T3 fibroblasts mediated by nitric oxide at lower concentrations. *Biochem Mol Biol Int* 1997; **41**: 625-631
243. Efron DT, Kirk SJ, Regan MC, Wasserkrug HL, Barbul A Nitric oxide generation from L-arginine is required for optimal human peripheral blood lymphocyte DNA synthesis. *Surgery* 1991; **110**: 327-334
244. Wu G, Flynn NE, Flynn SP, Jolly CA, Davis PK Dietary protein or arginine deficiency impairs constitutive and inducible nitric oxide synthesis by young rats. *J Nutr* 1999; **129**: 1347-1354
245. Iuvone T, Carnuccio R, Di Rosa M Modulation of granuloma formation by endogenous nitric oxide. *Eur J Pharmacol* 1994; **265**: 89-92
246. Iuvone T, Van Osselaer N, D'Acquisto F, Carnuccio R, Herman AG Differential effect of L-NAME and S-methyl-isothiourea on leukocyte emigration in carrageenin-soaked sponge implants in rat. *Br J Pharmacol* 1997; **121**: 1637-1644
247. Lee PC, Salyapongse AN, Bragdon GA, Shears LL, Watkins SC, Edington HD et al Impaired wound healing and angiogenesis in eNOS-deficient mice. *Am J Physiol* 1999; **277**: H1600-H1608
248. Imanishi J, Kamiyama K, Iguchi I, Kita M, Sotozono C, Kinoshita S Growth factors: importance in wound healing and maintenance of transparency of the cornea. *Prog Retin Eye Res* 2000; **19**: 113-129
249. Nill MR, Oberyszyn TM, Ross MS, Oberyszyn AS, Robertson FM Temporal sequence of pulmonary cytokine gene expression in response to endotoxin in C3H/HeN endotoxin-sensitive and C3H/HeJ endotoxin-resistant mice. *J Leukoc Biol* 1995; **58**: 563-574

250. Stallmeyer B, Kampfer H, Kolb N The function of nitric oxide in wound repair: inhibition of inducible nitric oxide-synthase severely impairs wound reepithelialization. *J Invest Dermatol* 1998; **113**: 1090-1098
251. Hood JD, Meininger CJ, Ziche M, Granger HJ VEGF upregulates ecNOS message, protein, and NO production in human endothelial cells. *Am J Physiol* 1998; **274**: H1054-H1058
252. Vander Z, Murohara T, Luo Z Vascular endothelial growth factor/vascular permeability factor augments nitric oxide release from quiescent rabbit and human vascular endothelium. *Circulation* 1997; **95**: 1030-1037
253. Ziche M, Morbidelli L, Choudhuri R, Zhang HT, Donnini S, Granger HJ et al Nitric oxide synthase lies downstream from vascular endothelial growth factor-induced but not basic fibroblast growth factor-induced angiogenesis. *J Clin Invest* 1997; **99**: 2625-2634
254. Parenti A, Morbidelli L, Cui XL, Douglas JG, Hood JD, Granger HJ et al Nitric oxide is an upstream signal of vascular endothelial growth factor-induced extracellular signal-regulated kinase1/2 activation in postcapillary endothelium. *J Biol Chem* 1998; **273**: 4220-4226
255. Morbidelli L, Chang CH, Douglas JG, Granger HJ, Ledda F, Ziche M Nitric oxide mediates mitogenic effect of VEGF on coronary venular endothelium. *Am J Physiol* 1996; **270**: H411-H415
256. Shizukuda Y, Tang S, Yokota R, Ware JA Vascular endothelial growth factor-induced endothelial cell migration and proliferation depend on a nitric oxide-mediated decrease in protein kinase Cdelta activity. *Circ Res* 1999; **85**: 247-256
257. Noiri E, Hu Y, Bahou WF, Keese CR, Giaever I, Goligorsky MS Permissive role of nitric oxide in endothelin-induced migration of endothelial cells. *J Biol Chem* 1997; **272**: 1747-1752
258. Noiri E, Lee E, Testa J, Quigley J, Colflesh D, Keese CR et al Podokinesis in endothelial cell migration: role of nitric oxide. *Am J Physiol* 1998; **274**: C236-C244

259. Brown LF, Yeo KT, Berse B, Yeo TK, Senger DR, Dvorak HF et al Expression of vascular permeability factor (vascular endothelial growth factor) by epidermal keratinocytes during wound healing. *J Exp Med* 1992; **176**: 1375-1379
260. Tsurumi Y, Murohara T, Krasinski K, Chen D, Witzanbichler B, Kearney M et al Reciprocal relation between VEGF and NO in the regulation of endothelial integrity. *Nat Med* 1997; **3**: 879-886
261. Lander HM, Sehajpal P, Levine DM, Novogrodsky A Activation of human peripheral blood mononuclear cells by nitric oxide-generating compounds. *J Immunol* 1993; **150**: 1509-1516
262. Barbul A, Fishel RS, Shimazu S, Wasserkrug HL, Yoshimura NN, Tao RC et al Intravenous hyperalimentation with high arginine levels improves wound healing and immune function. *J Surg Res* 1985; **38**: 328-334
263. Thornton FJ, Schäffer MR, Witte MB, Moldawer LL, MacKay SL, Abouhamze A et al Enhanced collagen accumulation following direct transfection of the inducible nitric oxide synthase gene in cutaneous wounds. *Biochem Biophys Res Commun* 1998; **246**: 654-659
264. Most D, Efron DT, Shi HP, Tantry US, Barbul A Characterization of incisional wound healing in inducible nitric oxide synthase knockout mice. *Surgery* 2002; **132**: 866-876
265. Bornstein P, Sage EH Matricellular proteins: extracellular modulators of cell function. *Curr Opin Cell Biol* 2002; **14**: 608-616
266. Puolakkainen PA, Bradshaw AD, Brekken RA, Reed MJ, Kyriakides T, Funk SE et al SPARC-thrombospondin-2-double-null mice exhibit enhanced cutaneous wound healing and increased fibrovascular invasion of subcutaneous polyvinyl alcohol sponges. *J Histochem Cytochem* 2005; **53**: 571-581
267. Bradshaw AD, Reed MJ, Sage EH SPARC-null mice exhibit accelerated cutaneous wound closure. *J Histochem Cytochem* 2002; **50**: 1-10

268. Wehrhan F, Rödel F, Grabenbauer GG, Amann K, Brückl W, Schultze-Mosgau S Transforming growth factor beta 1 dependent regulation of Tenascin-C in radiation impaired wound healing. *Radiother Oncol* 2004; **72**: 297-303
269. Liaw L, Birk DE, Ballas CB, Whitsitt JS, Davidson JM, Hogan BL Altered wound healing in mice lacking a functional osteopontin gene (spp1). *The Journal of clinical investigation* 1998; **101**: 1468-1478
270. Goh YY, Pal M, Chong HC, Zhu P, Tan MJ, Punugu L et al Angiopoietin-like 4 interacts with integrins beta1 and beta5 to modulate keratinocyte migration. *Am J Pathol* 2010; **177**: 2791-2803
271. Goh YY, Pal M, Chong HC, Zhu P, Tan MJ, Punugu L et al Angiopoietin-like 4 interacts with matrix proteins to modulate wound healing. *J Biol Chem* 2010; **285**: 32999-33009
272. Bornstein P Matricellular proteins: an overview. *Journal of cell communication and signaling* 2009; **3**: 163-165
273. Weber CE, Li NY, Wai PY, Kuo PC Epithelial-mesenchymal transition, TGF- β , and osteopontin in wound healing and tissue remodeling after injury. *J Burn Care Res* 2012; **33**: 311-318
274. Miyazaki KI, Okada Y, Yamanaka O, Kitano A, Ikeda K, Kon S et al Corneal wound healing in an osteopontin-deficient mouse. *Invest Ophthalmol Vis Sci* 2008; **49**: 1367-1375
275. Chong HC, Tan CK, Huang RL, Tan NS Matricellular proteins: a sticky affair with cancers. *Journal of oncology* 2012; **2012**: 351089
276. Kersten S, Mandard S, Tan NS, Escher P, Metzger D, Chambon P et al Characterization of the fasting-induced adipose factor FIAF, a novel peroxisome proliferator-activated receptor target gene. *J Biol Chem* 2000; **275**: 28488-28493
277. Ge H, Yang G, Huang L, Motola DL, Pourbahrami T, Li C Oligomerization and regulated proteolytic processing of angiopoietin-like protein 4. *J Biol Chem* 2004; **279**: 2038-2045

278. Mandard S, Zandbergen F, Tan NS, Escher P, Patsouris D, Koenig W et al The direct peroxisome proliferator-activated receptor target fasting-induced adipose factor (FIAF/PGAR/ANGPTL4) is present in blood plasma as a truncated protein that is increased by fenofibrate treatment. *The Journal of biological chemistry* 2004; **279**: 34411-34420

279. Mandard S, Zandbergen F, van Straten E, Wahli W, Kuipers F, Müller M et al The fasting-induced adipose factor/angiopoietin-like protein 4 is physically associated with lipoproteins and governs plasma lipid levels and adiposity. *J Biol Chem* 2006; **281**: 934-944

280. Huang RL, Teo Z, Chong HC, Zhu P, Tan MJ, Tan CK et al ANGPTL4 modulates vascular junction integrity by integrin signaling and disruption of intercellular VE-cadherin and claudin-5 clusters. *Blood* 2011; **118**: 3990-4002

281. Pal M, Tan MJ, Huang RL, Goh YY, Wang XL, Tang MBY et al Angiopoietin-like 4 regulates epidermal differentiation. *PloS one* 2011; **6**: e25377

282. Goh YY, Pal M, Chong HC, Zhu P, Tan MJ, Punugu L et al Angiopoietin-like 4 interacts with integrins beta1 and beta5 to modulate keratinocyte migration. *Am J Pathol* 2010; **177**: 2791-2803

283. Cheng B, Liu HW, Fu XB, Sun TZ, Sheng ZY Recombinant human platelet-derived growth factor enhanced dermal wound healing by a pathway involving ERK and c-fos in diabetic rats. *J Dermatol Sci* 2007; **45**: 193-201

284. Le Jan S, Amy C, Cazes A, Monnot C, Lamandé N, Favier J et al Angiopoietin-like 4 is a proangiogenic factor produced during ischemia and in conventional renal cell carcinoma. *Am J Pathol* 2003; **162**: 1521-1528

285. Bouleti C, Mathivet T, Coqueran B, Serfaty JM, Lesage M, Berland E et al Protective effects of angiopoietin-like 4 on cerebrovascular and functional damages in ischaemic stroke. *Eur Heart J* 2013; **34**: 3657-3668

286. Mitchell K, Szekeres C, Milano V, Svenson KB, Nilsen-Hamilton M, Kreidberg JA et al Alpha3beta1 integrin in epidermis promotes wound angiogenesis and keratinocyte-to-

endothelial-cell crosstalk through the induction of MRP3. *J Cell Sci* 2009; **122**: 1778-1787

287. Peranteau WH, Zhang L, Muvarak N, Badillo AT, Radu A, Zoltick PW et al IL-10 overexpression decreases inflammatory mediators and promotes regenerative healing in an adult model of scar formation. *J Invest Dermatol* 2008; **128**: 1852-1860

288. McGrouther DA Facial disfigurement. *BMJ* 1997; **314**: 991

289. Robert R, Meyer W, Bishop S, Rosenberg L, Murphy L, Blakeney P Disfiguring burn scars and adolescent self-esteem. *Burns* 1999; **25**: 581-585

290. Bayat A, McGrouther DA Clinical management of skin scarring. *Skinmed* 2005; **4**: 165-173

291. Ferguson MWJ, O'Kane S Scar-free healing: from embryonic mechanisms to adult therapeutic intervention. *Philos Trans R Soc Lond B Biol Sci* 2004; **359**: 839-850

292. Ferguson MW, Whitby DJ, Shah M, Armstrong J, Siebert JW, Longaker MT Scar formation: the spectral nature of fetal and adult wound repair. *Plast Reconstr Surg* 1996; **97**: 854-860

293. Bornstein P, Sage E Matricellular proteins: extracellular modulators of cell function. 2002; **14**: 608-616

294. Jun JI, Lau LF The matricellular protein CCN1 induces fibroblast senescence and restricts fibrosis in cutaneous wound healing. *Nat Cell Biol* 2010; **12**: 676-685

295. Goh YY, Pal M, Chong HC, Zhu P, Tan MJ, Punugu L et al Angiopoietin-like 4 interacts with matrix proteins to modulate wound healing. *J Biol Chem* 2010; **285**: 32999-33009

296. Espira L, Lamoureux L, Jones SC, Gerard RD, Dixon IMC, Czubryt MP The basic helix-loop-helix transcription factor scleraxis regulates fibroblast collagen synthesis. *J Mol Cell Cardiol* 2009; **47**: 188-195

297. Bagchi RA, Czubryt MP Synergistic roles of scleraxis and Smads in the regulation of collagen 1 α 2 gene expression. *Biochim Biophys Acta* 2012; **1823**: 1936-1944

298. Chong HC, Tan MJ, Philippe V, Tan SH, Tan CK, Ku CW et al Regulation of epithelial-mesenchymal IL-1 signaling by PPARbeta/delta is essential for skin homeostasis and wound healing. *J Cell Biol* 2009; **184**: 817-831

299. Chong HC, Chan JSK, Goh CQ, Gounko NV, Luo B, Wang X et al Angiopoietin-like 4 Stimulates STAT3-mediated iNOS Expression and Enhances Angiogenesis to Accelerate Wound Healing in Diabetic Mice. *Mol Ther* 2014;

PUBLICATIONS